

DESIGN OPTIMIZATION OF A HORIZONTAL WELL IN THIN OIL COLUMN  
RESERVOIR IN GULF OF THAILAND USING EXPERIMENTAL DESIGN  
METHODOLOGY

Mr. Jirasak Arunmongkol

A Thesis Submitted in Partial Fulfillment of the Requirements  
for the Degree of Master of Engineering Program in Petroleum Engineering  
Department of Mining and Petroleum Engineering  
Faculty of Engineering  
Chulalongkorn University  
Academic Year 2010  
Copyright of Chulalongkorn University

การออกแบบที่เหมาะสมสำหรับการเจาะหลุมแนวนอนในแหล่งกักเก็บน้ำมันชั้นบางใน

อ่าวไทยโดยใช้หลักการออกแบบการทดลอง

นาย จิรศักดิ์ อรุณมงคล

วิทยานิพนธ์นี้เป็นส่วนหนึ่งของการศึกษาตามหลักสูตรปริญญาวิศวกรรมศาสตรมหาบัณฑิต

สาขาวิชาวิศวกรรมปิโตรเลียม ภาควิชาวิศวกรรมเหมืองแร่และปิโตรเลียม

คณะวิศวกรรมศาสตร์ จุฬาลงกรณ์มหาวิทยาลัย

ปีการศึกษา 2553

ลิขสิทธิ์ของจุฬาลงกรณ์มหาวิทยาลัย

Thesis Title                                DESIGN OPTIMIZATION OF A HORIZONTAL  
WELL IN THIN OIL COLUMN RESERVOIR IN  
GULF OF THAILAND USING EXPERIMENTAL  
DESIGN METHODOLOGY

By    Mr. Jirasak Arunmongkol

Field of Study                                Petroleum Engineering

Thesis Advisor                               Assistant Professor Jirawat Chewaroungroj, Ph.D.

---

Accepted by the Faculty of Engineering, Chulalongkorn University in  
Partial Fulfillment of the Requirements for the Master's Degree

..... Dean of the Faculty of Engineering  
(Associate Professor Boonsom Lerdhirunwong, Dr.Ing.)

#### THESIS COMMITTEE

.....Chairman  
(Assistant Professor Suwat Athichanagorn, Ph.D.)

.....Thesis Advisor  
(Assistant Professor Jirawat Chewaroungroj, Ph.D.)

.....External Examiner  
(Thotsaphon Chaianansutcharit, Ph.D.)

จรัสศักดิ์ อรุณมงคล : การออกแบบที่เหมาะสมสำหรับการเจาะหลุมแนวนอนในแหล่งกักเก็บน้ำมันชั้นบางในอ่าวไทยโดยใช้หลักการออกแบบการทดลอง (DESIGN OPTIMIZATION OF A HORIZONTAL WELL IN THIN OIL COLUMN RESERVOIR IN GULF OF THAILAND USING EXPERIMENTAL DESIGN METHODOLOGY) อ. ที่ปรึกษาวิทยานิพนธ์หลัก: ผศ. ดร. จิรวัดน์ ชิวรุ่งโรจน์, 213 หน้า.

การเจาะหลุมแนวนอนในอ่าวไทยได้เริ่มมีมาตั้งแต่ปลายทศวรรษแห่งปีคริสต์ศักราช 1990 เพื่อให้สามารถกักปริมาณน้ำมันได้มากขึ้นและต่ออายุแหล่งผลิตให้ยาวนานยิ่งขึ้น เนื่องจากความซับซ้อนของสภาพทางธรณีวิทยาในอ่าวไทยทำให้แหล่งกักเก็บน้ำมันมีลักษณะเป็นชั้นบางและยากต่อการทำแผนที่เพื่อวางแผน ดังนั้นการตัดสินใจว่าควรเจาะหลุมแนวนอนแทนที่จะเป็นหลุมแนวตั้งหรือหลุมแนวเฉียงเบนจึงจำเป็นต้องเปรียบเทียบระหว่างความไม่แน่นอนของข้อมูลก่อนการเจาะและประโยชน์ที่จะได้รับ การวิจัยนี้นำเสนอการประยุกต์ใช้หลักการออกแบบการทดลองเพื่อเพิ่มประสิทธิภาพการออกแบบหลุมแนวนอนในแหล่งกักเก็บชั้นน้ำมันชั้นบางในอ่าวไทยให้เหมาะสมยิ่งขึ้น จากฐานข้อมูลหลุมแนวนอนที่มีอยู่ ข้อมูลทางปิโตรฟิสิกส์และวิศวกรรมได้ถูกรวบรวมมาวิเคราะห์เชิงสถิติเพื่อนำมาทำการทดลองเป็นชุดๆ ซึ่งแต่ละชุดถูกออกแบบโดยใช้หลักการออกแบบการทดลอง การทดลองสำหรับงานวิจัยนี้ทำโดยใช้วิธีการจำลองการไหลในแบบจำลองแหล่งกักเก็บน้ำมันอย่างง่าย ผลการวิเคราะห์ที่ได้จากการทดลองได้ถูกนำมาใช้คัดเลือกปัจจัยที่มีนัยสำคัญทางสถิติที่มีอิทธิพลต่อปัจจัยการกักน้ำมันสูงสุดและสร้างแบบจำลองตัวแทนสองแบบจำลอง แบบจำลองแรกสามารถทำนายปัจจัยการกักน้ำมันสูงสุดเนื่องจากการผลิตของหลุมแนวนอน ส่วนแบบจำลองที่สองสามารถทำนายปัจจัยการกักน้ำมันสูงสุดเนื่องจากการผลิตของหลุมแนวตั้งสองหลุมได้ วิธีการประยุกต์ใช้แบบจำลองทั้งสองในการระบุว่าแหล่งกักเก็บน้ำมันชั้นบางในอ่าวไทยแหล่งไหนมีความเหมาะสมสูงสำหรับการเจาะหลุมแนวนอนได้ถูกนำเสนอ ผลที่อาจจะได้รับคือการลดภาระในการสร้างและจำลองการไหลในแหล่งกักเก็บลง นอกจากนี้ ผลการวิเคราะห์เชิงสถิติยังระบุว่า ความพรุน, ความซึมผ่านได้, ผลเนื่องจากแคปิลารี, ระยะในแนวตั้งระหว่างหลุมแนวนอนถึงรอยต่อระหว่างชั้นน้ำและน้ำมัน, ความหนาในแนวตั้งของชั้นน้ำมัน, การควบคุมอัตราการผลิตของของเหลว, อัตราส่วนระหว่างความยาวของหลุมแนวนอนต่อความยาวของแหล่งกักเก็บ และอันตรกิริยาของปัจจัยเหล่านี้มีอิทธิพลอย่างมีนัยสำคัญทางสถิติต่อปัจจัยการกักน้ำมันสูงสุด

ภาควิชา ..... วิศวกรรมเหมืองแร่และปิโตรเลียม ..... ลายมือชื่อนิสิต.....  
 สาขาวิชา ..... วิศวกรรมปิโตรเลียม ..... ลายมือชื่อ อ.ที่ปรึกษาวิทยานิพนธ์หลัก.....  
 ปีการศึกษา ..... 2553 .....

# # 5071603521: MAJOR PETROLEUM ENGINEERING

KEYWORDS: EXPERIMENTAL DESIGN / HORIZONTAL WELL / THIN OIL COLUMN / GULF OF THAILAND / PROXY MODEL

JIRASAK ARUNMONGKOL: DESIGN OPTIMIZATION OF A HORIZONTAL WELL IN THIN OIL COLUMN RESERVOIR IN GULF OF THAILAND USING EXPERIMENTAL DESIGN METHODOLOGY. ADVISOR: ASST. PROF. JIRAWAT CHEWAROUNGROAJ, Ph.D., 213 pp.

Horizontal wells have been drilled in the Gulf of Thailand since the late 1990's to maximize oil recovery and prolong field life. Due to its complex geology, most of oil reservoirs have thin oil columns and are difficult to map. Decision to drill a horizontal well thus needs to compromise between pre-drill uncertainties and gain in benefits over traditional vertical or deviated wells. This research presents an application of experimental design methodology to optimize design method of a horizontal well in a thin-oil-column reservoir in the Gulf of Thailand. Petrophysical and engineering data from an existing horizontal well database was collated and statistically analyzed. Series of reservoir simulations on simplified reservoir models were conducted with respect to experimental designs to screen out significant factors and construct two proxy models. One is for predicting an ultimate recovery factor of a horizontal well. The other is for that of two vertical wells. By using the proxy models, a simple method capable of identifying thin-oil-column reservoirs which have high suitability for drilling a horizontal well is proposed. As a result, burden on reservoir modeling and simulation could be reduced. In addition, statistical analysis results of the designed experiments show that porosity, permeability, capillary effect, well standoff to oil-water contact, vertical thickness of oil column, liquid rate production control, a ratio of horizontal well length to reservoir length, and their interaction effects significantly influence ultimate recovery of the horizontal well.

Department: Mining and Petroleum Engineering..... Student's signature: .....

Field of Study: Petroleum Engineering..... Advisor's signature: .....

Academic Year: 2010.....

## **Acknowledgements**

I would like to express my deepest gratitude to Assistant Professor Dr. Jirawat Chewaroungroaj for his invaluable guidance, consistent support, patience, and hospitality from the initial to the final stage of this research. I also would like to extend my gratitude to Michael V. Madden and Michael S. Harr for their continuous support on engineering information and consultancy.

I am indebted to many of my friends who support me. Thank Jantakan Srisuriyon for introducing Schlumberger PETREL and sharing her technical knowledge to me. I am grateful to Piyamai Klinnoi, Pornthep Luasubsuk and Attawuth Disapirom for their advice on statistics and experimental designs.

I would like to thank the thesis committee members for their comments and recommendations.

Grateful thanks are also due to all faculty members of the Department of Mining and Petroleum Engineering, Chulalongkorn University, who provide technical knowledge, consultation, encouragement, and hospitality.

I am heartily thankful to my family. This thesis would not have been possible without their endless love, strong encouragement, and continuous support.

# Contents

	<b>Page</b>
<b>Abstract (Thai)</b> .....	<b>iv</b>
<b>Abstract (English)</b> .....	<b>v</b>
<b>Acknowledgements</b> .....	<b>vi</b>
<b>Contents</b> .....	<b>vii</b>
<b>List of Tables</b> .....	<b>xi</b>
<b>List of Figures</b> .....	<b>xiii</b>
<b>List of Abbreviations</b> .....	<b>xviii</b>
<b>Nomenclature</b> .....	<b>xx</b>

## **Chapter**

<b>I. Introduction</b> .....	<b>1</b>
1.1. Background .....	1
1.2. Objectives .....	3
1.3. Scope of Research .....	3
1.4. Expected Benefits.....	4
1.5. Methodology Outline .....	4
1.6. Thesis Outline .....	5
<b>II. Literature Review</b> .....	<b>7</b>
2.1. Horizontal Wells and Factors Affecting Their Performance .....	7
2.1.1 Horizontal Well Overview .....	7
2.1.2 Factors Affecting Horizontal Well Performance.....	9
2.2. Experimental Designs in Petroleum Industry .....	14
<b>III. Experimental Design and Response Surface Methodology</b> .....	<b>18</b>
3.1 Experimental Design Concepts .....	18
3.1.1 Procedure for Designing an Experiment.....	18
3.1.1.1 Statement of the Problems and Objectives .....	19
3.1.1.2 Selection of Response Variables.....	20

<b>Chapter</b>	<b>Page</b>
3.1.1.3	Selection of Input Factors ..... 20
3.1.1.4	Selection of Experimental Design..... 21
3.1.1.5	Performing the Experiment..... 21
3.1.1.6	Statistical Analysis of the Data ..... 21
3.1.1.7	Conclusions and Recommendations..... 22
3.1.2	Experimental Design Methods ..... 22
3.1.2.1	One-Variable-at-A-Time Designs (OVAT)..... 22
3.1.2.2	Full Factorial Designs (FD) ..... 23
3.1.2.3	Fractional Factorial Designs (FFD)..... 25
3.1.2.4	Response Surface Method Designs (RSM) ..... 28
3.1.2.4.1	Central Composite Designs (CCD)..... 28
3.1.2.4.2	Box-Behnken Designs (BBD) ..... 28
3.1.2.4.3	Space-Filling Designs (SFD)..... 30
3.1.3	Selection of Experimental Design Method ..... 31
3.2	Statistical Analysis of Result ..... 32
3.3	Response Surface Methodology (RSM)..... 35
3.3.1	First-Order Polynomial or Linear Model..... 37
3.3.2	Second-Order Polynomial or Quadratic Model..... 37
3.3.3	Gaussian Process Model ..... 38
<b>IV.</b>	<b>Research Methodology ..... 39</b>
4.1	Statement of Objectives and Response Factor..... 39
4.2	Selection of Input Factors ..... 39
4.3	Screening Experimental Design..... 41
4.4	Response Surface Designs ..... 42
4.5	Designed Experiments for Proxy Cross-Validation ..... 43
4.6	Reservoir Simulation Modeling ..... 44
<b>V.</b>	<b>Experimental Analyses and Results ..... 52</b>
5.1	Analysis and Result of Factor Screening Design..... 52
5.2	Analyses and Results of Response Surface Designs..... 56



<b>Chapter</b>	<b>Page</b>
5.2.1 Central Composite Design .....	56
5.2.1.1 Quadratic Proxy Fitting .....	56
5.2.1.2 Cross-Validation of Quadratic Proxy Model .....	63
5.2.2 Space-Filling Design: Maximum Entropy .....	66
5.2.2.1 Gaussian Process Proxy Fitting.....	66
5.2.2.2 Cross-Validation of Quadratic Proxy Model .....	76
5.2.3 Combined Central Composite and Maximum Entropy Design..	78
5.2.3.1 Design-Combined Proxy Fitting .....	78
5.2.3.2 Cross-Validation of Quadratic Proxy Model .....	86
5.3 Influence of Significant Factor Effects.....	89
5.3.1 Influence of Main Effects.....	89
5.3.1.1 Main Effect of Initial Oil Column Thickness .....	90
5.3.1.2 Main Effect of Horizontal Well Length to Reservoir Length Ratio .....	96
5.3.1.3 Main Effect of Well Standoff to Oil-Water Contact to Initial Oil Column Thickness Ratio .....	102
5.3.1.4 Main Effect of Porosity .....	109
5.3.1.5 Main Effect of Liquid Production Rate Control .....	117
5.3.2 Influence of Interaction Effects .....	128
5.4 Limitations of Design-Combined Gaussian Proxy .....	130
5.5 A Simple Reservoir Screening Method.....	136
5.6 Design Optimization of a Horizontal Well using a Proxy Model.....	151
5.7 Recommendations on Data Surveillance and Acquisition .....	152
<b>VI. Conclusions and Recommendations.....</b>	<b>154</b>
6.1 Conclusions.....	154
6.2 Recommendations .....	158
<b>References .....</b>	<b>159</b>
<b>Appendices .....</b>	<b>167</b>

<b>Appendices</b>	<b>Page</b>
Appendix A List of Potential Significant Factors Influencing Ultimate Recovery Factor of a Horizontal Well.....	168
Appendix B Probability Distribution and Associated Statistical Analysis of Design Factors .....	175
Appendix C Design Patterns of Experimental Designs Performed in this Research.....	188
Appendix D Generic Correlation Equations of Petrophysical Properties of Thin-Oil-Column Reservoirs in the Gulf of Thailand.....	194
Appendix E Experimental Analyses and Results for Building a Gaussian Process Proxy used to Predict URF due to Two Vertical Wells.....	199
Appendix F Estimation of Oil Production Volume at Break-Even Point of a Horizontal Well .....	211
<b>Vitae .....</b>	<b>213</b>

## List of Tables

<b>Table</b>	<b>Page</b>
Table 3.1: Summary of available 2-level factorial designs with resolution.....	27
Table 3.2: Guideline for selecting experimental design method .....	32
Table 4.1: Potential significant factors or design factors for experimental designs .....	41
Table 4.2: Probability Distribution of design factors for experimental designs...	42
Table 4.3: Fluid correlations used for fluid modeling .....	46
Table 4.4: Roughness of different types of pipe.....	48
Table 4.5: Economic limits and operational constraints of reservoir simulations .....	49
Table 5.1: Experimental results of Resolution IV $2^{13-8}$ fractional factorial design for horizontal well production.....	53
Table 5.2: Aliasing of two-factor effects of $2^{13-8}$ fractional factorial design for horizontal well production .....	55
Table 5.3: Experimental results of 6-factor face-centered central composite design for horizontal well production.....	57
Table 5.4: Regression coefficients of the fitted quadratic proxy model for horizontal well production .....	59
Table 5.5: Experimental results of the first 18-run maximum entropy design for validating the proxy model for horizontal well production.....	64
Table 5.6: Experimental results of 6-factor, 45-run maximum entropy design for horizontal well production.....	66
Table 5.7: JMP model report of the Gaussian process proxy model for horizontal well production .....	68
Table 5.8: Theta regression coefficients of the Gaussian process proxy for horizontal well production .....	70
Table 5.9: $\beta_j$ regression coefficients of the Gaussian process proxy for horizontal well production .....	70

<b>Table</b>	<b>Page</b>
Table 5.10: JMP model report of the design-combined Gaussian process proxy for horizontal well production.....	79
Table 5.11: Theta regression coefficients of the design-combined Gaussian process proxy for horizontal well production .....	80
Table 5.12: $\beta_i$ regression coefficients of the design-combined Gaussian process proxy for horizontal well production.....	81
Table 5.13: $\beta_j$ regression coefficients of the design-combined Gaussian process proxy for horizontal well production.....	81
Table 5.14: Experimental results of the second 18-run maximum entropy design for validating the proxy model for horizontal well production.....	87
Table 5.15: Summary of factor effects normalized by total sensitivity.....	89
Table 5.16: Experiments for determining HO main effect .....	92
Table 5.17: Experiments for determining LHRATIO main effect .....	97
Table 5.18: Experiments for determining WSTANDOFF main effect .....	104
Table 5.19: Experiments for determining PORO main effect.....	112
Table 5.20: Experiments for determining LRAT main effect .....	119
Table 5.21: Theta regression coefficients of the design-combined Gaussian process proxy model for vertical well production.....	137
Table 5.22: $\beta_i$ regression coefficients of the design-combined Gaussian process proxy model for vertical well production .....	138
Table 5.23: $\beta_j$ regression coefficients of the design-combined Gaussian process proxy model for vertical well production .....	138
Table 5.24: Summary of actual and predicted URFs of reservoir candidates for horizontal well development.....	147
Table 5.25: Validation of reservoir screening method for horizontal well development .....	149

## List of Figures

<b>Figure</b>	<b>Page</b>
Figure 2.1: Various completion techniques for horizontal wells .....	8
Figure 2.2: Effect of reservoir thickness and horizontal well length on productivity of horizontal and vertical wells .....	10
Figure 2.3: Effect of reservoir anisotropy and horizontal well length on productivity of horizontal and vertical wells .....	10
Figure 2.4: Influence of well eccentricity on well productivity .....	11
Figure 2.5: Comparison of pressure drawdown near horizontal and vertical wellbores .....	12
Figure 3.1: General model of a process or system .....	19
Figure 3.2: A two-factor one-variable-at-a-time experiment conducted at two levels .....	24
Figure 3.3: A two-factor full factorial experiment conducted at two levels .....	24
Figure 3.4: A 2-factor FD experiment (a) without AB interaction (b) with AB interaction .....	25
Figure 3.5: Cube plot of (a) $2^3$ full factorial design (b) $2^{3-1}$ fractional factorial design .....	27
Figure 3.6: Comparison of the three types of central composite designs .....	29
Figure 3.7: Cube plot of (a) 3-factor CCF (b) 3-factor BBD .....	29
Figure 3.8: Comparison between (a) 18-run two-factor Latin Hypercube design (b) 18-run two-factor Maximum Entropy design .....	31
Figure 3.9: An example of normal probability plot of $2^k$ factorial design .....	33
Figure 3.10: An example of half-normal probability plot of $2^k$ factorial design ...	34
Figure 3.11: General workflow for building a response surface model .....	36
Figure 4.1: A 3-dimensional simple reservoir model showing fluid zones, horizontal well modeling, and edge-drive aquifer .....	45

<b>Figure</b>	<b>Page</b>
Figure 4.2: A 3-dimensional simple reservoir model showing an updip impermeable fault, inactive cells modeling due to the fault, and a horizontal well.....	45
Figure 4.3: An example of typical placement of a horizontal well relative to existing vertical/deviated wells and trapping fault.....	50
Figure 4.4: Locations of two vertical wells relative to a corresponding horizontal well.....	51
Figure 5.1: Factor screening result of the $2^{13-8}$ fraction factorial experiments for horizontal well production .....	54
Figure 5.2: Regression coefficient estimates of the quadratic proxy model for horizontal well production .....	58
Figure 5.3: Actual by predicted plot and statistical analyses of the quadratic proxy for horizontal well production.....	60
Figure 5.4: Residual by predicted plot of the fitted quadratic proxy model for horizontal well production.....	60
Figure 5.5: JMP prediction profiler shows optimum factor setting of the quadratic proxy model for horizontal well production.....	61
Figure 5.6: 3D surface plot at the optimum setting of the quadratic proxy for horizontal well production.....	62
Figure 5.7: Matched pairs t-test for validating the quadratic proxy for horizontal well production .....	65
Figure 5.8: JMP marginal model plots of the Gaussian process proxy model for horizontal well production.....	71
Figure 5.9: Actual by jackknife predicted plot of the Gaussian process proxy for horizontal well production.....	72
Figure 5.10: JMP prediction profiler showing optimum factor setting of the Gaussian process proxy model for horizontal well production.....	73
Figure 5.11: 3D surface plot at optimum factor setting of the Gaussian process proxy model for horizontal well production .....	74

<b>Figure</b>	<b>Page</b>
Figure 5.12: Scatter plots of design points of the 45-run central composite design (square points) and the 45-run maximum entropy design (circular points) .....	75
Figure 5.13: Matched pairs t-test for validating the Gaussian process proxy model for horizontal well production .....	77
Figure 5.14: JMP prediction profiler shows optimum factor setting of the design-combined Gaussian process proxy model for horizontal well production.....	83
Figure 5.15: Actual by jackknife predicted plot of the design-combined Gaussian process proxy model for horizontal well production.....	84
Figure 5.16: 3D surface plot at optimum factor setting of the design-combined Gaussian process proxy for horizontal well production .....	84
Figure 5.17: JMP marginal model plots of the design-combined Gaussian process proxy model for horizontal well production .....	85
Figure 5.18: Matched pairs t-test for validating the design-combined Gaussian process proxy model for horizontal well production.....	88
Figure 5.19: Marginal plot of HO# showing design points of CCD Run ID 18 and 28.....	92
Figure 5.20: Production profiles of CCD Run ID (a) 18 (b) 28 .....	93
Figure 5.21: Pressure profiles of CCD Run ID (a) 18 (b) 28.....	94
Figure 5.22: 3D reservoir model showing initial water saturation and horizontal wellbore of CCD Run ID (a) 18 (b) 28.....	95
Figure 5.23: Marginal plot of LHRATIO showing design points of SFD Run ID 312 and 305A .....	97
Figure 5.24: Production profiles of SFD Run ID (a) 312 (b) 305A .....	98
Figure 5.25: Pressure profiles of SFD Run ID (a) 312 (b) 305A .....	99
Figure 5.26: 3D reservoir model showing fluid saturation at the end of production and horizontal wellbore of SFD Run ID (a) 312 (b) 305A.....	100

<b>Figure</b>	<b>Page</b>
Figure 5.27: 3D reservoir model showing fluid pressure at the end of production and horizontal well of SFD Run ID (a) 312 (b) 305A.....	101
Figure 5.28: Marginal plot of WSTANDOFF showing design points of CCD Run ID 20 and 26 .....	104
Figure 5.29: Production profiles of CCD Run ID (a) 20 (b) 26 .....	105
Figure 5.30: Pressure profiles of CCD Run ID (a) 20 (b) 26.....	106
Figure 5.31: 3D reservoir model showing initial water saturation with horizontal wellbore of CCD Run ID (a) 20 (b) 26 .....	107
Figure 5.32: 3D reservoir model showing fluid saturations at the end of production with horizontal wellbore of CCD Run ID (a) 20 (b) 26.....	108
Figure 5.33: A slice of 3D reservoir model showing gas saturations around the horizontal wellbore of CCD Run ID 26 on 01 May 2010 .....	109
Figure 5.34: Marginal plot of PORO showing design points of CCD Run ID 21 and 25.....	112
Figure 5.35: Production profiles of CCD Run ID (a) 21 (b) 25 .....	113
Figure 5.36: Pressure profiles of CCD Run ID (a) 21 (b) 25 .....	114
Figure 5.37: 3D reservoir model showing initial water saturation and horizontal wellbore of CCD Run ID (a) 21 and (b) 25.....	115
Figure 5.38: 3D reservoir model showing fluid saturations at the end of production and horizontal wellbore of CCD Run ID (a) 21 and (b) 25 .....	116
Figure 5.39: Marginal plot of HO# showing design points of CCD Run ID 22, 22A, 23, 23A, 24, and 24A .....	119
Figure 5.40: Production profiles of CCD Run ID (a) 22 (b) 22A .....	120
Figure 5.41: Pressure profiles of CCD Run ID (a) 22 (b) 22A .....	121
Figure 5.42: Production profiles of CCD Run ID (a) 23A (b) 23 .....	122
Figure 5.43: Pressure profiles of CCD Run ID (a) 23A (b) 23 .....	123
Figure 5.44: Production profiles of CCD Run ID (a) 24A (b) 24 .....	124
Figure 5.45: Pressure profiles of CCD Run ID (a) 24A (b) 24 .....	125



<b>Figure</b>	<b>Page</b>
Figure 5.46: Oil saturation distribution at the end of production of CCD Run ID 22A .....	126
Figure 5.47: Oil saturation distribution at the end of production of CCD Run ID 23A .....	126
Figure 5.48: Oil saturation distribution at the end of production of CCD Run ID 23.....	127
Figure 5.49: Oil saturation distribution at the end of production of CCD Run ID 24A .....	127
Figure 5.50: Oil saturation distribution at the end of production of CCD Run ID 24.....	128
Figure 5.51: JMP interaction profiles at optimum factor setting of design-combined Gaussian proxy model for horizontal well production .....	129
Figure 5.52: Corrected matched pairs t-test for validating design-combined Gaussian process proxy for horizontal well production .....	133
Figure 5.53: Marginal plots of design-combined proxy model with design points having URF = 0% and LRAT = 55 STB/day highlighted ...	134
Figure 5.54: Marginal plots of design-combined proxy model showing design points whose response is dominated by LRAT main effect .....	135
Figure 5.55: Workflow for screening out high potential reservoirs for drilling a horizontal well using the proxy models .....	143
Figure 5.56: Example of 5,000-run Monte Carlo analysis on the proxy model for horizontal well development.....	144
Figure 5.57: Cumulative probability density function and important quantiles of the example Monte Carlo analysis .....	145
Figure 5.58: Workflow for cross-validating the simple method for screening reservoir for drilling a horizontal well.....	146
Figure 5.59: Application of a proxy model as a substitute to reservoir simulator .....	151

## List of Abbreviations

3D	Three-Dimensional
ANOVA	ANalysis Of VARIance
API	American Petroleum Institute
BBD	Box-Behnken Designs
CCC	Circumscribed Central Composite designs
CCD	Central Composite Designs
CCF	Face-centered Central Composite designs
CCI	Inscribed Central Composite designs
CDF	Cumulative Density Function
CLM	Continuous Linear Model
DF	Degree of Freedom
DOE	Design Of Experiments
ECP	External Casing Packers
ED	Experimental Designs
EOR	Enhanced Oil Recovery
FD	Full Factorial Designs
FFD	Fractional Factorial Designs
GOR	Gas-Oil Ratio
HZ	HoriZontal
ID	Identity
ID	Inside Diameter
MMSTB	Millions of Stock Tank Barrel
MSCF	Thousands of Standard Cubic Foot
MULTPV	MULTIplier of Pore Volume
NIST	National Institute of Standards and Technology
OD	Outside Diameter
OFAT	One-Factor-at-A-Time
OOIP	Original Oil In-Place
OVAT	One-Variable-at-A-Time
PBD	Plackett-Burman Designs

PSE	Pseudo Standard Error
psi	pound per square inch
psia	pound per square inch (atmospheric)
psig	pound per square inch (gauge)
RF	Recovery Factor
RMSE	Root Mean Square Error
RSM	Response Surface Methodology
SEMATECH	SEmiconductor MANufacturing TECHnology
SFD	Space-Filling Designs
SME	Subject Matter Expert
STB	Stock Tank Barrel
STBO	Stock Tank Barrel of Oil
URF	Ultimate Recovery Factor
VLP	Vertical Lift Performance

## Nomenclature

ANISO	anisotropy or vertical-to-horizontal permeability ratio
ANISO#	$\ln(\text{ANISO}-0.0822)$
API	oil API gravity
AQFRATIO	ratio of the initial water pore volume of the aquifer to that of the oil
$B_{oi}$	initial oil formation volume factor
$c_f$	formation compressibility
$c_g$	gas compressibility
$c_j$	contrast or effect estimate of $j^{\text{th}}$ factor effect
$c_o$	oil compressibility
$c_w$	water compressibility
$d_{tb}$	tubing size
$d_w$	wellbore diameter
$h$	reservoir thickness
HO	initial oil column thickness
HO#	$\ln(\text{HO})$
HRES	reservoir thickness
$i$ and $j$	integer number
$J_h$	productivity of horizontal well
$J_v$	productivity of vertical well
$J_\delta$	horizontal well productivity at $\delta = \delta$
$J_{\delta=0}$	horizontal well productivity at $\delta = 0$
$k$	total number of design factors
$k_h$	horizontal permeability of rock
$k_{rg}$	relative permeability to gas
$k_{row}$	relative permeability to oil in oil-water system
$k_{rw}$	relative permeability to water
$k_v$	vertical permeability of rock

L	horizontal well length or the number of factor levels
LH	horizontal well length
LHRATIO	horizontal-well-length-to-reservoir-length ratio
LRAT	liquid production rate control
M	mobility ratio
m	ratio of the initial hydrocarbon pore volume of the gas cap to that of the oil or total number of contrasts or effect estimates of interest
MRATIO	ratio of the initial hydrocarbon pore volume of the gas cap to that of the oil
N	total number of experimental runs
OWC	initial oil-water contact depth
p	pressure
p	fraction of full factorial design
p(x)	pressure at a radial distance of x
p <sub>a</sub>	abandonment pressure
p <sub>b</sub>	bubble point pressure
p <sub>bi</sub>	initial bubble point pressure
p <sub>c</sub>	capillary pressure
p <sub>e</sub>	pressure at the external boundary
p <sub>i</sub>	initial reservoir pressure
PORO	porosity
p <sub>wf</sub>	bottom hole flowing pressure
R <sup>2</sup>	coefficient of determination
R <sup>2</sup> <sub>adj</sub>	adjusted coefficient of determination
r <sub>e</sub>	external boundary radius
RESDIP	average reservoir dip angle
RESDIP#	ln(RESDIP)
R <sub>si</sub>	initial solution gas-oil ratio
S <sub>gc</sub>	critical gas saturation

$S_{gi}$	initial gas saturation
$S_m$	mechanical skin factor
$S_{oi}$	initial oil saturation
$S_{org}$	residual oil saturation in oil-gas system
$S_{orw}$	residual oil saturation in oil-water system
$S_w$	water saturation
$S_{wi}$	initial water saturation
$t$	Student's t statistic
$T_{res}$	reservoir temperature
$T_{rf}$	fault transmissibility
WSTANDOFF	ratio of well standoff to oil-water contact to initial oil column thickness
$x$	radial distance from well
$x_k^i$ and $x_k^j$	the $k^{\text{th}}$ components of sample points $x^i$ and $x^j$ , respectively
$\hat{y}$	predicted process or system response
$Z$	gas compressibility factor
$z(x)$	a random function with mean zero, variance $\sigma_z^2$ , and correlation matrix $\mathbf{R}$ of Gaussian process model

### GREEK LETTERS

$\hat{\beta}_0$	regression intercept
$\hat{\beta}_i$	regression coefficient of the $i^{\text{th}}$ first-order term
$\hat{\beta}_{ii}$	regression coefficient of the $i^{\text{th}}$ second-order term
$\hat{\beta}_{ij}$	regression coefficient of interaction term of $x_i$ and $x_j$ factors
$\mu$	a normal distribution mean
$\mu_g$	gas viscosity
$\mu_o$	oil viscosity

$\alpha$	the distance from the center of design hyperspace to a star point of a central composite design
$\gamma_g$	gas gravity
$\delta$	vertical distance between horizontal well and reservoir center or horizontal well eccentricity
$\varepsilon$	random error or pipe roughness
$\theta$	a k-vector of exponential correlogram ranges, average reservoir dip angle, or contact angle between water and oil phases
$\sigma^2$	variance
$\sigma_{wo}$	surface tension between water and oil phases
$\phi$	porosity of rock

# CHAPTER I

## INTRODUCTION

This chapter provides detail about background and objectives of this research. Subsequently, scope of work and expected benefits are described. Finally, methodology and presentation of the research are outlined.

### 1.1 Background

The Pattani basin is the major oil and gas producing basin in the Gulf of Thailand. It is a pull-apart rift basin composed of a collection of Miocene stacked channel sands interrupted by normal (i.e. extensional) faulting. The final result is a 450-km-long of north/south trending graben and horst structures bounded by terraced fault blocks whose geological structures are difficult to predict and image [1].

To maximize the possibility of encountering trapped oil and gas, vertical/deviated wells are typically drilled through the stacked channel sands in parallel to the updip faults of the terraced fault blocks. Unfortunately, thin (< 40 ft) to medium (< 100 ft) thicknesses of the channel sand reservoirs cause early water/gas coning problem and short production lifetime of the wells. Consequently, extensive infill drilling has been used as a solution to recover significant amount of remaining hydrocarbons.

Owing to several advantages over vertical/deviated wells, horizontal wells have been drilled in the Gulf of Thailand since the late 1990's to maximize oil recovery and prolong field life [2 and 3]. However, utilization of a horizontal well may not yield a better economic result than a vertical/deviated well due to its higher cost of drilling, marginal amount of oil in-place and geological uncertainties. To have more confidence, a decision to select horizontal well drilling is usually made after early batches of vertical/deviated wells were drilled and logged to collect geological and petrophysical properties of the potential reservoir candidate. The challenge is that the decision must be made within a short time span among uncertainties. A process of geological study, reservoir simulation modeling, probabilistic analyses, well planning,



etc., must be completed within a short time frame while a drilling rig is working on wells of the second last batch.

Although technology in petroleum exploration and production has significantly advanced, uncertainties are still a major problem in the industry. The degree of the problem depends on knowledge of geological, petrophysical and engineering data of the reservoir being considered. Therefore, a sensitivity study using reservoir simulation is often performed to assess the uncertainties. One common approach, called One-Variable-at-A-Time (OVAT), is to do simulation experiment on 3 levels per input model factor (P10, P50, and P90). In each set of experiment, one factor is varied while the remaining factors are kept at a certain level. The major disadvantage of this method is failure to consider any possible interaction or interdependence between factors. Monte Carlo simulation is another widely used technique which relates model input-output uncertainty. However, its major disadvantage is the need to perform multiple model calculations. For large and/or complex simulation models, the associated computational burden can be exhaustive and prohibitive.

In recent years, many applications of experimental design (ED) in oil and gas industry have been increasingly published [4 and 5]. In brief, experimental design is a statistical method whose basic idea is to vary multiple parameters at the same time so that maximum inference can be attained with minimum cost. It offers not only an efficient way of assessing uncertainties by providing inference with minimum number of simulations, but also identify key or significant factors which influence response most early in the study.

By using response surface methodology (RSM), an interpolation model, so called a “response surface”, “proxy”, “meta”, or “surrogate” model, can be constructed. A proxy model is a mathematical model representing relationship between significant factors and an output response of interest from a process system. If the proxy model having an acceptable prediction tolerance is in hand, Monte Carlo simulation could be easily performed. As another application, the model could be used as a simple method for screening out reservoirs that could be economical for horizontal well development from many reservoir candidates. Thus, exhaustive effort

and time on reservoir simulation could be alleviated resulting in optimized design and decision-making process to drill a horizontal well.

In conclusion, experimental design and response surface methodology could be a cost effective and systematic approach for design optimization of a horizontal well in the Gulf of Thailand.

## **1.2 Objectives**

1) To propose an optimization method for designing a horizontal well in a thin-oil-column reservoir in the Gulf of Thailand using experimental designs.

2) To develop a simple screening method for deciding whether a horizontal well should be drilled into a particular thin-oil-column reservoir instead of traditional vertical/deviated wells.

3) To obtain a ranking list of factors having significant influence on a horizontal well performance.

## **1.3 Scope of Research**

1) Only one horizontal well in a thin-oil-column (< 40 ft) or a medium-thick-oil-column (< 110 ft) reservoir in the Gulf of Thailand is considered.

2) The presence of other vertical/deviated/horizontal wells in the same reservoir is out of this scope.

3) The reservoir is produced under primary depletion with a booster compressor. No other artificial lift or enhanced oil recovery methods are taken into account.

4) Lateral section of the well is assumed to be perfectly horizontal.

5) Computer experiments are performed using reservoir simulation. Since actual reservoir characteristics are very complex, simple hypothetical models approximating the actual characteristics are used in the simulation.

6) The existing horizontal well database used for this research is updated until June 2010.

## 1.4 Expected Benefits

With respect to the outlined objectives, the following benefits are expected:

1) An optimization method for horizontal well design is proposed. The proxy model approximating a horizontal well performance and the list of significant factors could be used as a guide for optimizing factor settings in subsequent detailed design.

2) The developed screening method could be used to quickly screen out oil reservoirs having high potential for horizontal well development from many probable ones. The obtained high potential reservoirs can then be evaluated in more detail at a later stage. Therefore, the amount of work for detailed reservoir simulation and probabilistic analysis is reduced resulting in saved time and cost.

3) Probabilistic analysis of incremental oil reserve due to horizontal well over traditional deviated wells can be easily performed with more confidence. Monte Carlo simulations can be quickly performed because the obtained proxy models provide deterministic solutions.

4) The list of ranked significant factors could help to collect the most useful information in data surveillance and acquisition program. If the available budget is limited, more resource and attention should be allocated on a factor having higher ranking. Good quality of collected data improves quality of design and prediction.

## 1.5 Methodology Outline

1) Define objectives and key performance factor of a horizontal well to be response of proxy models to be constructed.

2) Define a large set of factors which could influence ultimate recovery factor of a horizontal well by brainstorming. The factors are then grouped as controllable and uncontrollable factors.

3) Qualitatively screen out tentative significant factors from the listed factors by consulting with highly experienced geologists and reservoir engineers in the fields.

4) Collate probability distribution and range of the tentative significant factors from the existing horizontal well database.

5) Transform probability distribution of all factors to be or as much close to normal distribution as possible. This is because theories of statistical inference technique used in the subsequent steps require normality distribution of design factors.

6) Statistically screen out significant factors from the tentative ones by performing reservoir simulations based on 2-level screening experimental design. Resolution IV fractional factorial design is used for the screening.

7) After the final set of significant factors is obtained, perform a response surface design and corresponding reservoir simulations to fit a proxy model predicting ultimate recovery factor of a horizontal well.

8) Validate the obtained proxy model against a different set of cross-validation experiments. A hypothesis testing technique, called matched pairs t-test, is used for validating whether predicted ultimate recovery factors and the actual ones obtained from cross-validation experiments are statistically the same with 95% confidence.

9) If the null hypothesis in Step 8 is rejected, repeat Steps 7 and 8 by running more experiments or changing type of response surface design until the null hypothesis is accepted.

10) To develop the simple screening method, comparison in performance between horizontal and vertical wells is required. Repeat Steps 7 to 9 to construct a proxy model predicting ultimate recovery factors of vertical wells using the same set of significant factors. It is assumed that if horizontal well drilling is rejected, two vertical wells will be drilled instead. Each well is placed at targeted heel and toe locations of the rejected horizontal well.

11) Develop the simple screening criteria for deciding whether drilling a horizontal well is better from the proxy models obtained in Steps 9 and 10 using the cross-validation experiments.

## **1.6 Thesis Outline**

This thesis consists of six chapters and the outlines of each chapter are listed below.

Chapter II briefly reviews previous works related to horizontal wells and application of experimental design methodology in oil and gas industry.

Chapter III introduces the concept of experimental design and response surface methodology related to this research.

Chapter IV describes methodology of this research in more detail.

Chapter V presents the experimental analyses and results of designed experiments.

Chapter VI provides conclusions of the study and recommendations for the further study.

## **CHAPTER II**

### **LITERATURE REVIEW**

This chapter reviews formerly published literature relevant to the scope of the present study. It begins with an overview of horizontal wells and factors affecting their performance. In the end, published applications of experimental design methodology in petroleum industry are reviewed.

#### **2.1 Horizontal Wells and Factors Affecting Their Performance**

##### **2.1.1 Horizontal Well Overview**

The first recorded true horizontal oil well, drilled near Texon, Texas, was completed in 1929. Since then, the technology of horizontal well drilling and completion had been developed and more horizontal wells were drilled. However, horizontal drilling could not achieve its commercial success until 1980's. Subsequently, horizontal drilling technology has been increasingly developed and used by operators, drilling and service companies [6].

The main purpose of a horizontal well is to increase exposure of the producing wellbore for productivity improvement. Due to this advantage, horizontal wells have been effectively used for the following applications [7 and 8]:

- 1) Horizontal wells have been used to intersect fractures, and drain them and reservoir effectively.
- 2) In reservoirs with water and gas coning problems, horizontal wells have been used to minimize coning problems, enhance oil production and increase oil reserve.
- 3) In low-permeability gas reservoirs, horizontal wells can improve drainage area and reduce number of wells while in high-permeability gas reservoirs, horizontal wells can reduce near-wellbore gas velocities and improve well deliverability.

4) In EOR applications, horizontal wells have been used with heavy oil reservoir, especially for thermal oil recovery. A long horizontal well provides a large reservoir contact area and therefore enhances injectivity of an injection well.

5) Reducing cost by using fewer wells because size of offshore platforms, no. of well slots, water and/or gas separation and handling can be reduced.

There are generally 4 completion techniques for a horizontal well. Figure 2.1 shows a schematic of the four completion methods. Each type of completion is briefly described as follows:

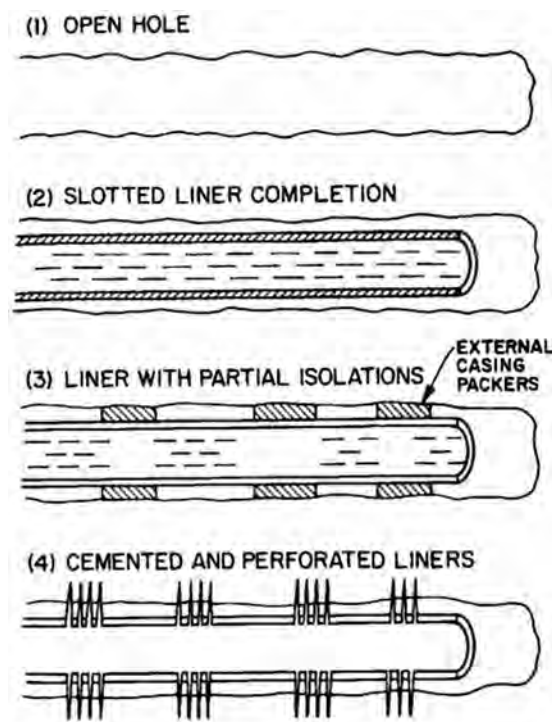


Figure 2.1: Various completion techniques for horizontal wells. (After Joshi [7])

1) Open hole or barefoot: This completion method is inexpensive. However, its main problems are that production/injection along the well length cannot be controlled, stimulation cannot be done on selective interval basis, production logging and cased hole saturation monitoring are difficult, and it is only suitable for stable formations.

2) Slotted liner completion: Slotted liners are usually used when sanding is a common problem in the wellbore. They can also guard the hole against collapsing.

They provide a convenient path to insert some tools but cause difficulty to selective production/injection and well stimulation.

3) Liner with partial isolations: The completion method is actually slotted liner installed with external casing packers (ECPs). The ECPs divide annulus between the slotted liner and the wellbore along horizontal section into smaller sections. Zone isolation, well stimulation and production control along the well length are thus feasible.

4) Cemented and perforated liners: This completion type is the best to effectively deal with water and/or gas entries. Well stimulation at desired intervals, production logging and saturation monitoring are relatively easier than the first two methods. However, cementing job of a horizontal well is usually difficult because the hole is not straight and cutting transport is not effective.

## 2.1.2 Factors Affecting Horizontal Well Performance

Owing to several advantages of a horizontal well over a vertical well, many researchers and practitioners have extensively studied its behavior and response against various factors. Some of their works related to this research are reviewed and summarized below.

Several theoretical solutions predicting single-phase flow with steady-state flow rate in a horizontal well are presented in the literature. Borisov [9], Giger et al. [10], and Joshi [11 and 12], and Renard and Dupuy [13] proposed similar solutions. All of these solutions represent a sum of two mathematical solutions. One represents horizontal flow while the other represents vertical flow. Besides, it is assumed that reservoirs are isotropic and a horizontal well can be represented as a limiting case of an infinite-conductivity fracture whose height equals to the wellbore diameter. This implies that diameter of a horizontal wellbore has an influence on its performance.

From the solutions, influence of horizontal well length and reservoir height,  $h$ , on well productivity is shown in Figure 2.2. For a given thickness of a reservoir, the horizontal-to-vertical productivity ratio,  $J_H/J_V$ , increases as the horizontal well is longer. Also, the incremental gain in productivity is much higher in a thinner reservoir than a thicker reservoir. These are because incremental contact area is greater for a longer horizontal well or a thinner reservoir.



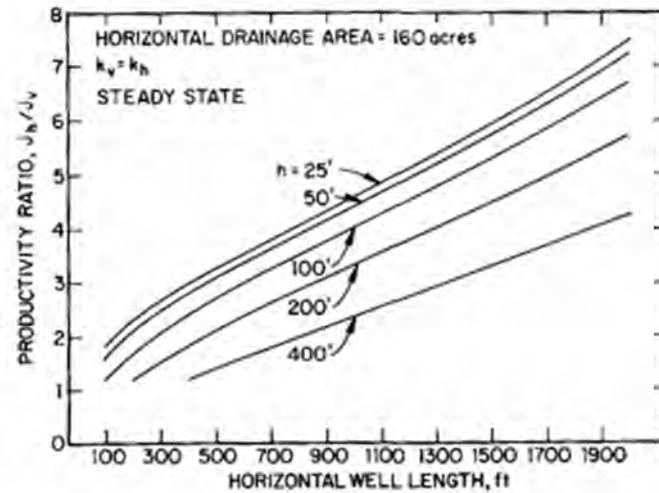


Figure 2.2: Effect of reservoir thickness and horizontal well length on productivity of horizontal and vertical wells (After Joshi [7])

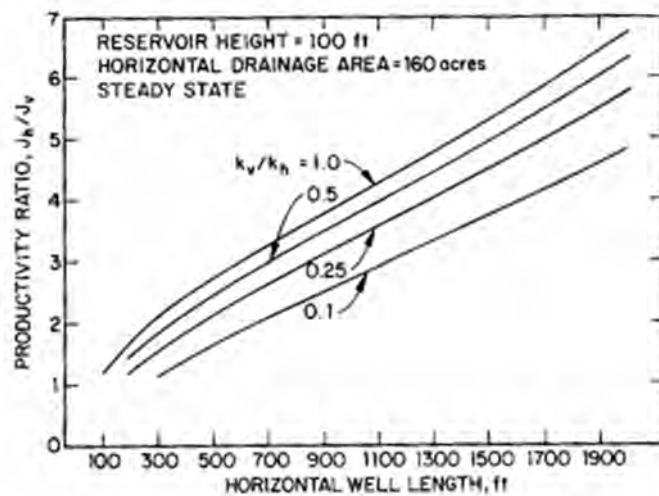


Figure 2.3: Effect of reservoir anisotropy and horizontal well length on productivity of horizontal and vertical wells (After Joshi [7])

Joshi [11], and Renard and Dupuy [13] modified the vertical flow component of their solutions to account for reservoir anisotropy. Calculations showing the influence of reduced vertical permeability on horizontal well productivity are shown in Figure 2.3. From the figure, it is indicated that, at a given horizontal length, productivity of a horizontal well significantly reduced as vertical permeability decreases.

Joshi [11] proposed an analytical solution for calculating oil flow rate of a horizontal well off-centered in a vertical plane. It is noted that no bottom water and top gas are considered in the solution. Its calculation results showing the influence of well eccentricity on well productivity are plotted and shown in Figure 2.4. The figure illustrates that horizontal well productivity decreases as the horizontal well eccentricity,  $\delta$ , increases. The horizontal well eccentricity,  $\delta$ , is defined as a vertical distance between horizontal well and reservoir center. However, the well can be placed anywhere without significant loss in productivity if it is long enough compared with reservoir thickness. Note that this conclusion is valid only for the case that bottom water and gas cap are absent in the reservoir.

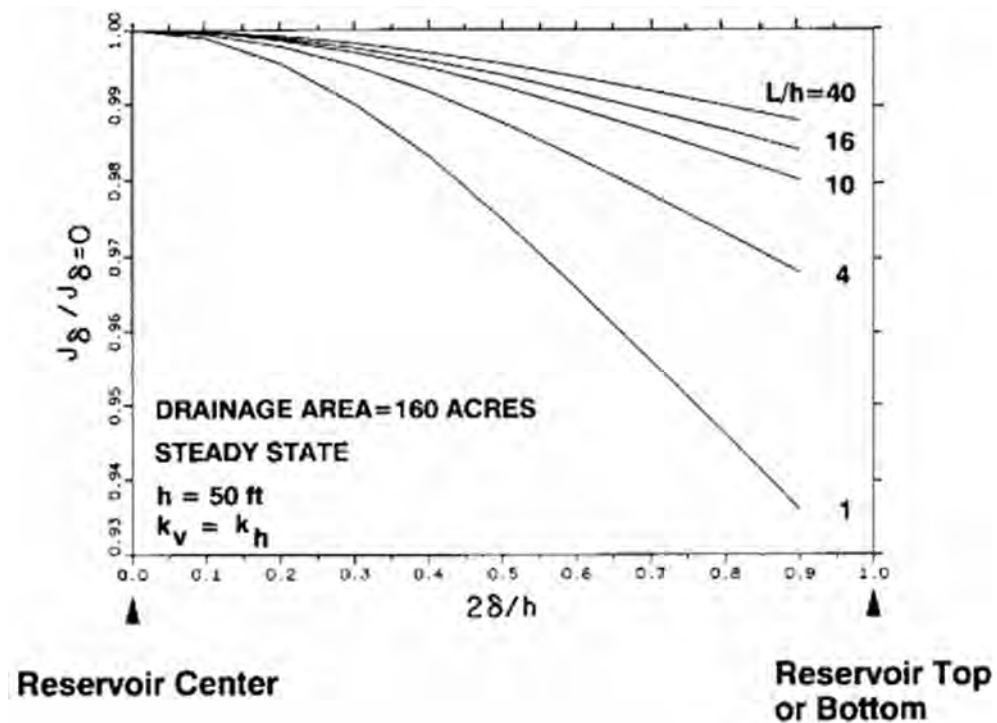


Figure 2.4: Influence of well eccentricity on well productivity (After Joshi [7])

In a reservoir having gas cap, bottom water or both, water and gas coning or cresting is a serious problem because it can significantly reduce oil production. Horizontal wells have been proven to handle water and gas cresting problem better than vertical wells in many fields [14, 15, 16 and 17]. One of the main reasons for coning or cresting is near-wellbore pressure drawdown. Figure 2.5 compares profiles of near-wellbore pressure drawdown between horizontal and vertical wells. It is

clearly illustrated in the figure that much more pressure drawdown occurs close to vertical wellbore region than that of horizontal well. This causes the vertical well to have more coning tendency than the horizontal well. Several experiments and theoretical analyses reveal that if production is produced below a certain rate, called a critical rate, water and gas production can be avoided. With an appropriate control of water and gas movement, the best possible sweep of the reservoir can be obtained [7].

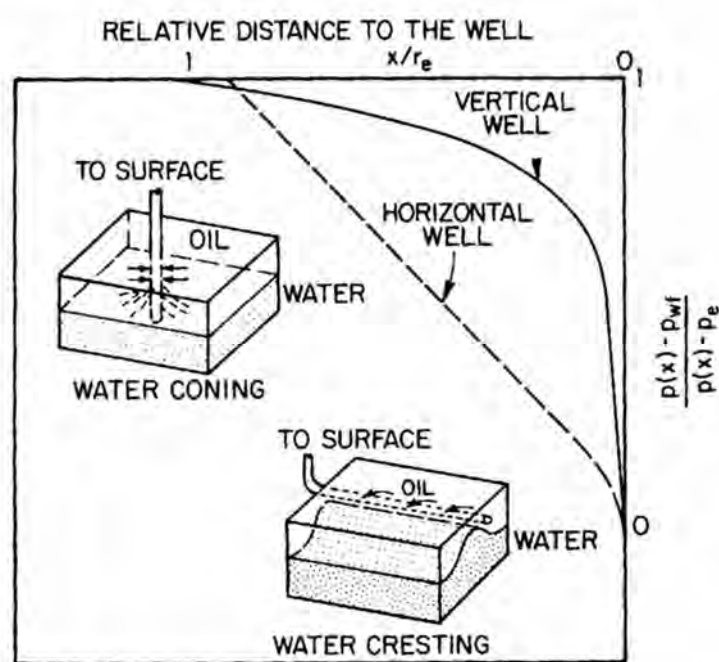


Figure 2.5: Comparison of pressure drawdown near horizontal and vertical wellbores  
(After Joshi [7])

Joshi [11], Chaperon [18], Giger and Karcher et al. [19 and 20], and Efros [21] proposed correlations for estimating horizontal well critical rate. One common conclusion from these correlations is that critical rates of horizontal wells are significantly higher than those for vertical wells. Therefore, horizontal wells can be produced at higher rates to obtain maximum recovery of oil in a shorter time span.

Ozkan and Raghavan [22] reported a theoretical correlation to calculate water breakthrough time for a horizontal well in a bottom water drive reservoir. The correlation yields a few conclusions that sweep efficiency of horizontal wells increases with increasing well length at a given well spacing. This implies that increasing well length at a fixed well spacing delays water breakthrough. At a given

well length, increasing well spacing up to a certain value can delay water breakthrough. For a bottom water drive reservoir without gas cap, a horizontal well placed at the top of oil column gives the highest value of sweep efficiency.

Papatzacos et al. [23] presented a solution to calculate breakthrough time for an infinitely long horizontal well in a reservoir having both gas cap and bottom water. The solution shows that the optimum well placement is closer to the oil-water contact as a ratio of density contrasts between water, oil, and gas,  $\psi$ , increases. As  $\psi$  increases, water and gas breakthrough time decreases. Beyond a certain flow rate, regardless of the value of  $\psi$ , the optimum well placement is at the center of oil column.

Mutalik, Godbole, and Joshi [24] presented a solution to calculate dimensionless pressure drop at a given dimensionless time of a horizontal well during pseudo-steady state. They concluded that top and bottom reservoir boundaries also affect horizontal well performance in addition to side boundaries.

Vo et al. [25] performed sensitivity analysis using reservoir simulation on simple reservoir model to select a drilling and completion strategy for horizontal wells in Attaka and Serang Fields, Indonesia. Horizontal well program in these two fields is targeted to thin-oil-column reservoirs under influence of gas cap and water support. They concluded that, for a reservoir having a small gas cap ( $m$ , free gas volume/oil inplace volume,  $< 1.0$ ), it is better to place the well horizontal as high as possible in the oil column. This is because reserve loss due to gas-cap blowdown is small. For large gas cap ( $m > 1$ ), it is prudent to place the horizontal section in the top half but close to the middle of oil column.

Drilling-related skin damage can cause additional pressure drop to a horizontal well resulting in reduction in productivity. However, for a given positive skin damage, pressure drop in the skin region around a horizontal well is significantly smaller than that of a vertical well. Thus, the detrimental effect of skin damage of a horizontal well has less influence on well productivity than that of a vertical well for a given skin factor [7].

In general, pressure drop along the horizontal well length is very small and can be ignored. However, under certain circumstances such as production of light oils with high flow rates, the pressure drop could cause overestimation of production and

smaller breakthrough time of water and gas. In general, pressure drop along the horizontal length becomes a concern for high-permeability reservoirs because high flow rate can be produced at relatively low pressure drawdown [7].

From reservoir engineering point of view, most of aforementioned analytical works on horizontal well productivity either assume that the well is infinitely conductive (no pressure loss) or the flow entering the wellbore is uniform along the well length. As a result, it is sometimes incorrect to conclude that horizontal well productivity improves as its horizontal length increases because of greater contact of the wellbore to the reservoir.

Penmatcha, Arbabi, and Aziz [26] developed a semi-analytical well-model to quantify the effects of pressure loss in the well on overall well performance for both single-phase oil and two-phase oil/gas flow. It was concluded that the ratio of wellbore pressure drop to reservoir drawdown gives a good indication of frictional effects on well productivity. The pressure drop in the wellbore becomes significant only when it is comparable to the drawdown at the heel of the wellbore. Errors in productivity calculations due to ignoring frictional effects increase with increasing well length, flow rates, wellbore roughness and reservoir permeability. However, they decrease with higher drawdown or higher fluid viscosity.

## **2.2 Experimental Designs in Petroleum Industry**

The initial concept of experimental designs was developed in the 1920's for agricultural production in the U.K. and the U.S. The concept was introduced after Fisher [27] developed fractional factorial and analysis of variance (ANOVA) methods in 1925. Box, Hunter, and Hunter [28] introduce the modern basic concept of experimental designs to manufacturing sector in 1978. Further development by Taguchi [29] and others result in establishment of many applications in chemistry, chemical engineering and industrial engineering.

The first publication of experimental design application in petroleum industry could be the one presented by Vogel [30]. The earliest application in reservoir work was presented by Sawyer et al. [31] whereas early references to reservoir simulation were reported by Chu [32] and Damsleth et al. [33]. All of these papers highlight the

main advantage of experimental designs over one-variable-at-a-time method (OVAT) on conducting fewer simulation runs with some understanding of possible interactions among variables. Due to fast development in computational facilities and more ability to deal with more complex reservoir models, many applications of experimental designs on reservoir modeling were published. Most of them are about managing uncertainties and finding optimal production scheme [34, 35, and 36].

Chewaroungroaj et al. [4] performed numerical simulation studies to compare efficiency of several techniques for handling uncertainty problems. Their main goal is to find the method which can evaluate uncertainty problems with fewer factors and satisfactory accuracy. Various approaches such as scaling analysis, first-order and second-order analyses, experimental design and response surface analysis were compared. They concluded that the combination of scaling, experimental design and response surface analysis provide a potential to predict uncertainty with less effort while maintaining accuracy in comparison with Monte Carlo simulation.

Subsequently, several authors, such as White and Royer [37], Peng and Gupta [38], Yeten et al. [39], and Zubarev [40], published papers to provide more detail about the pros and cons of different types of experimental designs. The design types compared in their studies vary from

- 1) 2-level screening design: Plackett-Burman (suitable for identifying main effects when interaction effects are negligible) and fractional factorial designs
- 2) 3-level design: D-Optimal and Central-Composite designs (suitable for creating first- and second-order polynomial proxy models when interaction and nonlinear effects are significant)
- 3) Latin Hypercube and other space-filling designs (suitable for kriging, thin-plate splines and artificial neural networks)

Comparison on the results obtained from exhaustive simulation run by Yeten et al. [39] show that space-filling experimental designs whose responses are fitted by kriging, splines and quadratic polynomials give the greatest accuracy when compared with those of traditional factorial designs fitted by associated response surfaces. However, if the number of experiments is very small, the space-filling design used, uniform design, is more likely to fail near the boundary of factor design space.

Zubarev [40] performed several reservoir simulations to compare efficiency of various proxy-modeling techniques for history matching, production optimization and forecasting applications. Experimental design used in the study is Latin Hypercube sampling. The types of proxy models compared are polynomial regression model, multivariate kriging model, thin-plate splines model, and artificial neural network. It was concluded that the appropriate choice of proxy-model type is problem specific. Kriging models showed the best performance, but require more computational efforts for model construction. The most reasonable solution suggested for use is thin-plate splines. However, it tends to have more error for small datasets. Artificial neural networks and polynomial regression models have smoothing effect on the predicted response surface. Therefore, precision of proxy prediction of computer experiments is reduced. Different topologies of artificial neural networks yield different quality of prediction.

From literature review, the objectives of applying experimental designs in reservoir modeling can be categorized as follows:

1) Sensitivity analysis to quantify uncertainty and probabilistic forecasting:

This objective could be the first reason for adopting experimental design methods to the petroleum industry. This is because the methods require fewer runs, can identify interaction effects and provide more understanding for factor effects on response. In addition, the generated proxy models can be used replace full reservoir simulations so that Monte Carlo simulation can be performed with less effort [33], [39], [41], [42], and [43].

2) History matching: In history matching, several optimization algorithms have been proposed to help engineers calibrate simulation models to production data. The process of history matching is frequently complex and require many simulation runs to find acceptable solutions. Proxy models which can adequately produce key output responses are thus an attractive tool. Cullick et al. [44] used an artificial neural network as a proxy model in history matching process and obtained acceptable results, provided that initial dataset is large enough. Similarly, Osterloh [45] used a kriging model with Latin Hypercube experimental design for history matching and achieved acceptable results. To obtain an adequate proxy model, one challenging problem must be overcome. Since actual response surface in reservoir simulations are

often highly non-linear, experimental designs which distribute design points uniformly over hyperspace of input factors may not be efficient enough. Jones et al. [46], Queipo et al. [47], Wang [48], and Li et al. [49] proposed iterative improvement methods to solve the problem. However, Zubarev [40] demonstrated that for increasing complexity of actual response surface and number of design factors, using a proxy model for history matching is not recommended.

3) Field development and production optimization: Experimental design methodology also plays an important role in this area. Infill well placement can be very complicated and exhaustive for running simulations if number, type, location and scheduling need to be optimized. Proxy models can thus help reduce efforts in the optimization process [39], [50], [51], [52], and [53].

It has been presented that experimental design methodology has been increasingly used in petroleum industry for about two decades due to its many advantages. Unfortunately, literature review reveals that none of its applications in petroleum industry in Thailand can be found.

In Chapter 3, the concepts of some important experimental design methods and response surface methodology used in this research are detailed.



## **CHAPTER III**

### **EXPERIMENTAL DESIGN AND RESPONSE SURFACE METHODOLOGY**

This chapter presents basic concepts and methods of experimental design which are relevant to the current research. Statistical analysis of experimental result is then described. Response surface methodology used to construct an empirical model for prediction and optimization purposes is finally overviewed.

#### **3.1 Experimental Design Concepts**

Experiment could be conceivably defined as a scientific procedure conducted to make a discovery of something about a process or system. In general, a process or system comprises inputs/variables/factors, process/system, and output/response as illustrated in Figure 3.1. Experimentation is performed by varying input factors and observing responses being interested to understand how the process system works and make useful conclusions. Experimental Design (ED) or Design Of Experiments (DOE) refers to the process of planning and conducting experiments so that valid, useful and objective conclusions can be drawn from the resulting data. In addition, all of this is done under the constraint of a minimum cost of engineering runs, time and money. To obtain meaningful conclusions, especially when experimental errors exist, statistical approach to experimental design is the only way of analysis which yields objective conclusions [54].

##### **3.1.1 Procedure for Designing an Experiment**

To adopt statistical approach in analysis and design of an experiment, understanding on the objectives of the experiment, data to be collected, how the data is to be analyzed should be recognized among experimenters in advance to obtain meaningful conclusions. Therefore, the below procedure is generally followed in designing an experiment.

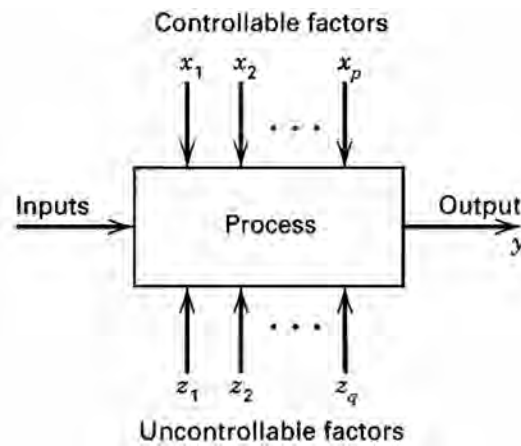


Figure 3.1: General model of a process or system (After Montgomery [54])

### 3.1.1.1 Statement of the Problems and Objectives

When a problem occurs and requirement of experimentation is identified, a clear and generally accepted statement of the problem and objectives should be developed. In a process system, there are usually several parties involved such as earth scientists, engineers, quality assurance personnel, construction crews, operators, etc. The objectives of an experiment are best determined by a team discussion. Objective prioritization during group discussion helps guide the direction to perform experiment design and selection of factors. In general, experimental design methodology can be applied to serve to following 4 objectives:

- 1) Comparative objective: assessing whether a change in a single factor has significant change/improvement to the process system as a whole.
- 2) Screening/characterizing objective: screening out the few important main effects from the many less important ones.
- 3) Modeling objective: functionally modeling the process with the output being a good-fitting mathematical function and to have good estimates of the coefficients in that function. The function can be used to find improved process settings, troubleshoot process problems and weak points, and make a process more robust against external and non-controllable influences.
- 4) Optimizing objective: determining optimal level of each factor that optimizes a process response.

### 3.1.1.2 Selection of Response Factors

Selection of response variables should be ascertained that they can provide useful information about the process system to serve the objective of the experiment. Issues relating to how to define and measure response variables should be identified before performing the experiment.

### 3.1.1.3 Selection of Input Factors

Understanding types of input factors which could impact performance of the process system could help the experimenter to plan, collect and analyze the input information. Input factors could be classified as potential design factors and nuisance factors. The potential design factors are the factors that the experimenter may wish to vary in the experiment. They can be further classified as

- 1) Design factors: factors actually selected for study in the experiment
- 2) Held-constant factors: factors that may exert some effect on the response but are out of interest in the study, so they are held constant at a certain level
- 3) Allowed-to-vary factors: factors whose effect may be caused by non-homogeneity of materials or unit-to-unit variation. Randomization process is usually adopted to balance out the effect of these factors.
- 4) Nuisance factors: factors are not interested in the present study, but their effect may be large enough to be concerned. They can be subdivided into
  - 4.1) Controllable factors: factors that can be controlled by the experimenter such as different batches of materials or different days of conducting experiment. Blocking principle is usually used to deal with these factors
  - 4.2) Uncontrollable factors: factors that cannot be controlled in the experiment but can be measured. Analysis of covariance is often used to compensate for these factor effects.
  - 4.3) Noise factors: factors which vary naturally and uncontrollably in the process system, but can be controlled for the purpose of the experiment. The settings of the controllable design factors which minimize variability due to noise factors are usually looked for.

### **3.1.1.4 Selection of Experimental Design**

Selection of experimental design involves determination of sample size, selection of suitable order of the experiment runs, whether and how randomization and blocking are applied, setting of each factor in each experimental run, etc. Ultimately, the selected experimental design must be able to serve the experimental objectives. Various methods of experimental designs involved in this research are described later in this chapter. Several statistical software packages are commercially available to aid in selection, design and analysis of experiments.

### **3.1.1.5 Performing the Experiment**

When performing the experiment, it is essential to monitor and control it as per the plan. Errors in the experimental procedure could cause invalidity of the experiment. The experiment can be conducted on physical process system which usually has run-to-run variation. Replication of each experimental setting is usually performed to deal with this type of variation. However, this type of variation is not present for experiment conducted using deterministic computer models of physical systems. This is because output responses of the models are not random variables and their values are determined from usually highly complex mathematical models.

### **3.1.1.6 Statistical Analysis of the Data**

Statistical methods should be used in the analysis of data to obtain objective conclusions. Hypothesis-testing, confidence interval determination, and analysis of variance are very useful to analyze and draw conclusions from experimental results. Representation of many experimental results in the form of an empirical, proxy or surrogate model, which mathematically describes relationship between important factors and response, is usually useful for further applications. It is essential to note that statistical methods do not allow us to experimentally prove that a factor has a

particular effect. However, they allow us to quantify probability of error or a level of confidence in a conclusion.

### **3.1.1.7 Conclusions and Recommendations**

After the analysis of the data is completed, practical conclusions from the results and recommendations are made. Follow-up runs and confirmation testing are subsequently performed to validate the conclusions. In practice, experimentation can be regarded as learning process because we do not perfectly know the answers of the problems. Successful experiment requires good knowledge of important factors, ranges of these factors and appropriate number levels for use in experimentation. Some factors may be dropped out and ranges of some factors may be adjusted after the first experiment. Therefore, the experimenter learns as the experimental program proceeds. As a result, experiment is usually conducted in a sequential manner.

## **3.1.2 Experimental Design Methods**

Several experimental design methods are available and presented in literature. As described previously, selection of experimental design method depends on the objectives of the experiment. This section describes concepts of some experimental design methods used in this study.

### **3.1.2.1 One-Variable-at-A-Time Designs (OVAT)**

One-Variable-at-A-Time (OVAT) or One-Factor-at-A-Time (OFAT) experimentation refers to a common approach of varying one factor over different levels while holding other factors constant at a specific level (usually at mid level). After determining importance of a single factor effect, focus of interest moves to another single factor. The effect of a factor is defined as a change in response produced by a change in the level of the factor. This effect is usually called “main effect” because it refers to the primary design factor in the experiment.

In 2-level experimental designs, each factor is assigned two levels in this type of designs. For computational purposes and avoiding a problem of different scale units of design factors, the factors are scaled so that the low and high levels of each factor are assigned a value of -1 and +1, respectively. For 3-level experimental designs, the mid level of a factor is assigned a value of 0.

Conventionally, effect of a factor is denoted by a capital Latin letter. For example, “A” refers to the effect of Factor A and “AB” refers to the effect of AB interaction. For notation of factor combinations of an experimental run, two different methods are widely used. For the first method, a series of capital Latin letters denotes names of factors varied in an experiment. Each factor name is followed by a superscript “-” or “+” referring to low or high level of the factor, respectively. As an example,  $A^-B^+$  refers to an experimental run at low level of Factor A and at high level of Factor B. Alternatively, high level of a factor is represented by corresponding a lower case letter while low level of a factor is represented by the absence of the corresponding letter. For instance, “b” represents an experimental run at low level of Factor A and at high level of Factor B.

Figure 3.2 shows the experimental plan or design of a 2-factor one-variable-at-a-time experiment. From the figure, estimates of Factors A and B are  $A^-B^+ - A^-B^-$  and  $A^+B^- - A^-B^-$ , respectively. Since experimental error is present in physical experiment, replication of experimental run at each design point is usually required. Effect estimate of each factor is thus performed based on average responses. If 2 response observations are required for each design point (2 replicates), a total number of six experimental runs are required.

### 3.1.2.2 Full Factorial Designs (FD)

Full factorial designs are the most efficient way to study the effects of several factors. This type of designs contains all possible combinations of low/high levels of all factors. Thus, levels of several design factors are varied together from run to run. If all design factors have the same number of levels, the total number of experiment can be calculated as  $L^k$ , where  $L$  = the number of levels of each design factor and  $k$  = the

number of design factors. A two-factor full factorial experiment conducted at two factor levels is presented in Figure 3.3.

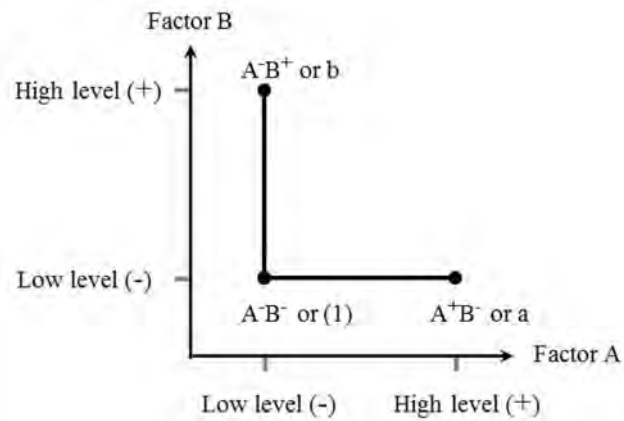


Figure 3.2: A two-factor one-variable-at-a-time experiment conducted at two levels  
(Adapted from Montgomery [54])

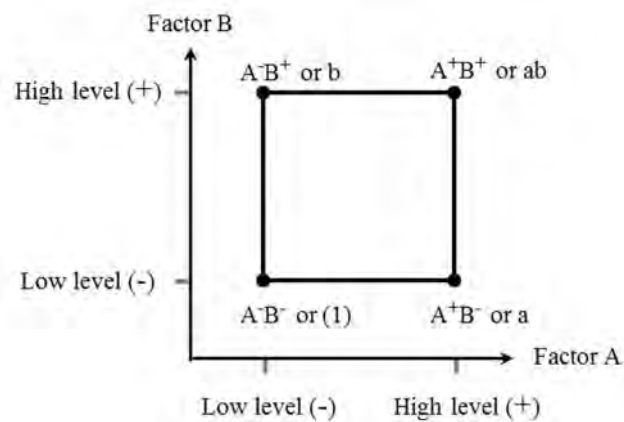


Figure 3.3: A two-factor full factorial experiment conducted at two levels  
(After Montgomery [54])

Full factorial designs have several advantages over one-variable-at-a-time designs. From the figure, two estimates of Factor A main effect can be determined as  $A^+B^+ - A^-B^+$  and  $A^+B^- - A^-B^-$ . Two estimates of Factor B main effect can also be evaluated in a similar manner. It can be shown that average main effects calculated from the two estimates of each main effect are as precise as those obtained from the one-variable-at-a-time experiment. However, only 4 experiment runs are required

meaning that FD is more efficient than OVAT. In general, the efficiency of full factorial designs over one-variable-at-a-time designs increases as the number of design factors increases.

In many process systems, effects due to interaction between factors can be important. As shown in Figure 3.4, due to the absence of experimental run at  $A^+B^+$ , one may conclude that the factor combination at  $A^+B^+$  produces the highest response since the responses at  $A^-B^+$  and  $A^+B^-$  show response increment in a one-variable-at-a-time experiment. If AB interaction effect exists, Figure 3.4(b) reveals that the conclusion can be seriously erroneous.

In addition, conclusions from full factorial designs are valid over a range of factor levels because the effects of a design factor are estimated over several levels of the other factors.

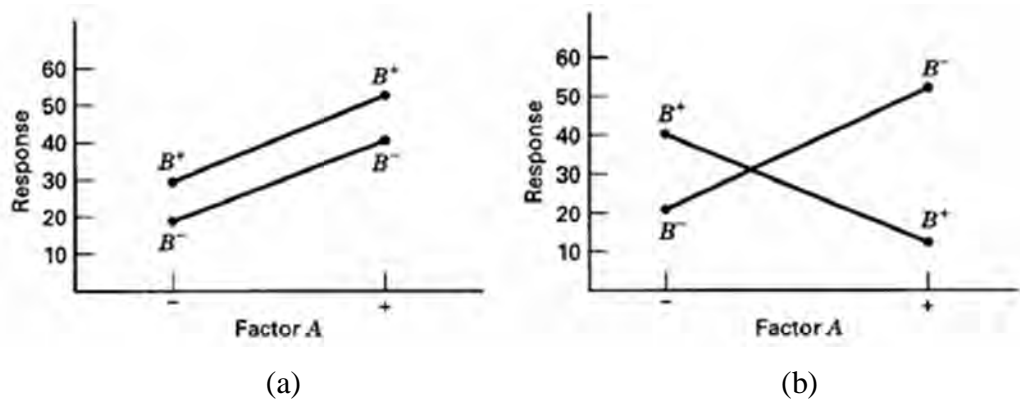


Figure 3.4: A 2-factor FD experiment (a) without AB interaction (b) with AB interaction (After Montgomery [54])

### 3.1.2.3 Fractional Factorial Designs (FFD)

Although full factorial designs have many advantages, their required number of runs become more impractical when the number of design factors is greater than about 4 because of limited experimental resource and time. It can be shown that the number of experimental runs of full factorial design can rapidly increase as “k” increases although L is as low as 2. Fortunately, it is usually not necessary to run all combinations of all factor levels. Fractional factorial designs (FFD) are variants of full factorial design which only a carefully chosen fraction or a subset of full factorial



combinations are experimented. A  $2^k$  full factorial design having  $2^{k-p}$  runs is called a  $1/p$  fraction of the  $2^k$  design. This can be simply called  $2^{k-p}$  fractional factorial design. Figure 3.5 compares cube plots of factor combinations between a  $2^3$  full factorial design and a  $2^{3-1}$  fractional factorial design.

Although the number of experimental runs can be decreased as “p” increases, the ability to differentiate response effects between factors decreases because more factor effects are aliases. For example, if main effect of Factor A and AB interaction effect are aliases (denoted by  $[A] = [AB]$ ), it is impossible to differentiate between A and AB. In fact, when either A or AB is estimated,  $A + AB$  is actually being estimated (denoted by  $[A] \rightarrow A + AB$ ). The notation of capital Latin letters in [ ] refers to factor effect evaluated from experimental design responses while the one without [ ] refers to actual factor effect.

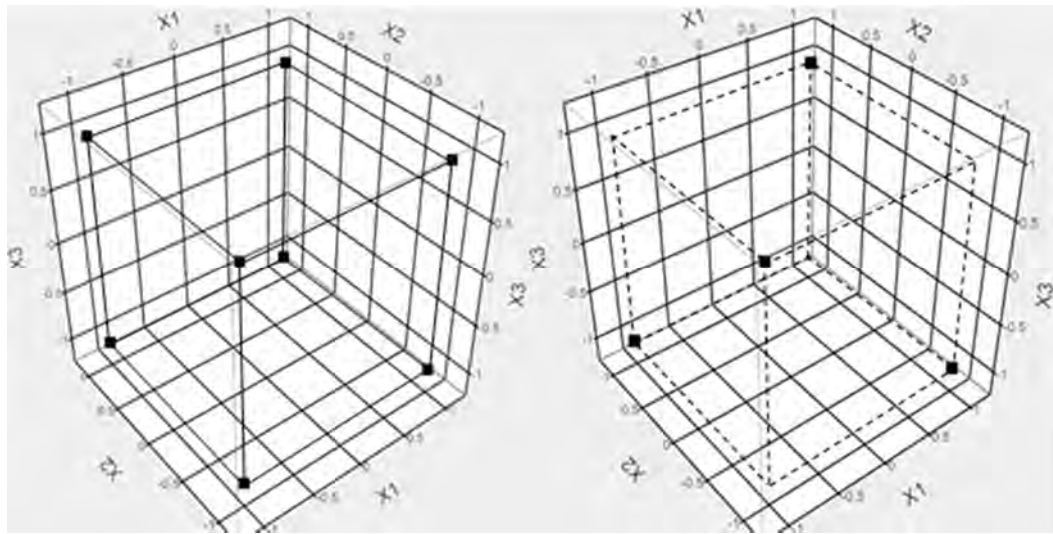
The ability to differentiate effects between factors can be indicated by resolution of the experimental design. Depending on available resource and time, the highest possible design resolution should be chosen. Table 3.1 shows available 2-level factorial designs with resolution. The definitions of important and mostly used resolution designs are described as follows:

1) Resolution III designs: no main effects are aliased with any other main effect. However, main effects are aliased with two-factor interactions and two-factor interactions may be aliased with each other.

2) Resolution IV designs: no main effects are aliased with any other main effect or any other two-factor interaction. However, two-factor interactions are aliased with each other.

3) Resolution V designs: no main effects or two-factor effects are aliased with any other main effect or two-factor interaction. However, two-factor interactions are aliased with any other three-factor interaction.

Plackett and Burman [56] developed and proposed a set of alternative 2-level fractional factorial matrices available for studying  $k = N-1$  factors in  $N$  runs where  $N$  is a multiple of 4. If  $N$  is a power of 2, these designs are the same as  $2^k$  full factorial designs. Plackett-Burman Designs (PBD) are Resolution III designs and often used as screening design because of their small number of experimental runs required. The designs have several special characteristics. First of all, the designs cannot be plotted



(a)

(b)

Figure 3.5: Cube plot of (a)  $2^3$  full factorial design (b)  $2^{3-1}$  fractional factorial design

Table 3.1: Summary of available 2-level factorial designs with resolution (After Minitab, Inc. [55])

	Factors														
Run	2	3	4	5	6	7	8	9	10	11	12	13	14	15	
4	Full	III													
8		Full	IV	III	III	III									
16			Full	V	IV	IV	IV	III	III	III	III	III	III	III	
32				Full	VI	IV	IV	IV	IV	IV	IV	IV	IV	IV	
64					Full	VII	V	IV	IV	IV	IV	IV	IV	IV	
128						Full	VIII	VI	V	V	IV	IV	IV	IV	

Available Resolution III Plackett-Burman Designs

Factors	Runs	Factors	Runs	Factors	Runs
2-7	12,20,24,28,...,48	20-23	24,28,32,36,...,48	36-39	40,44,48
8-11	12,20,24,28,...,48	24-27	28,32,36,40,44,48	40-43	44,48
12-15	20,24,28,36,...,48	28-31	32,36,40,44,48	44-47	48
16-19	20,24,28,32,...,48	32-35	36,40,44,48		

as cubes. So, they are sometimes called nongeometric designs. Their alias structures are very messy because every main effect is partially aliased with every two-factor interactions not involving itself. So, they are classified as irregular fractional factorial designs according to Box and Hunter [57 and 58]. As a result, they should be used as screening designs only when prior knowledge of the process system indicates that interaction effects are negligible.

### 3.1.2.4 Response Surface Method Designs (RSM)

Response surface method (RSM) designs are 3-level factor designs which are useful for modeling a curved quadratic surface to continuous design factors. The surface can be used for factor optimization if a minimum or maximum response exists inside the design factor region. The most popular type of response surface method designs are central composite designs (CCD) and Box-Behnken designs. A brief overview of these methods is presented as follows:

#### 3.1.2.4.1 Central Composite Designs (CCD)

Central composite designs are matrices corresponding to at most five-level experimental plans proposed by Box and Wilson [59]. A central composite design contains an imbedded full factorial or fractional factorial design with center points that is augmented with a group of star points that allow estimation of curvature. If the ranges of each design factor are coded so that its factorial points have either +1 or -1 unit, the distance from the center of the design hyperspace to a star point is  $\pm\alpha$  with  $|\alpha| \geq 1$ . There are 3 types of central composite designs which are circumscribed central composite designs (CCC) –  $\alpha > 1$ , Inscribed central composite designs (CCI) –  $\alpha = \pm 1$ , and face-centered central composite designs (CCF) –  $\alpha = \pm 1$ . Figure 3.6 shows comparison of the three types of central composite designs. Notice that star points of CCI and CCF are circular, spherical, or hyperspherical symmetry.

#### 3.1.2.4.2 Box-Behnken Designs (BBD)

A Box-Behnken design [61] is an independent quadratic designs that do not contain an embedded full factorial or fractional factorial design. In this design, factor combinations are at the midpoints of edges of the process design hyperspace and at the center. Figure 3.7 shows comparison between 3-factor CCF and 3-factor BBD. As illustrated in Fig. 3.7, the Box-Behnken design has no factor combinations or experiment points at vertices of the cube. Accuracy of prediction near vertices of this design is thus lower than CCF.

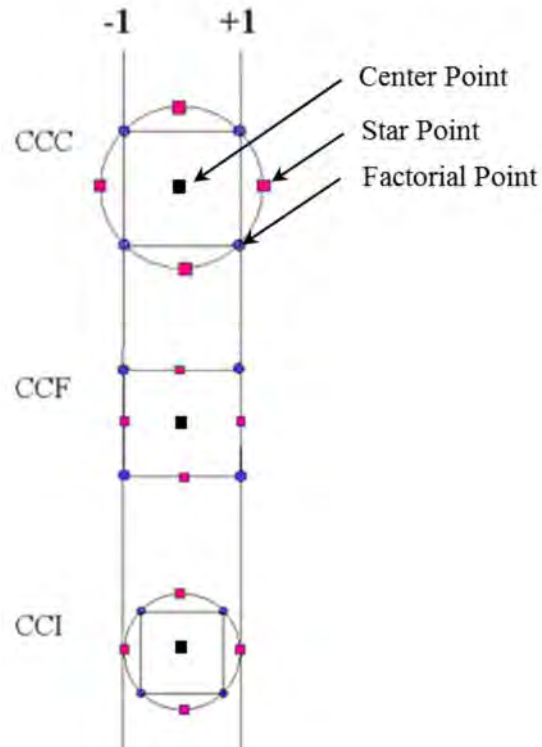


Figure 3.6: Comparison of the three types of central composite designs  
 (Adapted from United States Department of Commerce, NIST/SEMATECH [60])

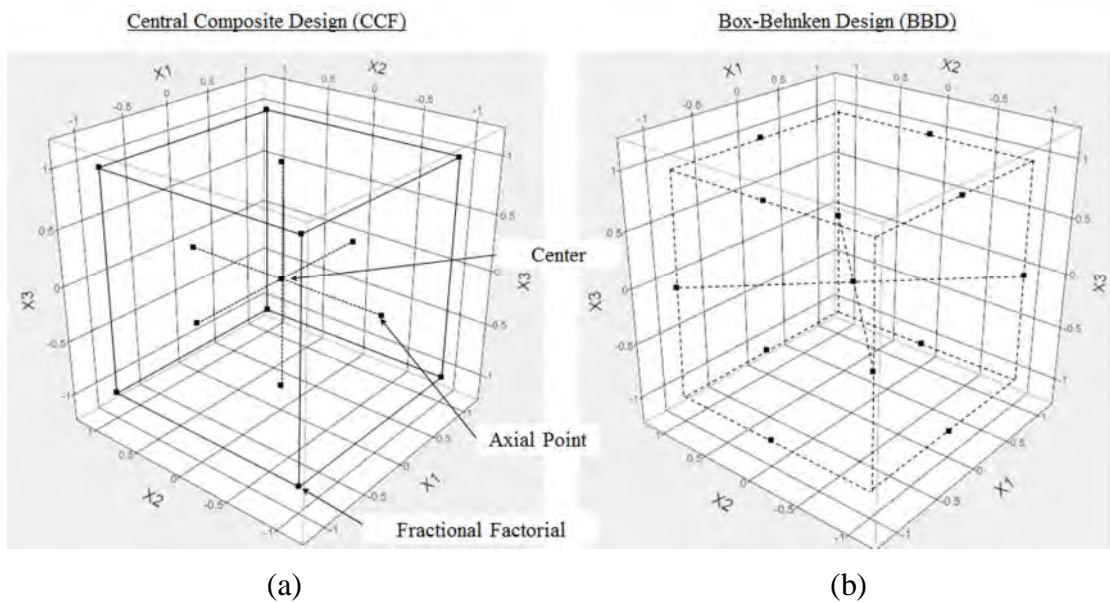


Figure 3.7: Cube plot of (a) 3-factor CCF (b) 3-factor BBD

### 3.1.2.4.3 Space-Filling Designs (SFD)

Space-filling designs (SFD) are useful for experiments whose run-to-run variability or random error is small enough to be neglected. Replication is thus not required because the same result will always be obtained when repeating the same run. Computer simulation, which is a deterministic system, is one of such experiments. In physical experiments where there is substantial random noise, the goal of experimental design is to minimize variance of prediction. However, in experiments on deterministic systems, there is no variance but bias. Bias is the difference between the approximation model and the true mathematical function. The goal of space-filling design is to bound the bias. There are two approaches to bound the bias. One is to prevent replication of design points or factor combinations by spreading out the distance between two points as maximum as possible. The other is to distribute the points as uniformly as possible over design hyperspace.

Descriptions of several space-filling designs such as sphere-packing designs, Latin Hypercube designs, uniform designs, maximum entropy designs, etc., are available in literature. Only Maximum entropy design method is described in this chapter because it is used in the current research. Note that maximum entropy design method is a competitor to Latin Hypercube design method which is widely used for computer experiments,

Maximum Entropy designs maximize a measure of the amount of information or Shannon information contained in an experiment [62]. Computationally, these designs maximize  $|\mathbf{R}|$ , the determinant of the correlation matrix of the design points. The matrix  $\mathbf{R}$  is defined as

$$\mathbf{R} = R(x^i, x^j) = \exp \left[ -\sum_{k=1}^k \theta_k (x_k^i - x_k^j)^2 \right] \quad (3.1)$$

where,

- i and j = the number of experimental runs
- k = the number of design factors
- $\theta$  = a k-vector of exponential correlogram ranges
- $x_k^i$  and  $x_k^j$  = the  $k^{\text{th}}$  components of sample points  $x^i$  and  $x^j$

This type of experimental designs is suitable for spatial correlation response surface model such as Gaussian process models, alternatively called kriging models. Figure 3.8 compares two-factor Maximum Entropy design with two-factor Latin Hypercube design. The figure shows that Latin Hypercube design does not always fill the design space well. Note that space-filling property improves as the number of runs increases.

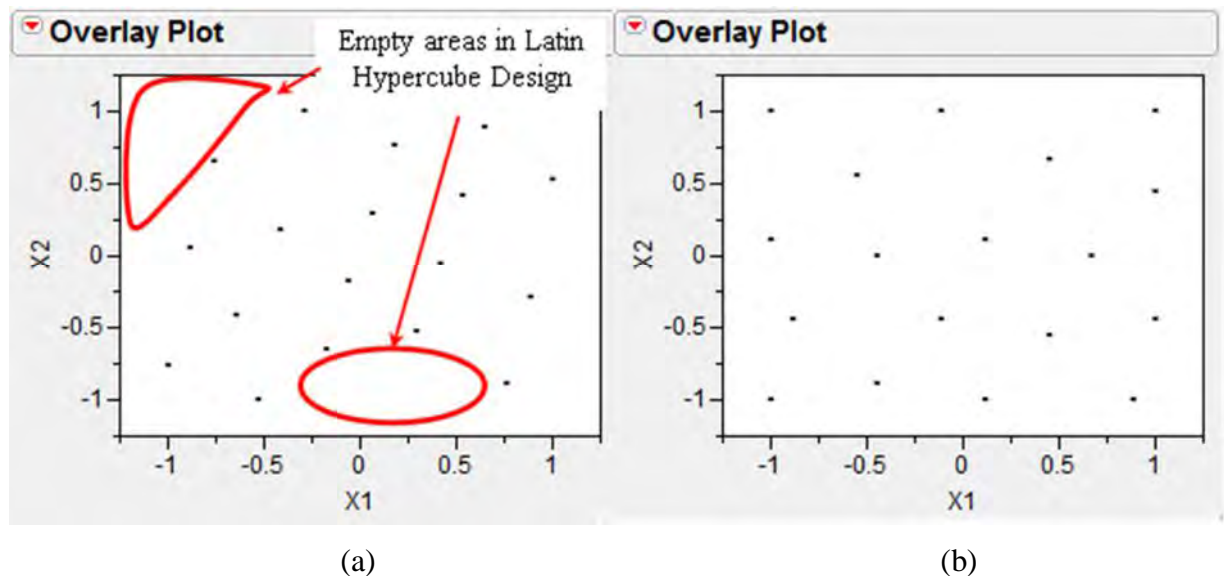


Figure 3.8: Comparison between (a) 18-run two-factor Latin Hypercube design  
(b) 18-run two-factor Maximum Entropy design

### 3.1.3 Selection of Experimental Design Method

As described in the previous sections, there are many experimental design methods published in literature and available in several statistical software packages for use. Different design methods have different advantages and limitations. Therefore, the method to be chosen for designing an experiment should be able to serve the objectives of the experiment and the number of factors to be investigated. Depending on the experiment objective and total number of design factors, Table 3.2 can be used as a guide line for choosing an experimental design method.

## 3.2 Statistical Analysis of Result

After conducting the designed experiment and obtaining process or system responses, it is usually required to identify and quantify sources of response variation, which factors are important or significant, and how they influence the sources of variation. To fulfill the requirement, statistical models and techniques are built and used. There are several statistical models available such as Continuous Linear Model (CLM), Analysis of Variance (ANOVA) model, and discrete model.

Table 3.2: Guideline for selecting experimental design method (Adapted from United States Department of Commerce, NIST/SEMATECH [60])

Number of Factors	Comparative Objective	Screening Objective	Modeling or Optimizing Objective
1	1-factor completely randomized design	-	-
2 - 4	Randomized block design	Full or fractional factorial	Central composite, Box-Behnken or space-filling
5 or more	Randomized block design	Fractional factorial or Plackett-Burman	Screen first to reduce number of factors

To employ either one of the aforementioned models, the following assumptions must be made. First, process system is sum of a systematic component and a random component. The systematic component can be described by a mathematical model while the random component represents error or noise present in the system. It is further assumed that the systematic component is fixed over the design range and the random component has a constant location, spread and distributional form. Second, the data used to fit these models are representative of the process system being modeled.

ANOVA models are commonly used in the data analysis because it can be used to compare effects of multiple levels of multiple factors. The basic concept of ANOVA is that the total variability in the process or system response can be partitioned into the variation due to factors (i.e. between factor levels) and the

variation due to pure error (i.e. within each factor level). All of the variations are assumed to be independently and normally distributed. After determining these total and partitioned variations, statistical hypothesis testing of equal means of factor level effects is performed. Consequently, factors whose change in their level can significantly influence response of the process system can be identified. These factors are called 'significant factors' herein. The detailed calculation method of ANOVA and its theories behind can be found in many statistical textbooks [54], [60], etc.

It is essential to note that, in computer experiments, there is no random or pure error to estimate mean square error in analysis of variance as usual because the experiments are performed on a deterministic model. Daniel [63] suggests a simple way to solve this problem. Daniel suggests that any effects which are negligible are normally distributed with mean zero and variance  $\sigma^2$ , and will tend to fall along a straight line on a normal or half-normal probability plot of the estimates of the effects. Significant effects will not have mean zero and will not lie along the straight line.

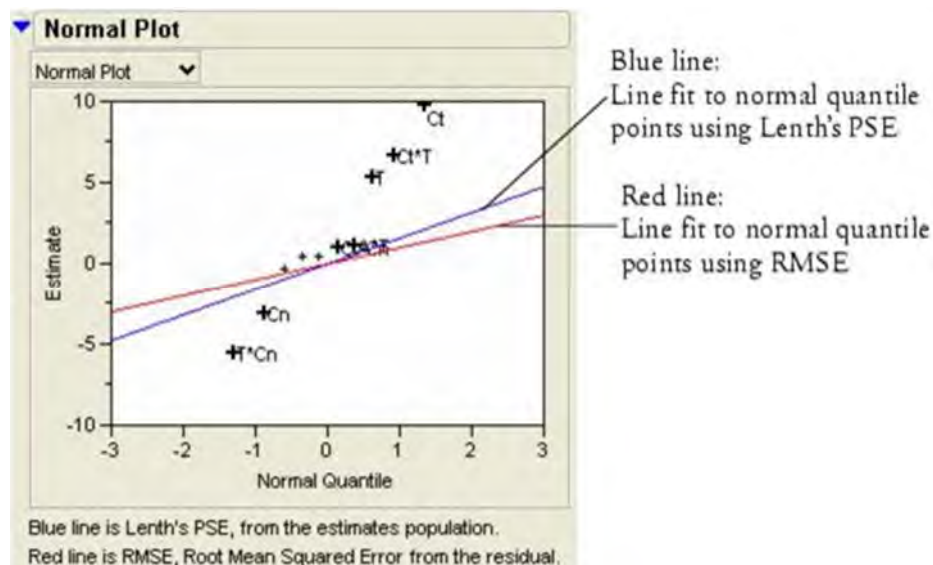


Figure 3.9: An example of normal probability plot of  $2^k$  factorial design [64]

As shown in Figure 3.9, a normal probability plot is a plot between effect estimates on the vertical axis and normal quantiles on the horizontal axis. It is shown in the figure that T, Ct, Cn, Ct\*T and Cn\*T are significant factor effects. Similarly, a half-normal probability plot is a plot between the absolute values of the estimates



against the normal quantiles for the absolute value normal distribution. Figure 3.10 shows the half-normal probability plot of the same factor effects plotted in Figure 3.9.

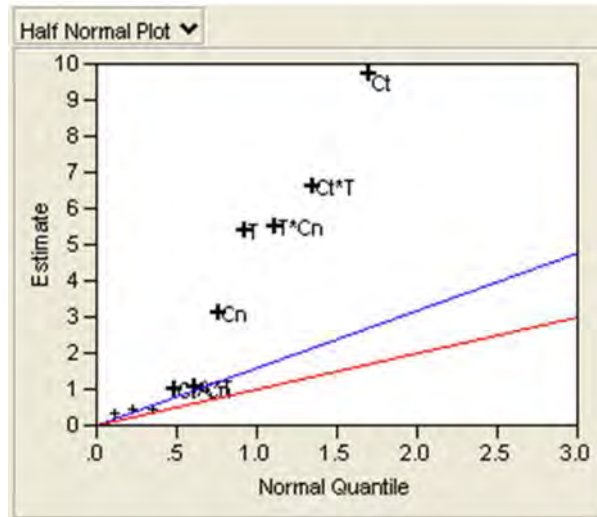


Figure 3.10: An example of half-normal probability plot of  $2^k$  factorial design [64]

Although normal or half-normal plot of factor effects are simple for use, interpretation of the effect significance is rather subjective. Alternatively, Lenth [65] proposed a good method to estimate standard error, called pseudo standard error (PSE) to detect significant factorial effects. The Lenth's PSE can be calculated as per Equation 3.2.

$$PSE = 1.5 \times median(|c_j| : |c_j| < 2.5S_0) \quad (3.2)$$

and

$$S_0 = 1.5 \times median(|c_j|) \quad (3.3)$$

where,

- $c_j$  = contrast or effect estimate of  $j^{\text{th}}$  factor effect
- $j$  = 1 to  $m$
- $m$  = total number of contrasts or effect estimates of interest
  - =  $2^k - 1$  factor effect estimates for an unreplicated  $2^k$  factorial or
  - $2^{k-p}$  fractional factorial designs
- $k$  = total number of design factors

In addition, there are two principles which play an important role in the analysis and interpretation of data. The first principle, called “sparsity of effects principle”, states that most systems are dominated by some of the main effects and low-order interactions, and most high-order interactions are negligible [54]. Thus, interaction effects of three or higher factors are usually assumed negligible and sometimes regarded as pure error in unreplicated experiments. The other is “hierarchy principle”. It states that if a model contains a high-order term (such as  $A^2B$ ), it should also contain all of the lower-order terms that compose it (in this case  $A^2$  and  $A^2B$ ). The objective of this principle is to promote a type of internal consistency in a model and many statistical model builders strictly follow the principle.

### **3.3 Response Surface Methodology (RSM)**

Response surface methodology or RSM is a collection of mathematical and statistical techniques used for modeling and analysis relationship between a response of interest and its influential factors. Therefore, response surface methodology is implemented when the objective of the experiment is modeling or optimizing. In other words, RSM is the method used to build a mathematical/statistical model mimicking actual process system illustrated as a box in Figure 3.1. A mathematical function relating process/system response to its independent influential factors and noise or error observed in the response is called response surface.

In many cases, the form of true response surface of a process system is unknown. Therefore, the first working step always starts with finding a suitable approximation form of the response surface in some region of independent factors. Least square techniques are then used to estimate parameters required for the model form. Consequently, a fitted surface is obtained for response surface analysis. Figure 3.11 schematizes a general workflow for building a response surface model. It is essential to note that the model parameters are effectively estimated when a proper experimental design method is used to collect data. Experiments designed for fitting response surface model are thus called response surface model designs.

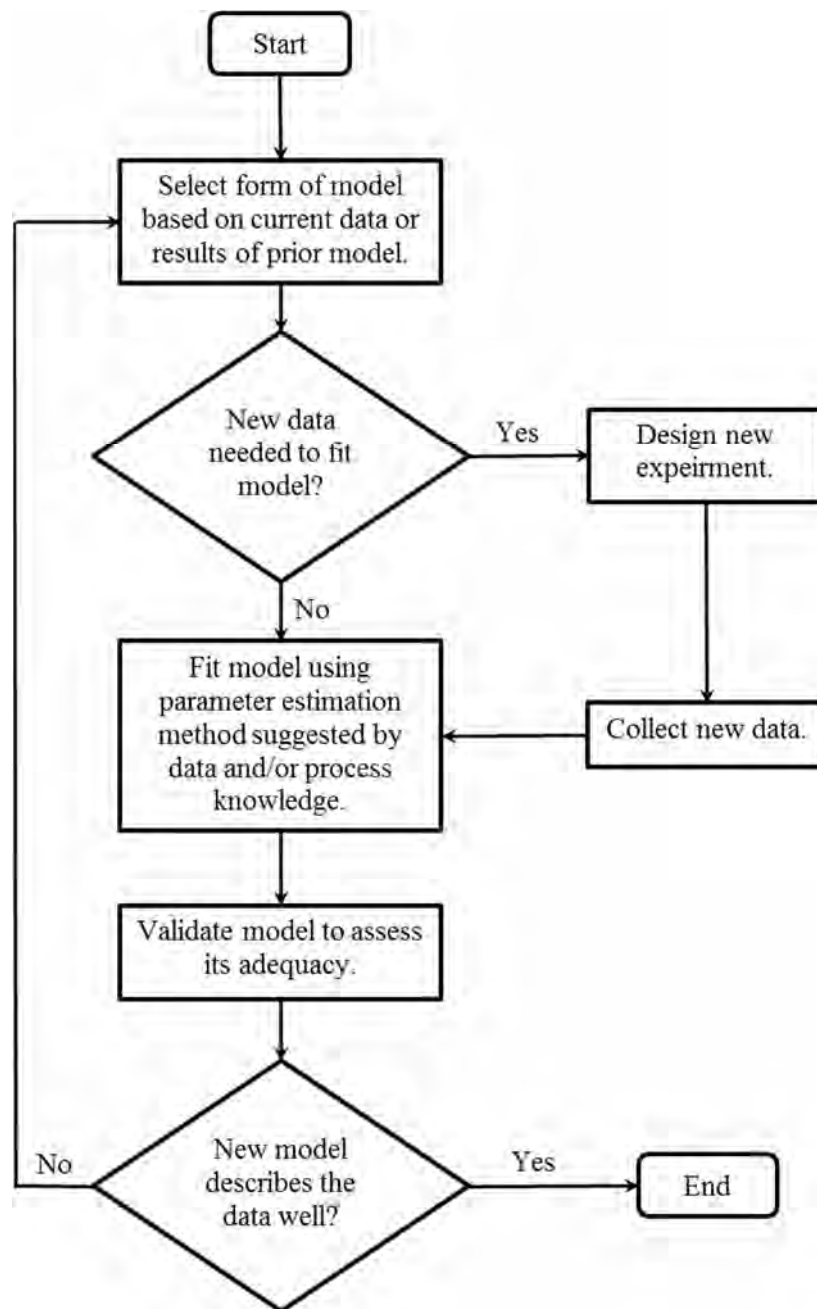


Figure 3.11: General workflow for building a response surface model (After United States Department of Commerce, NIST/SEMATECH [60])

If the experiment objective is optimization, first-order polynomial model may be firstly used to find the factor region which contains optimum (maximum or minimum) response of the process. A second-order polynomial model is then used to fit the response surface within a relatively small factor region. As a result, the RSM is a sequential procedure. On the other hand, if the objective is process modeling, a

more complex model form may be required to be able to imitate the process response as close as possible. Some forms of response surface models used in this research are briefly overviewed in the following sub-sections.

### 3.3.1 First-Order Polynomial or Linear Model

$$\hat{y} = \hat{\beta}_0 + \sum_{i=1}^k \hat{\beta}_i x_i + \varepsilon \quad (3.4)$$

where,

$\hat{y}$	=	predicted process or system response
$k$	=	number of design factors
$i$	=	integer from 1 to $k$
$\hat{\beta}_0$	=	regression intercept
$\hat{\beta}_i$	=	regression coefficient of first-order term, $x_i$
$\varepsilon$	=	random error

Notice that  $\hat{\beta}_i x_i$  is the estimated main effect of  $i^{\text{th}}$  design factor.

### 3.3.2 Second-Order Polynomial or Quadratic Model

This model is used in lieu of linear model when there is curvature in the response.

$$\hat{y} = \hat{\beta}_0 + \sum_{i=1}^k \hat{\beta}_i x_i + \sum_{i=1}^k \hat{\beta}_{ii} x_i^2 + \sum_{i < j} \hat{\beta}_{ij} x_i x_j + \varepsilon \quad (3.5)$$

where,

$\hat{y}$	=	predicted process or system response
$k$	=	number of design factors
$i, j$	=	integer from 1 to $k$
$\hat{\beta}_0$	=	regression intercept
$\hat{\beta}_i$	=	regression coefficient of first-order term, $x_i$
$\hat{\beta}_{ii}$	=	regression coefficient of second-order term, $x_i^2$

$$\begin{aligned}\hat{\beta}_{ij} &= \text{regression coefficient of interaction term, } x_{ij} \\ \varepsilon &= \text{random error}\end{aligned}$$

### 3.3.3 Gaussian Process Model

The Gaussian process models are powerful models for non-linear interpolation and often used to fit the data from a deterministic computer experiment. By definition, a Gaussian process is a stochastic process whose realizations consist of random values associated with every point in a range of times or space such that each such random variable has a normal distribution. Moreover, every finite collection of those random variables has a multivariate normal distribution. Historically, it is previously known as Gaussian process regression or Kriging [66]. Although this type of models can provide an exact fit to the responses from the experiment, it is important to note that there is no guarantee that interpolation is done well at locations having no response data.

The Gaussian process model used for this research has the following form:

$$y = \mu + z(x) \quad (3.6)$$

where,

$$\begin{aligned}y &= \text{process or system response} \\ \mu &= \text{a normal distribution mean} \\ z(x) &= \text{a random function with mean zero, variance } \sigma_z^2, \text{ and correlation} \\ &\quad \text{matrix } \mathbf{R} \text{ or } R(x^i, x^j) \text{ between two } z \text{ values at input vector } x^i \text{ and} \\ &\quad x^j; \text{ these are two } k\text{-dimensional vectors at distinct points } i \text{ and } j. \\ \mathbf{R} &= R(x^i, x^j) = \text{See Equation 3.1}\end{aligned}$$

Note that  $\mu$ ,  $\sigma_z^2$  and  $\theta_k$  in Equation 3.1 are estimated using the optimization method of maximum likelihood which is a measure of goodness-of-fit of model fitting like  $R^2$ .

In this chapter, the basic principles of experimental designs and response surface methodology relating to the current study have been presented. The next chapter describes methodology of this research.

# **CHAPTER IV**

## **RESEARCH METHODOLOGY**

This chapter describes the work carried out for this research according to the methodology outlined in Chapter 1. However, the scope of this chapter covers only from Step 1 to Step 5 of Section 1.5. The work performed in the remaining steps is presented in Chapter V. In the end of this chapter, description of simplified reservoir models for conducting designed experiments is provided.

### **4.1 Statement of Objectives and Response Factor**

According to the problem and opportunity stated in Section 1.1, it is decided to conduct designed experiments and response surface fitting to meet the objectives of this researched defined in Section 1.2. From the research objectives, it can be clearly identified that the main objectives of the designed experiments to be conducted are modeling and optimizing. However, because behavior and performance of a horizontal well can be influenced by several controllable and uncontrollable factors, the requirement of screening design is also identified.

Ultimate oil recovery factor (URF) of a horizontal well is selected to be the response factor of this study. This is due to the reason that horizontal wells are mainly used to maximize oil recovery to prolong field life in the Gulf of Thailand besides accelerating oil production. Intuitively, one can expect that horizontal well productivities from the experimental results could be more or less greater or equal to a equivalent vertical/deviated well. Therefore, defining well productivity as the response factor could not be as good as the URF.

### **4.2 Selection of Input Factors**

After the response factor was defined, potential significant factors that could influence ultimate oil recovery factor of a horizontal well was listed out based on literature review and consultation with subject matter experts (SMEs) of the oil fields.

As a result, a total of 48 potential significant factors could be listed out as shown in Table A1 of Appendix A. Table A1 presents potential significant factors grouped according to their geological and engineering characteristics and other different types of factor categorizations, i.e. controllable/uncontrollable and dependent/independent.

Subsequently, it is realized that the number of experimental runs is still impractical for screening 48 factors although an experimental design approach is used. For example, for Resolution III designs, 52 and 64 runs are required for Plackett-Burman and fractional factorial designs. For Resolution IV designs, 104 and 128 runs are required for folded Plackett-Burman and fractional factorial designs.

Therefore, it is decided to conduct factor screening based on SMEs' knowledge. To do so, each SME is independently requested for giving a score of factor significance or influence to each factor. The score increases from 0 to 10 as factor significance or influence on URF of horizontal well increases. Consequently, an average significance score of each factor can be calculated and ranked. See Table A1 for the detail.

In addition, the number of factors can be further reduced by grouping factors which have mutual correlation together. Also shown in Table A1 are two columns of additional categories of the potential significant factors. The symbol "I" in the first column indicates whether the factor of interest must be independently obtained from measurement/testing or can be calculated from physical relationship with other factors (labeled by "D"). The other column labels "C" to a factor if the factor can be calculated from available correlations, is fixed at a certain value as per SMEs' recommendation, or may be significant but its effect is beyond the objectives of this research. The label "X" means that the factor could be a potential significant factor and should be experimented.

By taking the factors which have a score of 4 or higher with labels "I" and "X", 13 significant factors can be screen out for screening experimental design. As remarked in the table, the remaining factors are either kept constant or varied together with other factors with respect to their known correlation. The screened out potential significant factors are re-tabulated in Table 4.1 for the ease of reference.

Then, probability distribution and range of the 13 potential significant factors are collated from the existing horizontal well database. The probability distributions

and associated statistics of the factors are presented in Table 4.2 and Appendix B. Note that transformed probability distributions of RESDIP, ANISO, and HO are also included in the table and appendix. As aforementioned in Section 1.5, factor transformation is performed so that the transformed distribution is as close to normal distribution as possible.

### 4.3 Screening Experimental Design

In the previous section, 13 out of 48 factors could be screened out by SMEs' experience and making use of known factor correlations. However, the number of experimental runs of response surface designs is still prohibitive. Therefore, the 13 design factors are screened out further using Resolution IV  $2^{13-8}$  fractional factorial design and reservoir simulation. By using screening experimental design, quantitative and objective conclusion can be obtained. A statistical software, called "JMP Statistical Discovery Software", is used to perform experimental design and analysis

Table 4.1: Potential significant factors or design factors for experimental designs

No.	Potential Significant Factor	Abbreviation	Unit	Controllable or Uncontrollable?
1	Reservoir thickness	HRES	ft	Uncontrollable
2	Ratio of horizontal-well-length to reservoir-length	LHRATIO	Fraction of reservoir length	Uncontrollable
3	Average reservoir dip angle	RESDIP	Degree	Uncontrollable
4	Porosity	PORO	Fraction	Uncontrollable
5	Anisotropy ( $k_v/k_h$ )	ANISO	Fraction	Uncontrollable
6	Oil gravity	API	°API	Uncontrollable
7	Initial oil column thickness	HO	ft TVD	Uncontrollable
8	Initial oil-water contact depth	OWC	ft TVDSS	Uncontrollable
9	Ratio of initial gas cap pore volume to initial oil pore volume	MRATIO	Fraction of oil PV	Uncontrollable
10	Ratio of initial aquifer pore volume to initial oil pore volume	AQFRATIO	Multiplier of oil PV	Uncontrollable
11	Horizontal well length	LH	ft	Controllable
12	Ratio of well standoff to OWC to initial oil column thickness	WSTANDOFF	Fraction of HO	Controllable
13	Liquid production rate control	LRAT	STB/day	Controllable



for this research. Table C1 in Appendix C shows factor settings or design patterns of  $2^{13-8}$  fractional factorial design for conducting reservoir simulations. The symbols “+” and “-” in Table C1 denote maximum and minimum values of a factor of interest as shown in Table 4.2. In addition, the order of factor level in each design pattern follows the order number of design factor shown in Table 4.2. It is essential to note that a 20-run Resolution III Plackett-Burman design is purposely not selected for this factor screening because some interaction effects of the 13 factors may be significant.

Table 4.2: Probability distribution of design factors for experimental designs

No.	Design Factor	Unit	Min.	Max.	P10	P50	P90
1	OWC	ft TVDSS	4119	8497	5294.29	6773.6	8116.77
2	HRES	ft	11.0	92.0	25.3	43.4	68.6
3	HO	ft TVD	25.0	159.0	35.6	65.0	109.2
	HO#	ft TVD	3.219	5.069	3.567	4.133	4.700
4	LH	ft	180	3476	574	1235	2279
5	LHRATIO	Fraction of reservoir length	0.10	1.00	0.10	0.55	1.00
6	RESDIP	Degree	1	8	1.67	2.96	5.24
	RESDIP#	Degree	0	2.079	0.504	1.084	1.663
7	MRATIO	Fraction of oil PV	0	1.65	0.00	0.08	0.155
8	AQFRATIO	Multiplier of oil PV	38.44	92.16	0.00	50.00	100.00
9	WSTANDOFF	Fraction of HO	0.11	0.95	0.46	0.46	0.76
10	PORO	Fraction	0.14	0.28	0.16	0.20	0.25
11	API	°API	34.74	47.75	36.2	38.9	41.6
12	ANISO	Fraction	0.1	1	0.1	0.21	1.00
	ANISO#	Fraction	-4.029	-0.086	-4.584	-2.057	-0.086
13	LRAT	STB/day	55	6000	3027.5	3027.5	6000.0

Note: 1) RESDIP# = Transformed RESDIP =  $\ln(\text{RESDIP})$

2) ANISO# = Transformed ANISO =  $\ln(\text{ANISO}-0.0822)$

3) HO# = Transformed HO =  $\ln(\text{HO})$

## 4.4 Response Surface Designs

After conducting screening experiment and analysis, the obtained significant factors are further experimented according to a response surface design. Unlike the

screening design, the low, mid, and high levels of a factor are set at P10, P50, and P90 values, respectively, so as to trim extreme and rarely encountered values out. The popular face-centered central composite design (CCF) is firstly chosen to be experimented to generate a quadratic proxy model. As described in Chapter 5, 6 out of the 13 design factors can be screened out for performing subsequent response surface designs. Level settings of the 6 designed factors are varied according to the design patterns shown in Table C2 in Appendix C. For the other factors, their settings are kept at their mid or P50 level.

Later on in Chapter 5, validation result of the quadratic proxy model shows that quadratic models cannot adequately describe the URF response surface. Therefore, 45-run maximum entropy designed experiments are performed. The number of experimental runs is selected to be the same as that of CCF so that their model fitting efficiencies could be compared. Refer to Table C3 for design patterns of the 45-run maximum entropy design.

## **4.5 Designed Experiments for Proxy Cross-Validation**

One approach to validate a fitted proxy model is comparing its predicted responses with actual responses obtained from another different set of experiments. For process systems that have random errors, the minimum number of sample experiments, which can statistically represent its population, can be calculated from sample variance. However, this type of calculation cannot be performed in this research because computer experiments are deterministic and random-error free. Thus, it is ideal to perform as many validation experiments as possible to better represent actual response surface. However, conducting too many cross-validation experiments could consume too much resource and omit the advantage of experimental designs on requiring fewer numbers of runs.

Therefore, it is subjectively decided to conduct 2 sets of 18-run (40% of 45-run CCF) maximum entropy designed experiments for the validation. Each set of the designs is differently generated by changing the number of random starts in JMP program. The first set of validation experiments is used for validating proxy models obtained from the 45-run central composite design and 45-run maximum entropy

design. The second set of validation experiment is combined with the first set to validate the proxy model obtained from 45-run central composite design and 45-run maximum entropy design points. See design patterns of the two cross-validation experimental designs from Tables C4 and C5 in Appendix C.

## 4.6 Reservoir Simulation Modeling

To perform the computer experiments, a commercial black-oil simulator “Schlumberger ECLIPSE E100” is used for simulating fluid flow in reservoirs. Due to its modeling and visualization capabilities, a seismic-to-simulation software “Schlumberger PETREL” is used for constructing an ECLIPSE model and exporting it to ECLIPSE E100 for flow simulation. After the simulation is completed, the results are imported to PETREL for better visualization.

During data collection stage, it is found that actual characteristics of the reservoirs in the Gulf of Thailand are complex and have a lot of variations. To obtain a proxy model that could represent all reservoirs as close as possible, all reservoir simulations are performed based on simple hypothetical models. A simple model is parallelogram-shaped and homogeneous reservoir having average reservoir and fluid properties assigned with respect to designed factor settings. By assuming that horizontal wellbore is placed at the middle of true reservoir thickness, HRES, boundary of any reservoir model can be calculated from geometry-related factors such as OWC, LH, LHRATIO, HO, HRES, RESDIP, MRATIO, and WSTANDOFF. A 3D graphical view of a simple reservoir model can be seen in Figure 4.1.

Since reservoirs under this stud

y are relatively thin, reservoir grid cells are modeled using corner-points rather than traditional block centers for better geometry and fluid flow modeling. Depending on length-to-width and length-to-height ratios of the reservoir of interest, the total number of grid cells in all models is limited not to exceed 100,000 grid cells to avoid excessive run time. The length-to-width ratios of all models are controlled to vary within a range of 0.8 to 1.2, except for the cases that the ratio is very high. The number of grid cell layers varies from 10 to 20 depending on the total number of grid cells. If feasible, the reservoir is divided into 15 grid layers as a base value.

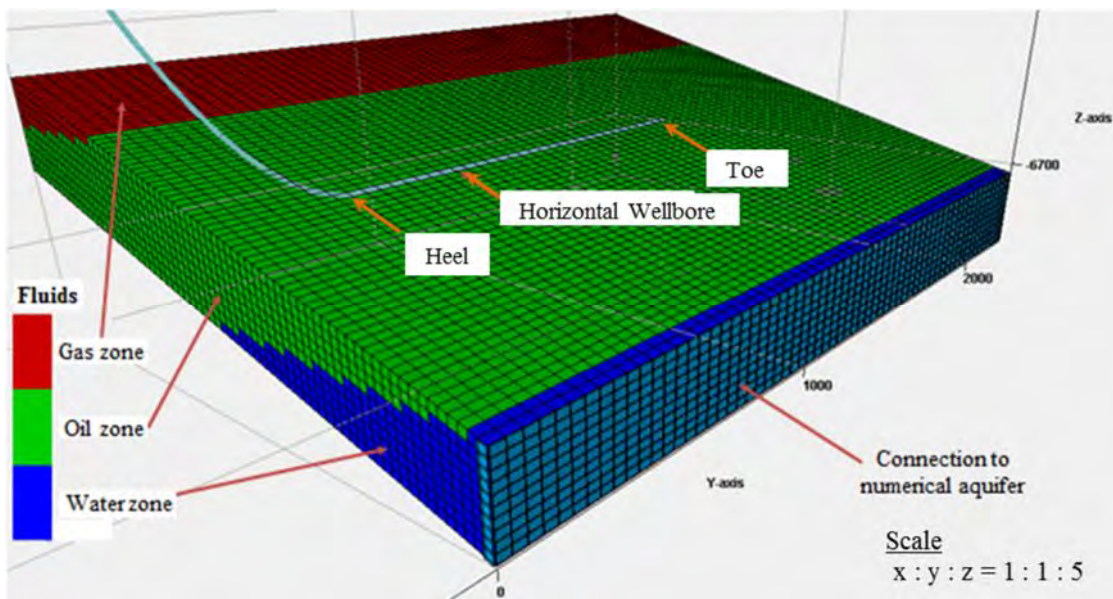


Figure 4.1: A 3-dimensional simple reservoir model showing fluid zones, horizontal well modeling, and edge-drive aquifer

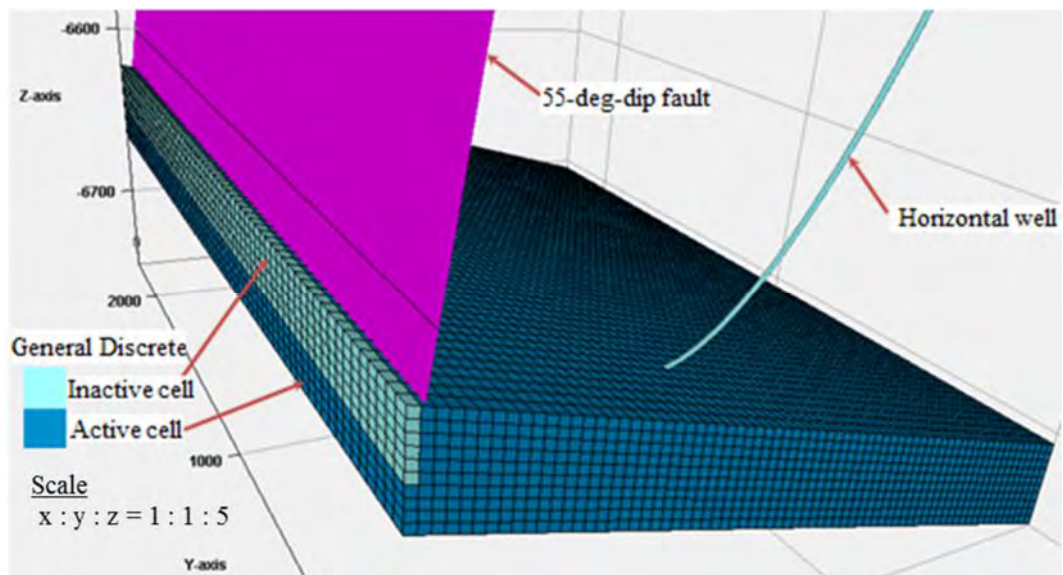


Figure 4.2: A 3-dimensional simple reservoir model showing an updip impermeable fault, inactive cells modeling due to the fault, and a horizontal well

In an attempt to represent a simple model as close to an actual one as possible, an updip fault is also simulated as shown in Figure 4.2. Since the fault is assumed to be impermeable, any grid cells whose cell centers are higher than the fault are modeled inactive for fluid flow. According to Table A1, fault dip angle is not

expected to significantly affect horizontal well URF for thin-oil-column reservoirs. Therefore, an average dip angle of 55 degree is simulated for all models.

Initial reservoir pressure and temperature in a reservoir model at the mid depth of oil column are calculated from generic correlation equations. The generic correlation equations are fitted from raw data collected from the existing horizontal well database. Refer to Figures D1 and D2 for regression of the correlation equations.

Based on initial reservoir pressure, temperature, oil & gas gravity and gas-oil contact elevation, fluid properties in a reservoir model can be calculated using correlations recommended by PETREL. Table 4.3 summarizes correlations used for fluid modeling in this research. Note that an average gas gravity of 0.77 is kept constant for all models as well as a water salinity of 1,000 ppm (fresh water).

For rock compaction, a constant rock compressibility of  $8 \times 10^{-6} \text{ psi}^{-1}$  is used for all models as per an SME's recommendation. This is because reservoir rocks in the Gulf of Thailand are generally consolidated. For relative permeability curves, available core plug data is collected and analyzed. The obtained average residual saturations, end points and Corey exponents are shown in Figure D5 and used for all simulations.

Table 4.3: Fluid correlations used for fluid modeling

<b>Description</b>	<b>Correlation</b>
Z Factor	Hall & Yarborough [67]
Gas Pseudocritical Properties	Piper, McCain & Corredor [68] from gas gravity
Gas Viscosity	Lee, Gonzales & Eakin [69]
Oil Bubble Point Pressure	Valko & McCain [70]
Gas-Oil Ratio	Standing [71]
Oil Formation Volume Factor ( $p \leq p_b$ )	Petrosky & Farshad [72]
Oil Formation Volume Factor ( $p > p_b$ )	McCain [73]
Oil Density ( $p \leq p_b$ )	McCain [73] mass balance
Oil Density ( $p > p_b$ )	McCain [73] mass balance
Dead Oil Viscosity	Beggs & Robinson [74]
Oil Viscosity ( $p \leq p_b$ )	Beggs & Robinson [74]
Oil Viscosity ( $p > p_b$ )	Vasquez & Beggs [75]
Water Formation Volume Factor ( $p > p_b$ )	McCain [73]
Water Compressibility ( $p > p_b$ )	Osif [76] revised by Spivey, Valko & McCain [77]
Water Viscosity	Meehan [78]

The horizontal permeability of rocks used in this research is correlated from extensive permeability tests of core plugs in the fields. The permeability-porosity correlation plot and equation which are commonly used by engineers working in the fields are shown in Figure D3 of Appendix D. In this research, level setting of horizontal permeability is directly varied in experimental design. Instead, it is indirectly varied when the factor level of porosity changes using the permeability-porosity correlation.

Initial water saturation in water-oil transition zone due to capillary effect is taken into account in the modeling. A generic J-function obtained from the existing database is plugged into PETREL to auto-generate oil-water capillary pressure curve in ECLIPSE. The initial water saturation distribution due to capillary effect in a model is generated during model equalization. Consequently, the initial saturations of water, oil and gas distributed under gravity are ready for the production simulation. Figure D4 presents a plot of Leverette J-function versus water saturation with correlation equation. From the formulas in the figure, initial water saturation at a given depth in oil-water transition zone can be calculated from permeability and porosity of the rock. Since permeability is correlated with porosity in this research, varying factor setting of porosity also changes thickness of the oil-water transition zone.

Horizontal well path is automatically generated by PETREL after specifying coordinates of heel and toe of the horizontal section. Besides its horizontal section, coordinates of horizontal well path are generated from the horizontal section up to kick-off point of the well. By default, the kick-off point is specified at 1/3 of the vertical depth from surface to the horizontal section. Above the kick-off point, the well is horizontal. Below the kick-off point, the build-up radius of 1,500 ft (classified as long radius [7]) is specified in PETREL for all horizontal wells. Examples of a modeled horizontal well can be viewed in Figures 4.1 and 4.2. In terms of simulation modeling, ECLIPSE will treat any grid cells intersected by perforated or open-hole sections of the well path generated by PETREL as wellbore.

As mentioned in Table A1 of Appendix A, all horizontal sections are modeled to be perfectly horizontal from heel to toe with open-hole completion. A wellbore size of 6-1/8" with a roughness of 0.066" (average value of unlined concrete in Table 4.4) is used for all models. By dividing the horizontal section into many segments, fluid

flow inside the open-hole section of a horizontal well can be calculated by ECLIPSE. Note that well segment size is set to be equal to the size of the grid cell that the horizontal well path intersects with. In the calculation, the effects of pressure loss due to friction, fluid acceleration and hydrostatic pressure are considered.

In all cases, the well section above the well heel is completed by a 5.000” API J-55 casing. A 2.875” API J-55 tubing (OD = 2.875” and ID = 2.441”) with a roughness of 0.0006” is installed from the well heel up to the surface. Fluid flow calculation inside the tubing is performed by means of using vertical lift performance (VLP) curves. The VLP curves are constructed using a software package, called “PROSPER”, which is developed by Petroleum Experts Limited. After the VLP curves are constructed, they are exported to ECLIPSE for well flow simulation. It is essential to note that all simulations are performed for fluids flowing from reservoir to horizontal wellbore and from horizontal wellbore to tubing head only.

Table 4.4: Roughness of different types of pipe [79]

Type of Pipe (New, clean condition)	Roughness $\epsilon$ (ft)	Roughness $\epsilon$ (in.)
Unlined Concrete	0.001–0.01	0.012–0.12
Cast Iron—Uncoated	0.00085	0.01
Galvanized Iron	0.0005	0.006
Carbon Steel	0.00015	0.0018
Fiberglass Epoxy	0.000025	0.0003
Drawn Tubing	0.000005	0.00006

*Increase by factor of 2–4 to allow for age and use.*

To explore the effect of water drive, a numerical aquifer model is connected to lower edge face of the reservoir model. See Figure 4.1 for connection between reservoir and aquifer models. A numerical aquifer is modeled by a one-dimensional row of cells. A cell or a set of cells in the simulation grid, usually inactive cell/cells, is nominated to represent the aquifer. The petrophysical properties of the aquifer are assigned to be the same as its corresponding reservoir model. The cross-sectional area of the aquifer is set to be the same as that of the lower edge face of the reservoir model. The length of the aquifer can be calculated from aquifer volume which depends on AQFRATIO setting of each experiment. Volume calculation tool in

PETREL is used to calculate reservoir volumes of in-place oil and gas cap by taking capillary effect into account. The depth of the aquifer is defined at the centroid of the aquifer volume. For gas cap modeling, a multiplier of pore volume keyword (MULTPV) is used to multiply with porosity of gas-bearing rock so that the desired MRATIO of the experiment is obtained.

After assigning all petrophysical properties to the reservoir model, a development strategy is then specified to control production operation of the well. Small simulation time steps are assigned during early production period and increased gradually to minimize running time of the simulation. However, the rate of increasing time step size is controlled to ensure that there are not any solving problems during simulation run. Given by an SME in the surveyed oil fields, limiting economic constraints shown in Table 4.5 are also specified.

Table 4.5: Economic limits and operational constraints of reservoir simulations

<b>Description</b>	<b>Economic Limit</b>
Max. water cut	0.90
Min. oil production rate (STB/day)	50
Max. GOR (MSCF/STB)	5.0
Min. tubing head pressure (psia)	114.7

In practice, in a drilling program, a few vertical/deviated wells are usually drilled at certain optimum distance apart passing through a reservoir candidate for horizontal well drilling. See Wells KPWD-11, D-12, D-13 and D-29 in Figure 4.3 for illustration. From the figure, it can be seen that the vertical wells are drilled parallel to the updip trapping fault. The purpose is to obtain more geological condition, petrophysical properties, and fluid contacts in the reservoir. After performing detailed simulation and economic analysis, the final decision whether to drill a horizontal well is made. If the analysis result indicates that production from a horizontal well is more economically viable than from the vertical wells, the horizontal well path will be designed to be parallel to the alignment of the vertical wells. However, a certain tolerance distance is maintained from the vertical wells to the horizontal well and from the horizontal well to the trapping fault to avoid collision.



According to Step 10) in Section 1.5, another proxy model for predicting URF of vertical wells is required to develop the simple screening method. Another set of experiments is thus performed by replacing a horizontal well with two vertical wells. Significant factors are varied in the same way as that of horizontal wells, i.e. same experimental designs. Note that LH in the experiments of vertical wells denotes distance between the two wells instead of horizontal length. Figure 4.4 shows the locations of the vertical wells in reservoir modeling. For well completion, the same casing and tubing sizes as those of horizontal well models are used. Perforated interval of the well is at the middle one-third of reservoir thickness according to the best practice of the fields for reservoirs having both gas cap and bottom water.

In this chapter, research methodology and reservoir simulation modeling to conduct designed experiments have been described. Experimental results, proxy model fittings and validations, and the development of a simple screening method for deciding whether to drill a horizontal well are presented in Chapter V.

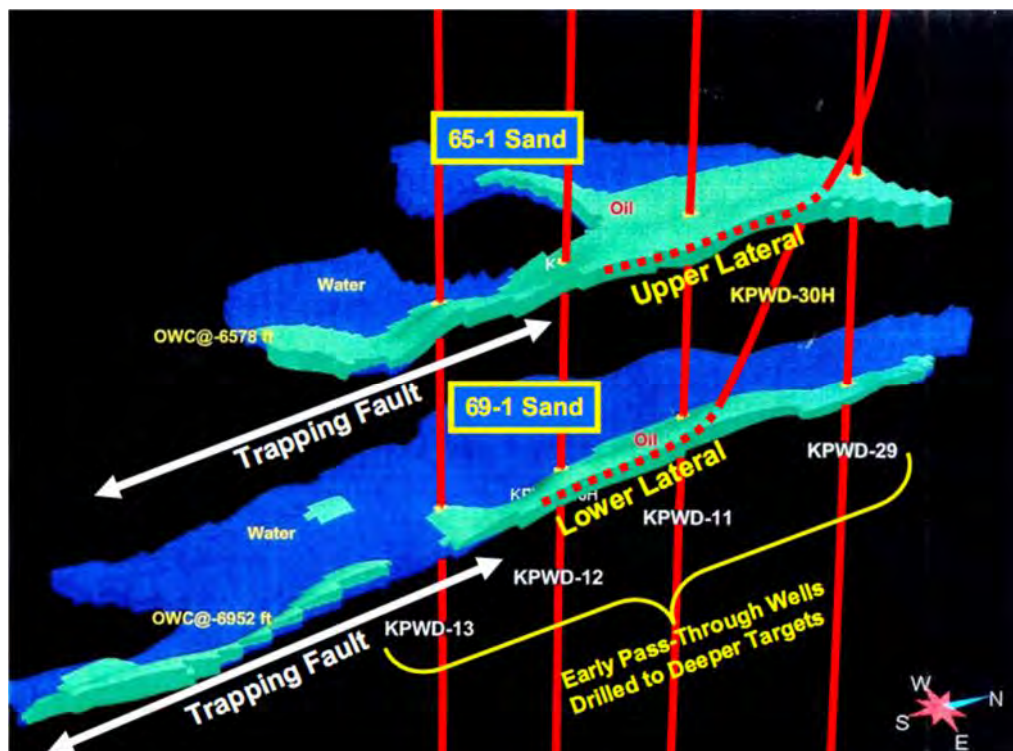


Figure 4.3: An example of typical placement of a horizontal well relative to existing vertical/deviated wells and trapping fault (After Eric et al. [1])



Figure 4.4: Locations of two vertical wells relative to a corresponding horizontal well

## CHAPTER V

### EXPERIMENTAL ANALYSES AND RESULTS

Analyses and results of designed experiments performed as described previously chapter are presented in this chapter. According to the workflow outlined in Section 1.5, the scope of this chapter covers from Step 6 to Step 11. In this chapter, a group of significant factors influencing an ultimate recovery factor of a horizontal well is identified. Proxy models predicting an ultimate recovery factor of a horizontal and two vertical wells are built with provision of its limitations of use. In the end, an application of the constructed proxy models to be used as a simple screening method for horizontal well development program is developed.

#### 5.1 Analysis and Result of Factor Screening Design

Factor screening experiments are performed to statistically screen out fewer significant factors for conducting response surface designs in the later step. 13 of the initial 48 design factors are screened out for screening experiments. According to the selected Resolution IV  $2^{13-8}$  fractional factorial design, 32 runs of reservoir simulation are carried out. The ultimate oil recovery factor obtained from each run is summarized in Table 5.1. Subsequently, statistical analysis of the experimental results is performed by using the screening platform of JMP software. The analysis result is presented in Figure 5.1.

Figure 5.1 shows contrasts or estimates of main and two-factor interaction effects. The factor effects are automatically sorted in descending order according to their absolute value by the software for the ease of comparison. To perform analysis of variance of the factor effects, Lenth's Pseudo Standard Error (Lenth PSE) is estimated. Lenth t-ratio is then calculated by dividing contrast by Lenth PSE. Consequently, calculation of individual p-value and statistical inference can be performed. As shown in Figure 5.1, the estimated Lenth PSE is 2.03684. JMP highlights that the effects of PORO, LRAT and PORO\*LRAT are statistically significant. Note that, by the default of JMP, factor effects whose individual p-value is

Table 5.1: Experimental results of Resolution IV  $2^{13-8}$  fractional factorial design for horizontal well production

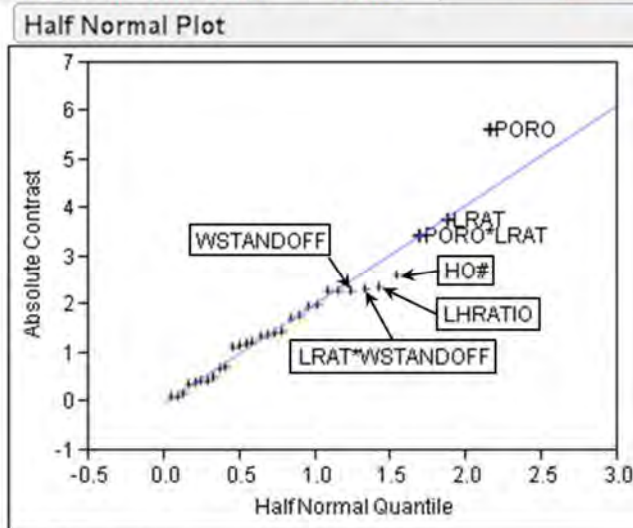
Run ID.	Design Pattern	URF (%)	Run ID.	Design Pattern	URF (%)
1	-----	0.000	17	+----+----++-	0.006
2	-----+++++	0.045	18	+----+----+--	0.011
3	---++++---+	0.000	19	+---+---+----	0.000
4	---+-----+	10.181	20	+-----+----+	21.145
5	--+---+----+	16.141	21	+-----+----+	17.089
6	--+---+----+	3.192	22	+-----+----+	0.000
7	--+---+----+	0.000	23	+-----+----+	0.000
8	-----+---+	0.000	24	+-----+----+	0.002
9	+----+----++	3.644	25	+-----+----+	18.386
10	+----+----++	0.000	26	+-----+----+	0.000
11	+----+----++	0.000	27	+-----+----+	0.000
12	+----+----++	0.000	28	+-----+----+	0.004
13	+----+----++	0.000	29	+-----+----+	0.001
14	+----+----++	17.205	30	+-----+----+	17.719
15	+----+----++	1.986	31	+-----+----+	0.000
16	+----+----++	10.669	32	+-----+----+	52.497

Note: 1) "+" = high-level value and "-" = low-level value  
 2) The order of design pattern is as follows: OWC, HRES, HO#, LH, LHRATIO, RESDIP#, MRATIO, AQFRATIO, WSTANDOFF, PORO, API, ANISO#, and LRAT.

less than or equal to 0.10 are automatically highlighted. In addition, as recommended by Montgomery [54], Lenth method should be used as a supplement to the usual normal or half-normal probability plot, not a replacement. Thus, HO#, LHRATIO, LRAT\*WSTANDOFF, and WSTANDOFF should be regarded as significant effects as well.

Since the  $2^{13-8}$  fractional factorial design has Resolution IV, the estimated main effects are the actual main effects of the factors. Thus it can be concluded at this point that the main effects of PORO, LRAT, HO#, LHRATIO, and WSTANDOFF are significant. However, two-factor interaction effects of the design are aliased with each other as shown in Table 5.2. The alias patterns shown in Table 5.2 imply that;

Contrasts			Lenth t-Ratio	Individual p-Value	Simultaneous p-Value
Term	Contrast				
PORO	5.61068		2.75	0.0160*	0.2791
LRAT	3.74796		1.84	0.0741	0.7996
HO#	2.59622		1.27	0.1984	0.9943
LHRATIO	2.35672		1.16	0.2405	0.9990
WSTANDOFF	2.28727		1.12	0.2533	0.9992
OWC	1.99363		0.98	0.3140	1.0000
HRES	1.69677		0.83	0.3891	1.0000
API	1.37510		0.68	0.4922	1.0000
RESDIP#	1.10677		0.54	0.6105	1.0000
ANISO#	0.71256		0.35	0.7390	1.0000
AQFRATIO	-0.40710		-0.20	0.8476	1.0000
LH	0.09516		0.05	0.9664	1.0000
MRATIO	0.09342		0.05	0.9672	1.0000
PORO*LRAT	3.42515		1.68	0.0985	0.8876
PORO*HO#	2.27301		1.12	0.2543	0.9993
LRAT*HO#	0.41747		0.20	0.8442	1.0000
PORO*LHRATIO	2.28144		1.12	0.2535	0.9992
LRAT*LHRATIO	0.17063		0.08	0.9380	1.0000
HO#*LHRATIO	1.77236		0.87	0.3686	1.0000
PORO*WSTANDOFF	1.96280		0.96	0.3193	1.0000
LRAT*WSTANDOFF	2.31645		1.14	0.2480	0.9991
HO#*WSTANDOFF	0.67794		0.33	0.7516	1.0000
LHRATIO*WSTANDOFF	1.18204		0.58	0.5845	1.0000
HO#*OWC	0.38852		0.19	0.8540	1.0000
LHRATIO*OWC	1.13665		0.56	0.6001	1.0000
LRAT*HRES	-0.48223		-0.24	0.8210	1.0000
WSTANDOFF*HRES	1.34069		0.66	0.5288	1.0000
OWC*HRES	1.45023		0.71	0.4606	1.0000
PORO*HO#*WSTANDOFF	0.35473		0.17	0.8659	1.0000
LRAT*LHRATIO*WSTANDOFF	1.21212		0.60	0.5748	1.0000
HO#*LHRATIO*WSTANDOFF	1.41627		0.70	0.4727	1.0000



Lenth PSE=2.03684  
P-Values derived from a simulation of 10000 Lenth ratios.

Figure 5.1: Factor screening result of the  $2^{13-8}$  fraction factorial experiments for horizontal well production

Table 5.2: Aliasing of two-factor effects of  $2^{13-8}$  fractional factorial design for horizontal well production

Effects	Aliases
OWC*HRES	= LHRATIO*ANISO# = RESDIP#*MRATIO = AQFRATIO*WSTANDOFF = PORO*API
OWC*HO#	= LHRATIO*API = RESDIP#*AQFRATIO = MRATIO*WSTANDOFF = PORO*ANISO#
OWC*LH	= LHRATIO*WSTANDOFF = RESDIP#*PORO = MRATIO*API = AQFRATIO*ANISO#
OWC*LHRATIO	= HRES*ANISO# = HO#*API = LH*WSTANDOFF = RESDIP#*LRAT
OWC*RESDIP#	= HRES*MRATIO = HO#*AQFRATIO = LH*PORO = LHRATIO*LRAT
OWC*MRATIO	= HRES*RESDIP# = HO#*WSTANDOFF = LH*API = ANISO#*LRAT
OWC*AQFRATIO	= HRES*WSTANDOFF = HO#*RESDIP# = LH*ANISO# = API*LRAT
OWC*WSTANDOFF	= HRES*AQFRATIO = HO#*MRATIO = LH*LHRATIO = PORO*LRAT
OWC*PORO	= HRES*API = HO#*ANISO# = LH*RESDIP# = WSTANDOFF*LRAT
OWC*API	= HRES*PORO = HO#*LHRATIO = LH*MRATIO = AQFRATIO*LRAT
OWC*ANISO#	= HRES*LHRATIO = HO#*PORO = LH*AQFRATIO = MRATIO*LRAT
OWC*LRAT	= LHRATIO*RESDIP# = MRATIO*ANISO# = AQFRATIO*API = WSTANDOFF*PORO
HRES*HO#	= LH*LRAT = LHRATIO*PORO = RESDIP#*WSTANDOFF = MRATIO*AQFRATIO = API*ANISO#
HRES*LH	= HO#*LRAT = LHRATIO*AQFRATIO = RESDIP#*API = MRATIO*PORO = WSTANDOFF*ANISO#
HRES*LRAT	= HO#*LH = LHRATIO*MRATIO = RESDIP#*ANISO# = AQFRATIO*PORO = WSTANDOFF*API

$$\begin{aligned} \text{Apparent PORO*LRAT} &= [\text{PORO*LRAT}] = 3.42515 & (5.1) \\ &= \text{OWC*WSTANDOFF} + \text{HRES*AQFRATIO} + \\ &\quad \text{HO\#*MRATIO} + \text{LH*LHRATIO} + \text{PORO*LRAT} \end{aligned}$$

$$\begin{aligned} \text{Apparent WSTANDOFF*LRAT} &= [\text{WSTANDOFF*LRAT}] = 2.31645 & (5.2) \\ &= \text{OWC*PORO} + \text{HRES*API} + \text{HO\#*ANISO\#} + \\ &\quad \text{LH*RESDIP\#} + \text{WSTANDOFF*LRAT} \end{aligned}$$

To find out which actual interaction effect contributes most to the apparent PORO\*LRAT and WSTANDOFF\*LRAT, hierarchy principle is applied. Since PORO\*LRAT is an interaction of two significant main effects whereas OWC\*WSTANDOFF, HRES\*AQFRATIO, HO#\*MRATIO, and LH\*LHRATIO are interactions of at least one insignificant main effect. Therefore, the actual PORO\*LRAT should contribute most to the apparent PORO\*LRAT and be regarded as significant interaction. Similarly, WSTANDOFF\*LRAT is regarded as significant interaction. It is essential to note that all three-factor or higher interaction effects are assumed insignificant herein according to the principle of sparsity effects.

As a conclusion, PORO, LRAT, HO#, LHRATIO, and WSTANDOFF are the significant factors for subsequent response surface designs. Since the screening

experiments are conducted at only 2 levels of factors, the analysis of screening might miss some significant factors out if the actual response surface is highly non-linear, the sixth factor, i.e. OWC, is added into the list of significant factors to perform response surface experiments. If subsequent analysis report of the fitted proxy model confirms that the effects of OWC are not significant, it could be ensured that no significant factors are missed out. Note that the drawback of introducing extra factors is that too many response surface experiments are conducted. Therefore, the desire to accurately screen factors and the extra efforts to conduct more experiments due to the presence of insignificant factors in response surface designs should be compromised. As a result, only one extra factor is added.

## 5.2 Analyses and Results of Response Surface Designs

### 5.2.1 Central Composite Design

#### 5.2.1.1 Quadratic Proxy Fitting

After obtaining the list of significant factors, 45 runs of the popular center-faced central composite design (CCF) are then performed and their results are presented in Table 5.3. Afterwards, “Fit Model” platform of JMP is used to fit a quadratic proxy model using least square regression technique. As a result, regression coefficients of the fitted quadratic proxy model can be obtained as shown in Figure 5.2. Also shown in the figure is the test statistics for the hypothesis that each factor effect is zero. If the null hypothesis is true, it can be interpreted that the factor effect is significantly different from zero with 95% confidence (“Prob>|t|” < 0.05). For significant factor effect, JMP automatically marks “\*” at the end of each row. The quadratic proxy model can be expressed in a mathematical form as follows:

$$\sqrt{URF} = \beta_0 + \sum_{i=1}^6 \beta_i x_i + \sum_{i<j} \beta_{ij} x_i x_j + \sum_{i=1}^6 \beta_{ii} x_i^2 \quad (5.3)$$

where,

URF = ultimate oil recovery due to a horizontal well

$\beta_0$  = regression intercept in Table 5.4

- $\beta_i$  = regression coefficient of main effect  $x_i$  in Table 5.4  
 $\beta_{ij}$  = regression coefficient of interaction effect  $x_{ij}$  in Table 5.4  
 $\beta_{ii}$  = regression coefficient of quadratic effect  $x_i$  in Table 5.4

Table 5.3: Experimental results of 6-factor face-centered central composite design for horizontal well production

Run ID.	Design Pattern	URF (%)	Run ID.	Design Pattern	URF (%)
1	-----+	0.000	24	00000A	15.338
2	-----+-	0.001	25	0000A0	28.177
3	----+---	0.001	26	000A00	20.860
4	----++++	6.902	27	00A000	18.877
5	---+----	0.000	28	0A0000	22.036
6	---+-++	10.905	29	+-----	0.000
7	---+--+	0.000	30	+-----+	5.329
8	---++++-	0.009	31	+-----+	0.104
9	a00000	13.702	32	+-----+	0.001
10	-+-----	0.000	33	+-----+	0.001
11	-+-----+	7.021	34	+-----+	0.006
12	-+-----+	3.086	35	+-----+	0.006
13	-+-----+	39.904	36	+-----+	26.179
14	-+-----+	0.000	37	A00000	16.804
15	-+-----+	0.002	38	+-----+	0.000
16	-+-----+	0.004	39	+-----+	0.000
17	-+-----+	42.026	40	+-----+	0.000
18	0a0000	7.495	41	+-----+	31.140
19	00a000	6.588	42	+-----+	0.000
20	000a00	6.708	43	+-----+	10.021
21	0000a0	0.830	44	+-----+	12.137
22	00000a	0.003	45	+-----+	47.912
23	000000	15.667			

- Note: 1) "+", "0", and "-" = high-, mid-, and low-level values, respectively.  
2) "A" and "a" = high- and low-level of face-centered point.  
3) The order of design pattern is as follows: OWC, HO#, LHRATIO, WSTANDOFF, PORO, and LRAT.



Sorted Parameter Estimates					
Term	Estimate	Std Error	t Ratio		Prob> t
PORO(0.16,0.25)	1.2749017	0.189675	6.72		<.0001*
WSTANDOFF(0.16,0.76)	0.8617934	0.189675	4.54		0.0003*
LRAT(55,6000)	0.7940086	0.189675	4.19		0.0006*
HO#(3.5665,4.7002)	0.717453	0.189675	3.78		0.0015*
HO#*WSTANDOFF	0.6934978	0.195513	3.55		0.0025*
WSTANDOFF*PORO	0.4951945	0.195513	2.53		0.0215*
LRAT*LRAT	-1.654244	0.717484	-2.31		0.0340*
OWC*LHRATIO	0.4373029	0.195513	2.24		0.0390*
HO#*PORO	0.3982065	0.195513	2.04		0.0576
PORO*LRAT	0.383748	0.195513	1.96		0.0662
LHRATIO(0.1,1)	0.264288	0.189675	1.39		0.1815
LHRATIO*LRAT	0.1723013	0.195513	0.88		0.3905
PORO*PORO	-0.529676	0.717484	-0.74		0.4704
OWC*WSTANDOFF	0.1432025	0.195513	0.73		0.4739
LHRATIO*PORO	0.1279781	0.195513	0.65		0.5215
OWC(5294,3.8116.8)	0.121871	0.189675	0.64		0.5291
LHRATIO*WSTANDOFF	0.1235632	0.195513	0.63		0.5358
HO#*LRAT	-0.114485	0.195513	-0.59		0.5659
OWC*LRAT	0.0813938	0.195513	0.42		0.6824
OWC*OWC	0.261322	0.717484	0.36		0.7202
LHRATIO*LHRATIO	-0.183454	0.717484	-0.26		0.8013
HO#*HO#	0.0768426	0.717484	0.11		0.9160
WSTANDOFF*LRAT	0.0166349	0.195513	0.09		0.9332
WSTANDOFF*WSTANDOFF	-0.060491	0.717484	-0.08		0.9338
HO#*LHRATIO	0.0138226	0.195513	0.07		0.9445
OWC*PORO	-0.012406	0.195513	-0.06		0.9501
OWC*HO#	-0.000134	0.195513	-0.00		0.9995

Figure 5.2: Regression coefficient estimates of the quadratic proxy model for horizontal well production

Table 5.4: Regression coefficients of the fitted quadratic proxy model for horizontal well production

$\beta$	j	1	2	3	4	5	6	Ultimate Recovery Factor of HZ Well
i	X	[OWC]	[HO#]	[LHRATIO]	[WSTANDOFF]	[PORO]	[LRAT]	
0	Intercept	.	.	.	.	.	.	3.6682
1	[OWC]	0.2613	-0.0001	0.4373	0.1432	-0.0124	0.0814	0.1219
2	[HO#]	.	0.0768	0.0138	0.6935	0.3982	-0.1145	0.7175
3	[LHRATIO]	.	.	-0.1835	0.1236	0.1280	0.1723	0.2643
4	[WSTANDOFF]	.	.	.	-0.0605	0.4952	0.0166	0.8618
5	[PORO]	.	.	.	.	-0.5297	0.3837	1.2749
6	[LRAT]	.	.	.	.	.	-1.6542	0.7940

where,

$$\begin{aligned}
 [OWC] &= \left( \frac{OWC - 6705.55}{1411.25} \right) & [WSTANDOFF] &= \left( \frac{WSTANDOFF - 0.46}{0.3} \right) & HO\# &= \ln(HO) \\
 [HO\#] &= \left( \frac{HO\# - 4.13335}{0.56685} \right) & [PORO] &= \left( \frac{PORO - 0.205}{0.045} \right) \\
 [LHRATIO] &= \left( \frac{LHRATIO - 0.55}{0.45} \right) & [LRAT] &= \left( \frac{LRAT - 3027.5}{297.25} \right)
 \end{aligned}$$

Notice that the URF in Equation 5.3 is transformed so that the model has a better goodness-of-fit.

Figure 5.3 shows statistical analysis results of the fitted model. In the figure, actual by predicted plot graphically shows model goodness-of-fit. If the model can perfectly fit to responses of the design points, all data points will align on the 45-degree straight line. Therefore, it is clearly seen from the figure that the model can fit the predicted URF well when the predicted URF < 20% and shows high variance at the higher URF. This is the reason why  $R^2_{adj}$  is only 0.754 in the summary of fit. The analysis of variance shown confirms that the model can be used to significantly explain variance of the URF over design hyperspace. Validity check of the fitted model can be done by investigating residual by predicted plot in Figure 5.4. Figure 5.4 reveals that residual of the predicted URF randomly distribute at all values of predicted URF. Thus, the proxy is properly fitted to the responses by complying with a statistical assumption of random error.

The optimum factor setting of the quadratic proxy model to obtain the maximum URF can be found using an optimizer, called Prediction Profiler, of JMP. To be able to show a response surface in hyperspace on 2D plane, the profiler presents

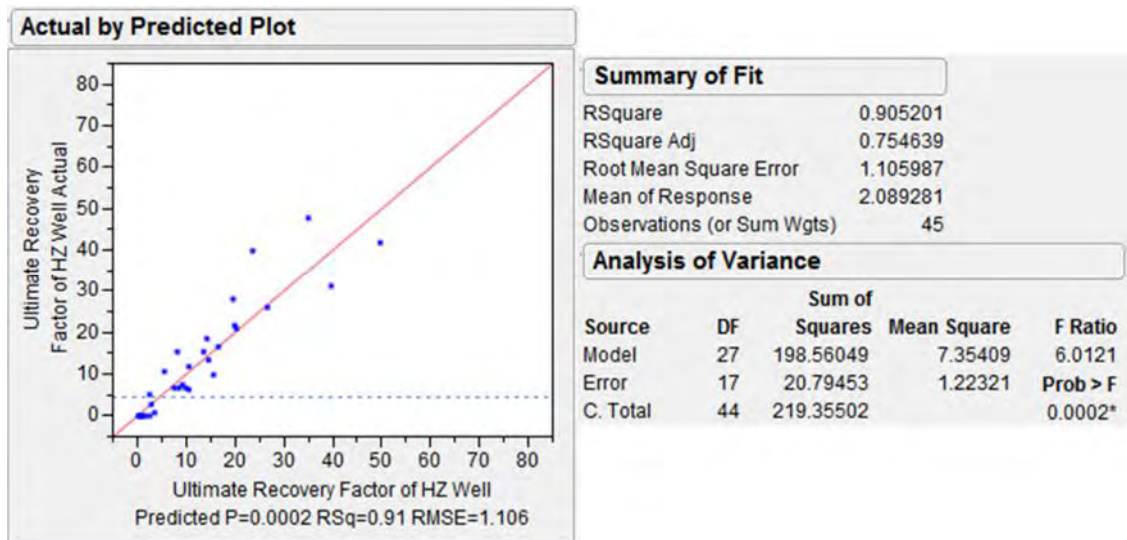


Figure 5.3: Actual by predicted plot and statistical analyses of the quadratic proxy for horizontal well production

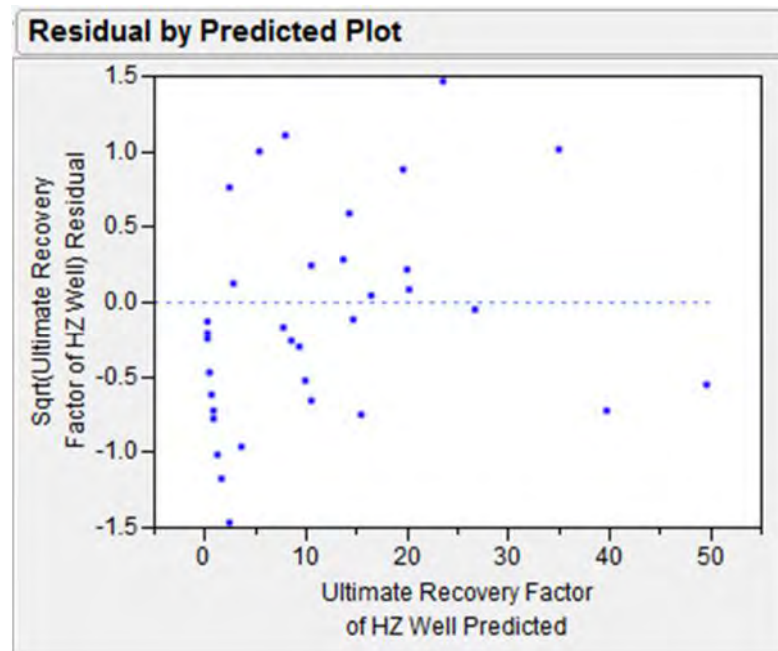


Figure 5.4: Residual by predicted plot of the fitted quadratic proxy model for horizontal well production

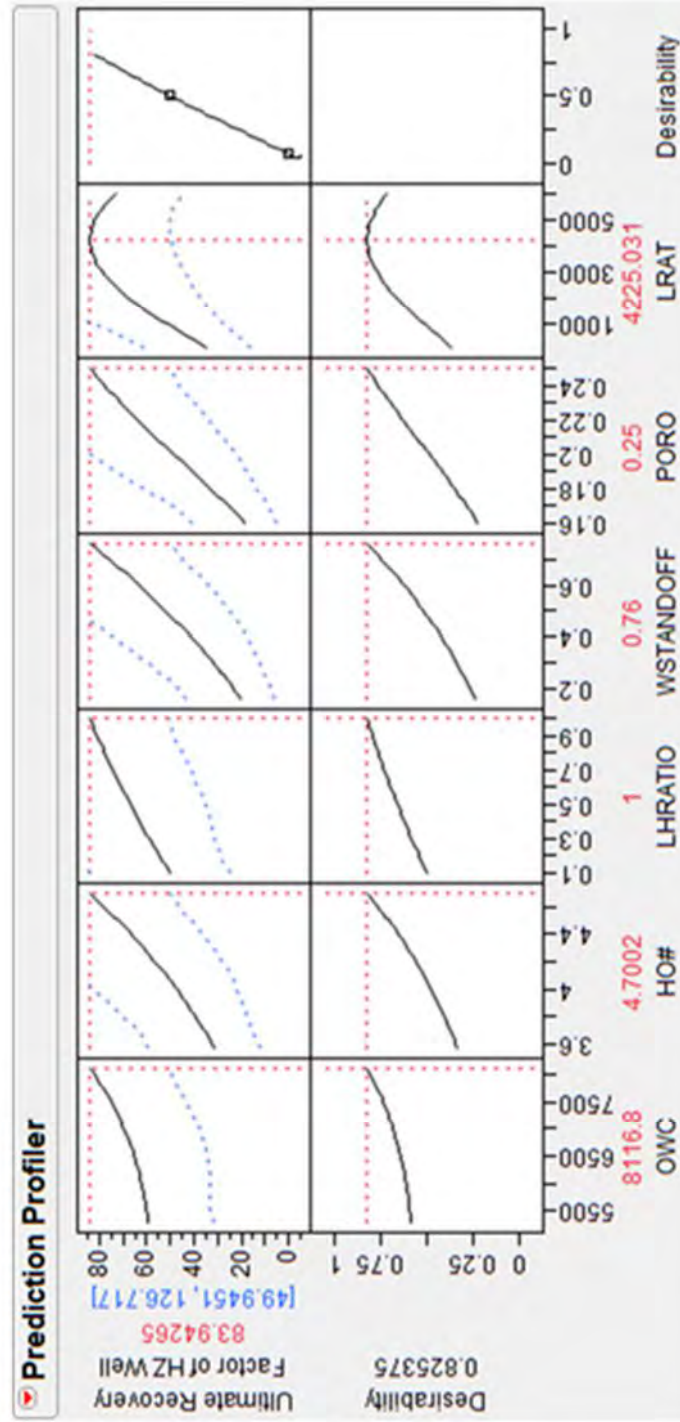


Figure 5.5: JMP prediction profiler shows optimum factor setting of the quadratic proxy model for horizontal well production

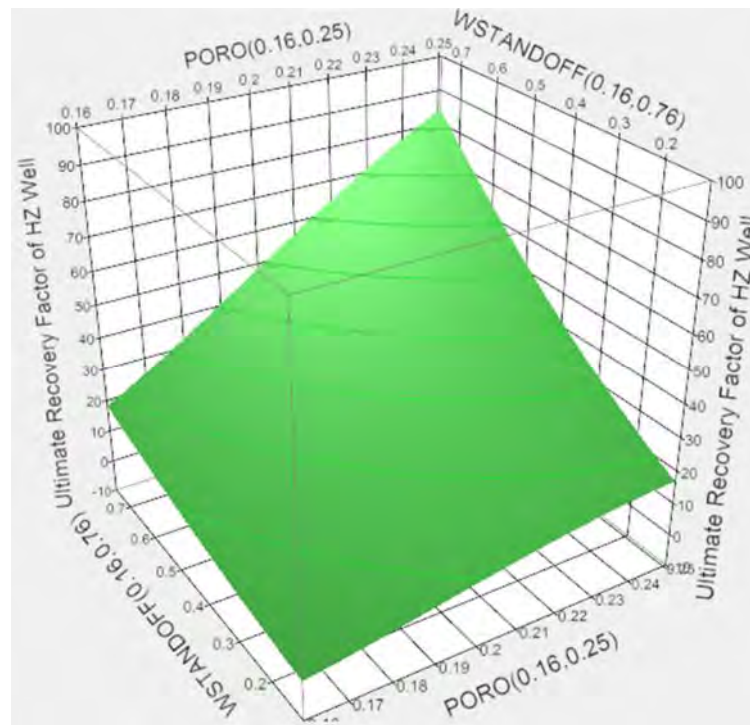


Figure 5.6: 3D surface plot at the optimum setting of the quadratic proxy for horizontal well production

the fitted surface in the form of plots between each factor level and the predicted response. In other words, the profiler shows how the fitted surface looks like when it is sliced along each factor axis at the location of a design point of interest in hyperspace. Factor setting of the design point of interest is displayed above the name of each design factor. The corresponding predicted response is displayed on the right of response factor name.

Figure 5.5 shows prediction profiler of the fitted quadratic proxy model with its optimum factor setting. From the figure, it can be seen that the predicted URF increases as level of each factor increases except for LRAT which shows an optimum setting at 4225.03 STB/day. At the optimum design point, the predicted maximum URF of the proxy model is 83.94%. When compared with the actual URF of 52.5% of Run ID 32 in Table 5.1 whose design point is close to the predicted optimum design point, the proxy model seems to significantly over-predict the URF. This observation is supported by the 3D response surface plot in Figure 5.6. From the figure, it is clearly seen that the quadratic proxy predicts rapid increment in URF as PORO and

WSTANDOFF increase. Moreover, the 3D surface shows low degree of non-linearity of the fitted response surface inside the design space.

### 5.2.1.2 Cross-Validation of Quadratic Proxy Model

In the previous section, the proxy model is checked for goodness of model fitting and it is shown that the fitting quality is reasonably acceptable. However, it should be highlighted that the checking is performed between responses from design points used to construct the model and the predicted responses from the model. Therefore, a cross-validation of the model predictability at different locations in design hyperspace is required.

The first cross-validation experiments are carried out as described in Section 4.5. The obtained experimental results are presented in Table 5.5. To have an objective conclusion, a matched pairs t-test between predicted URF and actual URF from the cross-validation experiments is performed. The analysis result of the t-test can be seen in Figure 5.7. Figure 5.7 plots differences between predicted and actual URFs on the vertical axis, and mean of the predicted and actual URFs on the horizontal axis. The vertical cross-hair line represents mean mean of the predicted and actual URFs. The horizontal cross-hair line represents mean difference between predicted and actual URFs. The horizontal dotted lines next to the mean difference line show 95% confidence interval boundary. Graphically, if the horizontal axis falls into the 95% confidence interval boundary, it can be interpreted that means of predicted and actual URFs are not statistically different with 95% confidence.

Interpretation of the plot in Figure 5.7 reveals that mean of URFs predicted by the quadratic proxy is statistically different from the cross-validation ones. The interpretation is confirmed by the t-test result, i.e. “Prob<t” < 0.05, at the bottom of the figure. Furthermore, at a mean of mean value greater than about 15%, the proxy model tends to yield significant under-prediction.

Thus, it can be concluded that the quadratic proxy cannot adequately fit the actual surface response of ultimate oil recovery of a horizontal well in a thin-oil-column reservoir in the Gulf of Thailand. Another response surface model which is more capable of fitting higher degree of non-linearity is required.

Table 5.5: Experimental results of the first 18-run maximum entropy design for validating the proxy model for horizontal well production

<b>Run ID.</b>	<b>OWC</b>	<b>HO#</b>	<b>LHRATIO</b>	<b>WSTANDOFF</b>	<b>PORO</b>	<b>LRAT</b>	<b>URF (%)</b>
101	7959.99	3.755	0.950	0.293	0.165	55.0	0.000
102	7332.77	4.259	0.100	0.160	0.185	5339.4	3.023
103	7803.19	4.322	0.800	0.493	0.180	5009.2	16.152
104	6548.74	4.700	0.450	0.160	0.210	4348.6	12.734
105	6705.55	3.692	0.650	0.660	0.230	1376.1	25.821
106	6548.74	4.133	0.200	0.627	0.180	3027.5	4.767
107	6548.74	4.259	0.900	0.160	0.225	2036.7	9.226
108	6391.94	3.567	0.350	0.393	0.235	4678.9	10.335
109	5451.11	3.944	0.100	0.360	0.200	2697.2	3.257
110	5294.30	4.385	0.150	0.493	0.170	5669.7	1.809
111	5764.72	4.196	0.450	0.327	0.245	2036.7	26.356
112	6078.33	3.755	0.900	0.727	0.160	3688.1	0.548
113	8116.80	4.574	0.250	0.293	0.230	3027.5	24.888
114	5294.30	4.511	0.850	0.527	0.235	2697.2	26.530
115	6862.36	4.385	0.400	0.693	0.220	1045.8	30.772
116	5294.30	3.692	0.650	0.260	0.185	385.3	0.000
117	6705.55	3.818	0.700	0.327	0.165	2366.9	0.000
118	6862.36	4.385	0.800	0.560	0.160	715.6	2.941

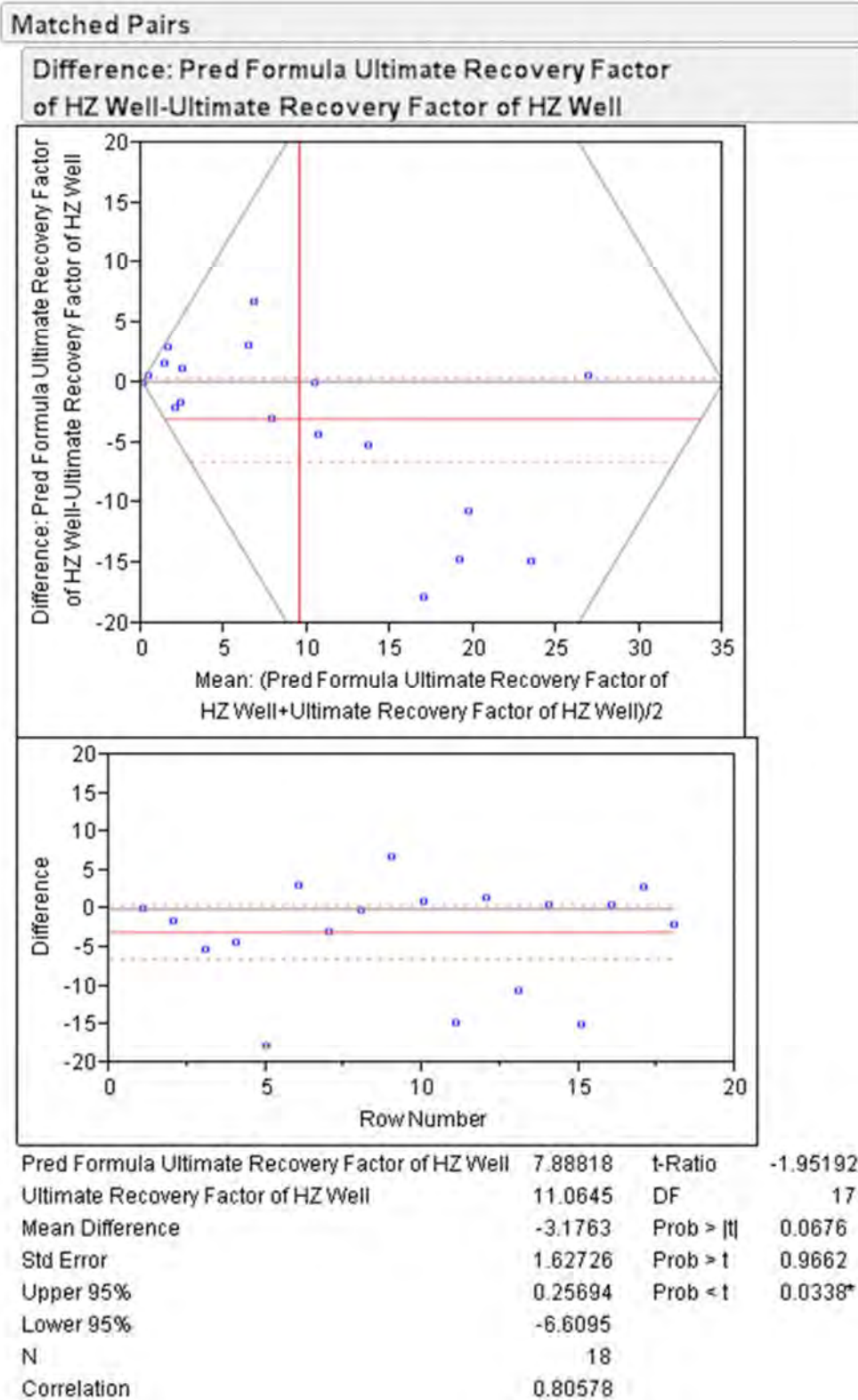


Figure 5.7: Matched pairs t-test for validating the quadratic proxy for horizontal well production



## 5.2.2 Space-Filling Design: Maximum Entropy

### 5.2.2.1 Gaussian Process Proxy Fitting

The results of the maximum entropy designed experiments described in Section 4.4 are tabulated in Table 5.6. JMP Gaussian Process platform is used for analyzing and fitting Gaussian process proxy model of the experimental results. The analysis results reported by JMP can be seen from Table 5.7 and Figures 5.8 to 5.11. Table 5.7 presents report of Gaussian process model of the maximum entropy experiments. In the table, the estimates of main and interaction effects are reported together with total sensitivity and model parameter estimates. In this report, the reported factor effect is (Functional factor effect)/(Total variation). Functional factor effect is the integrated total variation due to that effect alone while total variation is the integrated variability over the entire experimental space. The amount of influence a factor and its two-factor interactions have on the response, i.e. URF, is the total sensitivity of that factor. Thus, it is shown in Table 5.7 that PORO has 70.6% influence, the highest, on the URF followed by WSTANDOFF, LHRATIO, HO#, and OWC, accordingly. However, LRAT is reported to have no influence on URF at all.

From the estimated model parameters,  $\theta$ ,  $\mu$ ,  $\sigma^2$ , the fitted Gaussian process proxy model can be mathematically expressed as shown in Equations 5.4. Note that the minimum allowable URF predicted by the proxy model is limited to zero in Equation 5.4.

Table 5.6: Experimental results of 6-factor, 45-run maximum entropy design for horizontal well production

Run ID.	OWC	HO#	LHRATIO	WSTANDOFF	PORO	LRAT	URF (%)
301	7301.41	3.567	0.380	0.240	0.240	2697.2	13.779
302	6360.58	4.171	0.180	0.360	0.160	2565.1	0.001
303	7175.97	3.692	0.820	0.400	0.174	2697.2	2.289
304	5294.30	3.818	0.940	0.307	0.236	5735.8	14.922
305	5796.08	4.473	0.980	0.320	0.224	4414.7	15.999
306	7426.86	4.322	0.940	0.427	0.246	715.6	27.280
307	5294.30	3.995	0.640	0.387	0.160	55.0	0.000

Table 5.6: Experimental results of 6-factor, 45-run maximum entropy design for horizontal well production (Continued)

Run ID.	OWC	HO#	LHRATIO	WSTANDOFF	PORO	LRAT	URF (%)
308	6276.04	3.793	0.687	0.360	0.190	55.0	0.003
309	7991.36	4.675	0.280	0.440	0.220	4578.4	25.925
310	5482.47	4.599	0.600	0.213	0.164	3225.7	0.000
311	7928.63	4.222	0.540	0.587	0.234	4150.4	26.682
312	5482.47	4.448	0.120	0.320	0.206	2036.7	8.454
313	6297.86	4.247	0.620	0.413	0.206	1993.6	24.263
314	5796.08	4.297	0.420	0.160	0.212	3754.1	11.562
315	7489.58	4.020	0.320	0.421	0.194	847.7	11.980
316	5984.24	4.574	0.420	0.400	0.160	847.7	1.048
317	5607.91	3.617	0.760	0.160	0.200	2036.7	0.000
318	7928.63	4.322	0.440	0.293	0.162	2433.0	1.194
319	7050.52	4.222	0.360	0.760	0.188	55.0	0.002
320	5294.30	4.133	0.160	0.613	0.204	3357.8	7.829
321	7238.69	3.894	0.740	0.173	0.164	4943.1	0.000
322	5921.52	4.675	0.100	0.520	0.188	3357.8	3.236
323	7113.24	4.010	0.220	0.693	0.160	4546.8	0.999
324	7748.65	4.549	0.300	0.160	0.198	55.0	0.000
325	7050.52	3.567	0.780	0.533	0.214	2168.8	16.347
326	7050.52	3.642	0.260	0.627	0.186	2697.2	3.660
327	6736.91	4.196	0.880	0.173	0.224	2961.4	12.035
328	6548.74	3.567	0.380	0.627	0.250	5867.9	20.574
329	7426.86	3.692	0.260	0.467	0.234	319.2	15.691
330	5294.30	3.692	0.520	0.320	0.228	4414.7	11.113
331	6705.55	4.257	0.433	0.160	0.178	55.0	0.000
332	5733.36	3.970	0.660	0.680	0.246	5339.4	27.898
333	6486.02	4.448	0.560	0.547	0.164	4150.4	4.358
334	7135.06	4.574	0.280	0.317	0.208	2565.1	17.997
335	7994.08	4.020	0.100	0.267	0.210	3225.7	5.988
336	6172.41	4.096	0.120	0.440	0.232	5867.9	10.859
337	7113.24	4.096	0.300	0.307	0.210	5471.6	13.563
338	7740.47	4.599	0.880	0.707	0.186	5735.8	18.809
339	6674.19	4.524	0.980	0.707	0.160	715.6	6.172
340	7865.91	4.574	0.960	0.653	0.214	583.4	33.355
341	6674.19	3.768	0.760	0.360	0.236	4018.3	17.492
342	5482.47	3.869	0.100	0.520	0.224	1244.0	8.332
343	5357.02	3.642	0.840	0.653	0.212	3489.9	15.507
344	6109.69	3.739	0.180	0.160	0.236	2300.9	8.020
345	5733.36	3.617	0.800	0.640	0.174	1508.2	2.174

Table 5.7: JMP model report of the Gaussian process proxy model for horizontal well production

<b>Model Report</b>												
Column	Theta	Sensitivity	Total	Main Effect	OWC	HO#	LHRATIO	WSTANDOFF	PORO	LRAT	Interaction	Interaction
OWC	1.267e-8	0.0138269	0.0116042	0.000015	0.0001294	0.0008343	0.001244	0.0001294	0.0008343	0.001244	0	0
HO#	0.4220006	0.0943928	0.0574185	0.000015	0.0001294	0.002827	0.0263857	0.0077465	0.002827	0.0263857	0	0
LHRATIO	1.6356843	0.1117901	0.062742	0.0001294	0.0008343	0.0182312	0.022941	0.0077465	0.0182312	0.022941	0	0
WSTANDOFF	5.5540543	0.1666999	0.1208703	0.0008343	0.002827	0.0182312	0.0239371	0.002827	0.0182312	0.0239371	0	0
PORO	1751.5893	0.7060463	0.6315384	0.001244	0.002827	0.0239371	0	0.001244	0.0239371	0	0	0
LRAT	0	0	0	0	0	0	0	0	0	0	0	0
	$\mu$											
	7.8526797	91.907449										
	$\sigma^2$											
	-2*LogLikelihood											
	274.45755											

Fit using the Gaussian correlation function.

$$URF = \begin{cases} 0, & [URF] < 0 \\ [URF], & [URF] \geq 0 \end{cases} \quad (5.4)$$

where,

- URF = ultimate oil recovery due to a horizontal well
- $[URF] = \mu + [R]_{1 \times j} [\beta_j]_{j \times 1}$
- $\mu = 7.8527$
- $[R]_{1 \times j} = [ \text{Exp}(\sum_{j=1}^j \sum_{k=1}^k \theta_k (x_k - x_k^j)^2) ]$
- k = total number of design factors = 6
- $x_k$  =  $k^{\text{th}}$  design factor. See Table 5.8
- $x_k^j$  = level setting of Design factor  $x_k$  of the design point of Run ID. (300+j) in Table 5.6
- j = total number of design points = 45
- $\theta_k$  = Fitted model parameter of Design factor  $x_k$ . See Table 5.8
- $[\beta_j]_{j \times 1}$  = regression coefficient corresponding to  $j^{\text{th}}$  design point. See Table 5.9

As a supplement to the model report, JMP marginal model plots graphically show the average value of each factor across all other factors. A change in the average values due to a change in one factor could be envisaged as the main effect of that factor. Marginal model plots of the Gaussian process proxy in Figure 5.8 show some conclusions similar to that of the quadratic proxy model. On average, URF increases as OWC, HO#, or PORO increases whereas PORO has the greatest influence on the URF because of its greatest increasing trend. However, the average of LHRATIO and WSTANDOFF shows convex trend as the factor level increases. Moreover, LRAT does not affect URF at all. The cause of these differences could be revealed by investigating goodness-of-fit analysis and model validity check.

The actual by jackknife predicted plot shown in Figure 5.9 plots the actual URFs on the vertical axis and the jackknife predicted values on the horizontal axis. This type of plot is one useful measure of goodness-of-fit of a model which exactly fits responses of design points. Similar to the plot in Figure 5.3, the objective of this

Table 5.8: Theta regression coefficients of the Gaussian process proxy for horizontal well production

k	1	2	3	4	5	6
$x_k$	OWC	HO#	LHRATIO	WSTANDOFF	PORO	LRAT
$\theta_k$	1.267E-08	0.4220	1.6357	5.5541	1751.59	0.00

Table 5.9:  $\beta_j$  regression coefficients of the Gaussian process proxy for horizontal well production

j	$\beta_j$	j	$\beta_j$	j	$\beta_j$	j	$\beta_j$
1	14.67667	13	44.53645	24	-54.37531	35	-0.801296
2	-8.117091	14	37.69997	25	-4.01689	36	-33.48179
3	28.15762	15	86.79344	26	8.746887	37	-63.08974
4	24.09221	16	2.961039	27	-0.120426	38	25.50667
5	-25.18994	17	12.7904	28	-11.51445	39	-8.113582
6	20.94334	18	-5.110951	29	38.09013	40	17.37488
7	-7.254986	19	-35.57995	30	-3.11339	41	-40.88303
8	-88.46217	20	-18.04062	31	22.76275	42	-1.170111
9	23.51438	21	-9.333644	32	20.77859	43	-5.050839
10	-6.85406	22	-15.84103	33	14.64843	44	-7.695652
11	-2.075494	23	-3.871208	34	41.48849	45	-8.339818
12	-18.06491						

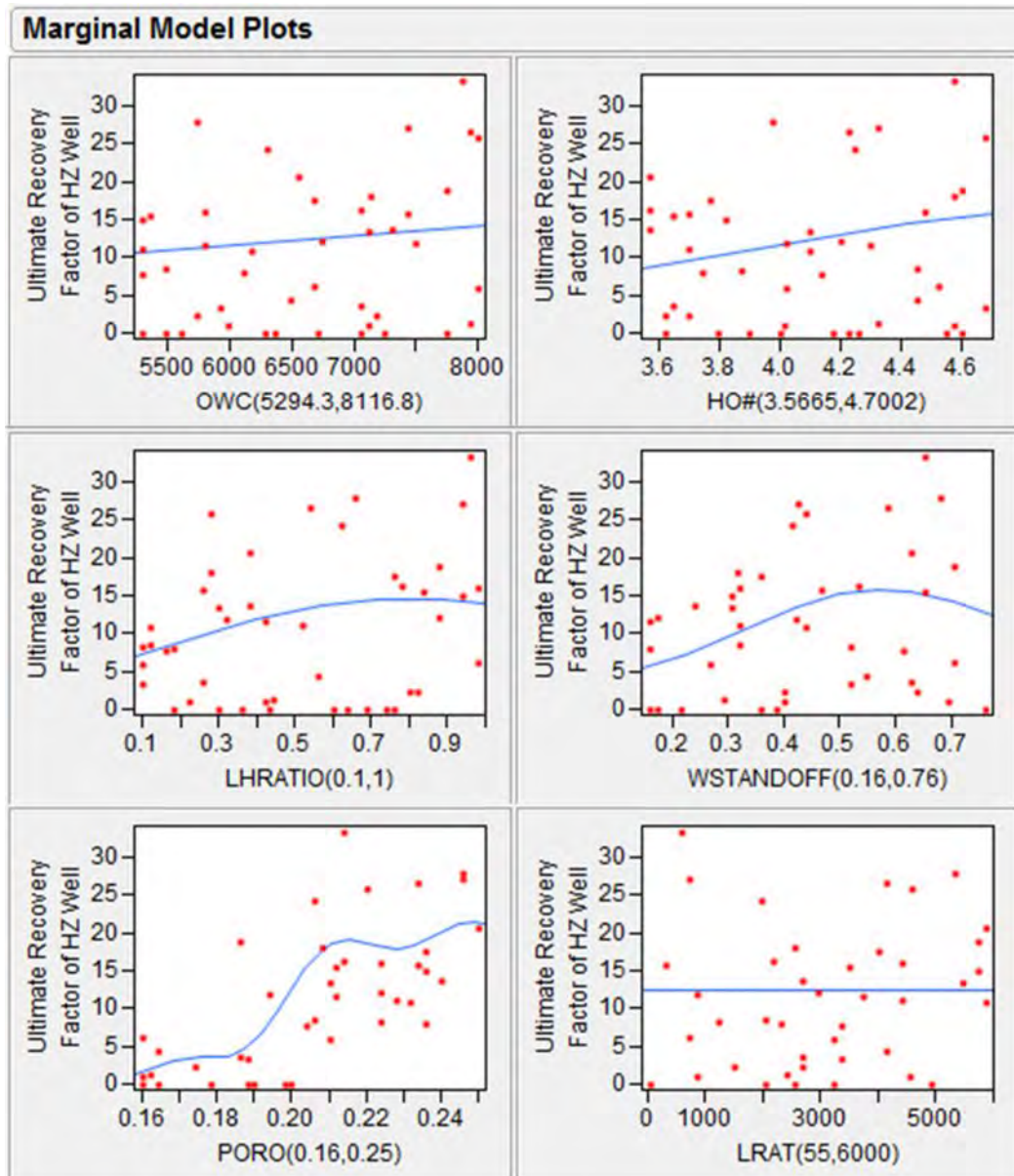


Figure 5.8: JMP marginal model plots of the Gaussian process proxy model for horizontal well production

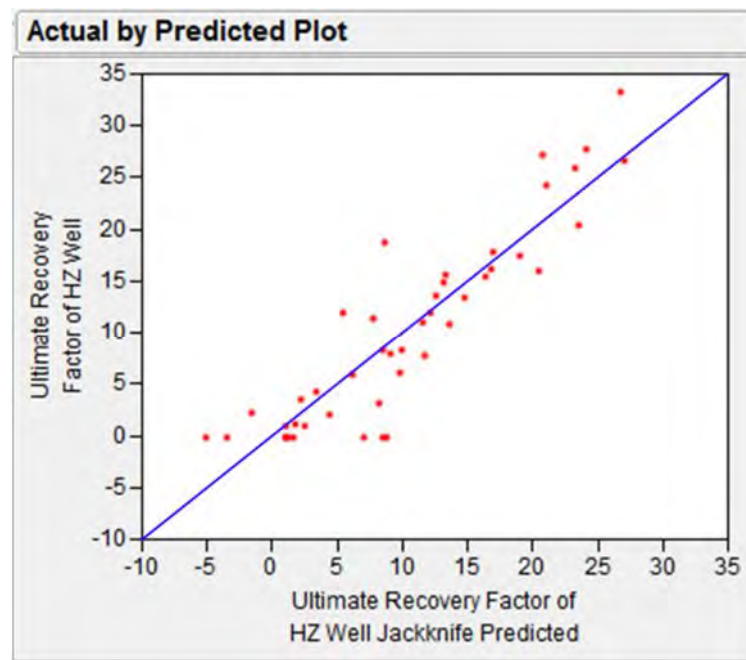


Figure 5.9: Actual by jackknife predicted plot of the Gaussian process proxy for horizontal well production

method is determining how well the points lie along the 45 degree diagonal line [64]. So, it can be seen from Figure 5.9 that in general the proxy model fits the data points well except for the actual URF at 0% which has relatively high variance.

The prediction profiler in Figure 5.10 shows that the predicted optimum factor setting of the Gaussian process proxy shifts closer to the inner side of the design hyperspace when compared with that of the quadratic proxy model. Besides, at a significantly different design point, the predicted maximum URF of only 38.33% is much lower than that of the quadratic model and the actual URF of Run ID 32 in Table 5.1.

In contrast to the quadratic proxy, the 3D surface plot of the fitted Gaussian process model in Figure 5.11 shows high non-linearity inside the design space. The difference in the fitted response surface of the two proxy models can be explained by observing Figure 5.12. An observation on Figure 5.12 shows that, with the same number of runs, most of design points of central composite design are distributed at the boundary of the design hyperspace while there is only one design point at the center of design hyperspace. Besides, the capability of the quadratic proxy model on

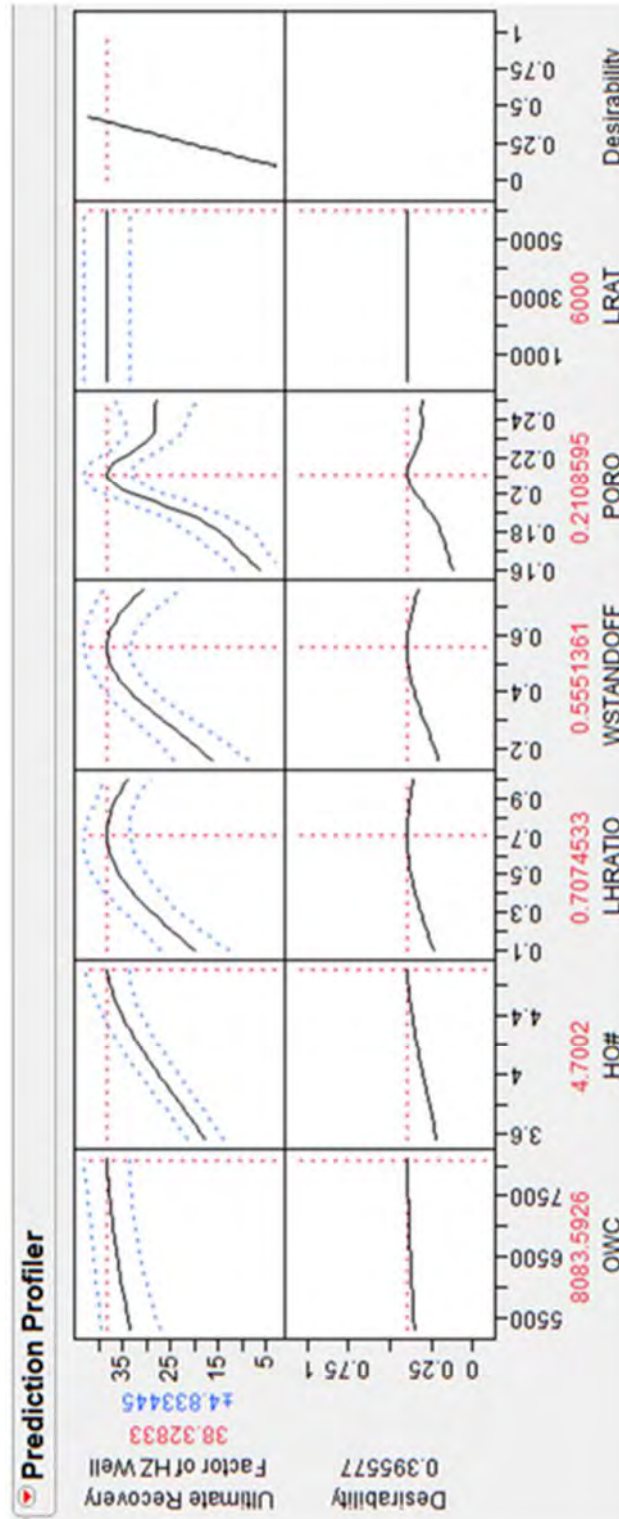


Figure 5.10: JMP prediction profiler showing optimum factor setting of the Gaussian process proxy model for horizontal well production



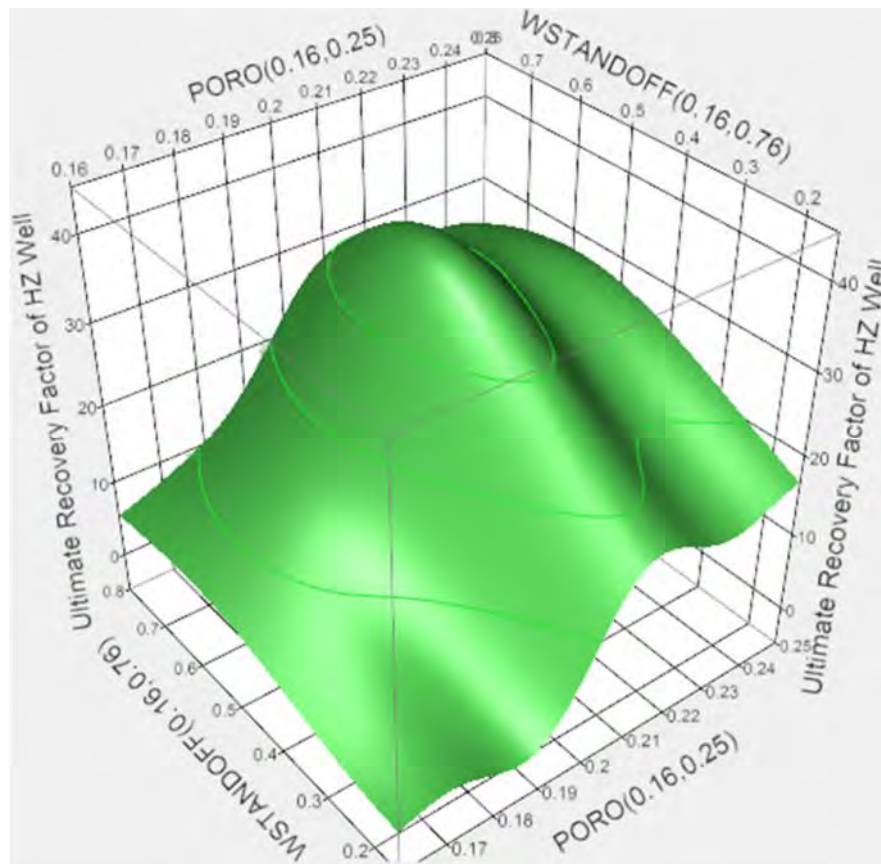


Figure 5.11: 3D surface plot at optimum factor setting of the Gaussian process proxy model for horizontal well production

fitting non-linearity of the actual response surface is limited by the quadratic terms of the model. Therefore, these reasons explain why the quadratic model highly over-predicts URF at a certain design region, i.e. at the design point of Run ID 32 in Table 5.1, while it significantly under-predicts URF at a certain design region. See Figure 5.7.

For the maximum entropy design, its design points are intended to spread inside the design region, so relatively fewer design points are at the boundary of the design hyperspace. This explains why the Gaussian process proxy model can describe non-linearity of the actual response surface inside the design hyperspace better than the quadratic model. However, the prediction near to the space boundary seems to be quite poor because Gaussian process interpolation method is poor in extrapolating responses outside its data points.

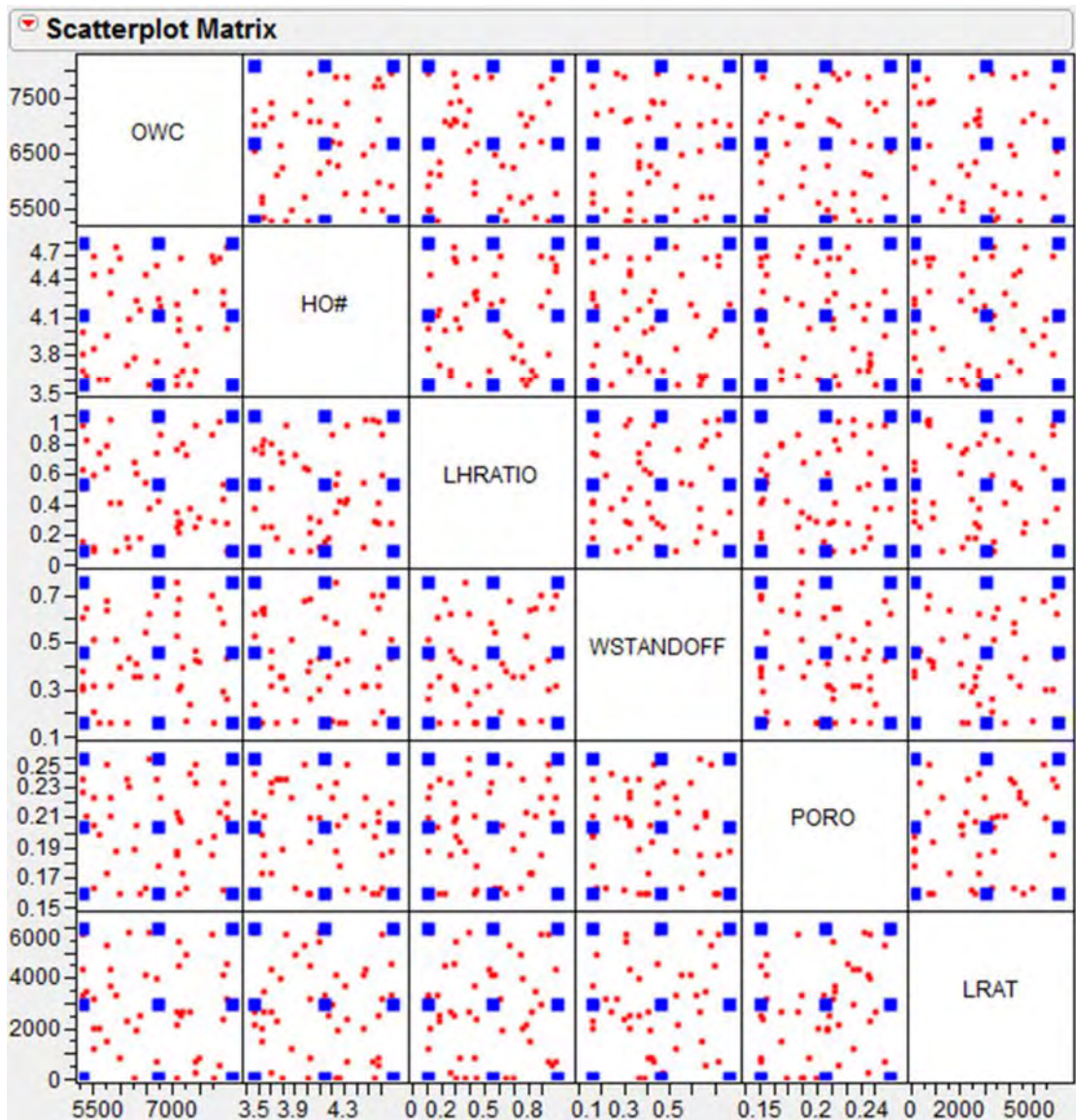


Figure 5.12: Scatter plots of design points of the 45-run central composite design (square points) and the 45-run maximum entropy design (circular points)

### 5.2.2.2 Cross-Validation of Gaussian Process Proxy Model

The Gaussian process proxy is validated against the same cross-validating experiments as the quadratic proxy model. See Section 5.2.1.2. JMP analysis result of a matched pairs t-test of the Gaussian process proxy is presented in Figure 5.13. From the figure, it can be observed that the horizontal axis of the plots is within the 95% confidence interval boundary. All of “Prob>|t|”, “Prob>t”, and Prob<t” are greater than a p-value of 0.05. Thus, it can be concluded that on average URFs predicted by the Gaussian process proxy model is not significantly different from the actual URF. In other words, the difference will be within a range of -3.3576 to 0.71756 with 95% confidence level. In addition, comparison between the plots in Figures 5.7 and 5.13 indicates that the Gaussian process proxy can predict URFs with significantly less variance than the quadratic proxy model. As it can be seen in Figure 5.7, the standard error (a variant of variance) and the maximum difference of 1.627 and -17.8 are much greater than the ones of 0.966 and -9.1 of the Gaussian process proxy shown in Figure 5.13.

In conclusion, on average the Gaussian process proxy can predict the URF without significant difference from the actual one. Its prediction variance is significantly smaller than that of the quadratic model. These could be attributed to the capability of Gaussian process method which can model non-linearity of the actual response surface within design hyperspace better than quadratic model.

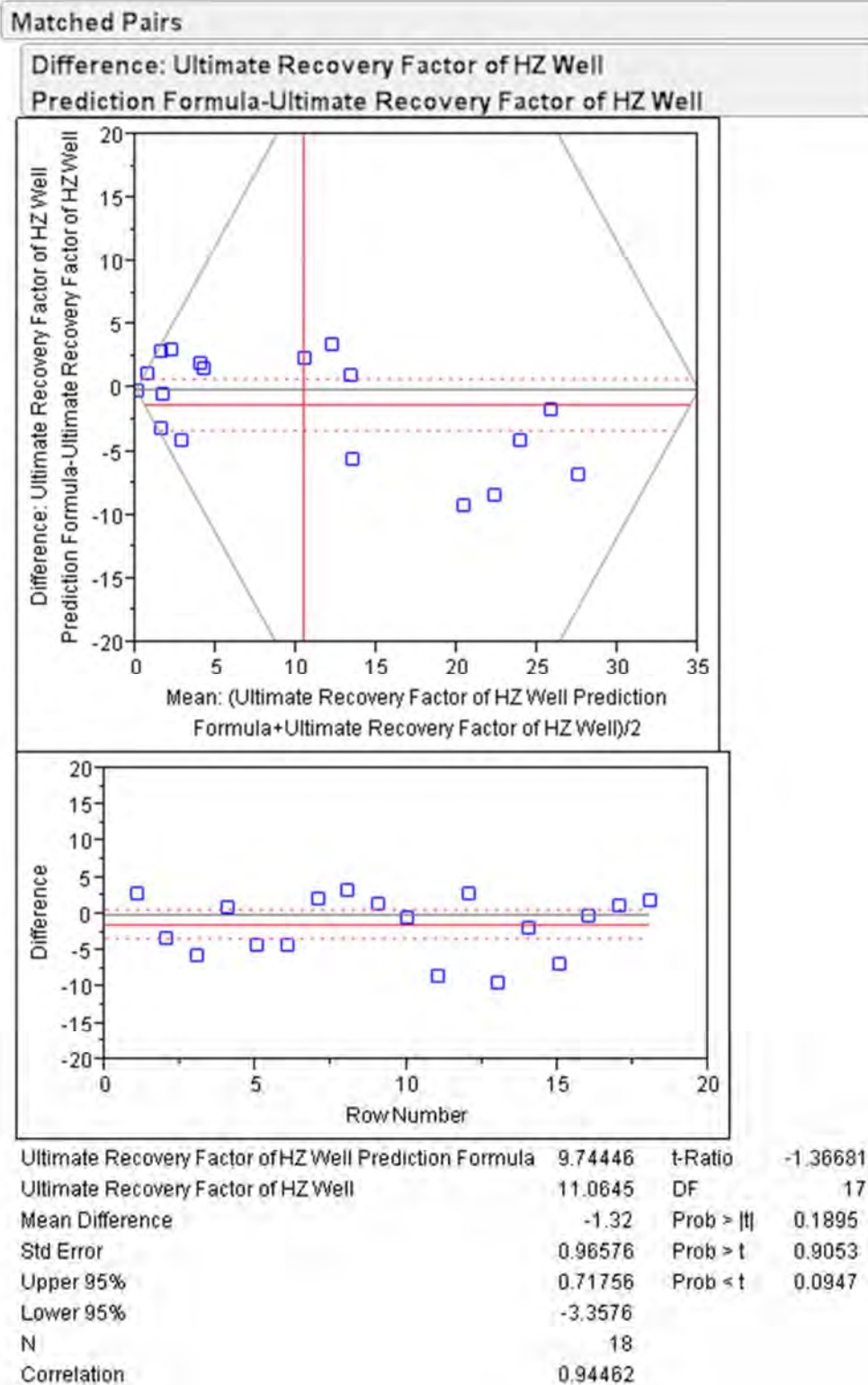


Figure 5.13: Matched pairs t-test for validating the Gaussian process proxy model for horizontal well production

## 5.2.3 Combined Central Composite and Maximum Entropy Design

### 5.2.3.1 Design-Combined Proxy Fitting

To improve predictability of the Gaussian process proxy, experimental results of the central composite design are combined with those of the maximum entropy design. This combination strategy stems from the finding that the Gaussian process model fitted from the maximum entropy design is poor in predicting URF near the boundary of the design hyperspace whereas majority of design points of the central composite designs are at the boundary. Therefore, if design points and experimental results of these two designs are combined and fitted using Gaussian process method, a more efficient proxy model should be obtained.

Consequently, the experimental design points and their results in Table 5.3 and 5.6 are combined. Gaussian Process platform of JMP is used to perform statistical analyses and fits a new Gaussian process proxy model. The obtained Gaussian process proxy model is called herein “design-combined Gaussian process proxy”. Table 5.10 presents estimates of factor effects and model parameters of the design-combined proxy. The estimated total sensitivities reveal that PORO and WSTANDOFF are still the first and second most influence factors. HO# and LRAT are ranked as the third and fourth places, but their values are quite close to WSTANDOFF. LHRATIO and OWC are ranked as the fifth and the last places, respectively.

It should be recalled that OWC is the extra design factor added to prevent misinterpretation of factor screening result as discussed in Section 5.1. The estimated total sensitivity of only about 2.067% of OWC confirms that all significant factors are completely screened out. Although OWC seems to be insignificant, its terms in the design-combined proxy are not removed because fewer degree of freedom of the proxy model could cause less prediction accuracy. Based on the estimated model parameters, the design-combined proxy model can be mathematically expressed as shown in Equation 5.5.

Table 5.10: JMP model report of the design-combined Gaussian process proxy for horizontal well production

<b>Model Report</b>																
Column	Theta	Total			OWC		HO#		LHRATIO		WSTANDOFF		PORO		LRAT	
		Sensitivity	Main Effect	Interaction	Interaction	Interaction	Interaction	Interaction	Interaction	Interaction	Interaction	Interaction	Interaction	Interaction	Interaction	Interaction
OWC	1.1763e-8	0.0206683	0.0145097				7.2544e-5		0.0002201		0.0003745		0.0018249		0.0036667	
HO#	0.8285008	0.1508914	0.1163183	7.2544e-5					0.0013159		0.0150981		0.0120219		0.0060646	
LHRATIO	0.4335244	0.0654019	0.0462833	0.0002201			0.0013159				0.0103199		0.0030581		0.0042045	
WSTANDOFF	5.8414367	0.1587521	0.1021529	0.0003745			0.0150981		0.0103199				0.0222187		0.008588	
PORO	214.11848	0.5378685	0.4871449	0.0018249			0.0120219		0.0030581		0.0222187				0.0116	
LRAT	1.7905e-7	0.1210191	0.0868952	0.0036667			0.0060646		0.0042045		0.008588		0.0116			
$\mu$																
$\sigma^2$																
5.4068878	147.90589															
-2*LogLikelihood																
587.74976																

Fit using the Gaussian correlation function.

$$URF = \begin{cases} 0, & [URF] < 0 \\ [URF], & [URF] \geq 0 \end{cases} \quad (5.5)$$

where,

- URF = ultimate oil recovery due to a horizontal well
- $[URF] = \mu + [R]_{1xi} [\beta_j]_{ix1} + [R]_{1xj} [\beta_j]_{jx1}$
- $\mu = 5.4069$
- $[R]_{1xi} = [ \text{Exp}(\sum_{i=1}^i \sum_{k=1}^k \theta_k (x_k - x_k^i)^2) ]$
- $[R]_{1xj} = [ \text{Exp}(\sum_{j=1}^j \sum_{k=1}^k \theta_k (x_k - x_k^j)^2) ]$
- k = total number of design factors = 6
- $x_k$  =  $k^{\text{th}}$  design factor. See Table 5.11
- $x_k^i$  = level setting of Design factor  $x_k$  of the design point of Run ID. “i” in Table 5.6
- $x_k^j$  = level setting of Design factor  $x_k$  of the design point of Run ID. “300+j” in Table 5.3
- i = total number of design points of maximum entropy design = 45
- j = total number of design points of central composite design = 45
- $\theta_k$  = fitted model parameter of Design factor  $x_k$ . See Table 5.11
- $[\beta_i]_{ix1}$  = regression coefficient corresponding to  $i^{\text{th}}$  design point. See Table 5.12
- $[\beta_j]_{jx1}$  = regression coefficient corresponding to  $j^{\text{th}}$  design point. See Table 5.13

Table 5.11: Theta regression coefficients of the design-combined Gaussian process proxy for horizontal well production

k	1	2	3	4	5	6
$x_k$	OWC	HO#	LHRATIO	WSTANDOFF	PORO	LRAT
$\theta_k$	1.176E-08	0.8285	0.4335	5.8414	214.12	1.79E-07

Table 5.12:  $\beta_i$  regression coefficients of the design-combined Gaussian process proxy for horizontal well production

i	$\beta_i$	i	$\beta_i$	i	$\beta_i$	i	$\beta_i$
1	9.204278	13	172.7847	24	10.65058	35	-52.865
2	74.9619	14	39.2372	25	-2.884248	36	-66.073
3	18.03561	15	70.48655	26	4.474735	37	54.2226
4	-4.330527	16	-16.54314	27	-48.07775	38	-16.671
5	-34.66287	17	-29.39563	28	78.93651	39	20.8075
6	-13.05811	18	-59.35606	29	117.4737	40	20.4946
7	22.57846	19	-7.251607	30	-33.33996	41	51.0991
8	4.246784	20	26.14089	31	16.40215	42	-84.253
9	54.5243	21	-0.589437	32	-6.485041	43	10.668
10	-3.772873	22	-66.87557	33	45.60985	44	21.1235
11	-23.67601	23	-14.56781	34	100.7172	45	-35.004
12	-120.3701						

Table 5.13:  $\beta_j$  regression coefficients of the design-combined Gaussian process proxy for horizontal well production

j	$\beta_j$	j	$\beta_j$	j	$\beta_j$	j	$\beta_j$
1	-4.270754	13	36.33787	24	7.759279	35	3.97052
2	-17.85464	14	-4.007128	25	13.06272	36	0.43699
3	11.27446	15	3.486673	26	26.43336	37	-52.727
4	-55.27938	16	-19.68219	27	-27.64479	38	-15.398
5	0.094318	17	37.81114	28	-1.251913	39	-9.4633
6	7.803672	18	-3.530573	29	-20.90658	40	-1.6976
7	-9.828017	19	-7.0287	30	-10.16098	41	12.2171
8	-8.653845	20	22.65567	31	4.661682	42	-10.138
9	-6.122594	21	-41.50035	32	-33.66551	43	-0.3168
10	3.9379	22	-136.2446	33	-5.857823	44	15.0761
11	-3.503427	23	-12.35089	34	-13.08094	45	29.9323
12	-9.563717						



Figure 5.14 shows the optimum factor setting calculated by JMP prediction profiler. It can be seen that the factor setting is quite similar to that of quadratic proxy model except LRAT. It should be noticed that the predicted optimum URF is 52.29%, which is much less than that of the quadratic proxy. This is evidenced by the 3D surface plot in Figure 5.16. Although the shape of the surface in Figure 5.16 looks similar to that of the quadratic model, it should be reminded that the actual model is 6-dimensional. Comparison of the models in other different 2D design spaces shows some differences in their shapes. Figure 5.17 shows marginal model plots of the design-combined proxy model. When compared with Figure 5.8, the average effect of each factor across the other factors have similar trend to that of the Gaussian process model except LRAT. The effects of each design factor on the URF are discussed later in Section 5.3.

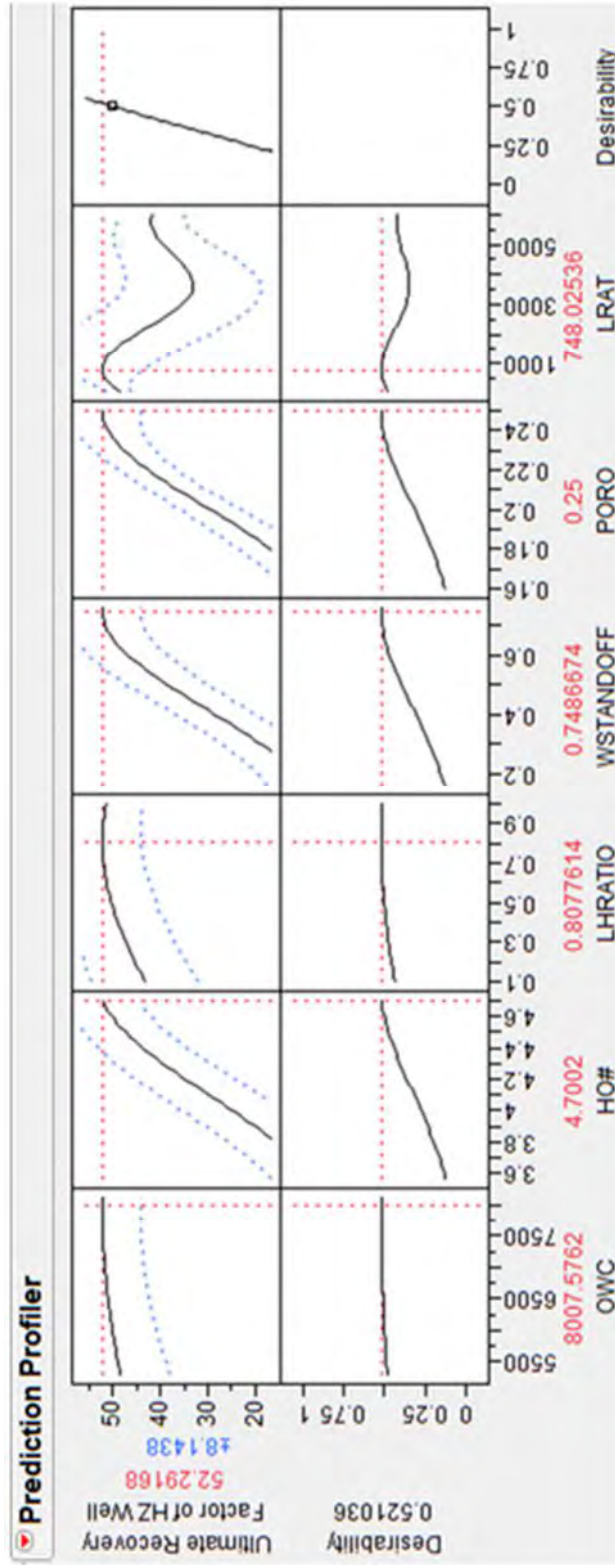


Figure 5.14: JMP prediction profiler shows optimum factor setting of the design-combined Gaussian process proxy model for horizontal well production

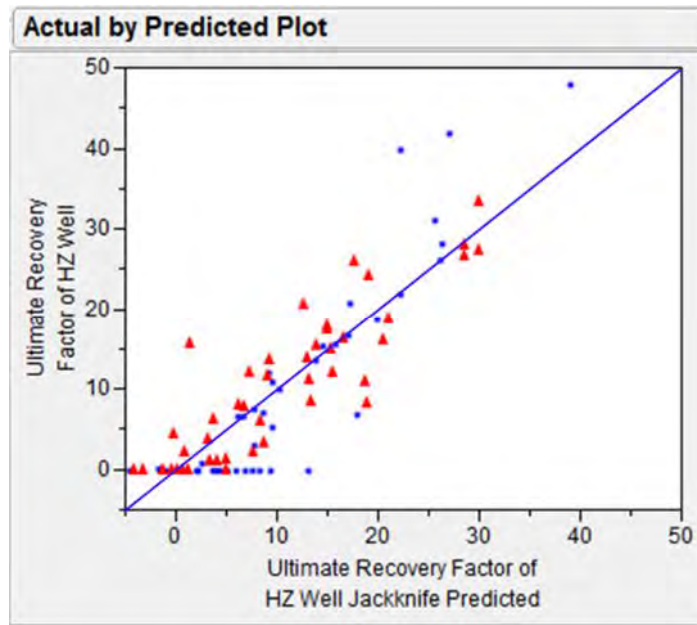


Figure 5.15: Actual by jackknife predicted plot of the design-combined Gaussian process proxy model for horizontal well production

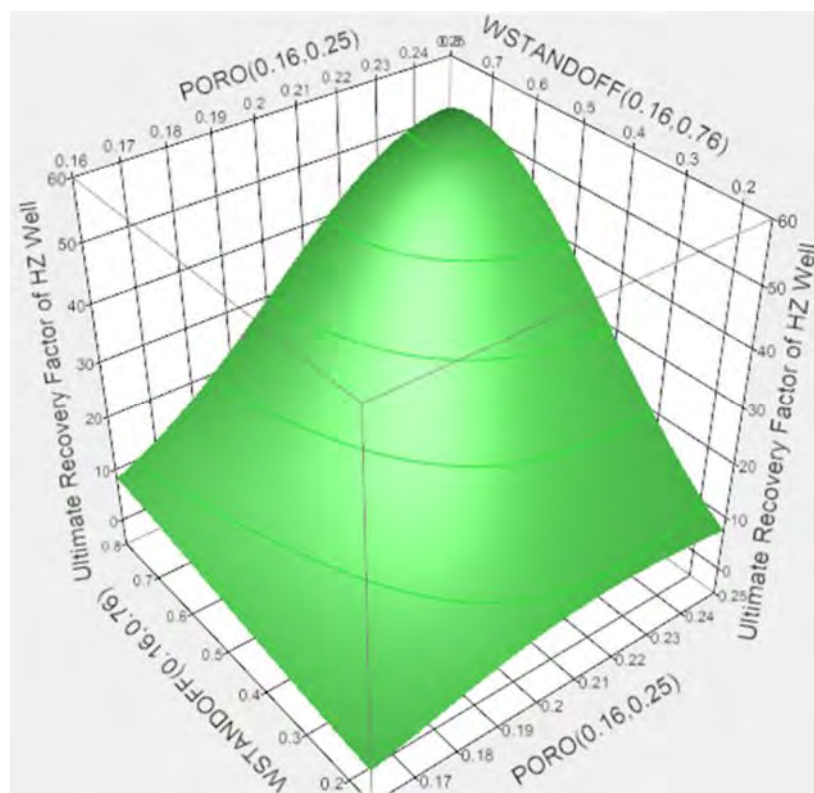


Figure 5.16: 3D surface plot at optimum factor setting of the design-combined Gaussian process proxy for horizontal well production

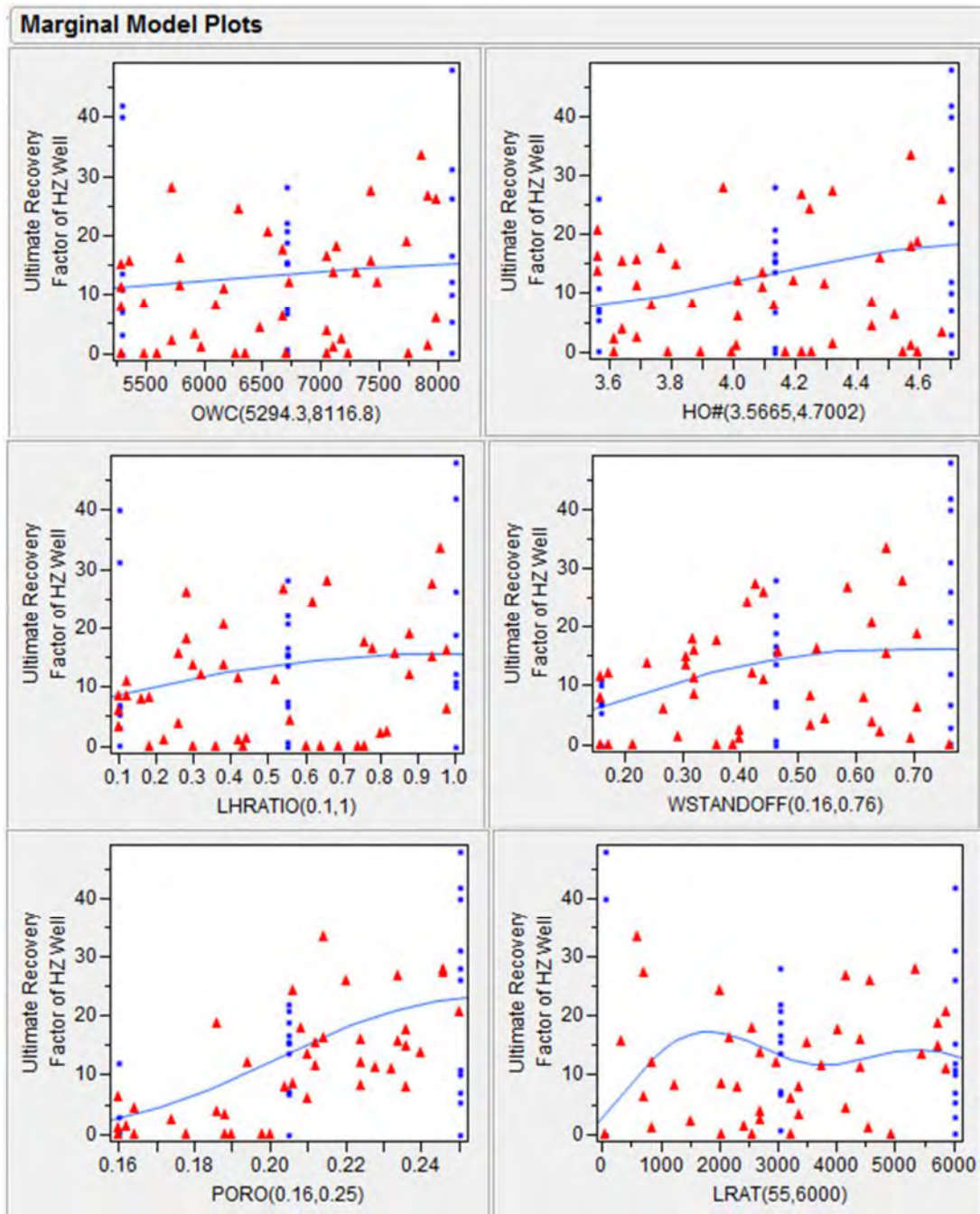


Figure 5.17: JMP marginal model plots of the design-combined Gaussian process proxy model for horizontal well production

### **5.2.3.2 Cross-Validation of Design-Combined Proxy Model**

The cross-validation of the design-combined proxy model is performed as described in Section 4.5. Results of the second cross-validating experiments are shown in Table 5.14. The matched pairs t-test against the validating experiments is then performed and its result is presented in Figure 5.18. Observation on Figure 5.18 reveals that on average URF predictions of the proxy model are not significantly different from the ones of actual response surface. A mean difference and a standard error of 0.433 and 0.739 are significantly smaller than -1.32 and 0.966 of the Gaussian proxy of maximum entropy design, respectively. Most of the differences between predicted and actual URF are within a range of -5% to + 5%. The maximum difference in URFs is 11.6 in absolute value.

In conclusion, combining the existing central composite and maximum entropy designed experiments could improve prediction accuracy of the proxy model. Rather than re-running a new whole set of maximum entropy design, e.g. 90 runs, the combination strategy can help reduce time and cost. In addition, the disadvantage of maximum entropy design is diminished because most of design points of central composite design are at boundary of design hyperspace. Therefore, the design-combined proxy model is selected to be the best representative of the actual response surface. Factor effects described by the proxy are thus discussed in the next section.

Table 5.14: Experimental results of the second 18-run maximum entropy design for validating the proxy model for horizontal well production

<b>Run ID.</b>	<b>OWC</b>	<b>HO#</b>	<b>LHRATIO</b>	<b>WSTANDOFF</b>	<b>PORO</b>	<b>LRAT</b>	<b>URF (%)</b>
201	5607.91	3.818	0.150	0.427	0.205	2366.9	4.106
202	5294.30	3.755	0.650	0.627	0.220	5009.2	17.436
203	5921.52	3.567	0.250	0.727	0.190	4018.3	2.725
204	7175.97	3.818	0.250	0.493	0.160	5339.4	0.008
205	5294.30	4.637	0.150	0.593	0.195	1706.4	8.723
206	5294.30	4.700	0.900	0.460	0.180	2036.7	11.684
207	7803.19	4.511	0.400	0.727	0.205	3688.1	27.880
208	7959.99	4.133	0.800	0.327	0.160	4348.6	0.004
209	6862.36	4.574	0.600	0.527	0.170	4018.3	10.014
210	5607.91	4.259	0.100	0.327	0.185	5339.4	3.548
211	6391.94	3.692	0.950	0.427	0.225	385.3	16.043
212	6078.33	4.070	0.500	0.160	0.225	3688.1	10.644
213	6862.36	3.567	0.850	0.493	0.180	2697.2	3.241
214	7646.38	4.322	0.350	0.327	0.165	715.6	1.921
215	7175.97	3.567	1.000	0.227	0.180	55.0	0.000
216	5764.72	4.448	0.550	0.627	0.225	5669.7	24.922
217	5294.30	4.259	0.800	0.160	0.175	2366.9	0.000
218	5921.52	4.511	0.400	0.260	0.205	385.3	10.790

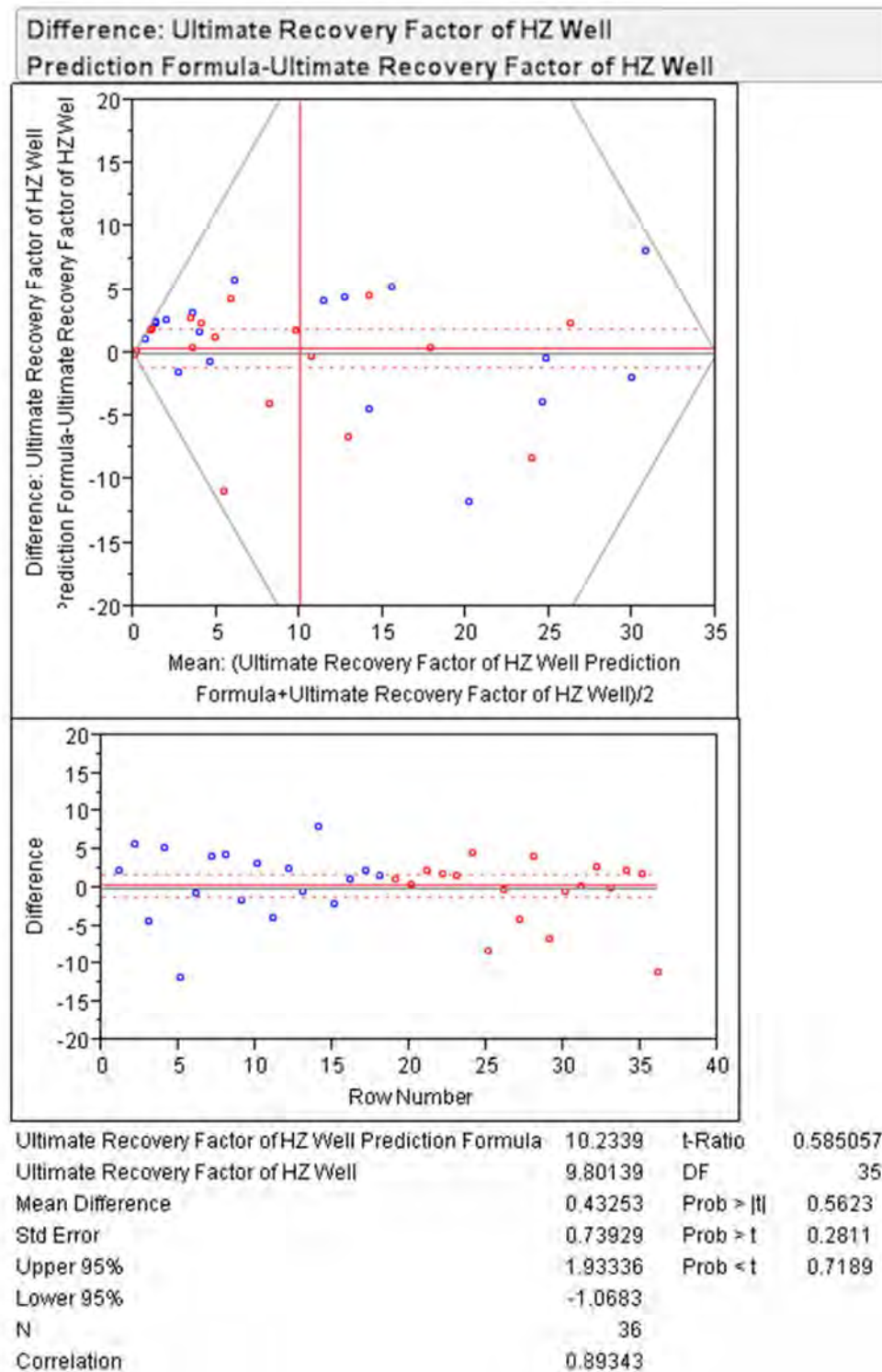


Figure 5.18: Matched pairs t-test for validating the design-combined Gaussian process proxy model for horizontal well production

### 5.3 Influence of Significant Factor Effects

To investigate the influence of significant factors and their interactions on URF, the model report in Table 5.10 is modified and re-represented in Table 5.15. Table 5.15 presents estimates of main and interaction effects normalized by total sensitivity. Factor effects whose influences are relatively significant are highlighted and discussed in this section. As it can be seen, main effects contribute 80.91% of total influence on URF. However, only 1.71% of the total main effects is attributed to OWC. Besides, all of OWC interaction effects also show negligible influence. This observation supports the discussion described in Section 5.2.3.1.

Table 5.15: Summary of factor effects normalized by total sensitivity

Column	Total Sensitivity	Main Effect	OWC Interaction	HO# Interaction	LHRATIO Interaction	WSTANDOFF Interaction	PORO Interaction	LRAT Interaction
OWC	1.96%	1.38%	.	0.01%	0.02%	0.04%	0.17%	0.35%
HO#	14.31%	11.03%	0.01%	.	0.12%	1.43%	1.14%	0.58%
LHRATIO	6.20%	4.39%	0.02%	0.12%	.	0.98%	0.29%	0.40%
WSTANDOFF	15.05%	9.69%	0.04%	1.43%	0.98%	.	2.11%	0.81%
PORO	51.00%	46.19%	0.17%	1.14%	0.29%	2.11%	.	1.10%
LRAT	11.48%	8.24%	0.35%	0.58%	0.40%	0.81%	1.10%	.
<b>Sum =</b>	100.00%	80.91%	0.58%	3.28%	1.81%	5.37%	4.81%	3.24%

#### 5.3.1 Influence of Main Effects

Influence of main effect is investigated by comparing two or more experimental results whose level of the factor being interested is varied whereas the others are kept the constant. This is essentially one-variable-at-a-time approach. Since marginal plot shows a line of average response of the factor of interest across the other factors, it is actually approximately representing main effect of the factor. Thus, the existing experiments whose design points and responses are closest to the average line are chosen for comparison. If none of the existing experiments can be a good representative, a new experiment is the conducted. In the subsequent sub-sections, only main effects of HO, LHRATIO, WSTANDOFF, PORO, and LRAT are



discussed. Discussion of OWC, whose total sensitivity in Table 5.15 is insignificant, is omitted.

### 5.3.1.1 Main Effect of Initial Oil Column Thickness

The main effect of initial oil column thickness,  $HO\#$  or  $\ln(HO)$ , can be investigated by comparing the results of CCD Run ID 18 and 28 of Table 5.3. See Table 5.16 and Figure 5.19 for more detail about the design points. Figures 5.20 and 5.21 compare production profiles and pressure profiles of the two experiments on the same time scale. Comparison between initial water saturation in 3D of the two experiments is also shown in Figure 5.22.

As shown in Figure 5.20a, CCD Run ID 18 which has a thinner vertical oil column thickness starts production with an oil and gas rates of 2,240 STB/day and 0.64 MSCF/STB. The observed initial water cut is 0.26. As the well produce, oil production rate sharply declines whereas water cut rapidly increases from the beginning. Shortly afterwards, free gas from the gas cap breaks into the well as signaled by the drastic increase in gas-oil ratio. Then, the well keeps on producing and totally depletes within only 52 days with an URF of 7.50%.

In contrast, Figure 5.20b shows that the reservoir having a thicker vertical oil thickness has much later water and gas breakthrough. A higher oil production rate can be maintained at a rate of approximately 3000 STB/day for about 4.5 months before declining at a slower rate. After 13 months, the well depletes with an URF of 22.04%.

The pressure profiles in Figure 5.21a reveal that, after free gas breakthrough, total pressure drop in the reservoir increases. This could be attributed to the increase in non-Darcy flow friction loss due to increasing gas flow rate. However, the higher amount of gas in the well helps retard the decreasing rate of oil production as seen in the zoom-in view of the figure. In addition, because of higher gas-oil ratio and lesser hydrostatic pressure in the well, bottom hole pressure of the well significantly decreases whereas tubing head pressure increases.

When compared with the profiles of Figure 5.21b, it is obviously seen that reservoir pressure of CCD Run ID 18 decreases at faster rates and depletes at a higher pressure than those of CCD Run ID 28. This could be attributed to higher water cut at

a given time of CCD Run ID 18 because early water production of the well causes higher hydrostatic pressure in the well, i.e. increase in bottom hole pressure. As a result, greater pressure drop or pressure loss in the reservoir is required to produce the well. In addition, it causes the well to reach its maximum water cut and depletes early.

The reason that causes the well in CCD Run ID 18 produces water at the beginning and higher rate of water cut increment can be explained by comparing Figure 5.22a with Figure 5.22b. It can be obviously seen that, at the same WSTANDOFF, the horizontal well of CCD Run ID 18 is placed inside oil-water transition zone while that of the other run is in oil zone. Consequently, water can be immediately produced at the beginning. Since fluid and rock properties of the two models are the same, the J-function correlation and capillary pressure formula in Figure D3 indicate that their thickness of the oil-water transition zone must be the same.

Thus, it can be concluded that as vertical thickness of oil column,  $HO$ , increases, the horizontal well is farther away from oil-water and gas-oil contacts at a given WSTANDOFF. As a result, bottom water and free gas from gas cap can enter the well at later time resulting higher sweep of oil volume prior to well depletion. Production of bottom water has detrimental effect to URF because it causes higher hydrostatic pressure the well. Thus, higher pressure drop in reservoir is required to lift reservoir fluids up to the surface besides decreasing oil holdup. If  $HO$  is so small enough that the oil-water transition zone dominates the reservoir, the high initial water saturation in the vicinity of the wellbore can cause the well to produce higher water cut, lower oil production rate, and earlier breakthrough of bottom water.

Table 5.16: Experiments for determining HO main effect

Run ID	Reference Table	OWC	HO#	LHRATIO	WSTANDOFF	PORO	LRAT	URF (%)	Time to Reach URF (days)
18	5.3	6705.55	3.5665	0.55	0.46	0.21	3027.5	7.50	52.20
28	5.3	6705.55	4.7002	0.55	0.46	0.21	3027.5	22.04	399.00

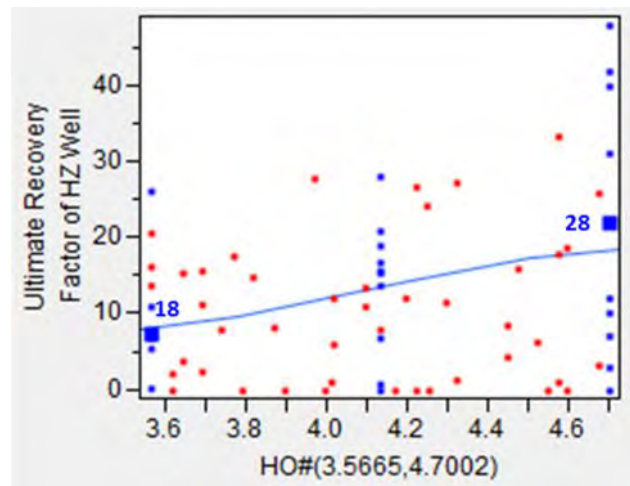


Figure 5.19: Marginal plot of HO# showing design points of CCD Run ID 18 and 28

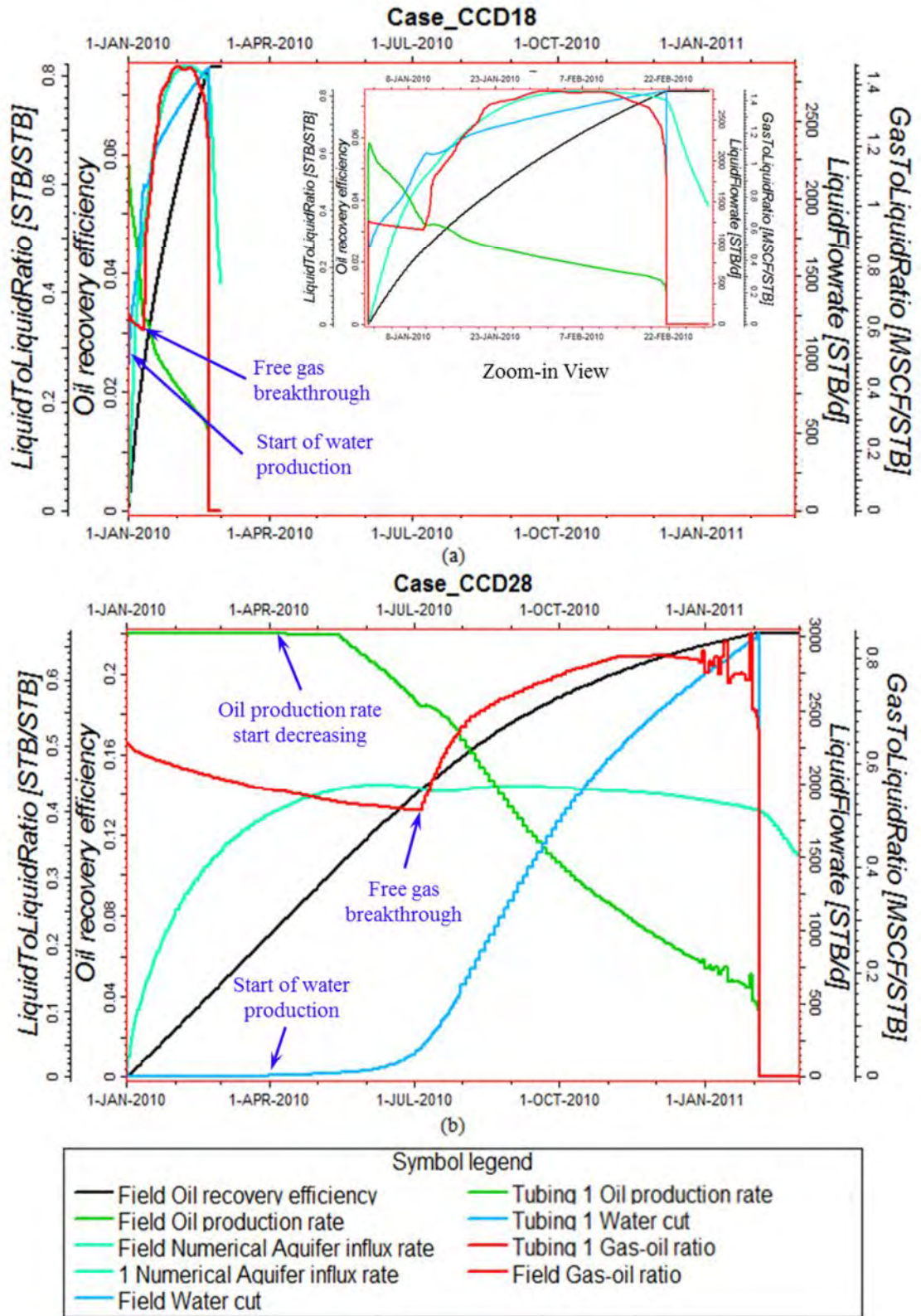


Figure 5.20: Production profiles of CCD Run ID (a) 18 (b) 28

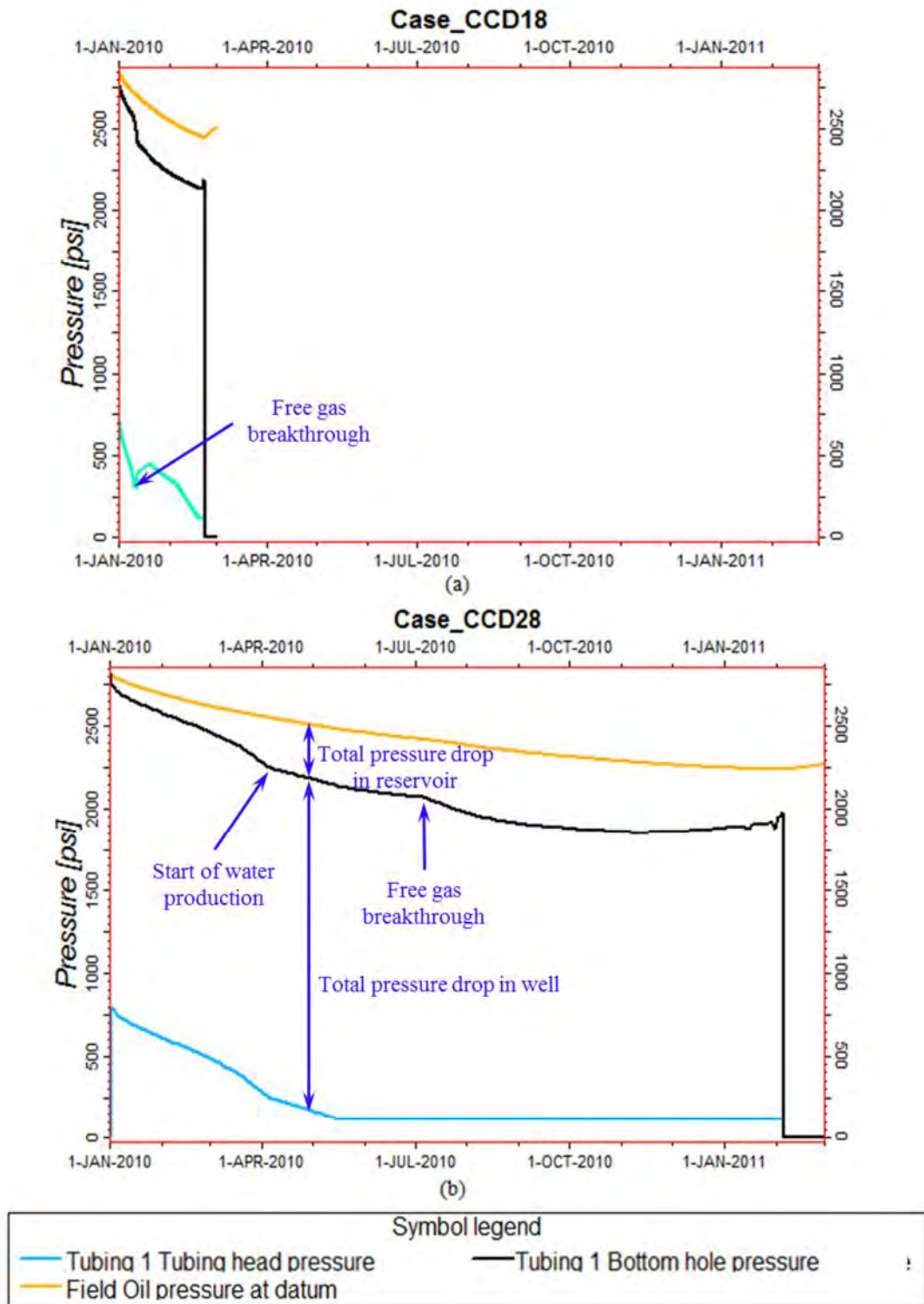
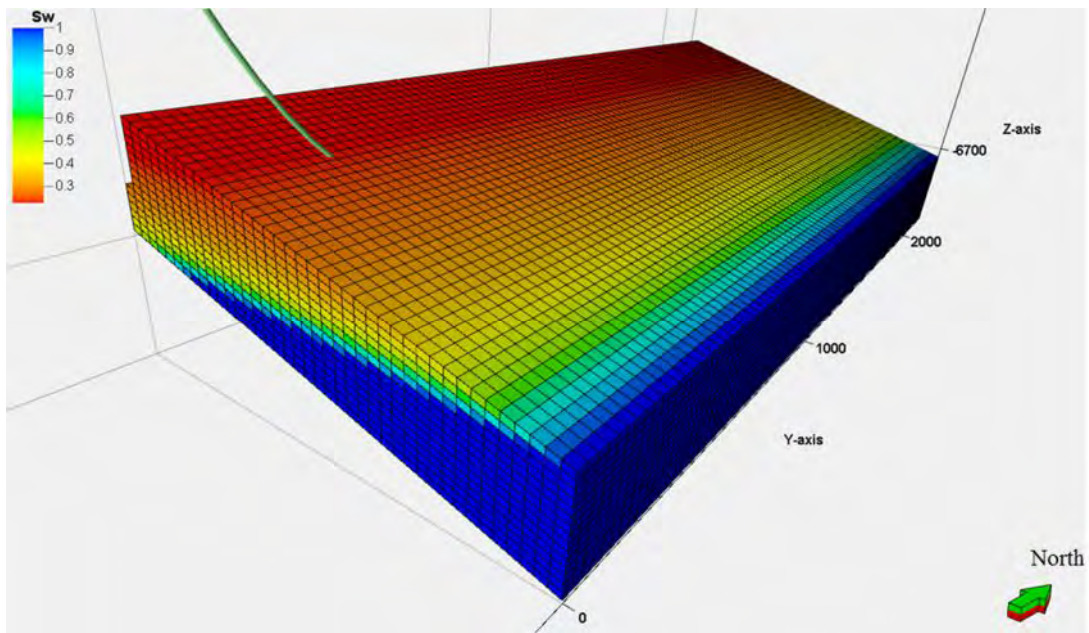


Figure 5.21: Pressure profiles of CCD Run ID (a) 18 (b) 28



(a)

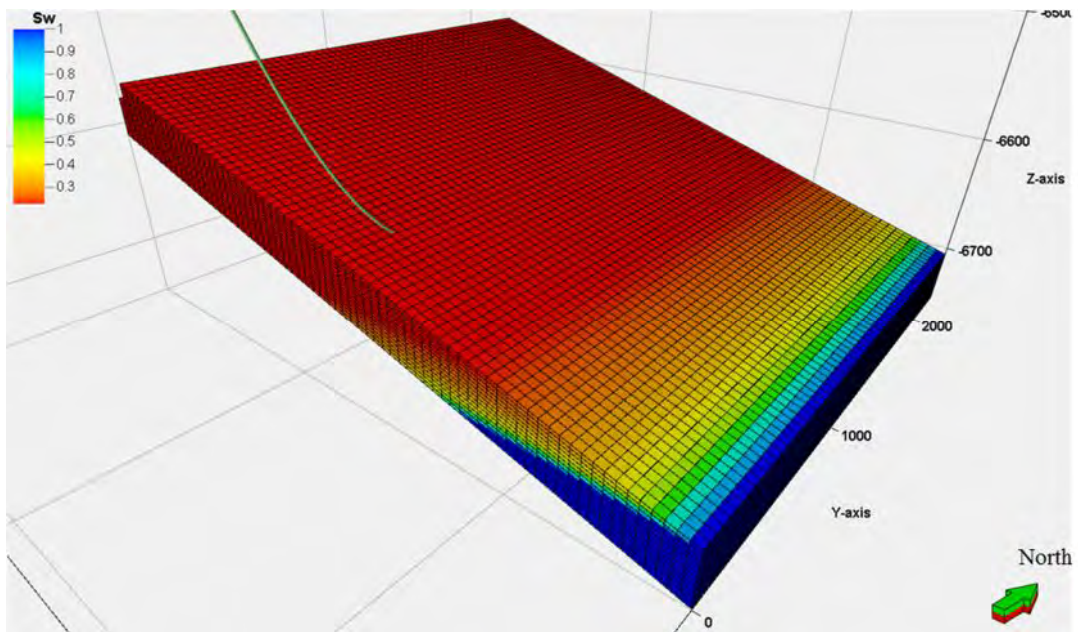


Figure 5.22: 3D reservoir model showing initial water saturation and horizontal wellbore of CCD Run ID (a) 18 (b) 28

### **5.3.1.2 Main Effect of Horizontal Well Length to Reservoir Length Ratio**

Main effect of horizontal well length to reservoir length ratio or LHRATIO is investigated by comparing the existing SFD Run ID 312 of maximum entropy design and a new experiment SFD Run ID 305A. The new experiment is specifically conducted to investigate the main effect of LHRATIO. Table 5.17 and Figure 5.23 present design points and URF of the two experiments. Figure 5.24 presents comparison of production profiles between the two experiments. It can be obviously seen from the figure that oil in the reservoir of SFD Run ID 305A can be produced so fast that its URF is reached before free gas breaks into the well. No plateau period of oil rate and strong aquifer influx can be observed for both experiments. Therefore, bottom water drive does not play an important role in the responses of these two experiments. This is evidenced by the absence of pressure maintenance sign in Figure 5.25. Figure 5.25 also shows that at any given time, pressure drop in the reservoir of SFD Run ID 305A is smaller than that of SFD Run ID 312 although it has faster oil recover rate. This could imply that the well of SFD Run ID 305A could have less severity of water and gas cresting.

More evidences can be found from observations on Figures 5.26 and 5.27. Figure 5.26 presents fluid saturation distribution within the reservoir just before the end of production of both experiments. Figure 5.26a reveals that there is gas cresting in inverted-bell shape on plan while there is still large amount of oil left in the reservoir. An observation on water cresting which is not shown here also shows a similar behavior. In contrast, Figure 5.26b shows that both gas and bottom water approach the well uniformly along the horizontal section. At the end of production, free gas from gas cap does not reach the well yet.

The difference in shapes of water and gas cresting can be explained using reservoir pressure distributions in Figure 5.27. For the reservoir having smaller LHRATIO, i.e. SFD Run ID 312, higher pressure drops are concentrated around the wellbore in elliptical shape. Thus, farther fluids near the reservoir ends are less susceptible to pressure drop from the well. Hence, fluids closer to the wellbore tend to flow faster to the wellbore resulting water and gas cresting in inverted-bell shape. On

the other hand, pressure drops in the SFD Run ID 305A are smaller and more evenly distributed resulting in more uniform fronts of free gas and bottom water. Since every fluid drop at a given elevation in the reservoir can perceive the same amount of pressure drawdown, more volume of oil can thus be recovered from the reservoir. In addition, the lesser required pressure drop can delay free gas breakthrough. In other words, it could be claimed that the larger LHRATIO improves sweep efficiency of oil volume.

Table 5.17: Experiments for determining LHRATIO main effect

Run ID	Reference Table	OWC	HO#	LHRATIO	WSTANDOFF	PORO	LRAT	URF (%)	Time to Reach URF (days)
305A	New Run	5796.08	4.473	0.98	0.32	0.21	2036.67	15.08	230.00
312	5.6	5482.47	4.448	0.12	0.32	0.21	2036.67	8.45	1461.27

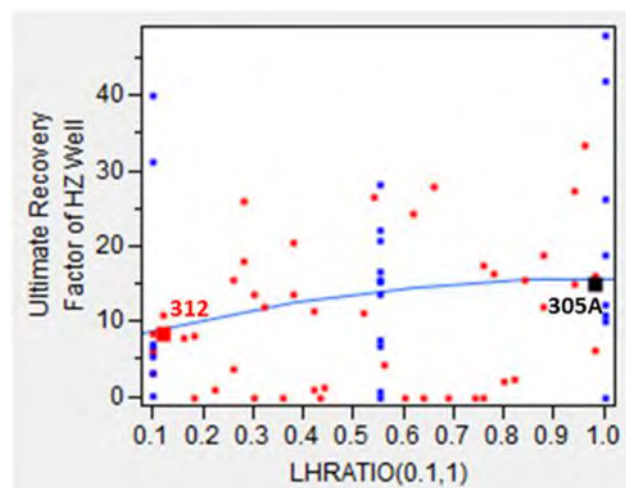


Figure 5.23: Marginal plot of LHRATIO showing design points of SFD Run ID. 312 and 305A



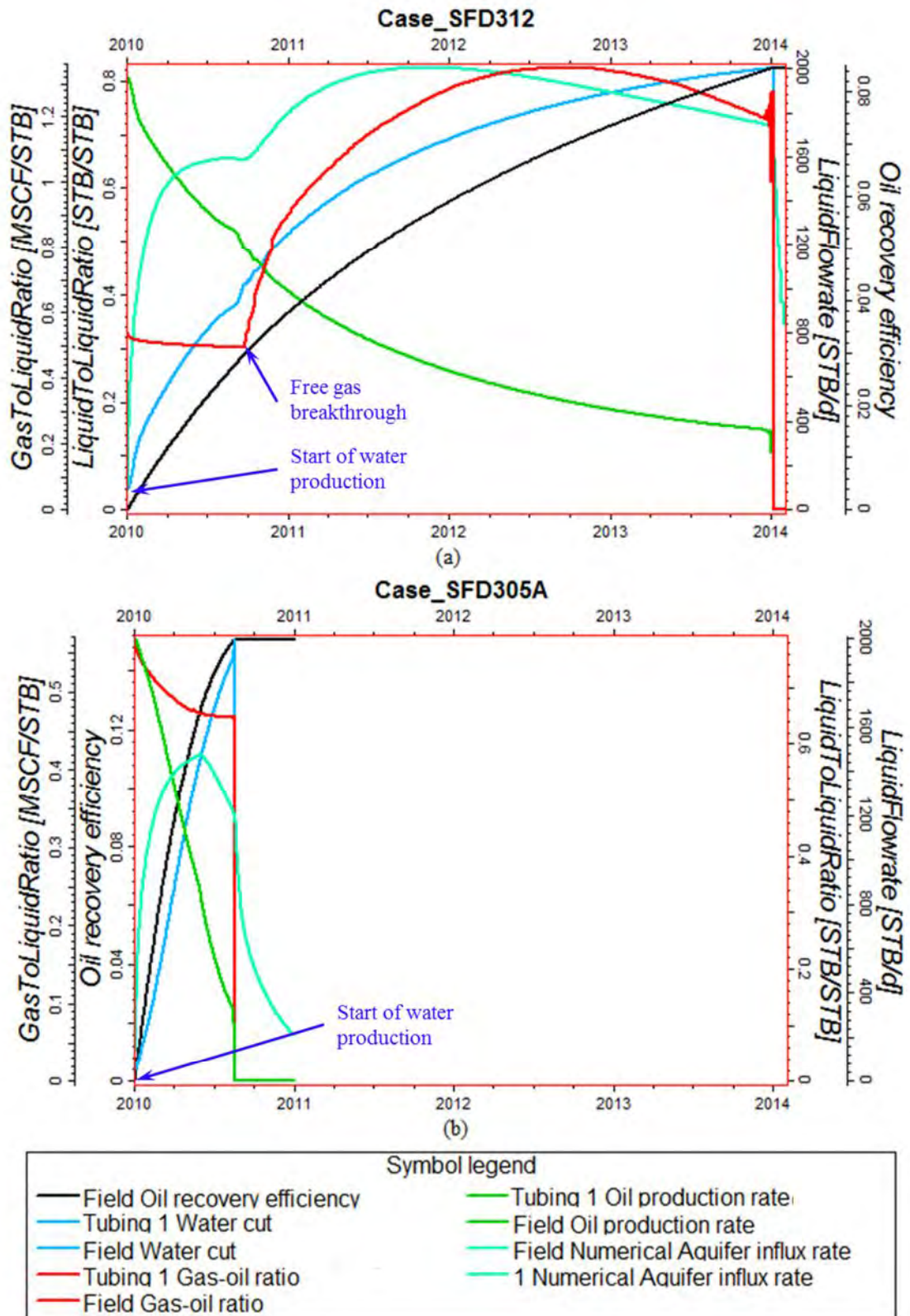


Figure 5.24: Production profiles of SFD Run ID (a) 312 (b) 305A

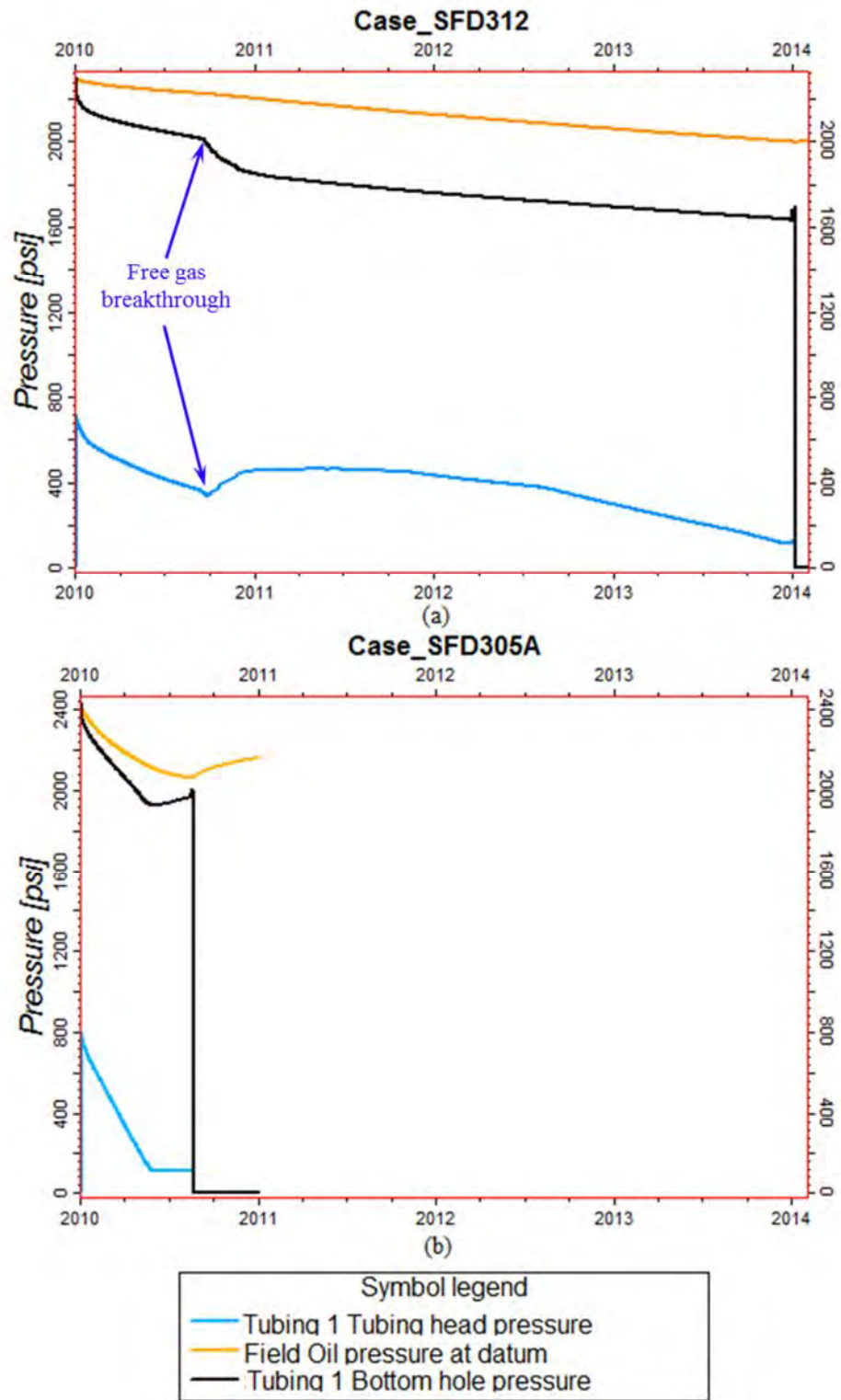
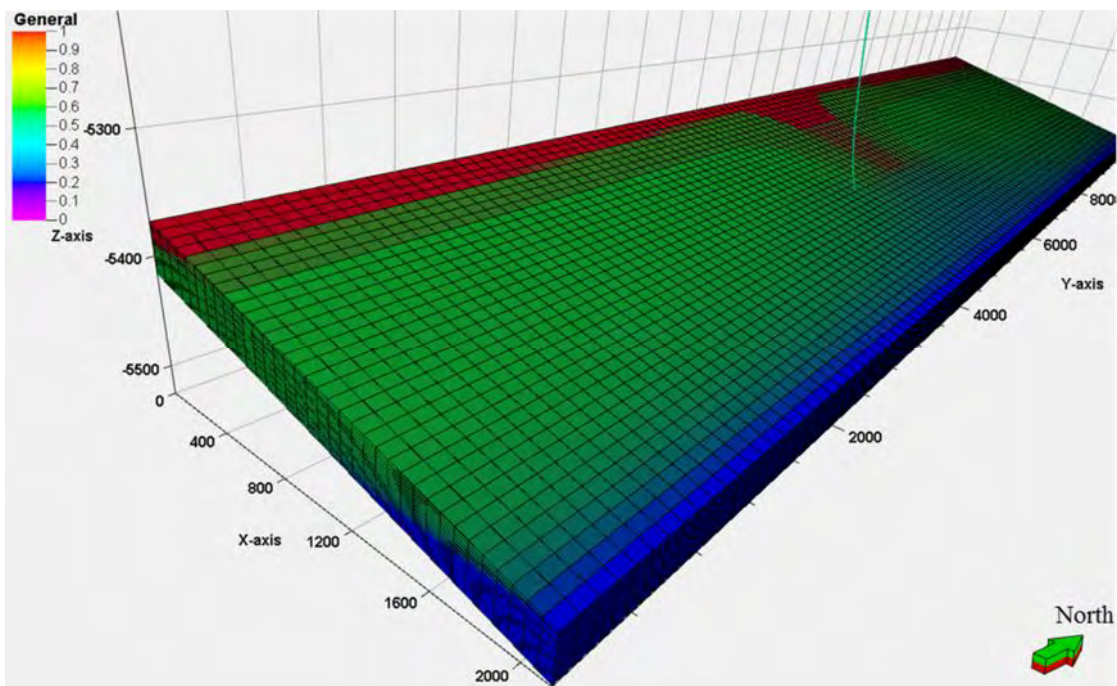


Figure 5.25: Pressure profiles of SFD Run ID (a) 312 (b) 305A



(a)

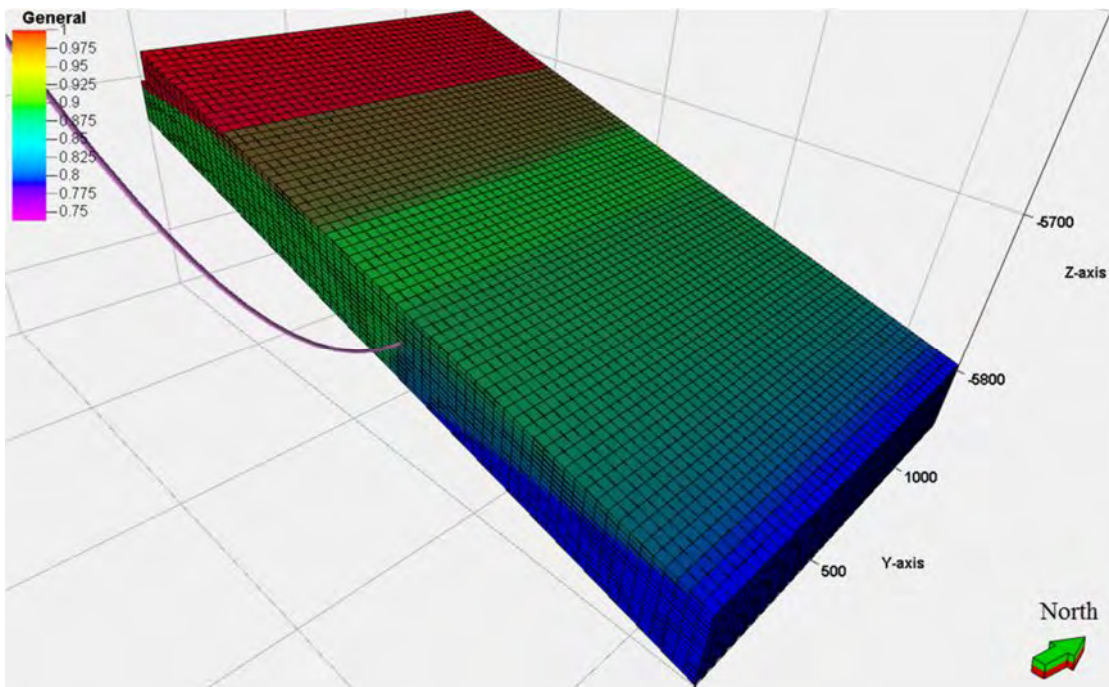
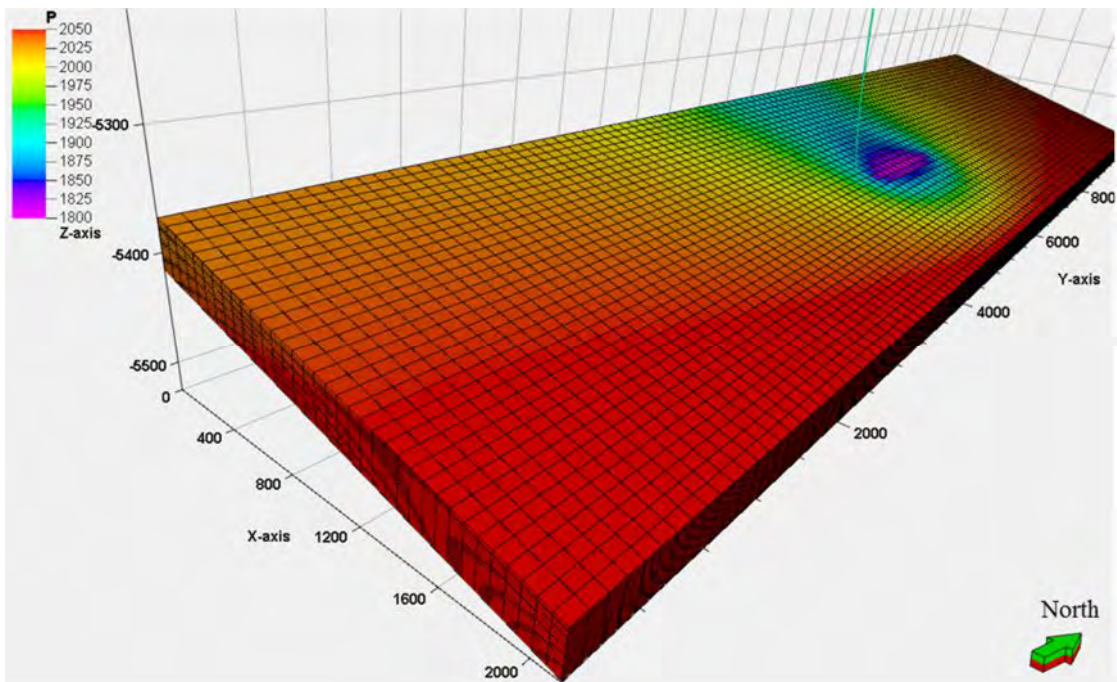


Figure 5.26: 3D reservoir model showing fluid saturation at the end of production and horizontal wellbore of SFD Run ID (a) 312 (b) 305A



(a)

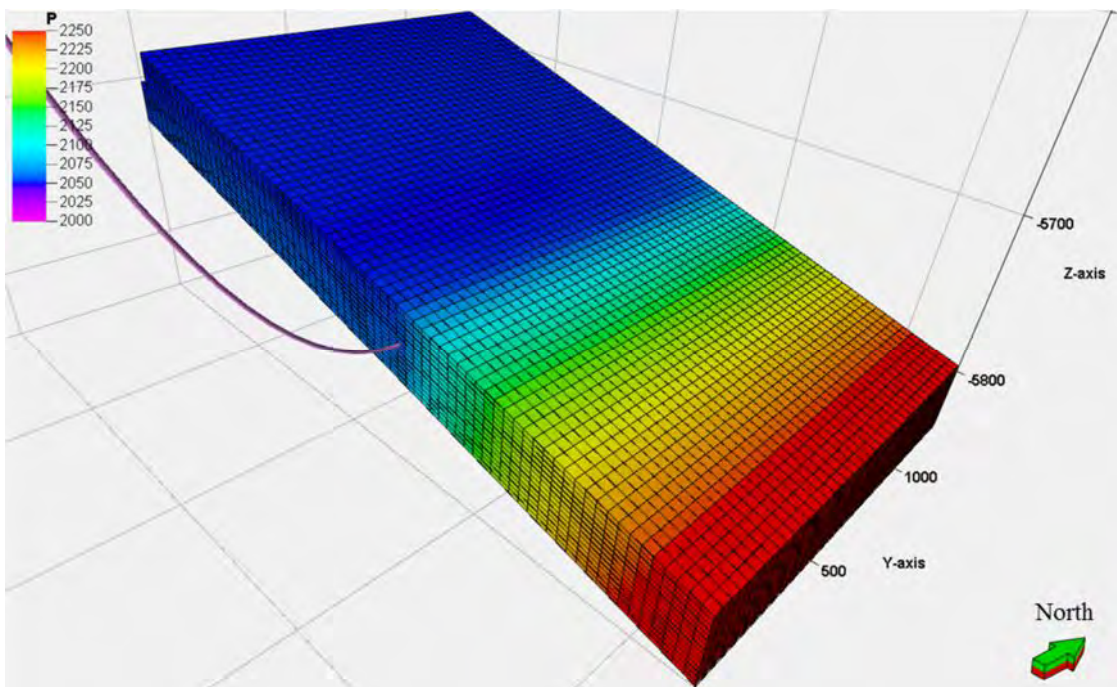


Figure 5.27: 3D reservoir model showing fluid pressure at the end of production and horizontal well of SFD Run ID (a) 312 (b) 305A

### 5.3.1.3 Main Effect of Well Standoff to Oil-Water Contact to Initial Oil Column Thickness Ratio

Table 5.18 shows factor settings of CCD Run ID 20 and CCD Run ID 26 experiments used to investigate main effect of WSTANDOFF, a ratio of well standoff to oil-water contact to vertical thickness of oil. Responses of the two design points on marginal plot of WSTANDOFF relative to the line of average URF across the other factors are presented in Figure 5.28. From the table and the plot, it can be clearly seen that WSTANDOFF has strong positive effect on the URF. In other words, the horizontal wellbore is moved closer to gas-oil contact, more volume of oil can be significantly recovered from the reservoir.

Figure 5.29 presents comparison between production profiles of CCD Run ID 20 and CCD Run ID 26. From the figure, production of CCD Run ID 20 begins with a very high initial water cut of 0.74 and a relatively low oil production rate of 840 STB/day. As the well produces, oil production rate rapidly increases where corresponding water cut and gas-oil ratio decreases. After oil production rate reaches its maximum value, the oil production rate and gas-oil ratio gradually decline whereas water cut increases until the end of production. The presence of oil peak rate could be attributed to the rapid increase in water production. Shortly after the beginning, the solution drive mechanism is interfered by water produced from the bottom aquifer. Since the horizontal well is placed inside oil-water transition zone and close to the oil-water contact, flowing water can reach the well within a short time. See Figure 5.32a. The influence of increasing of water in the well is that it tends to increase bottom hole pressure and pressure loss of the well. As a result, liquid and oil flowing rates decline as water cut increases. This is evidenced by the change in the slope of bottom hole pressure after the production starts as shown in Figure 5.30a. Note that the weak influence of aquifer influx can be observed as indicated by the slight increase in declining rate of oil production rate after the aquifer influx reaches its maximum rate. However, its influence on pressure support seems to be much weaker than that of CCD Run ID 26. This could be because some of the influx water is produced by the horizontal well.

For CCD Run ID 26, the horizontal wells start its production with a high initial oil production rate of about 3,000 STB/day without water production. However, the well can maintain its constant oil rate for only about one month before water cresting breaks into the well. A sudden change in declining rate of oil is observed about 3 weeks afterwards after the influx from aquifer reaches its peak. Subsequently, the oil production rate fluctuates as the reservoir is produced until the end of production. For this run, it can be noticed that free gas enters into the well very early and before water cresting. This is not a surprise because the horizontal well in this experiment is located closer to gas-oil contact. See Figure 5.32.

However, it is interesting to notice that, as the oil and gas flow rates fluctuate, their corresponding bottom hole pressure shows an opposite trend. For example, as oil and gas flow rates reach their valley value on Mar 01, 2010, their bottom hole pressure just reaches its peak. Since only produced gas has a lifting effect, i.e. reducing hydrostatic pressure in the well, it could be deduced that the fluctuation in production rates is caused by the free gas entering into the wellbore. This is evidenced by observing Figure 5.32b. Figures 5.32a and 5.32b show distribution of reservoir fluids at the end of production of CCD Run IDs 20 and 26, respectively. It is quite obvious that almost all of gas cap in CCD Run ID 26 is produced by the horizontal well. Figure 5.33 shows that, during the fluctuation period, there is free gas entrance along the length of the horizontal wellbore. This implies that as liquid and gas flows along the wellbore, the new gas at the locations closer to the well heel could enter into the wellbore and causes more turbulence to the flow. In addition, the amount of entering gas should be so much that the well can produce almost the entire gas cap. In terms of oil recovery, Figure 5.32 also shows that placing the horizontal well farther from the oil-water contact results in higher sweep of oil volume.

In conclusion, the main effect of WSTANDOFF has positive influence on the URF of a horizontal well. As the well is placed farther away from oil-water contact, it is less prone to the detrimental influence of oil-water transition zone on producing high initial water cut. Besides, it also results in longer time for bottom water cresting to reach the wellbore. As the well is moved closer to gas-oil contact, gas breakthrough time is less and more volume of gas cap can be produced. Observations from the experiments reveal that if the free gas is produced, it could help increase liquid

production rate. However, if the gas production is higher than a certain rate, fluctuation in production rates can occur due to turbulence from high gas flow rate.

Table 5.18: Experiments for determining WSTANDOFF main effect

Run ID	Reference Table	OWC	HO#	LHRATIO	WSTANDOFF	PORO	LRAT	URF (%)	Time to Reach URF (days)
20	5.3	6705.55	4.133	0.55	0.16	0.21	3027.5	6.71	311.00
26	5.3	6705.55	4.133	0.55	0.76	0.21	3027.5	20.86	277.50

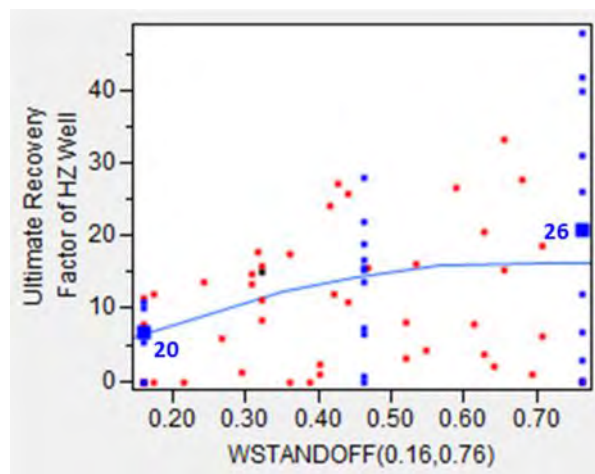


Figure 5.28: Marginal plot of WSTANDOFF showing design points of CCD Run ID.

20 and 26

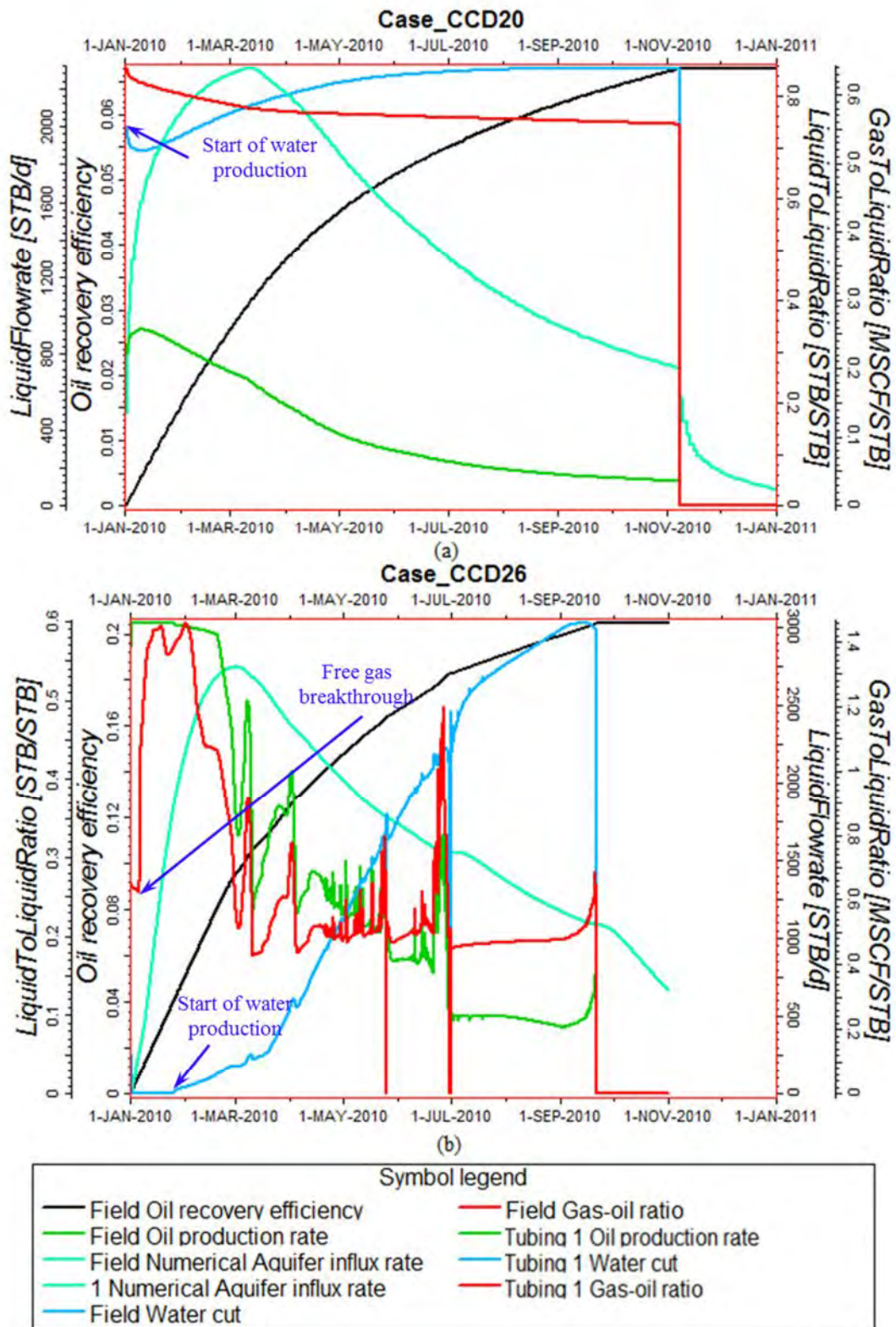


Figure 5.29: Production profiles of CCD Run ID (a) 20 (b) 26



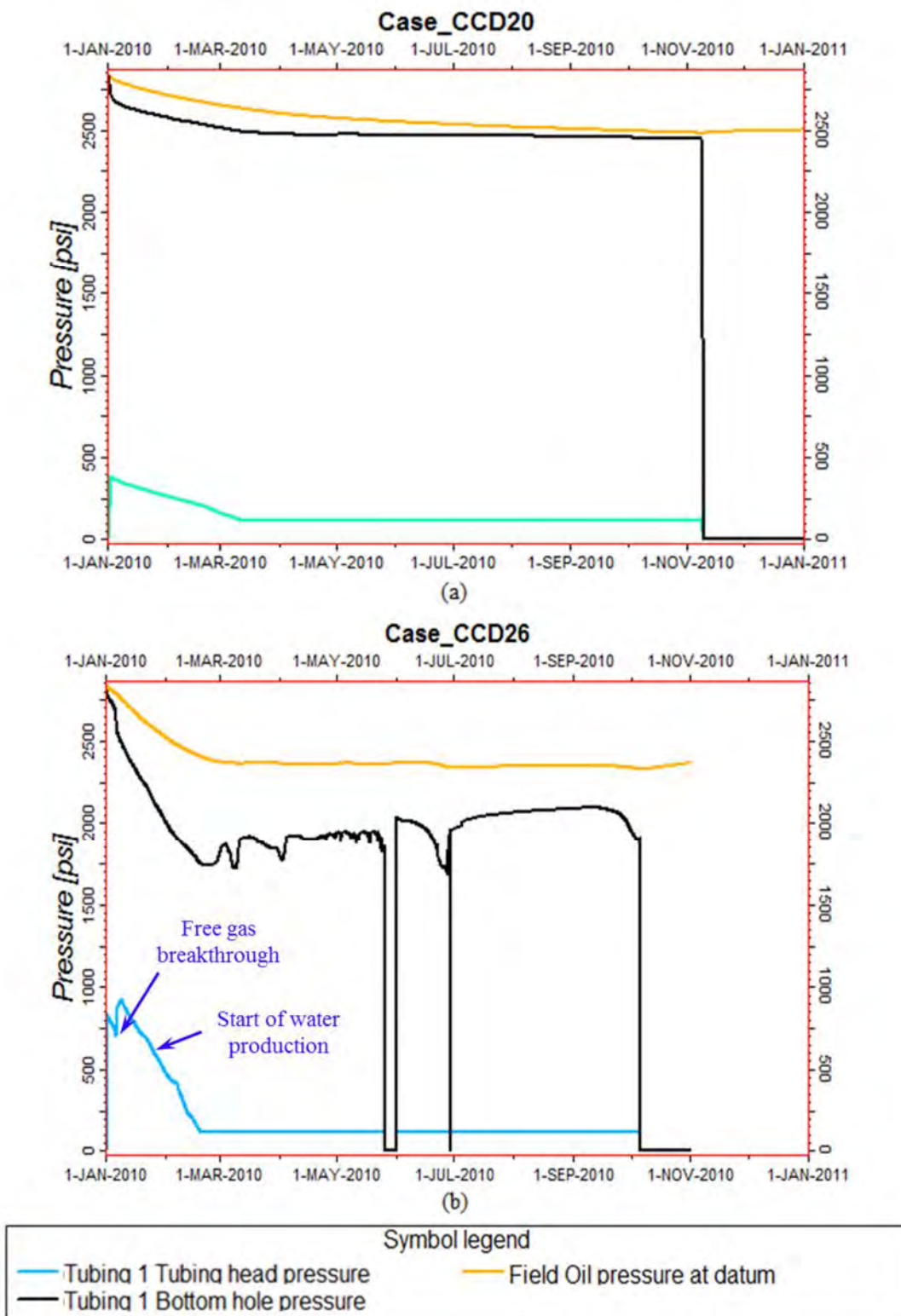
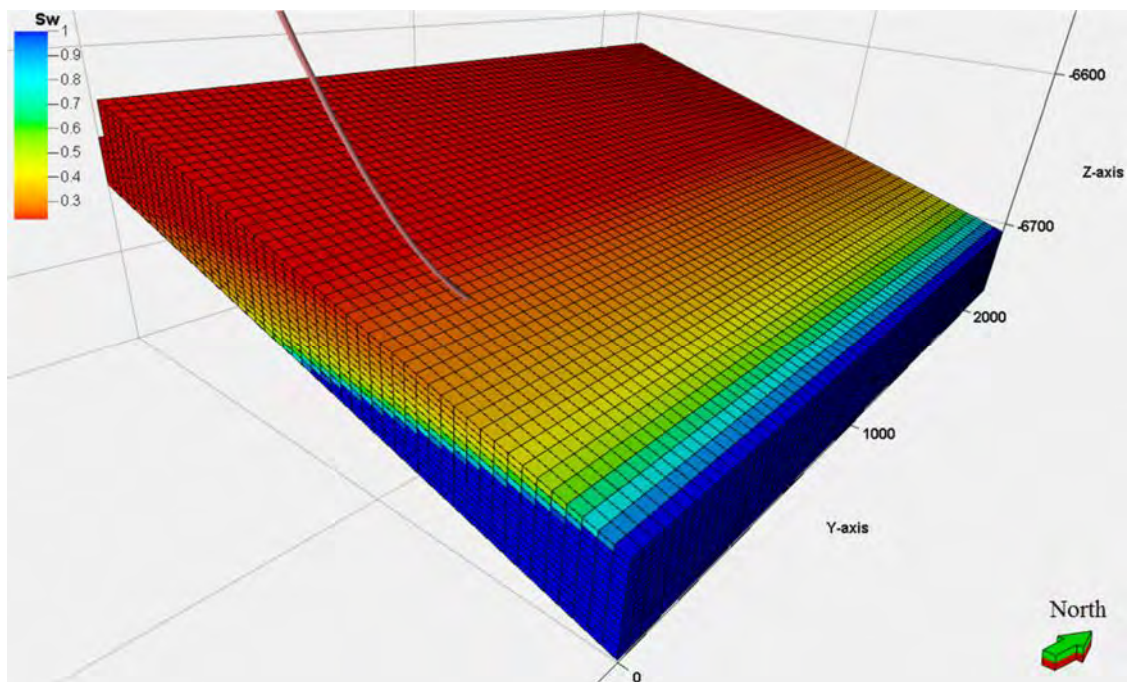


Figure 5.30: Pressure profiles of CCD Run ID (a) 20 (b) 26



(a)

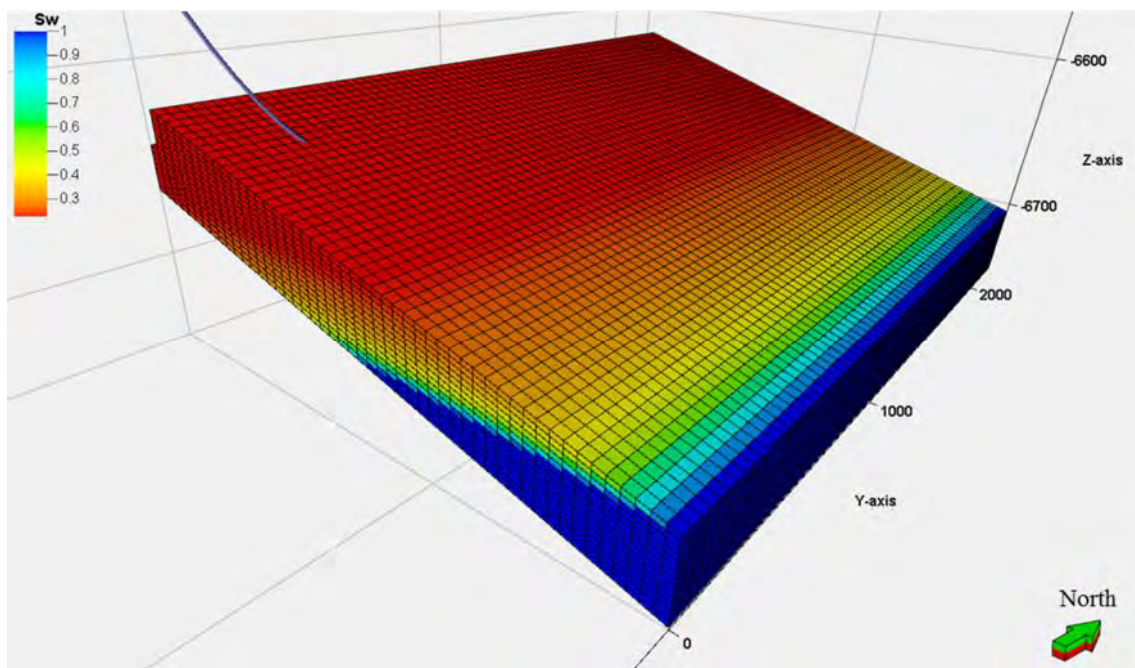
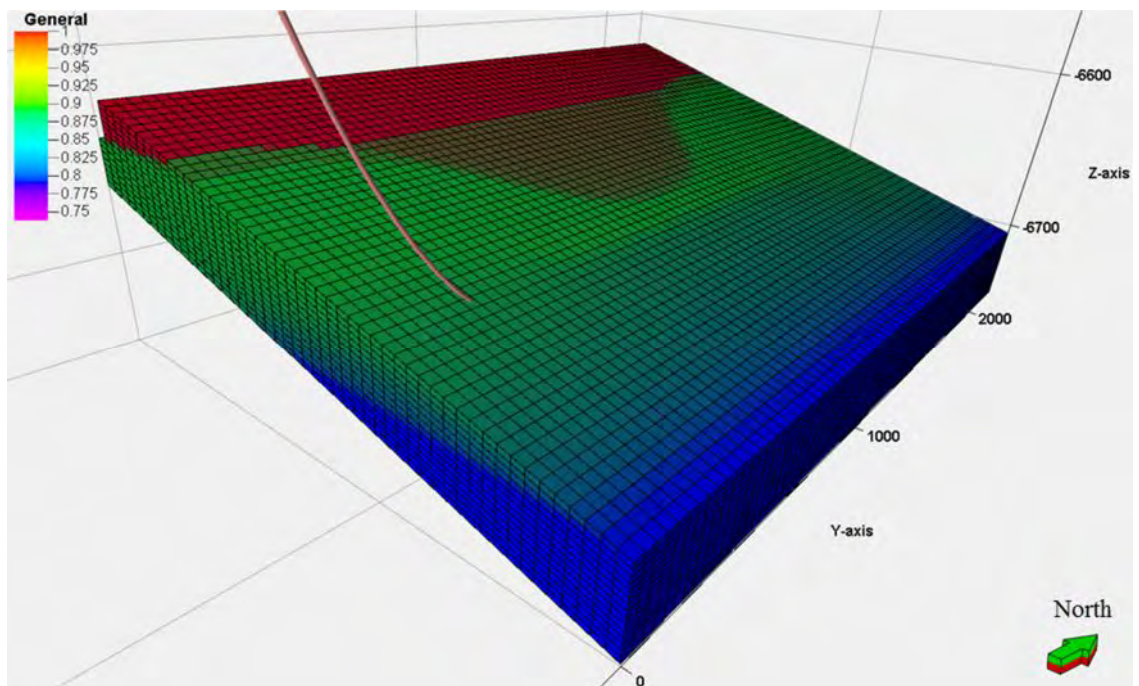


Figure 5.31: 3D reservoir model showing initial water saturation with horizontal wellbore of CCD Run ID (a) 20 (b) 26



(a)

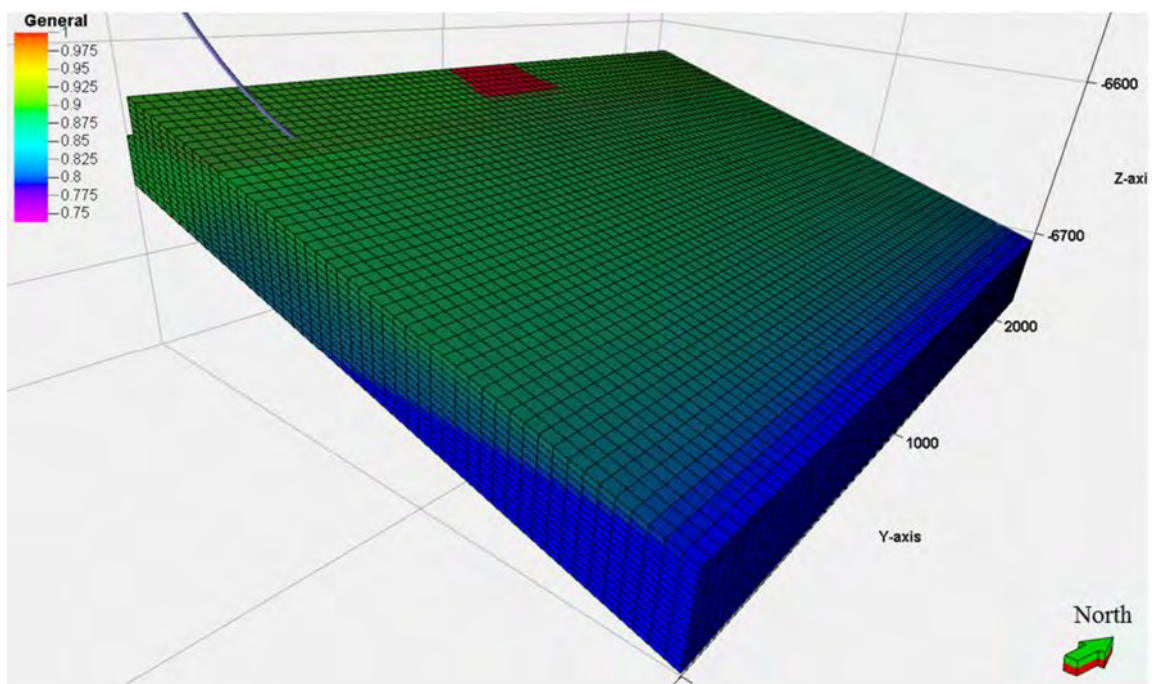


Figure 5.32: 3D reservoir model showing fluid saturations at the end of production with horizontal wellbore of CCD Run ID (a) 20 (b) 26

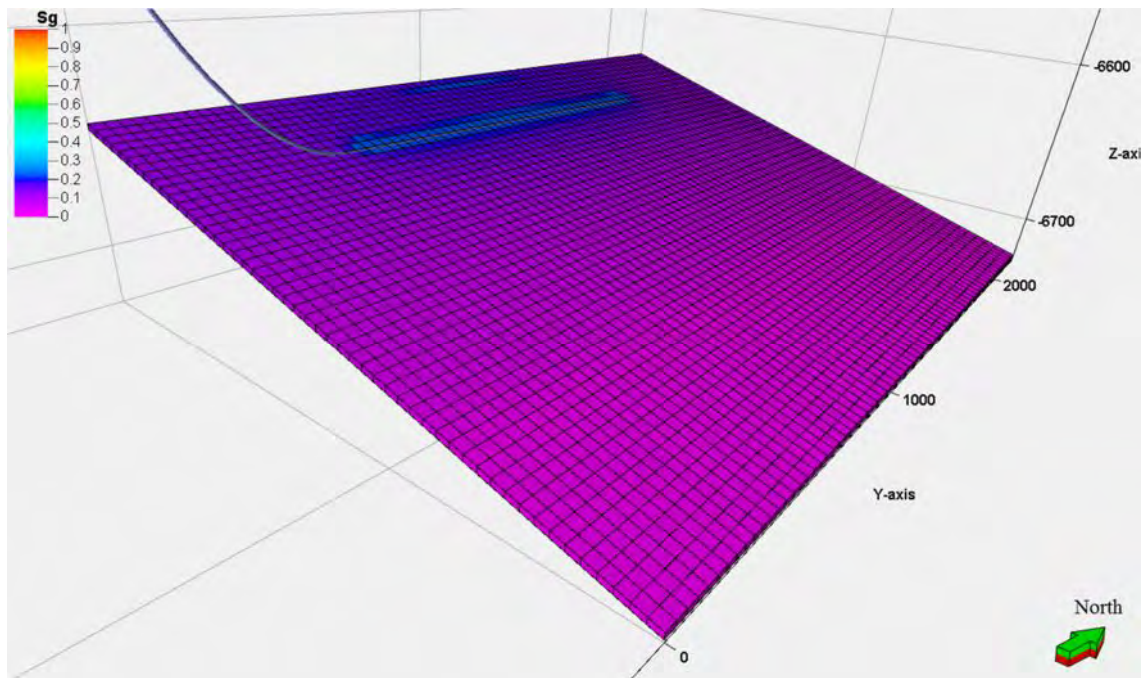


Figure 5.33: A slice of 3D reservoir model showing gas saturations around the horizontal wellbore of CCD Run ID 26 on 01 May 2010

### 5.3.1.4 Main Effect of Porosity

Porosity or PORO is a design factor representing porosity and its correlated factors which are horizontal permeability and initial water saturation in oil-water transition zone. By increasing PORO, porosity and horizontal permeability of the reservoir rock increases whereas thickness of oil-water transition zone is decreased. Refer to Section 4.6 for more description. Similar to the previous section, CCD Run IDs 21 and 25 are selected for determining main effect of PORO. Table 5.19 and Figure 5.34 show setting of design point, URF, and marginal plot of the experiments. Both of the table and figure obviously show that PORO has a very strong positive effect on the URF. To find out the reasons, production and pressure profiles of both experiments are plotted and compared in Figures 5.35 and 5.36, respectively.

Figure 5.35a shows production profiles of CCD Run ID 21. From the figure, it can be seen that the initial production has a very high water cut of 0.78 whereas the initial oil flow rate is only 350 STB/day. As the oil flow rate rapidly declines with time, its corresponding water cut still roughly remains the same. Only about two

weeks later, the horizontal well is completely depleted without free gas breakthrough observed. Subsequently, the well is tried to be re-opened on weekly basis in a hope that the approaching bottom water could help recover more significant amount of oil. However, production from the well can last for only a few days for each time with high water cut observed. The attempt of well re-production is ceased on Apr 01, 2010, when an average rate of oil production of 50 STB/day is reached. Figure 5.36a discloses pressure profiles of the experiment. It is shown that, shortly after the well is opened, pressure loss or drawdown in the reservoir rapidly increases to produce reservoir fluid as much as possible. However, because initial tubing head pressure is already a minimum value of 114.7 psia, the pressure drawdown thus can no longer be increased from Jan 03, 2010 onwards. Since the influx or pressure maintenance from bottom water is quite small, the pressure drawdown then gradually decreases together with oil production rate until the well is depleted. It is also shown in Figure 5.36 that subsequent re-productions of the well are unsuccessful because the reservoir has not enough pressure to lift well fluids.

On the other hand, CCD Run ID 25 shows much better well performance as shown in Figure 5.35b. The well starts with a high initial oil flow rate of about 3,000 STB/day without water production. The initial oil rate can sustain at a constant rate for about 2.5 months before water breakthrough. The gas produced from the well during this time period is the gas dissolved from solution gas as indicated by the gentle declining trend of gas-oil ratio. Also shown is the rapid increase in aquifer influx rate. Thus, a certain degree of pressure maintenance from the bottom water could occur. After water breakthrough, oil production rate declines whereas water cut continuously increases.

About 7 months after the beginning of the production, it can be noticed that the profiles of oil flow rate and water cut in Figure 5.35b are less steep. Investigation on fluid distribution in 3D model indicates that gas cresting almost reaches the horizontal wellbore. Small amount of free gas enters into the wellbore and slightly helps lift liquid in the well. However, the amount of gas is not great enough to significantly alter the trend of gas-oil ratio. This is another example of lifting effect from free gas cap. One month later, when free gas from gas cap almost fully enters

along the length of the wellbore, gas-oil ratio significantly increases continuously until the end of production.

Comparison of pressure profiles between CCD Run IDs 21 and 25 is shown in Figure 5.36. Obviously, it is shown that CCD Run ID 25 requires far smaller pressure drawdown than that of CCD Run 21 at a given time to produce far higher oil production rate. This observation implies that reservoir fluids lose less of its pressure or energy to flow to the wellbore to achieve the specified oil flow rate. Inevitably, this is attributed to higher rock permeability of the experiment. Comparison of initial water saturation of the two experiments is also shown in Figure 5.37. It can be seen that the horizontal well of CCD Run ID 21 is placed inside oil-water transition zone. This is the reason why initial water cut of the experiment is high and causes the well depleted very fast.

From the observations, it can be concluded that the URF significantly increases as PORO increases. As porosity of the reservoir increases initial water saturation around horizontal wellbore tends to decrease because of thinner oil-water transition zone. As a result, smaller initial water cut or delay in water breakthrough could be observed. Higher liquid production rate with smaller pressure drawdown could also be expected because of greater reservoir permeability. As a by-product, lesser degree of oil and gas cresting due to lesser pressure drawdown results in higher oil sweep efficiency. See Figure 5.38 for fluid saturations at the end of production of CCD run ID 21 and 25. Although gas cresting can be observed, Figure 5.38b reveals that there is no water cresting at the end of production of CCD run ID 25.

Table 5.19: Experiments for determining PORO main effect

Run ID	Reference Table	OWC	HO#	LHRATIO	WSTANDOFF	PORO	LRAT	URF (%)	Time to Reach URF (days)
21	5.3	6705.55	4.133	0.55	0.46	0.16	3027.5	0.83	88.00
25	5.3	6705.55	4.133	0.55	0.46	0.25	3027.5	28.18	406.33

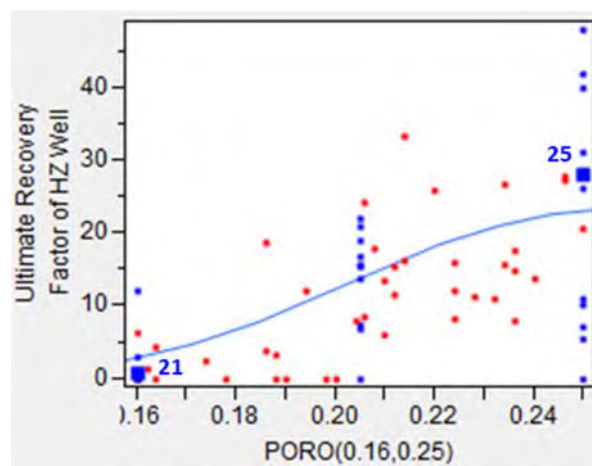


Figure 5.34: Marginal plot of PORO showing design points of CCD Run ID 21 and 25

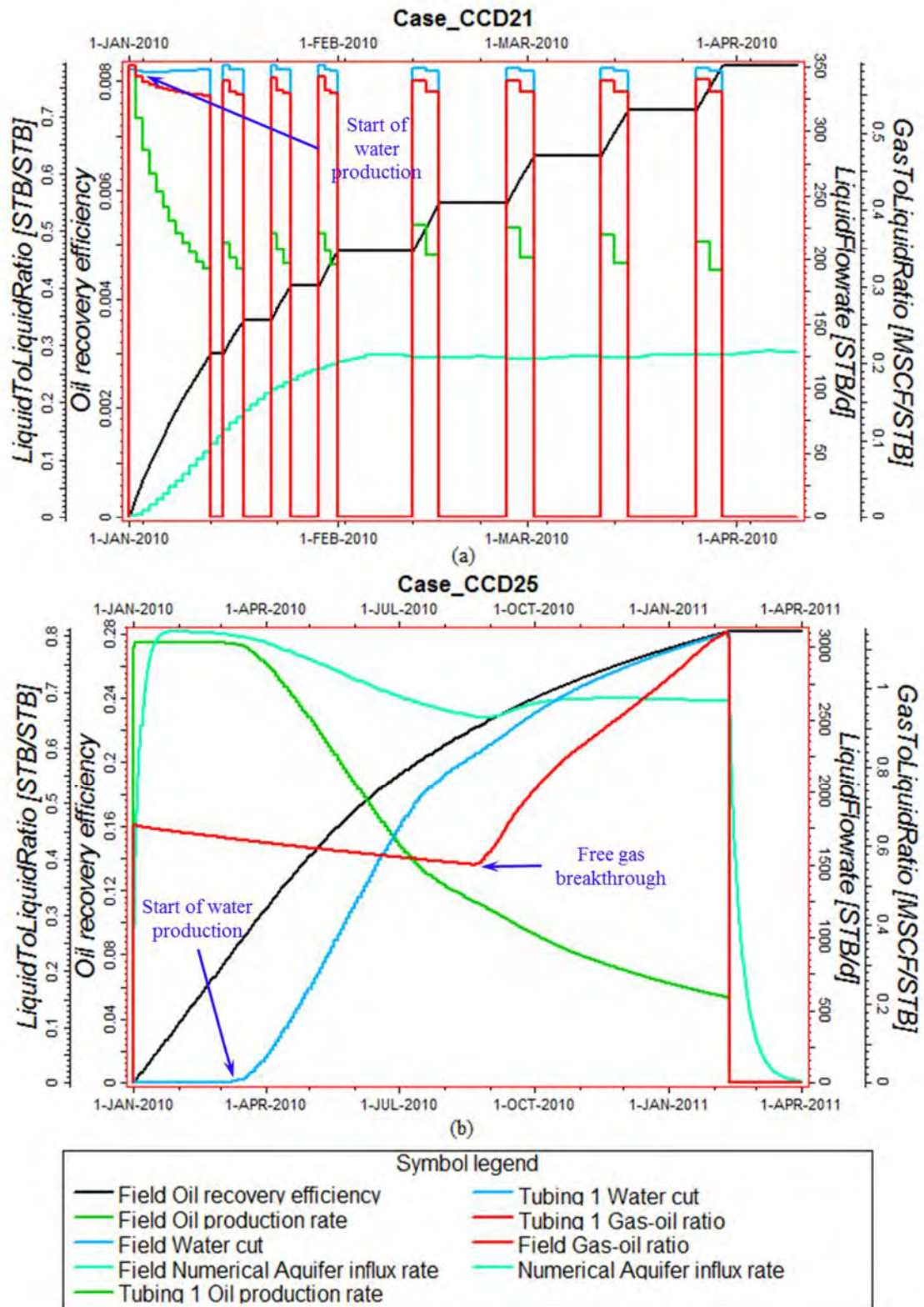


Figure 5.35: Production profiles of CCD Run ID (a) 21 (b) 25



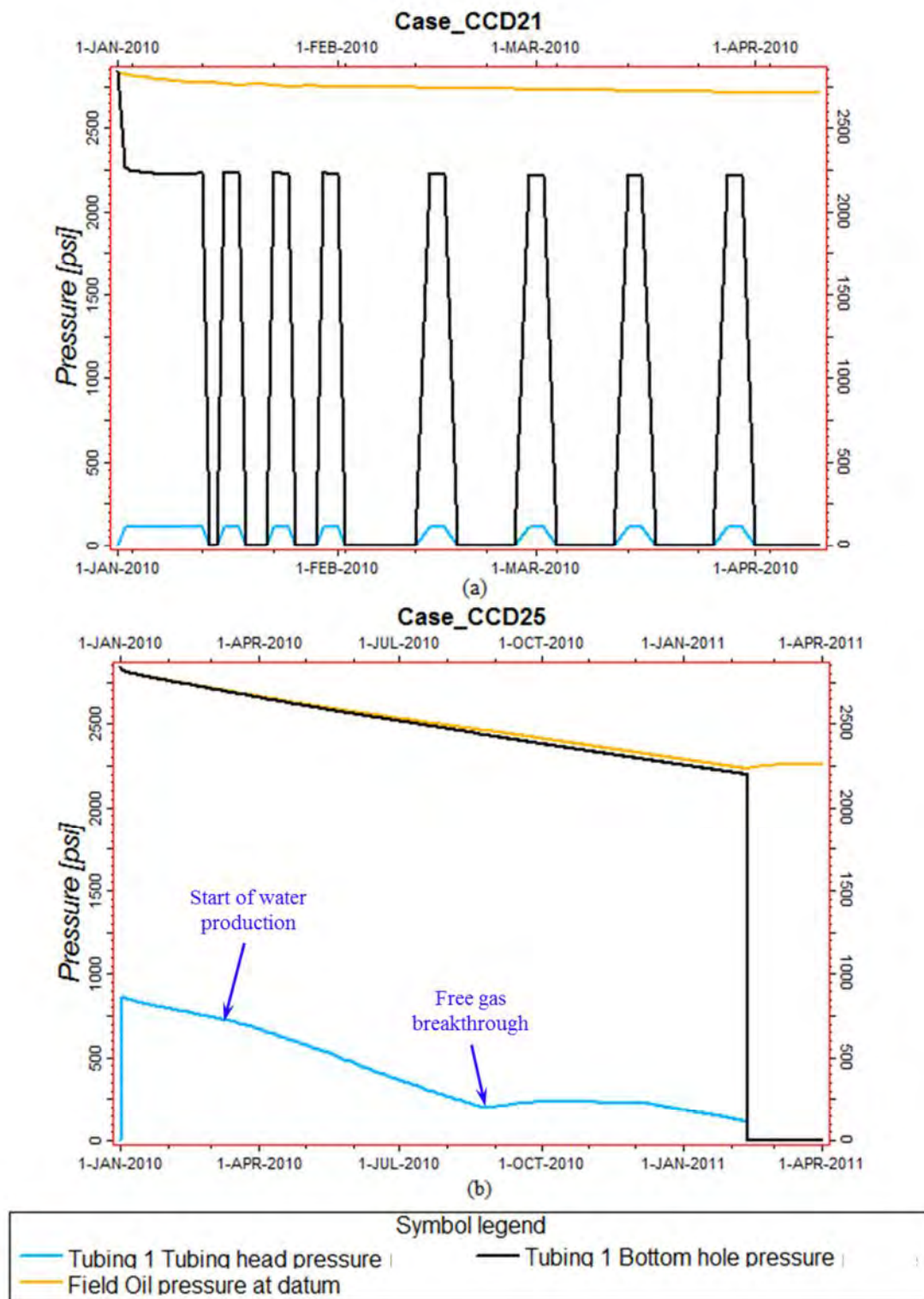
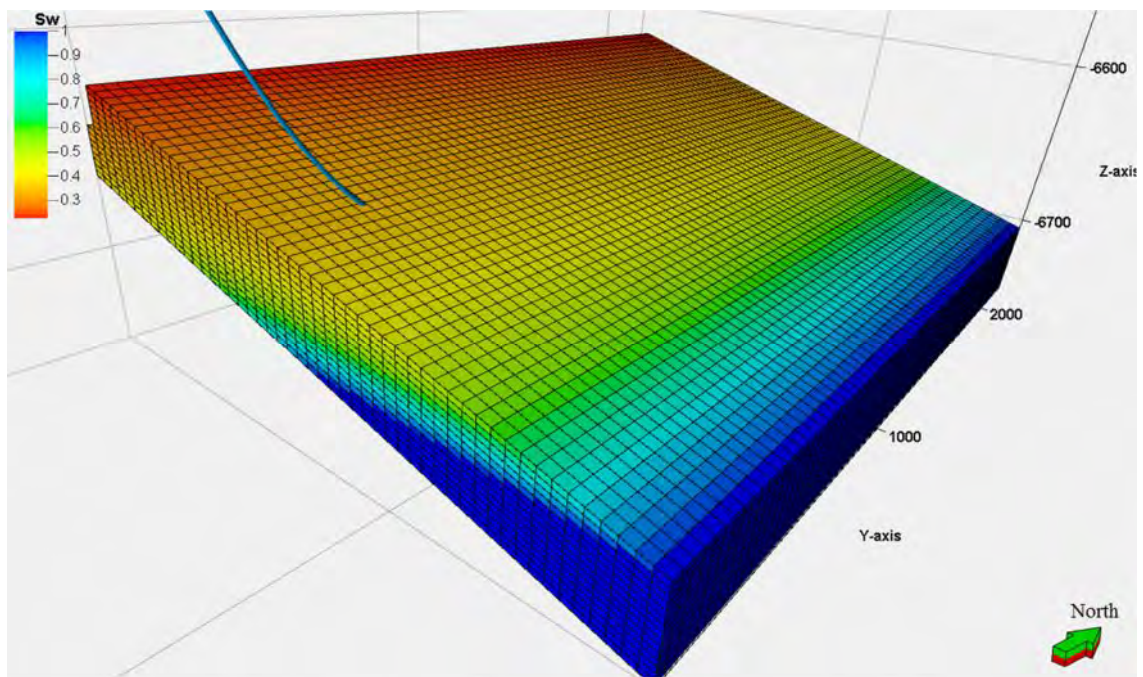


Figure 5.36: Pressure profiles of CCD Run ID (a) 21 (b) 25



(a)

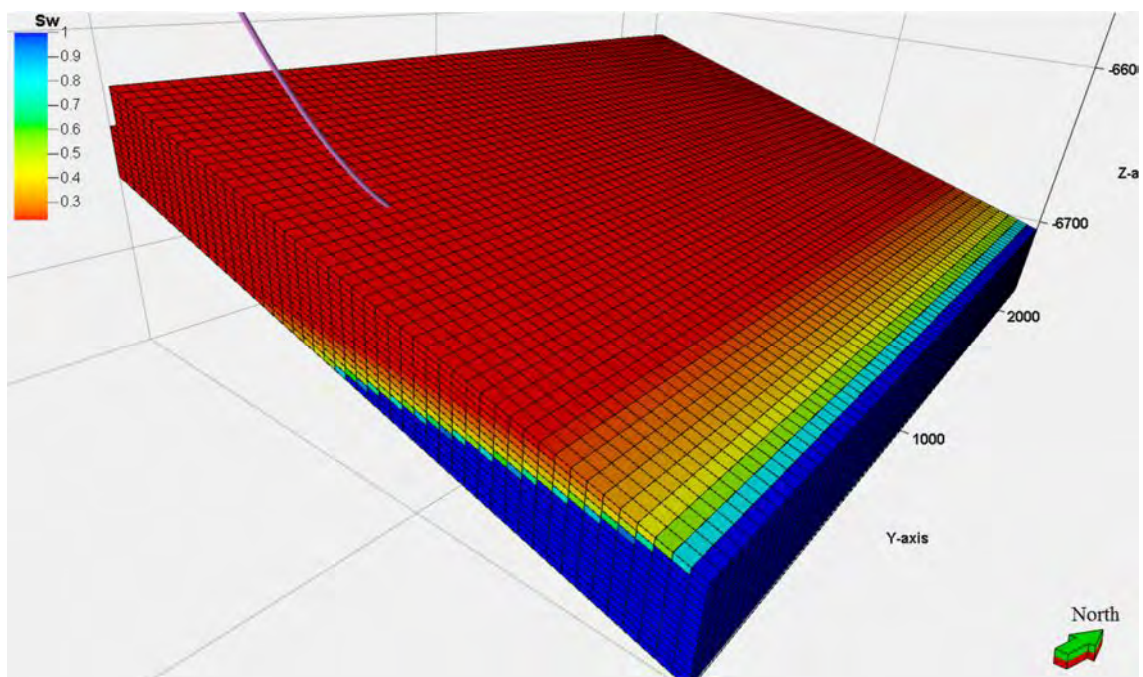
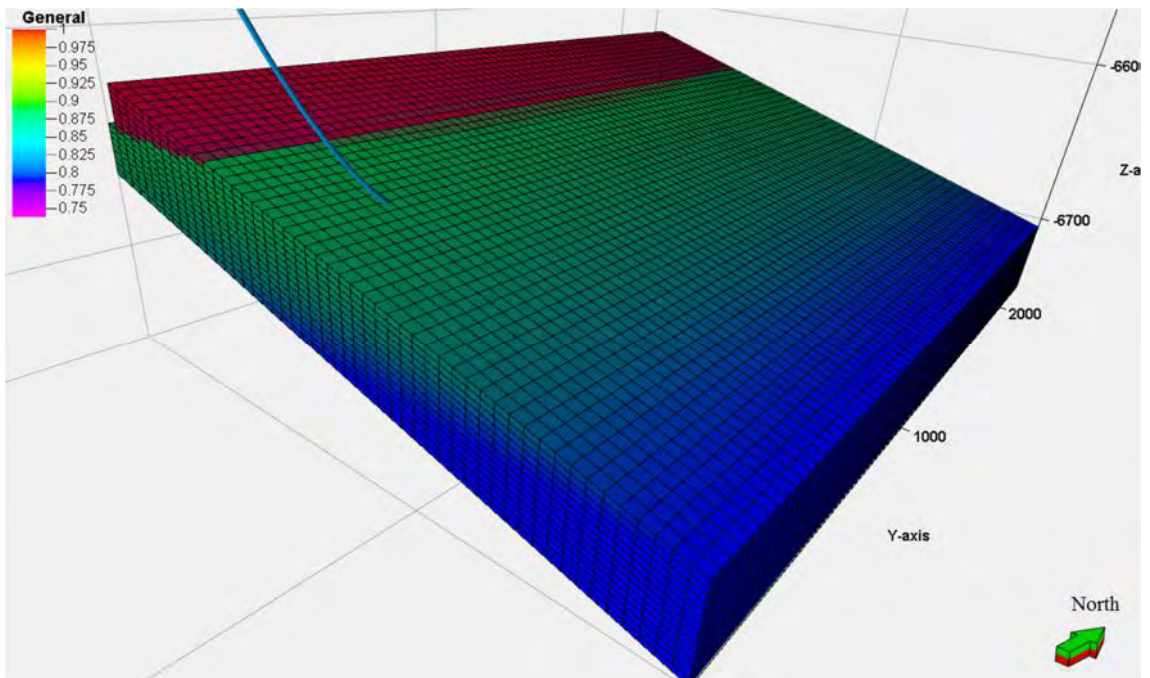


Figure 5.37: 3D reservoir model showing initial water saturation and horizontal wellbore of CCD Run ID (a) 21 and (b) 25



(a)

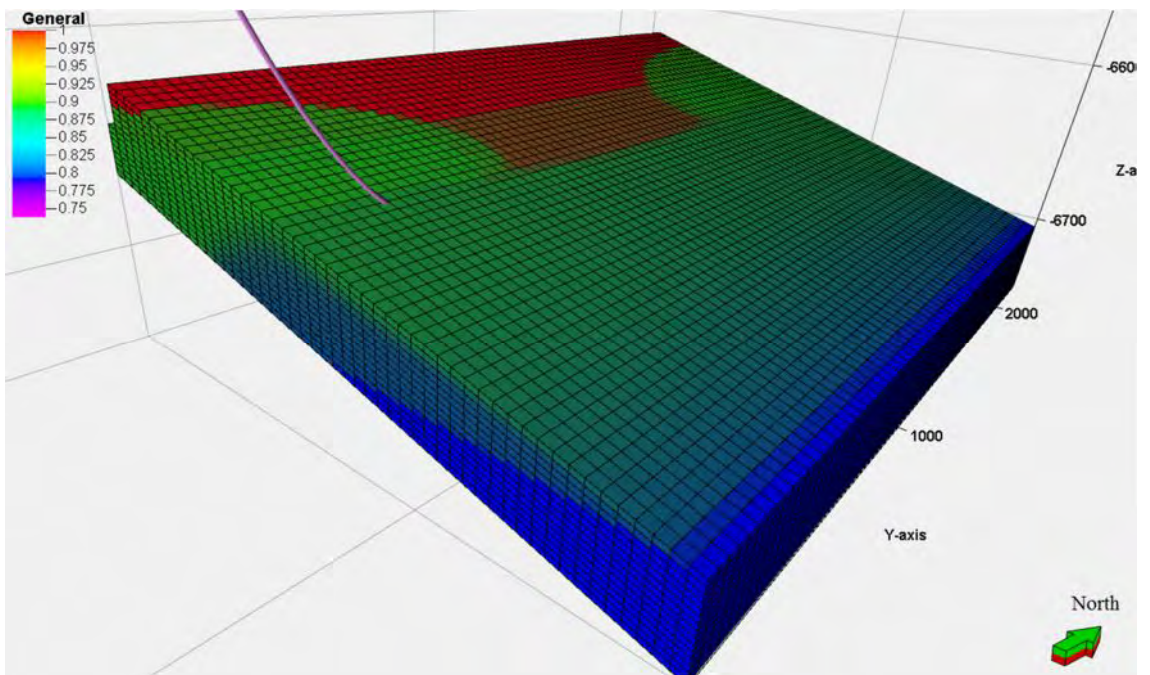


Figure 5.38: 3D reservoir model showing fluid saturations at the end of production and horizontal wellbore of CCD Run ID (a) 21 and (b) 25

### 5.3.1.5 Main Effect of Liquid Production Rate Control

In this section, six experimental results are compared to investigate the main effect of liquid production rate control or LRAT. Table 5.20 presents factor settings or design points of the six experiments. As shown, 3 new experiments are specifically performed to investigate the main effect in more detail. In fact, the 6 experiments constitute a one-variable-at-a-time design. Figure 5.39 shows the marginal plot of LRAT. Also shown in the figure is the average URF due to LRAT across the other factors. In fact, the average URF line could be considered as the model fitting of LRAT main effect. Joshi [7] mentions that, for a reservoir having potential gas or water cresting, oil recovery can be improved if oil production is properly controlled under a critical rate. This implies that if well production rate is higher, the tendency for water and gas cresting to occur should be higher and lower URF as a result. However, the average URF line at  $LRAT < 1,500$  STB/day shows a different conclusion as shown in Figure 5.39. Thus, the additional experiments are run for validating the model prediction.

After conducting all 3 new experiments, their URF and Run ID are plotted on LRAT marginal plot together with the other 3 existing points as shown in Figure 5.39. A dash line of interpolated trend of LRAT main effect is drawn by connecting these points. It can be seen from the dash line that main effect of LRAT decreases URF as LRAT increases. This result complies with what Joshi [7] mentioned. However, the maximum difference in URF over the factor range is only 5%. As LRAT is less than 1,500 STB/day, the proxy model tends to under-predict LRAT main effect. Investigation on the experimental results show that the well of many experiments having  $LRAT = 55$  STB/day cannot produce from the beginning because they have an initial oil flow rate less than a minimum economic limit of 50 STBO/day. This is the reason why the average URF line in the marginal plot converges to  $URF = 0$  as LRAT is reduced. Note that a correction method of the model due to this error is presented later in Section 5.4.

This is the reason why the average line shows a strange trend. Without the economic limit, the average response at an LRAT of 55 STB/day could be about 20%, which is an extrapolated value of the dash line shown in Figure 5.39. The importance

of this observation will be highlighted again when limitations of the proxy model are discussed.

Comparison of production and pressure profiles from Figures 5.40 to 5.45 shows that increasing LRAT can result in shorter gas breakthrough time and increasing water cut rate. This indicates that the problem of gas and water cresting is more severe. The negative impacts of early gas breakthrough are that it can cause sudden increase in gas flow rate, overload gas-handling facility on the surface, and increase required pressure drawdown in the reservoir. However, if gas handling is not an issue, it could help maintain oil flow rate due to its lifting effect. See Figure 5.40b for oil rate profile after free gas breakthrough. In addition, although oil production can be accelerated as LRAT increases, the resulting faster water production rate could cause the well be killed by liquid loadup faster as well. Consequently, less volume of oil can be swept by rising bottom water into the wellbore. See Figures 5.46 to 5.48 for unrecovered oil in the reservoir of all experiments except CCD Run ID 22.

Table 5.20: Experiments for determining LRAT main effect

Run ID	Reference Table	OWC	HO#	LHRATIO	WSTANDOFF	PORO	LRAT	URF (%)	Time to Reach URF (days)
CCD22	5.3	6705.55	4.133	0.55	0.46	0.21	55	0.00	1.00
CCD22A	New Run	6705.55	4.133	0.55	0.46	0.21	500	20.06	1669.00
CCD23A	New Run	6705.55	4.133	0.55	0.46	0.21	1500	18.69	553.00
CCD23	5.3	6705.55	4.133	0.55	0.46	0.21	3027.5	15.67	171.33
CCD24A	New Run	6705.55	4.133	0.55	0.46	0.21	5000	15.34	144.67
CCD24	5.3	6705.55	4.133	0.55	0.46	0.21	6000	15.34	144.67

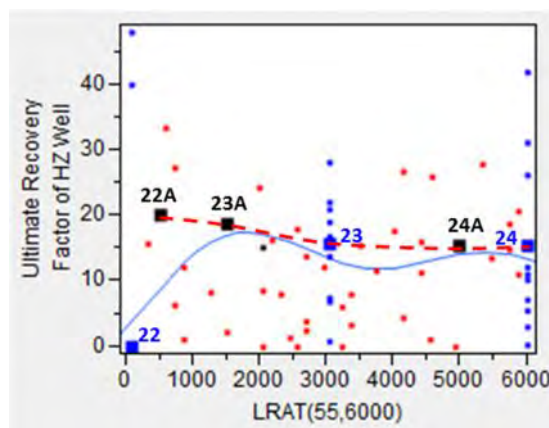


Figure 5.39: Marginal plot of HO# showing design points of CCD Run ID 22, 22A, 23, 23A, 24, and 24A

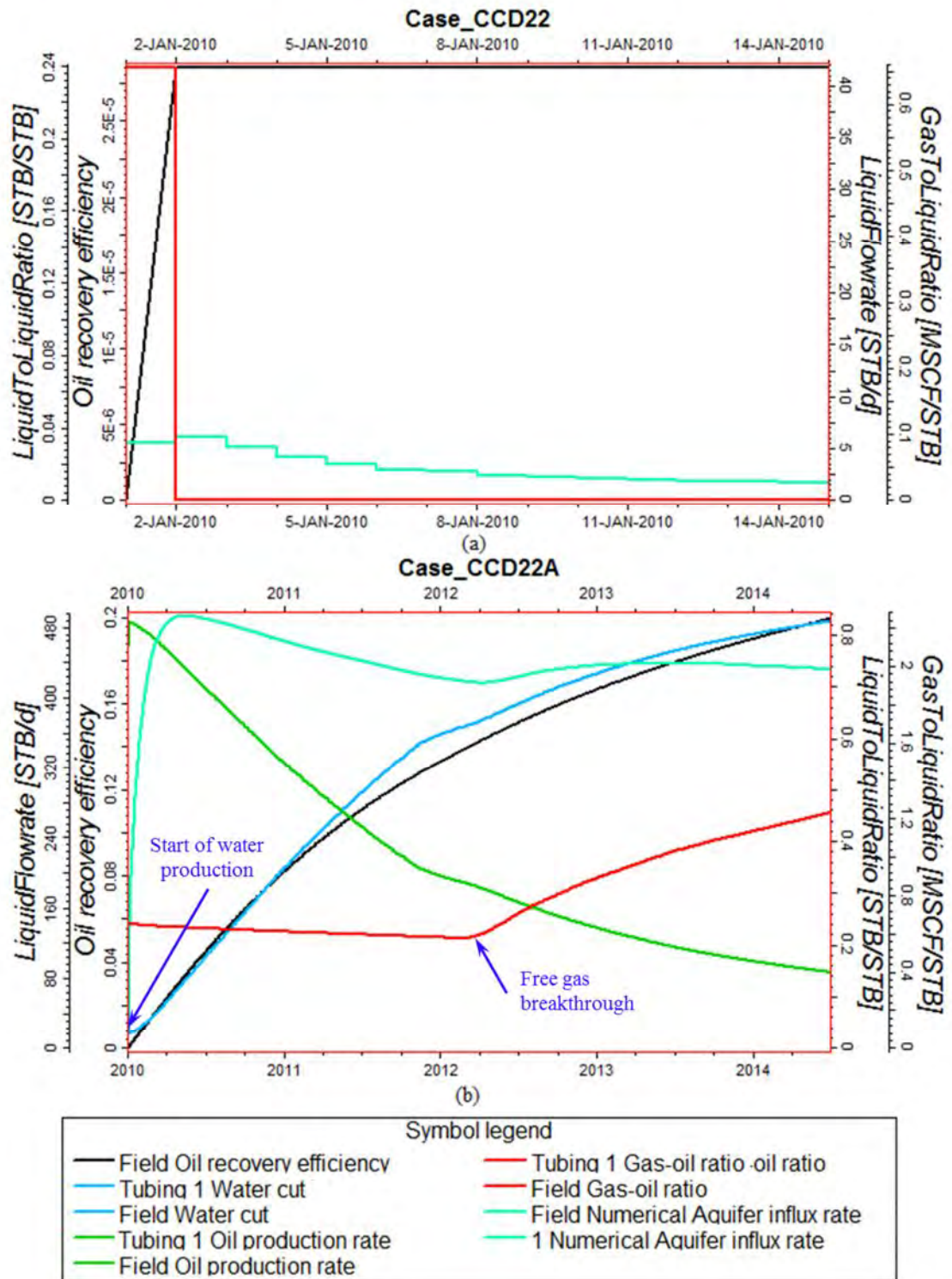


Figure 5.40: Production profiles of CCD Run ID (a) 22 (b) 22A

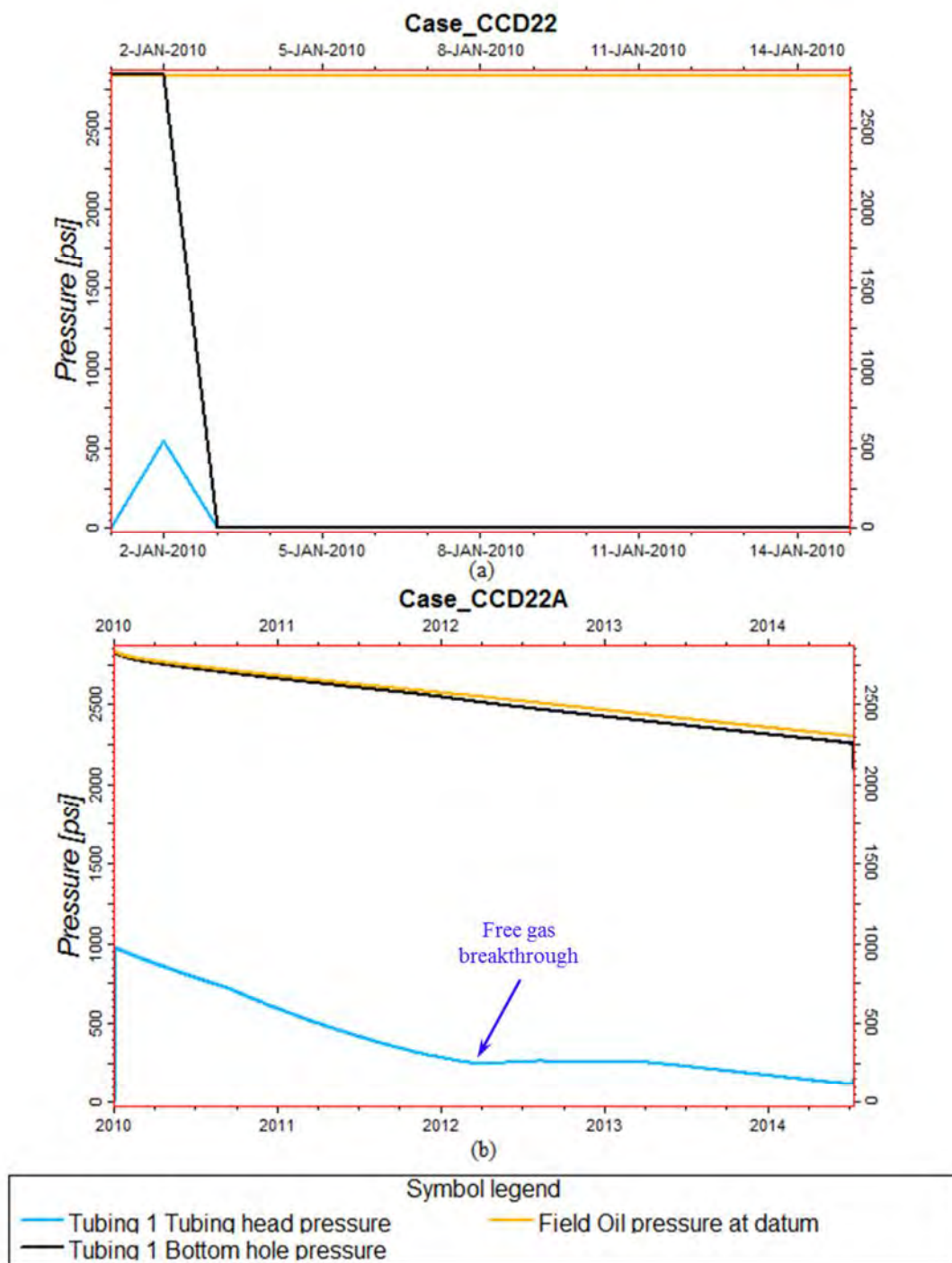


Figure 5.41: Pressure profiles of CCD Run ID (a) 22 (b) 22A



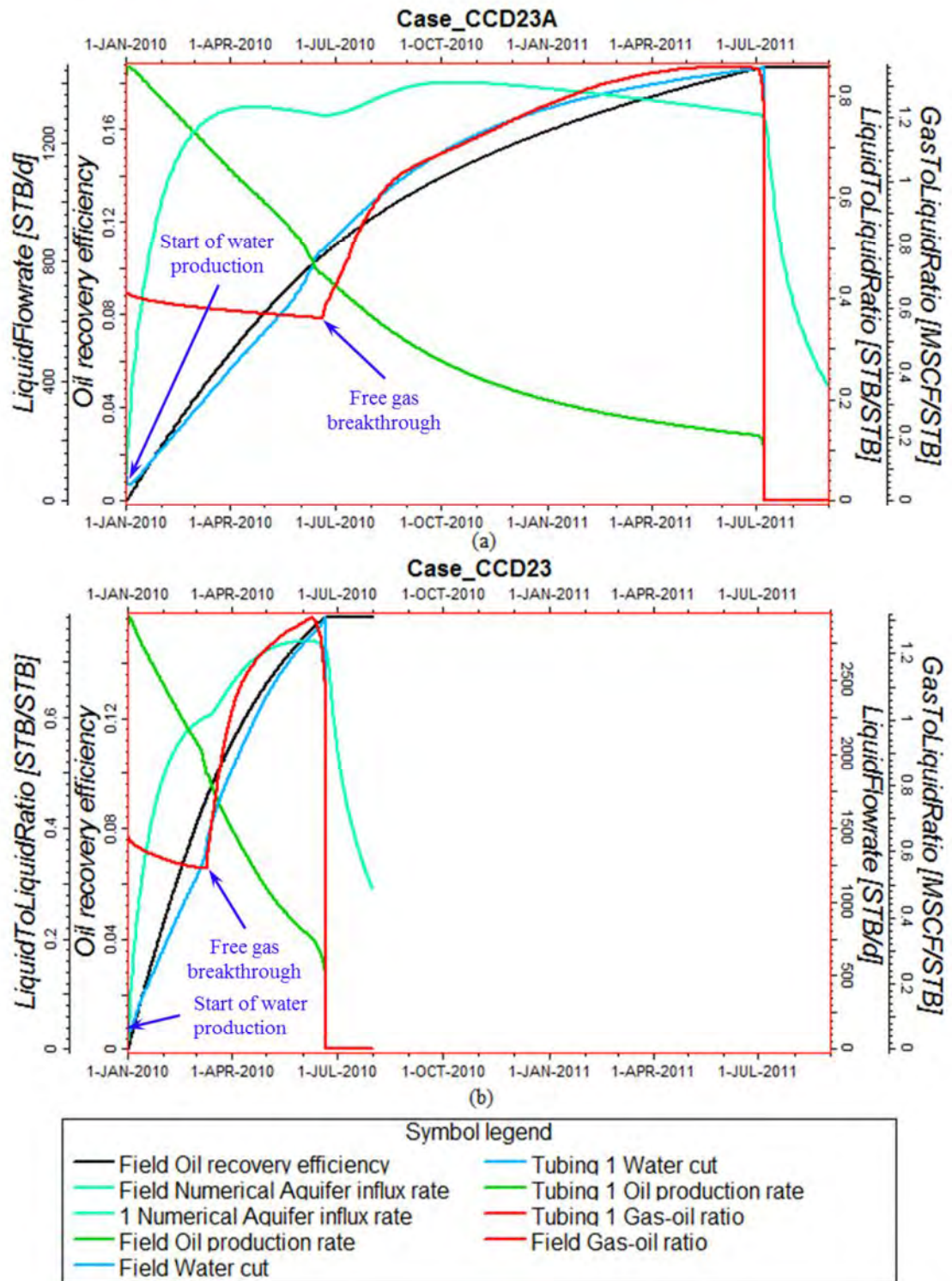


Figure 5.42: Production profiles of CCD Run ID (a) 23A (b) 23

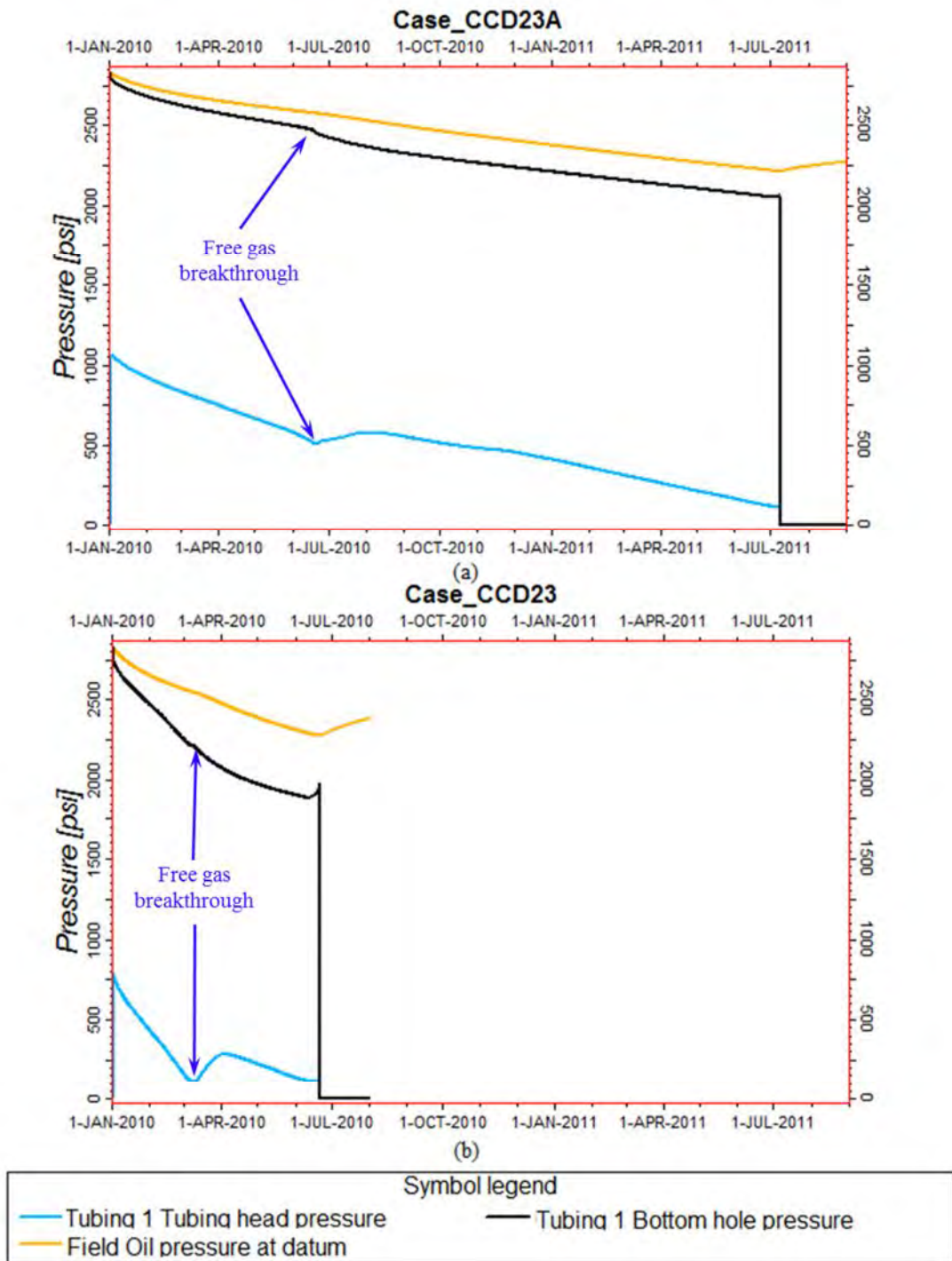


Figure 5.43: Pressure profiles of CCD Run ID (a) 23A (b) 23

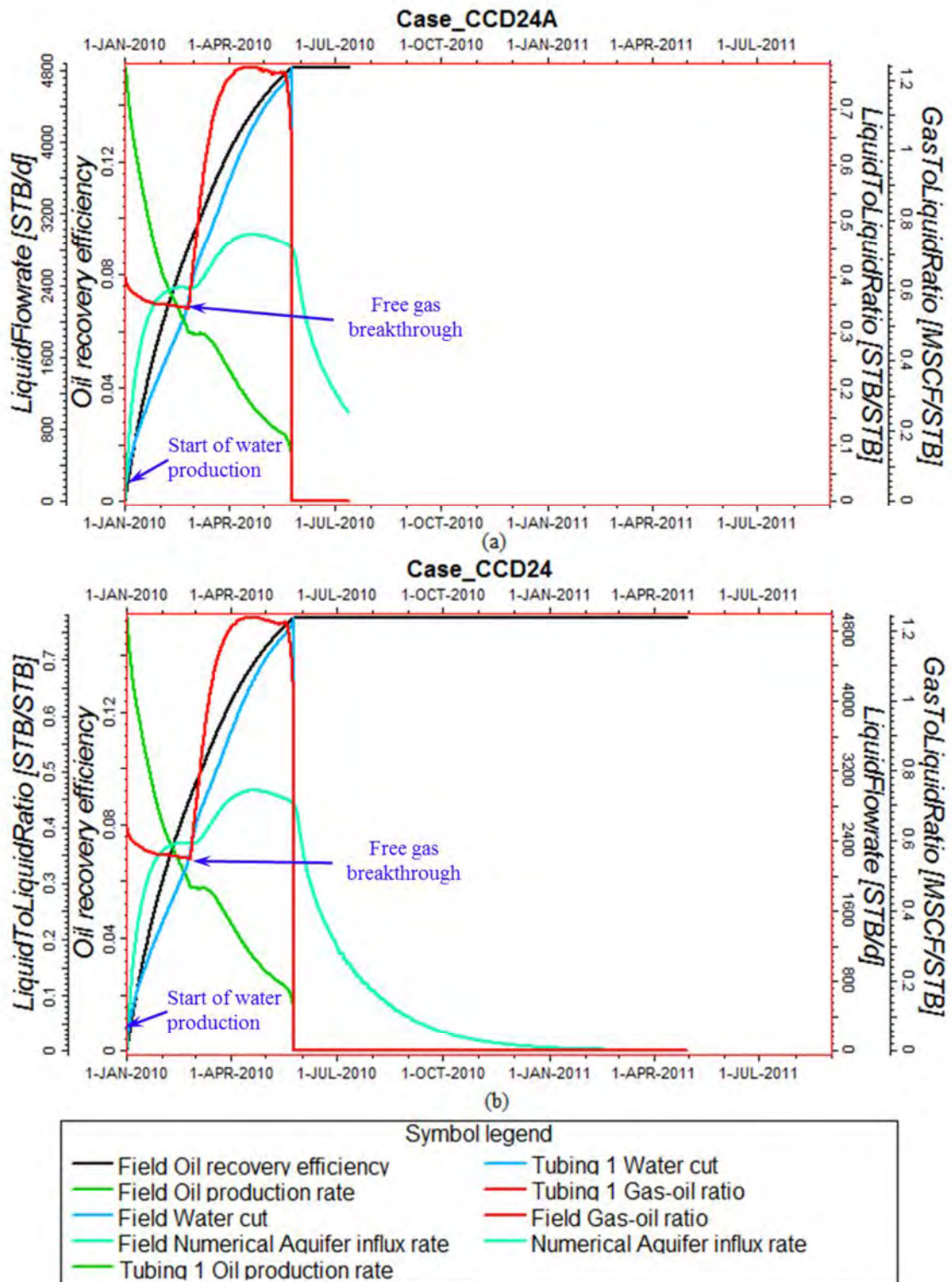


Figure 5.44: Production profiles of CCD Run ID (a) 24A (b) 24

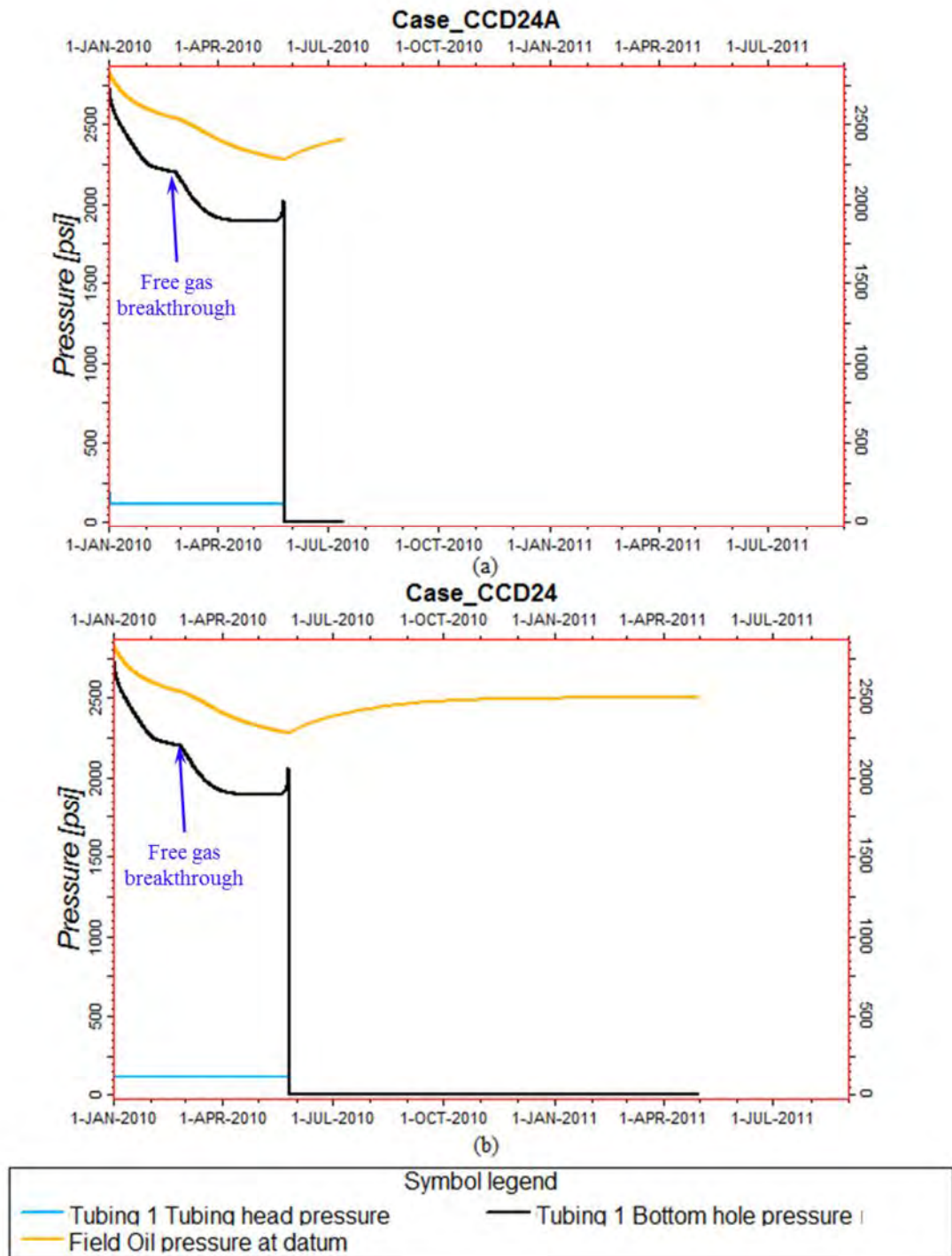


Figure 5.45: Pressure profiles of CCD Run ID (a) 24A (b) 24

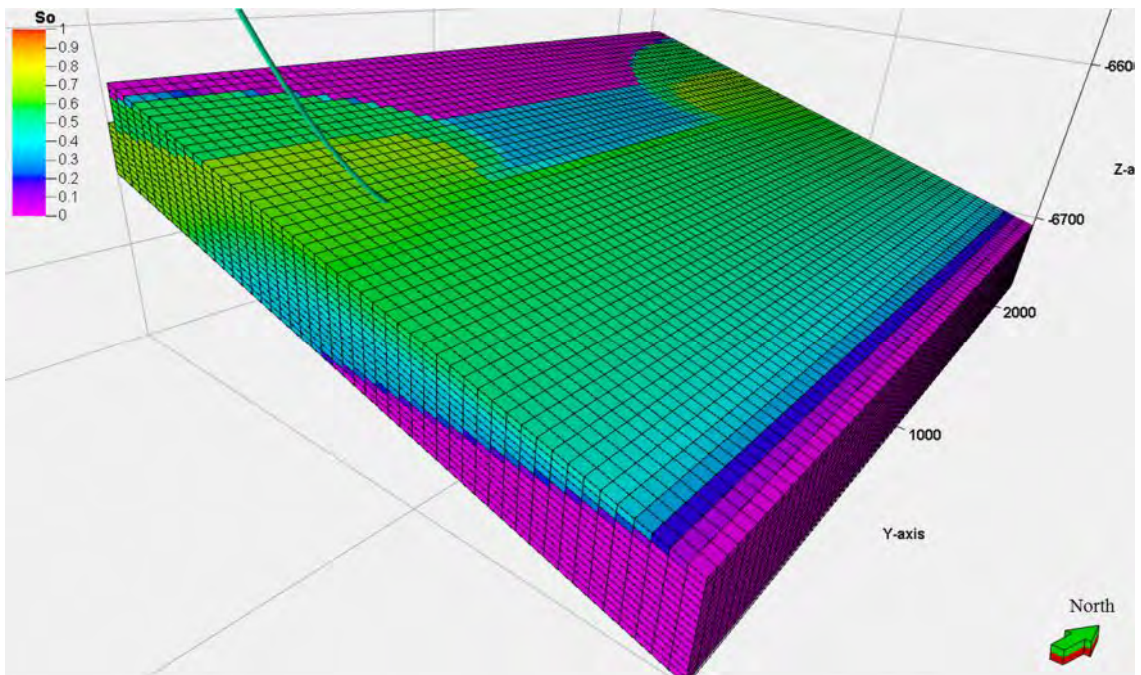


Figure 5.46: Oil saturation distribution at the end of production of CCD Run ID 22A

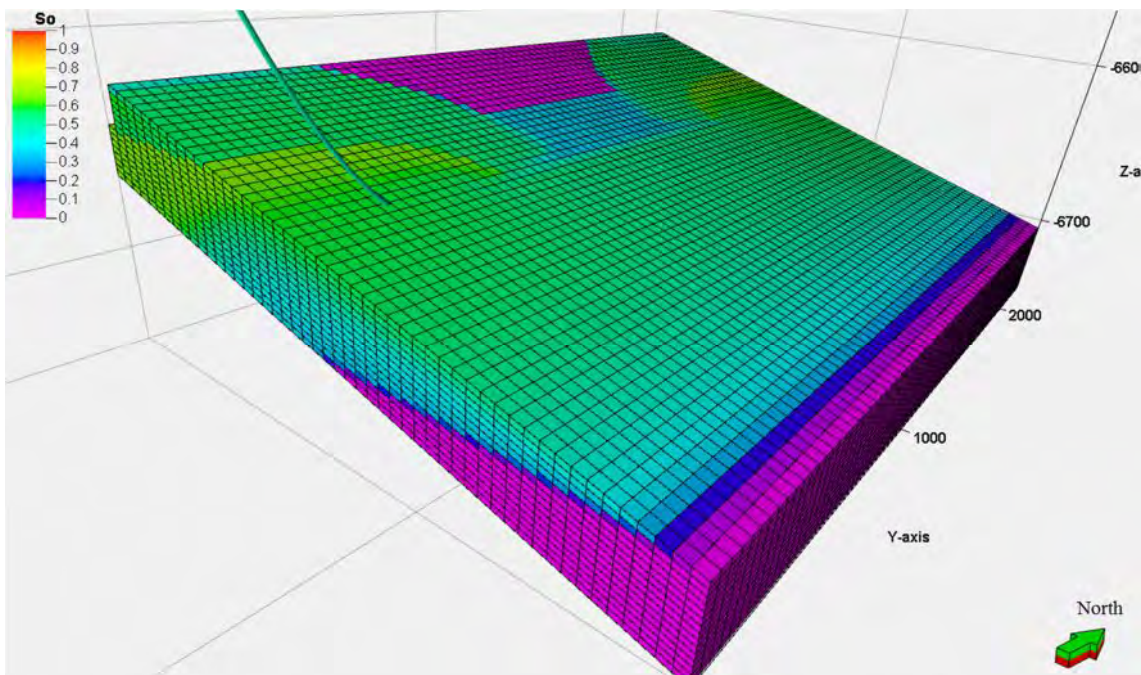


Figure 5.47: Oil saturation distribution at the end of production of CCD Run ID 23A

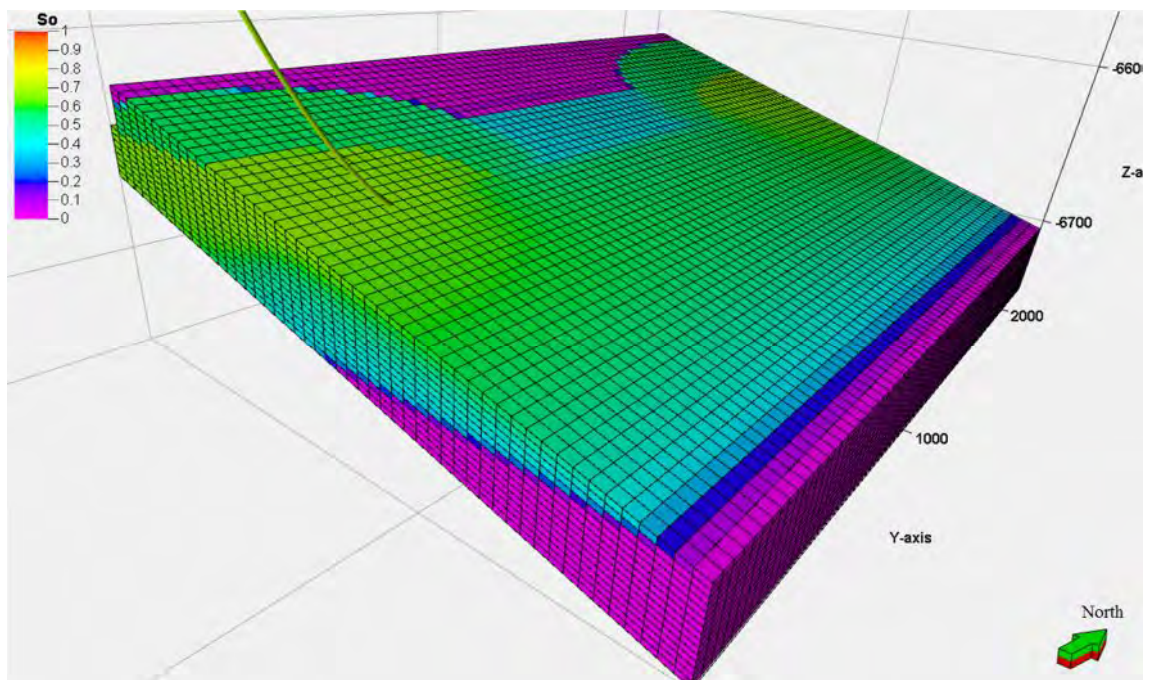


Figure 5.48: Oil saturation distribution at the end of production of CCD Run ID 23

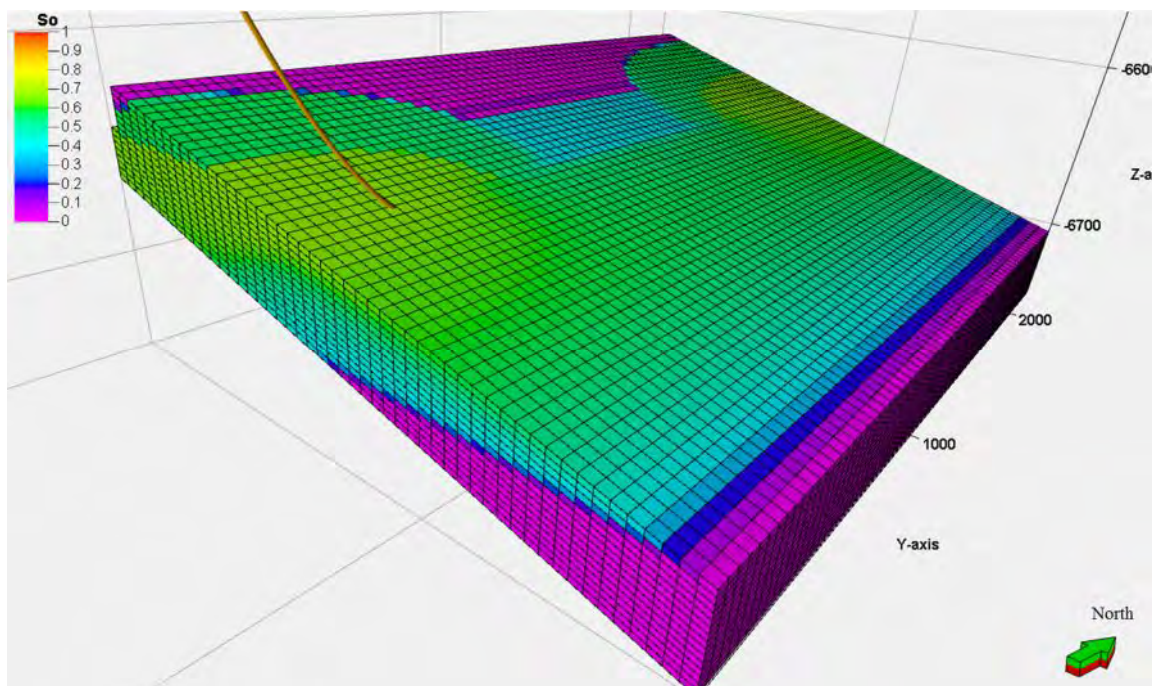


Figure 5.49: Oil saturation distribution at the end of production of CCD Run ID 24A

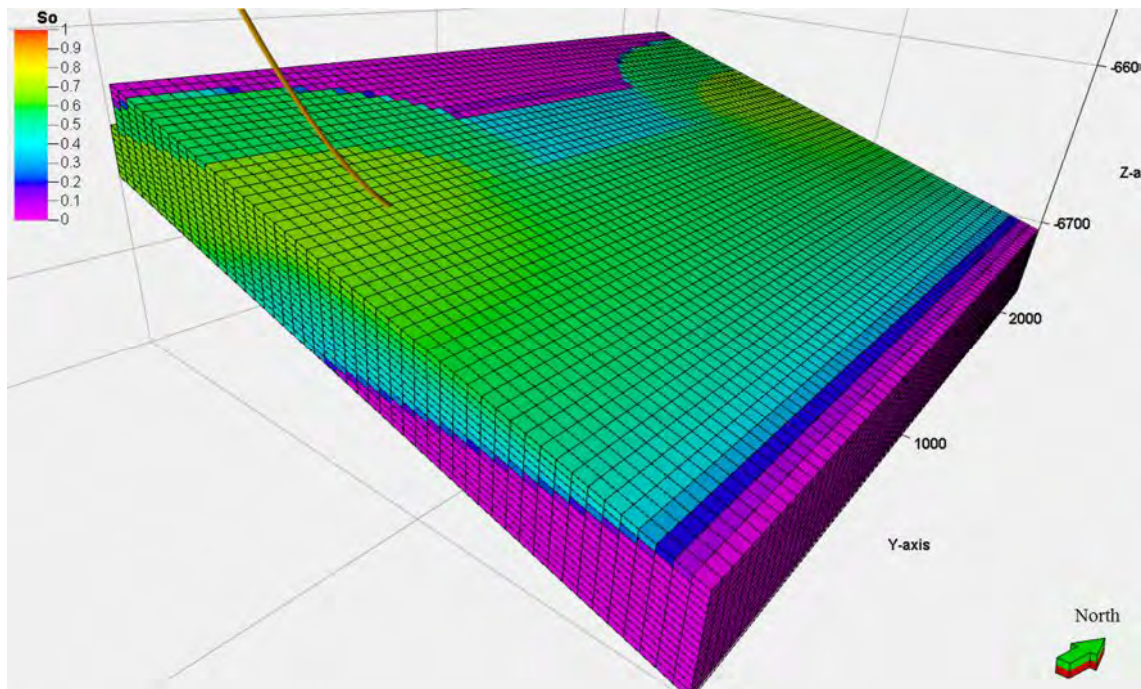


Figure 5.50: Oil saturation distribution at the end of production of CCD Run ID 24

### 5.3.2 Influence of Interaction Effects

This section discusses effects of factor interactions on the URF. As described in Chapter 3, interaction effects cannot be identified by conducting one-variable-at-a-time experiments, but factorial ones. For this research, summary of main and interaction effects of the six significant design factors calculated using Gaussian process method is reported in Table 5.15. The factors effects are normalized by total sensitivity of combined 45-run central composite and 45-run maximum entropy designed experiments for the ease of understanding.

From the table, it can be seen that about 19% of total variation of URF in the design hyperspace is contributed by two-factor interactions. Thus, neglecting factor interaction in proxy fitting could cause significant prediction error. However, one assumption based on the principle of sparsity effects is that three- or higher factor effects are negligible and can be ignored. However, this assumption is not totally the case in this research because it is found that two-factor interaction profiles generated by JMP can slightly change as a factor level is varied. To be meaningful, only the factor interactions whose effect is greater than 1% of total sensitivity are discussed.

Figure 5.51 presents JMP two-factor interaction profiles of the design-combined Gaussian proxy model at the optimum factor setting. Refer to Figure 5.14 for the optimum factor setting. In the plots, the evidence of interaction is nonparallel lines. Relatively significant factor interactions highlighted in Table 5.15 are enclosed by a red box. Each of two plotting aspects of the same factor interaction is assigned by a numeric and an alphabetic characters which have the same sequential order for each, e.g. 1 and A, 2 and B, etc.

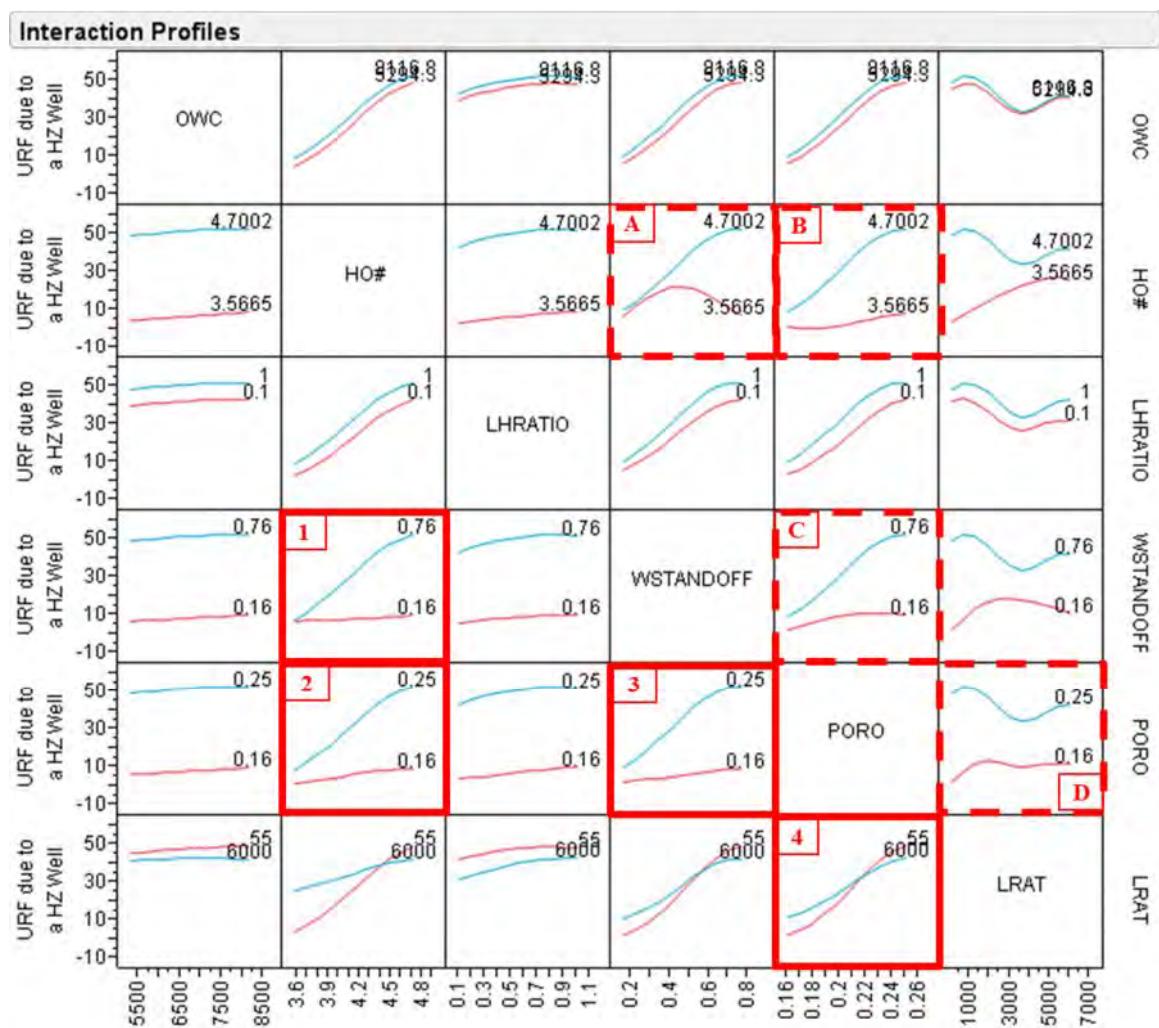


Figure 5.51: JMP interaction profiles at optimum factor setting of design-combined Gaussian proxy model for horizontal well production



A careful observation on the interaction plots reveals that three of the four relatively significant interactions are interactions of PORO. Three out of them, which are WSTANDOFF\*HO#, PORO\*HO#, and PORO\*WSTANDOFF, are interactions of the top three most significant factors listed in Table 5.10. Besides, they also show similar characteristic of interaction. For example, Interaction plot 1 shows that the effect of WSTANDOFF on the URF is greater as the level of HO# increases. On the other hand, as WSTANDOFF increases in Interaction plot A, the effect of HO# also increases. In other words, the effect on URF of either one of PORO, WSTANDOFF, and HO# can be amplified as the level of either one or two of the other factors increases. As discussed in Section 5.3.1, vertical thickness of oil-water transition zone can be decreased if PORO is increased. If only WSTANDOFF increases, the well will be farther away from oil-water contact and transition zone resulting in delay in water breakthrough. And, initial water saturation around a horizontal well can be decreased as HO# increases at a constant WSTANDOFF. Since PORO, WSTANDOFF, and HO# interact with the thickness of oil-water transition zone, they interact with one another.

For PORO\*LRAT interaction, Interaction plot 4 shows that, at the low level of PORO, the lesser LRAT results in the smaller URF. However, it is discussed in Section 5.3.1.5 that more oil can be recovered from a reservoir if LRAT is smaller because of less severity of gas and water cresting problem. This is attributed to prediction error of the proxy model. Later in Section 5.4, it is shown that URF prediction of the design-combined proxy model is not adequately accurate for some regions of the design hyperspaces and some correction is required. Therefore, the interaction profiles of LRAT\*PORO in Figure 5.51 could be incorrect and not discussed here.

## 5.4 Limitations of Design-Combined Gaussian Proxy

This section discusses limitations on using the design-combined Gaussian proxy model. In Section 5.3.1.5, a discussion on prediction error of LRAT main effect and its cause are described. It is found that on average, when  $LRAT < 1,500$  STB/day, the proxy model tends to under-predict the main effect of LRAT. Figure 5.52 re-

presents marginal plots of the design-combined proxy model. In the figure, the design points, whose LRAT setting is at the low level and URF equals to zero because of a minimum required oil flow rate of 50 STB/day, are highlighted. It can be observed from the figure that the highlighted design points are equally distributed over the factor range of OWC, HO#, and LHRATIO. However, most of them tend to flocculate when  $LRAT \leq 1,500$  STB/day,  $WSTANDOFF \leq 0.46$ , and  $PORO \leq 0.205$ . Thus, it could be prudent to set predicted URF of a design point equal to zero when  $LRAT \leq 1,500$  STB/day,  $WSTANDOFF \leq 0.46$ , and  $PORO < 0.205$ .

To find out region in the design hyperspace which LRAT main effect is dominant, the design points in the vicinity of the dash line in Figure 5.39 are bold and re-presented in Figure 5.53. It should be noted again that the dash line is obtained from one-variable-at-a-time experiments having LRAT varied, but the other factors set at their mid value. Thus, it represents the effect of LRAT main effect. Figure 5.53 shows that LRAT main effect plays an important role on URF when  $PORO \geq 0.205$  and  $WSTANDOFF \leq 0.46$ . From the figure, it can be seen that the optimum URF predicted by the proxy model is about 17% when LRAT equals to 1,500 STB/day. By extrapolating to the dash line to the low level of LRAT, the obtained URF is approximately 20% which is slightly larger than 17%. To obtain a more accurate URF prediction, an LRAT of 1,500 STB/day should be input into the proxy model when a design point has  $LRAT \leq 1,500$  STB/day,  $WSTANDOFF \leq 0.46$ , and  $PORO \geq 0.205$ .

By applying the above corrective actions on the prediction of proxy model, the obtained result is cross-validated again against 36-run validating experiments as described in Sections 4.5 and 5.2.3.2. Figure 5.54 presents the matched pairs t-test of the corrected URF prediction. When compared with the original result shown in Figure 5.18, the new result shows slight improvement on prediction precision as the standard error of URF difference is reduced from 0.739 to 0.645. The correlation between predicted URF and actual URF increases from 0.89 to 0.92. In addition, it should be noticed that almost all differences in URFs fall within a range of  $\pm 5\%$ .

In conclusion, the conditions and limitations of the design-combined proxy model in Equation 5.5 are as follows:

- 1) The predicted URF is for a reservoir depleted by a horizontal well under primary depletion.

- 2) The horizontal well has open-hole completion with a wellbore diameter of 6-1/8". A 2.875" API J-55 tubing is used and installed from the well heel to the surface.
- 3) Generic correlations and petrophysical properties presented in Appendix D are used in reservoir modeling. The proxy model should be used with caution when lab test or field measurements show significant deviations from the correlations.
- 4) Economic limits and operational constraints shown in Table 4.5 are used.
- 5) The reservoir rock is homogenous and consolidated sand having a constant rock compressibility of  $8 \times 10^{-6} \text{ psi}^{-1}$ .
- 6) On average, gravity of free gas in gas cap is 0.77 and bottom water salinity is 1,000 ppm
- 7) The proxy model is valid only within the design hyperspace used to construct the model. In other words, Levels of design factors to be used in the model must be within the P10 to P90 values as shown in Table 4.2.
- 8) If  $\text{LRAT} \leq 1,500 \text{ STB/day}$ ,  $\text{WSTANDOFF} \leq 0.46$ , and  $\text{PORO} < 0.205$ , the predicted URF should be reset to zero.
- 9) If  $\text{LRAT} \leq 1,500 \text{ STB/day}$ ,  $\text{WSTANDOFF} \leq 0.46$ , and  $\text{PORO} \geq 0.205$ , an LRAT of 1,500 STB/day should be used to substitute in the proxy model instead of that of the design point.

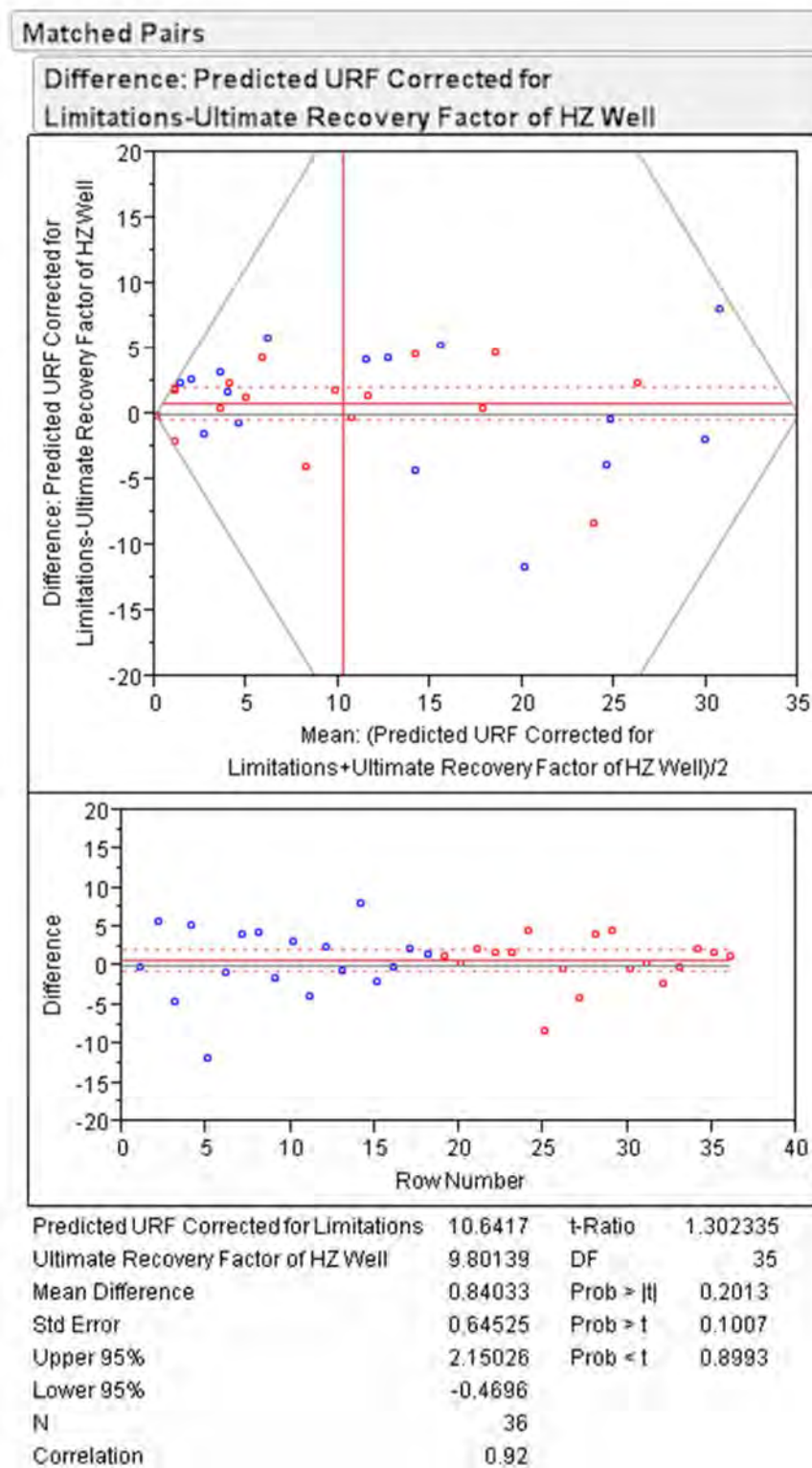


Figure 5.52: Corrected matched pairs t-test for validating design-combined Gaussian process proxy for horizontal well production

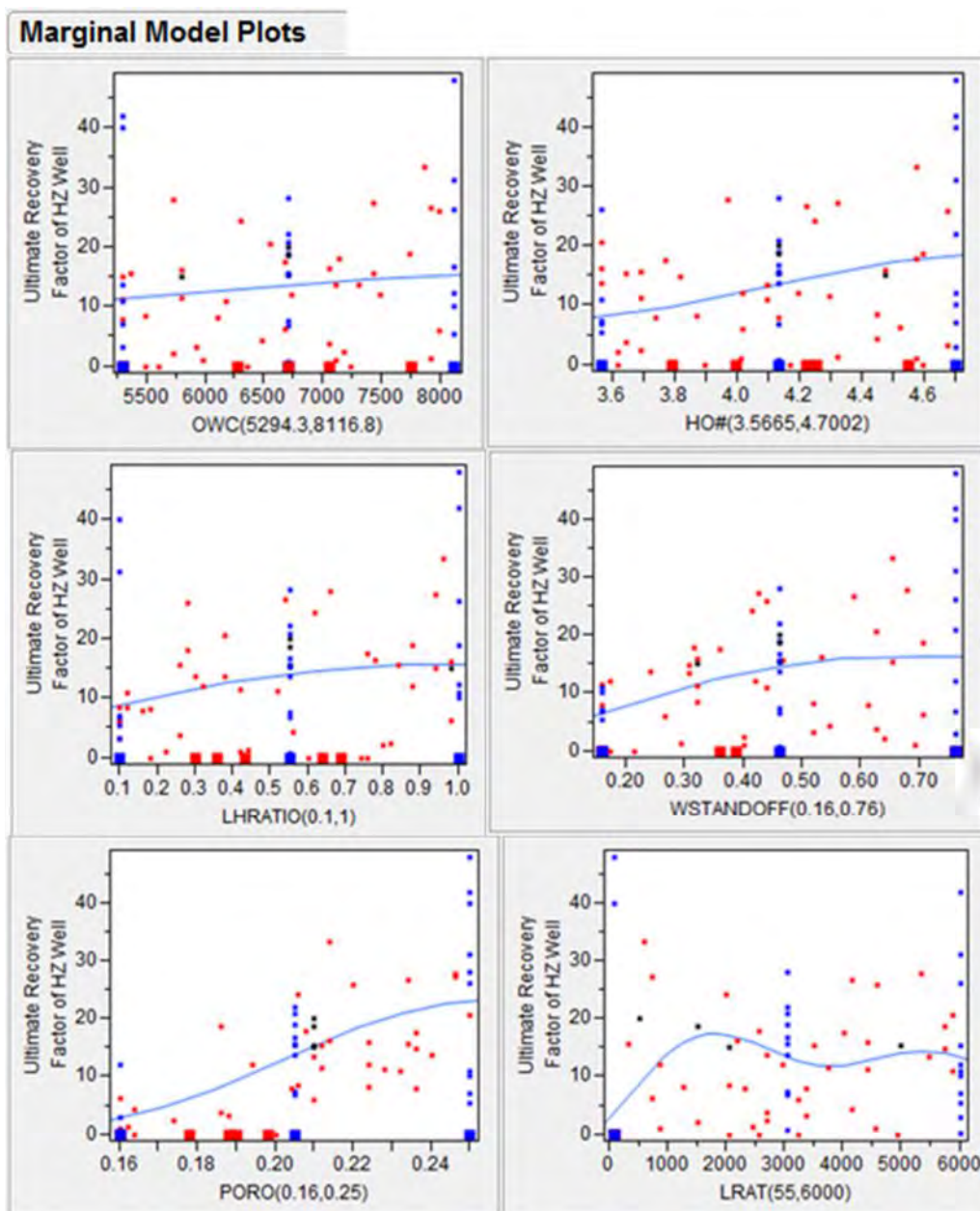


Figure 5.53: Marginal plots of design-combined proxy model with design points having URF = 0% and LRAT = 55 STB/day in bold

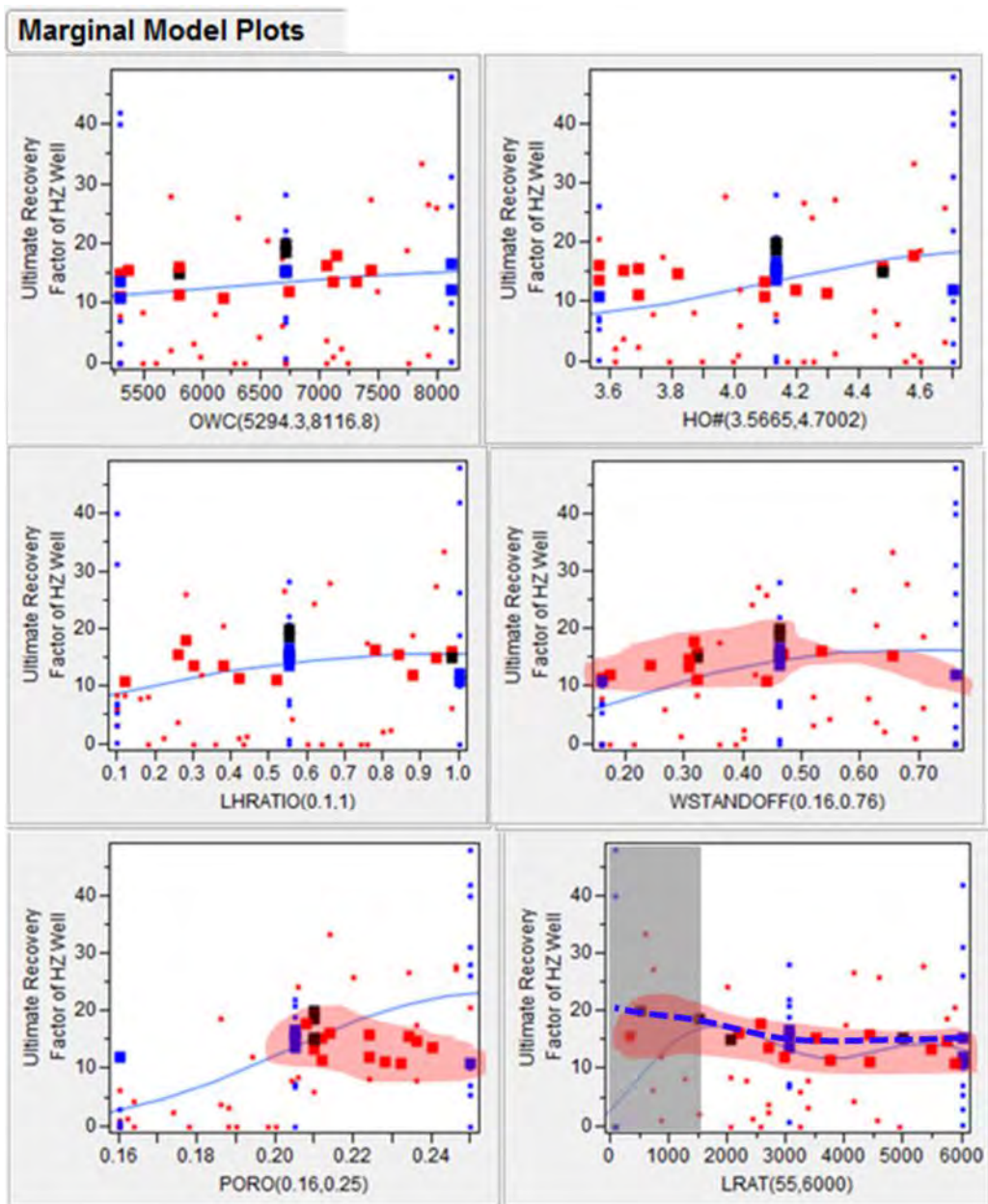


Figure 5.54: Marginal plots of design-combined proxy model showing design points whose response is dominated by LRAT main effect

## 5.5 A Simple Reservoir Screening Method

This section describes an application of experimental designs and proxy models to be used as a simple method for screening out high potential reservoir candidates for horizontal well development. Steps 10 and 11 as outlined in Section 1.6 are followed to develop the screening method. First of all, develop a design-combined proxy model which predicts a URF due to production of two vertical wells equivalent to a horizontal well. Refer to Figure 4.4 for a horizontal well and its equivalent vertical wells. The basic strategy behind is that one horizontal well will be replaced by two vertical wells if there is no improvement in economic result. Thus, the 45-run central composite and 45-run maximum entropy designs described in earlier sections are re-experimented as described in Section 4.6. Their results are shown in Tables E1 and E2 in Appendix E. JMP software is then used to analyze the data and fit a Gaussian process proxy model. Table E3 presents estimates of factor effects and fitted parameters of the proxy model. Equation 5.6 and Tables 5.21 to 5.23 show mathematical expression of the proxy model and its corresponding fitted model parameters.

$$URF = \begin{cases} 0 & , [URF] < 0 \\ [URF] & , [URF] \geq 0 \end{cases} \quad (5.6)$$

where,

URF = ultimate oil recovery due to a horizontal well

$[URF] = \mu + [R]_{1xi} [\beta_j]_{ix1} + [R]_{1xj} [\beta_j]_{jx1}$

$\mu = -0.63118$

$[R]_{1xi} = [ \text{Exp}(\sum_{i=1}^i \sum_{k=1}^k \theta_k (x_k - x_k^i)^2) ]$

$[R]_{1xj} = [ \text{Exp}(\sum_{j=1}^j \sum_{k=1}^k \theta_k (x_k - x_k^j)^2) ]$

k = total number of design factors = 6

$x_k$  =  $k^{\text{th}}$  design factor. See Table 5.21

$x_k^i$  = level setting of Design factor  $x_k$  of the design point of Run ID. "iV" in Table E1

- $x_k^j$  = level setting of Design factor  $x_k$  of the design point of Run ID. “300+jV” in Table E2
- $i$  = total number of design points of maximum entropy design = 45
- $j$  = total number of design points of central composite design = 45
- $\theta_k$  = fitted model parameter of Design factor  $x_k$ . See Table 5.21
- $[\beta_i]_{i \times 1}$  = regression coefficient corresponding to  $i^{\text{th}}$  design point. See Table 5.22
- $[\beta_j]_{j \times 1}$  = regression coefficient corresponding to  $j^{\text{th}}$  design point. See Table 5.23

Table 5.21: Theta regression coefficients of the design-combined Gaussian process proxy model for vertical well production

k	1	2	3	4	5	6
$x_k$	OWC	HO#	LHRATIO	WSTANDOFF	PORO	LRAT
$\theta_k$	8.306E-09	0.1879	0.2333	6.5841	169.405	2.945E-08

Goodness-of-fit of the proxy model is checked by plotting actual and jackknife URFs predicted by the proxy model in Figure E1. From the figure, it can be seen that the proxy model can fit most of the experimental results reasonably well. The total sensitivity report in Table E3 reveals that the effects of PORO, WSTANDOFF, and HO# contribute approximately 93% of the total response variation. Out of 93%, 56% is attributed to PORO. This is evidenced by the average URF lines shown in the marginal plots in Figure E2. Similar to the marginal plots of the proxy model of horizontal well, on average, the URF due to production of two vertical wells increases as level of each design factor increases except for LRAT which is rather constant. JMP prediction profiler with optimum factor setting, 3D surface plot, and interaction profiles of the proxy model are presented in Figures E3 to E5. In general, these figures show similar characteristics to those of the proxy for a horizontal well.

Cross-validation of the proxy model is performed in the same manner as that of the proxy for a horizontal well. Validating experiments for vertical wells are conducted by using the same validating experimental designs for a horizontal well.



Table 5.22:  $\beta_i$  regression coefficients of the design-combined Gaussian process proxy model for vertical well production

i	$\beta_i$	i	$\beta_i$	i	$\beta_i$	i	$\beta_i$
1	58.34985	13	238.2109	24	162.7032	35	-97.672
2	16.28633	14	207.8171	25	-56.19676	36	-11.975
3	-145.3565	15	396.2389	26	-41.74342	37	141.277
4	-169.1814	16	58.32066	27	-79.75463	38	95.2761
5	-36.0924	17	93.39882	28	192.0911	39	-38.149
6	139.5931	18	-111.7942	29	129.327	40	100.244
7	-51.41102	19	47.94214	30	-234.4837	41	289.986
8	230.918	20	123.5254	31	-177.3766	42	26.7881
9	94.95335	21	149.3219	32	-14.28267	43	-3.0963
10	-4.639537	22	-87.60384	33	-137.0022	44	26.2764
11	-292.7149	23	29.49347	34	-173.1456	45	94.1614
12	24.06836						

Table 5.23:  $\beta_j$  regression coefficients of the design-combined Gaussian process proxy model for vertical well production

i	$\beta_i$	i	$\beta_i$	i	$\beta_i$	i	$\beta_i$
1	-16.93389	13	48.16975	24	9.018896	35	2.83232
2	-20.85215	14	-24.69543	25	-53.32167	36	26.7774
3	-20.66776	15	-2.769955	26	-25.26214	37	-533.8
4	-123.3425	16	-4.693111	27	-345.7763	38	-5.8089
5	-6.496468	17	11.22516	28	101.5489	39	-20.382
6	91.91617	18	-103.1503	29	-4.15286	40	-9.7647
7	-1.700459	19	-469.1679	30	-31.31432	41	55.1079
8	-51.14677	20	-242.3355	31	2.099514	42	39.8515
9	-508.2705	21	141.3872	32	-31.4289	43	23.0523
10	21.72758	22	-774.8881	33	-40.45099	44	-52.797
11	-18.54855	23	1795.27	34	-66.67888	45	41.464
12	-3.751108						

Results of the two validating experiments are presented in Tables E4 and E5. The experimental results are then analyzed using matched pairs t-test technique. Figure E6 presents JMP result of the matched pairs t-test. Compared to the result of the proxy for horizontal well production, it can be seen that the proxy for vertical well production can fit the experiment responses better as evidenced by a lower standard error of 0.645 and a higher correlation of 0.92. As a result, it is validated that the proxy model has adequate prediction accuracy for further use.

In practice, management decision to invest on a project usually relies on economic analysis result. To perform the analysis, revenue from oil production, capital investment costs, and expense costs throughout the well life need to be estimated to take into account time value of money. Because of many advantages over other methods, oil production profiles are usually predicted using reservoir simulation method. However, each detailed reservoir simulation requires significant effort and time for a building reliable geological model, upscaling, simulation and optimization. Within a limited timeframe, more extra effort is required for accomplishing all of these steps for all reservoir candidates. Therefore, a proxy model which could adequately represent the reservoir production system could be used to replace the reservoir modeling and reservoir simulation. Since the proxy model is in a mathematical form of continuous function, prediction and optimization of production system response can be easily done.

Unfortunately, the two formulated proxy models cannot be directly used to produce an oil production profile, but only an ultimate oil recovery factor. Moreover, they are developed based on simplified reservoir models which are not specific to any reservoir. Therefore, it could not be justifiable to use the proxy models alone without detailed reservoir modeling and simulation. However, they can be used as a simple screening tool to screen out high potential reservoir candidates for reservoir modeling and simulation in the next step. As a result, burden on the modeling and simulation can be reduced.

A full economic analysis involves many factors ranging from production to financial factors. Since URF is the response factor which is not related to time value of money, an indirect economic comparison can thus be only done by comparing whether one horizontal well can produce a certain amount of oil faster than two

equivalent vertical wells or not. To be profitable, the amount of produced oil should be at least able to pay back investment cost of the development. Appendix F presents an estimation of oil production volume at break-even point of a horizontal well. It is noted that, for conservatism, the total cost of development is estimated on the high side. At the end of the estimation, it is concluded that the oil volume for economic comparison is governed by the minimum required oil volume to develop a project, which is 100,000 STBO.

Figure 5.55 presents a workflow of the simple method for screening out high potential reservoirs for drilling a horizontal well using the proxy models. The method starts with qualitative screening of reservoirs which have appropriate characteristics for horizontal well drilling from a large portfolio. Unfortunately, because there might be too many reservoir candidates to be screened out, performing reservoir simulation on every reservoir could be impractical and prohibitive. Besides, some petrophysical information of some reservoirs may not be available in pre-drill stage to make the decision with high confidence. Therefore, when there is a drilling program in the same proximity of these reservoir candidates, vertical or deviated wells should be designed to be drilled pass through them so that well logging can be used to collect the missing information.

Afterwards, the design-combined proxy models are used to predict URF due to production of one horizontal well and two equivalent vertical wells of each reservoir, respectively. If the predicted URF due to production of one horizontal well is greater, the reservoir is screened out and classified as the reservoir having high potential for horizontal well drilling. Otherwise, drop the reservoir from horizontal well development program. After screening all reservoir candidates, perform Monte Carlo analysis on the high potential reservoirs. As a result, probabilistic URFs and recoverable oil volumes of each reservoir are obtained. Figure 5.56 shows an example or JMP Monte Carlo analysis result. Based on the result, a cumulative probability density function of URFs can be plotted as shown in Figure 5.57. Subsequently, prioritize the reservoirs based on the probabilistic recoverable oil volumes and perform reservoir simulation on the reservoir having higher priority first. It may be noticed that the simple method helps identify which reservoirs are worthy to spend effort and time on reservoir simulation. Thus, the design process is optimized.

Figure 5.58 presents the workflow for validating the simple reservoir screening method. In brief, decision based on the simple reservoir screening method is validated against that of reservoir simulation results. For this research, the decision made based on reservoir simulation results is regarded as the actual decision. For the simple screening method, the reservoir being considered is suitable for horizontal well drilling when

$$\text{Predicted URF}_{\text{one HZ well}} > \text{Predicted URF}_{\text{two equivalent vertical wells}} \quad (5.7)$$

The decision criteria based on reservoir simulations are as follows;

$$\text{Actual URF}_{\text{one HZ well}} > \text{Actual URF}_{\text{two equivalent vertical wells}} \quad (5.8)$$

$$\text{Break-even Point}_{\text{one HZ well}} < \text{Break-even Point}_{\text{two equivalent vertical wells}} \quad (5.9)$$

Table 5.24 presents proxy prediction and reservoir simulation results of the validating experiments. Decisions to drill a horizontal well based on each method are then made according to the work flow in Figure 5.58 and presented in Table 5.25. To investigate the effectiveness of the simple screening method, all analysis results in Table 5.25 are sorted by Column (9) in descending order. Interestingly, the validation results can be divided into 3 groups as follows;

1)  $\Delta$  predicted URF > 5% - decision based on the simple screening method and that of reservoir simulation results are the same. Thus, the simple method can be effectively used without requiring subsequent reservoir simulations, provided limitations of the proxy models are not violated.

2)  $0\% < \Delta$  predicted URF  $\leq 5\%$  - the screening method sometimes wrongly suggests that the reservoir being considered should be drilled by one horizontal well rather than two equivalent vertical wells. This type of error is defined as “Type II error” herein.

3)  $\Delta$  predicted URF  $\leq 0\%$  - the screening method sometimes incorrectly suggests that the reservoir being considered should be dropped out of horizontal well development program. This type of error is defined as “Type I error” herein.

For reservoir screening purpose, Type II error decision is considered acceptable because the suitability of the reservoir for horizontal well drilling will be confirmed again by a subsequent detailed reservoir simulation. In contrast, Type I error decision is unacceptable because it will cause the decision-maker to miss the development opportunity of the reservoir being considered out.

In conclusion, it has been proven that the simple screening method can be effectively used to optimize horizontal well design process with acceptable accuracy. Out of 36 validating cases, 26 cases are correctly predicted by the method while 9 cases have Type II error decision. Only one unacceptable decision is made with Type I error. When  $\Delta$  predicted URF  $> 5\%$ , the simple method can be effectively used without confirmation from subsequent reservoir simulations, provided limitations of the proxy models are not violated. For the remaining cases, subsequent reservoir simulations should be performed for final confirmation.

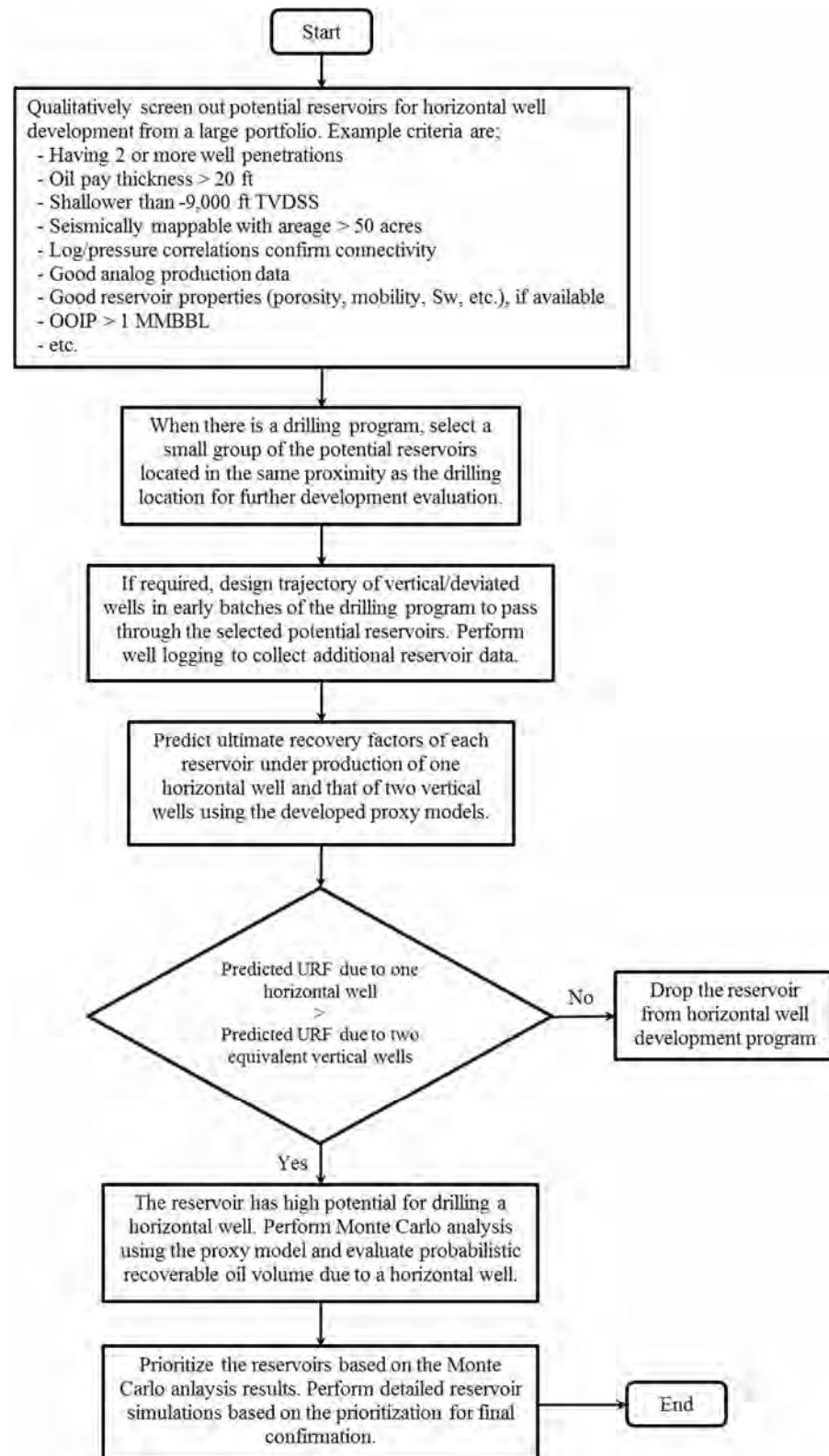


Figure 5.55: Workflow for screening out high potential reservoirs for drilling a horizontal well using the proxy models

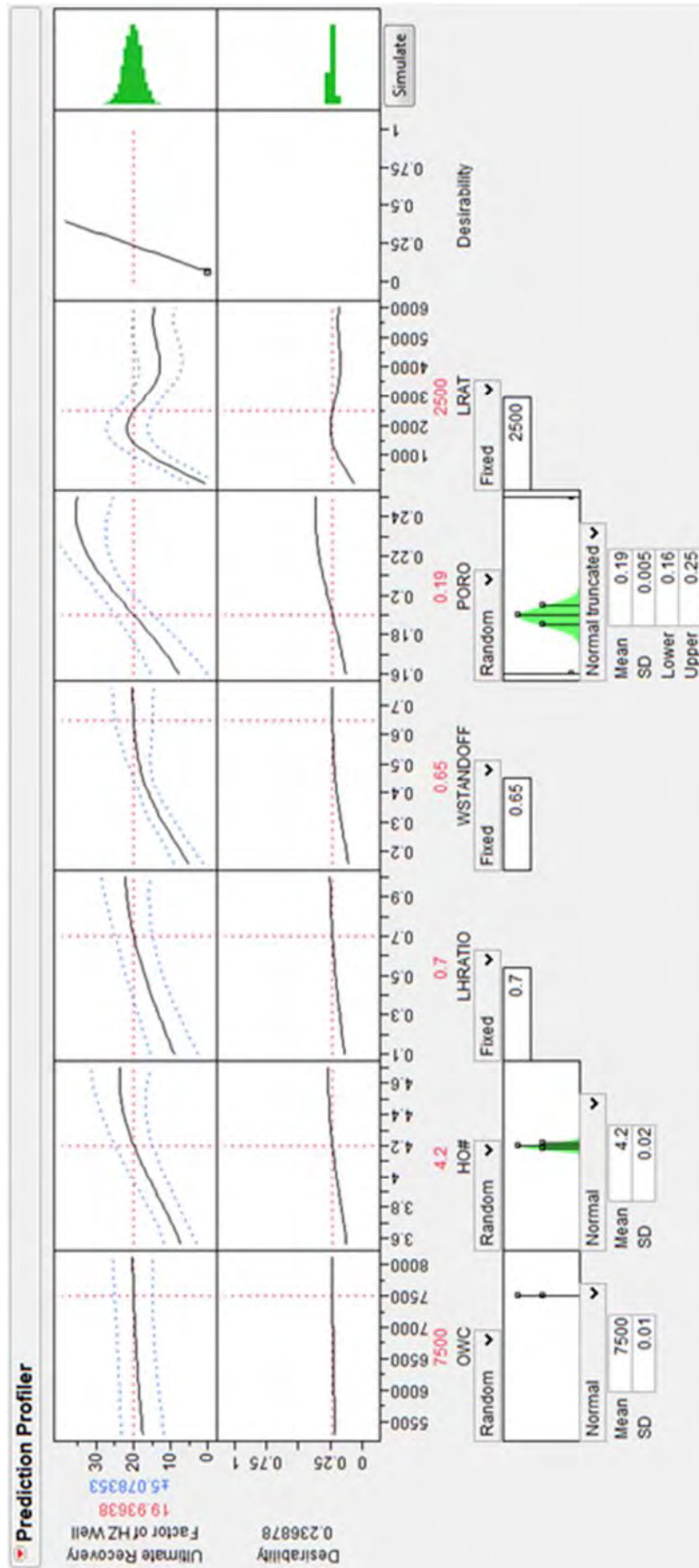


Figure 5.56: Example of 5,000-run Monte Carlo analysis on the proxy model for horizontal well development

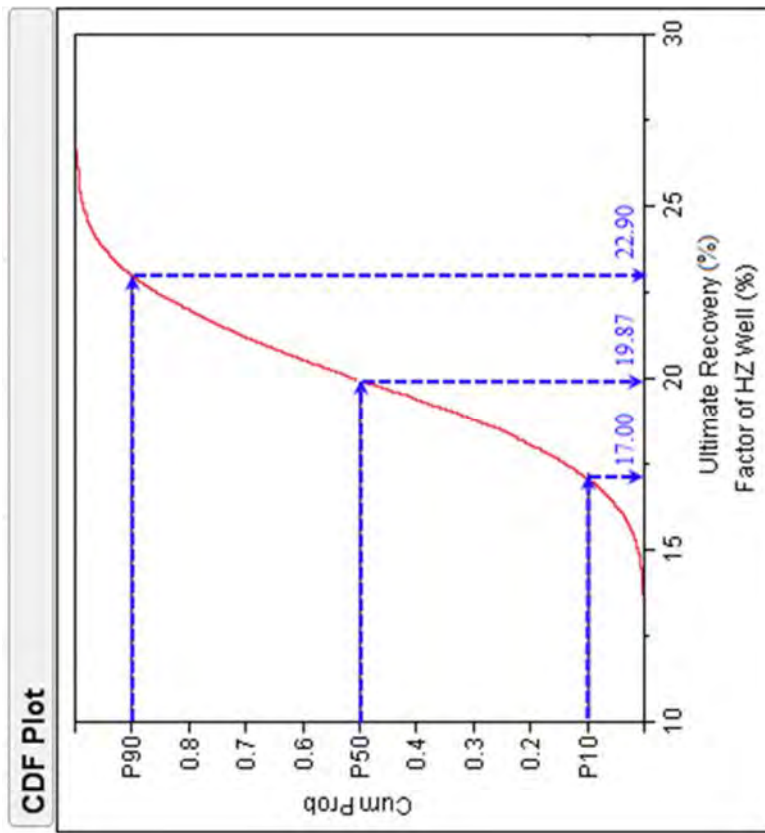
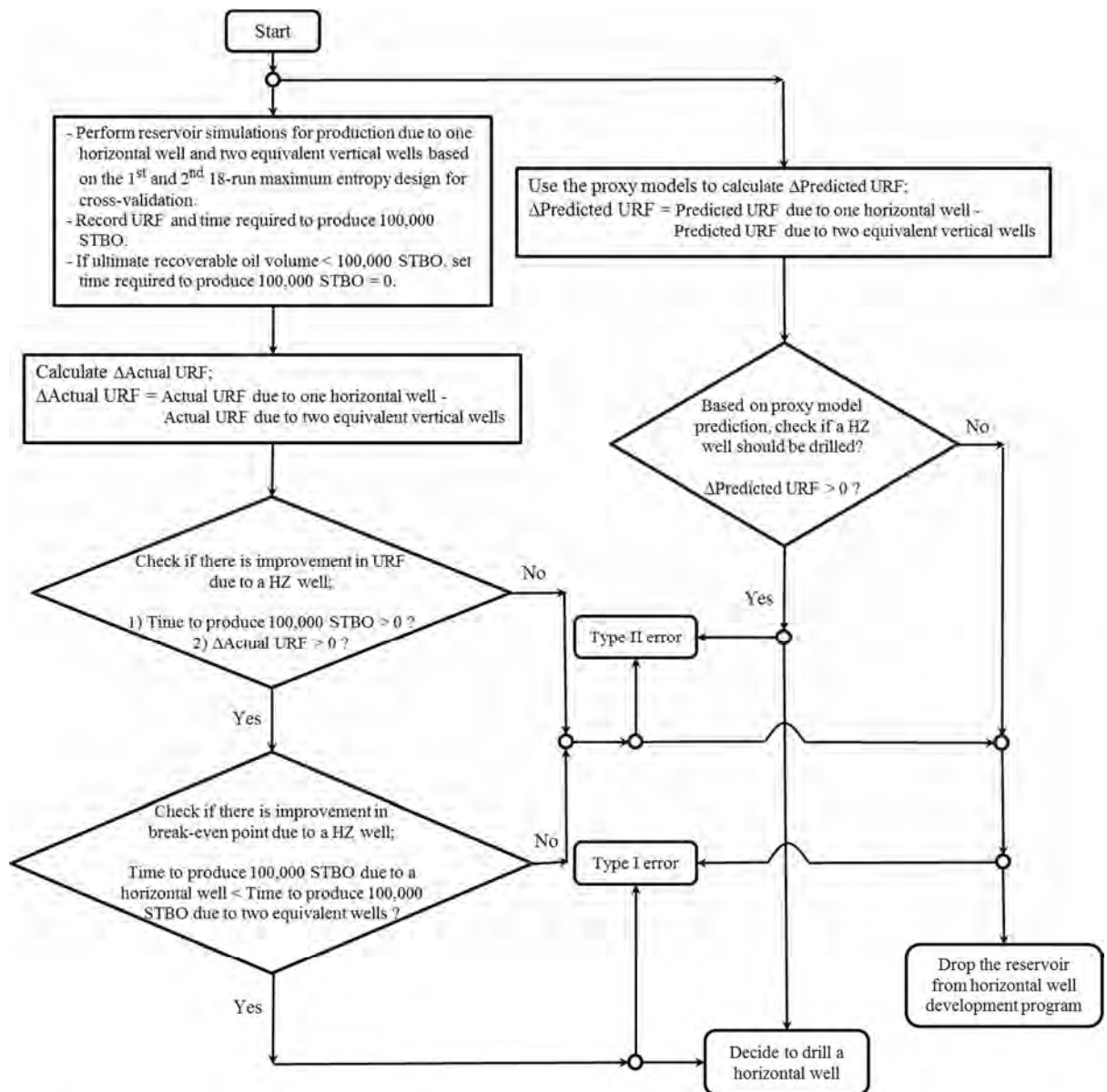


Figure 5.57: Cumulative probability density function and important quantiles of the example Monte Carlo analysis





Note:

Type of prediction error	Should a horizontal well be drilled?	
	Simple method	Reservoir simulation
Type I error	No	Yes
Type II error	Yes	No

Figure 5.58: Workflow for cross-validating the simple method for screening reservoir for drilling a horizontal well

Table 5.24: Summary of actual and predicted URFs of reservoir candidates for horizontal well development

Run ID	OWC	HO#	LHRATIO	WSTANDOFF	PORO	LRAI	Production from a Horizontal Well				Production from Vertical Wells			
							Predicted URF (%)	Actual URF (%)	Time to Produce 100,000 STBO (days)	RF @ 100,000 STBO (%)	Predicted URF (%)	Actual URF (%)	Time to Produce 100,000 STBO (days)	RF @ 100,000 STBO (%)
101	7959.99	3.755	0.95	0.293	0.165	55.00	0.00	0.00	0	0	0.40	0.00	0	0
102	7332.77	4.259	0.10	0.160	0.185	5339.44	8.98	3.02	297	1.05	0.00	0.00	0	0
103	7803.19	4.322	0.80	0.493	0.180	5009.17	11.94	16.15	67	8.29	3.90	2.86	0	0
104	6548.74	4.700	0.45	0.160	0.210	4348.61	18.14	12.73	37	2.14	3.24	2.41	424	2.11
105	6705.55	3.692	0.65	0.660	0.230	1376.11	14.24	25.82	78	10.59	6.39	13.25	92	10.51
106	6548.74	4.133	0.20	0.627	0.180	3027.50	4.24	4.77	73	2.7	3.60	1.87	0	0
107	6548.74	4.259	0.90	0.160	0.225	2036.67	13.52	9.23	133	6.31	2.06	3.11	0	0
108	6391.94	3.567	0.35	0.393	0.235	4678.89	14.82	10.34	40	6.72	9.30	8.36	76	6.74
109	5451.11	3.944	0.10	0.360	0.200	2697.22	1.93	3.26	83	1.37	0.00	0.21	0	0
110	5294.30	4.385	0.15	0.493	0.170	5669.72	5.19	1.81	415	1.51	0.00	0.00	0	0
111	5764.72	4.196	0.45	0.327	0.245	2036.67	22.62	26.36	51	2.96	20.48	12.98	35	2.96
112	6078.33	3.755	0.90	0.727	0.160	3688.06	3.27	0.55	0	0	1.94	0.00	0	0
113	8116.80	4.574	0.25	0.293	0.230	3027.50	24.55	24.89	34	1.29	14.04	14.82	23	1.27
114	5294.30	4.511	0.85	0.527	0.235	2697.22	34.78	26.53	38	3.99	28.95	21.16	35	3.93
115	6862.36	4.385	0.40	0.693	0.220	1045.83	28.99	30.77	96	2.61	20.64	22.80	48	2.61
116	5294.30	3.692	0.65	0.260	0.185	385.28	0.00	0.00	0	0	2.21	0.00	0	0
117	6705.55	3.818	0.70	0.327	0.165	2366.94	2.57	0.00	0	0	1.56	0.00	0	0
118	6862.36	4.385	0.80	0.560	0.160	715.56	4.75	2.94	0	0	0.00	0.00	0	0

Table 5.24: Summary of actual and predicted URFs of reservoir candidates for horizontal well development (Continued)

Run ID	OWC	HO#	LHRATIO	WSTANDOFF	PORO	LRAI	Production from a Horizontal Well				Production from Vertical Wells			
							Predicted URF (%)	Actual URF (%)	Time to Produce 100,000 STBO (days)	RF @ 100,000 STBO (%)	Predicted URF (%)	Actual URF (%)	Time to Produce 100,000 STBO (days)	RF @ 100,000 STBO (%)
201	5607.91	3.818	0.15	0.427	0.205	2366.94	5.55	4.11	85	2.35	0.85	0.49	0	0
202	5294.30	3.755	0.65	0.627	0.220	5009.17	18.05	17.44	33	10.18	8.49	8.13	0	0
203	5921.52	3.567	0.25	0.727	0.190	4018.33	5.18	2.73	0	0	1.78	0.03	0	0
204	7175.97	3.818	0.25	0.493	0.160	5339.44	1.96	0.01	0	0	0.00	0.00	0	0
205	5294.30	4.637	0.15	0.593	0.195	1706.39	10.66	8.72	59	0.8	6.99	9.71	193	0.79
206	5294.30	4.700	0.90	0.460	0.180	2036.67	16.42	11.68	90	5.1	3.70	0.57	0	0
207	7803.19	4.511	0.40	0.727	0.205	3688.06	19.75	27.88	28	2.6	23.25	21.74	57	2.54
208	7959.99	4.133	0.80	0.327	0.160	4348.61	0.00	0.00	0	0	0.00	0.00	0	0
209	6862.36	4.574	0.60	0.527	0.170	4018.33	6.15	10.01	108	4.79	2.66	0.44	0	0
210	5607.91	4.259	0.10	0.327	0.185	5339.44	7.99	3.55	165	0.99	0.00	0.00	0	0
211	6391.94	3.692	0.95	0.427	0.225	385.28	20.84	16.04	447	15.73	7.76	8.71	0	0
212	6078.33	4.070	0.50	0.160	0.225	3688.06	10.52	10.64	71	4.48	2.32	1.53	0	0
213	6862.36	3.567	0.85	0.493	0.180	2697.22	3.78	3.24	0	0	0.00	0.00	0	0
214	7646.38	4.322	0.35	0.327	0.165	715.56	0.00	1.92	0	0	1.47	0.00	0	0
215	7175.97	3.567	1.00	0.227	0.180	55.00	0.00	0.00	0	0	0.30	0.00	0	0
216	5764.72	4.448	0.55	0.627	0.225	5669.72	27.39	24.92	21	3.08	25.60	23.77	44	3.03
217	5294.30	4.259	0.80	0.160	0.175	2366.94	2.03	0.00	0	0	0.00	0.00	0	0
218	5921.52	4.511	0.40	0.260	0.205	385.28	12.29	10.79	332	2.35	4.19	3.34	394	2.35

Table 5.25: Validation of reservoir screening method for horizontal well development

Run ID	$\Delta$ Predicted URF (%)		$\Delta$ Actual URF Improvement in URF due to a HZ Well?		Improvement in Break-Even Point?		Should a HZ Well be Drilled?		Remark
	(1) - (5)	(2) - (6)	(3) > 0 AND (10) > 0?	(11)	(12)	(13)	(14)		
104	14.91	10.32	YES	YES	YES	YES	YES	YES	
211	13.08	7.34	YES	YES	NO	NO	YES	YES	
206	12.73	11.12	YES	YES	NO	NO	YES	YES	
107	11.45	6.11	YES	YES	NO	NO	YES	YES	
113	10.51	10.07	YES	YES	NO	NO	YES	YES	
202	9.56	9.31	YES	YES	NO	NO	YES	YES	
102	8.98	3.02	YES	YES	NO	NO	YES	YES	
115	8.34	7.97	YES	YES	NO	NO	YES	YES	
212	8.20	9.11	YES	YES	NO	NO	YES	YES	
218	8.10	7.45	YES	YES	YES	YES	YES	YES	
103	8.04	13.29	YES	YES	NO	NO	YES	YES	
210	7.99	3.55	YES	YES	NO	NO	YES	YES	
105	7.85	12.57	YES	YES	YES	YES	YES	YES	
114	5.83	5.37	YES	YES	NO	NO	YES	YES	
108	5.52	1.97	YES	YES	YES	YES	YES	YES	
110	5.19	1.81	YES	YES	NO	NO	YES	YES	
118	4.75	2.94	NO	NO	NO	NO	YES	NO	Type II Error
201	4.71	3.62	YES	YES	NO	NO	YES	YES	

Table 5.25: Validation of reservoir screening method for horizontal well development (Continued)

Run ID	$\Delta$ Predicted URF (%)		$\Delta$ Actual URF (%)		Improvement in URF due to a HZ Well ?		Improvement in Break-Even Point ?		Should a HZ Well be Drilled?		Remark
	(1) - (5)	(2) - (6)	(3) - (7)	(4) - (8)	(9) > 0 ?	(10) > 0 ?	(11) > 0 ?	(12) < (7) ?	Decide by Using Proxy If (9) > 0 ?	Decide by Using Simulation If (11) = YES OR (12) = YES ?	
	(9)	(10)	(11)	(12)	(13)	(14)					
213	3.78	3.24	NO	NO	YES	NO	NO	YES	NO	NO	Type II Error
205	3.68	-0.99	NO	YES	YES	NO	YES	YES	YES	YES	
209	3.49	9.57	YES	NO	YES	NO	NO	YES	YES	YES	
203	3.40	2.69	NO	NO	YES	NO	NO	YES	NO	NO	Type II Error
111	2.14	13.37	YES	NO	YES	NO	NO	YES	YES	YES	
217	2.03	0.00	NO	NO	YES	NO	NO	YES	NO	NO	Type II Error
204	1.96	0.01	NO	NO	YES	NO	NO	YES	NO	NO	Type II Error
109	1.93	3.05	YES	NO	YES	NO	NO	YES	YES	YES	
216	1.79	1.15	YES	YES	YES	YES	YES	YES	YES	YES	
112	1.33	0.55	NO	NO	YES	NO	NO	YES	NO	NO	Type II Error
117	1.01	0.00	NO	NO	YES	NO	NO	YES	NO	NO	Type II Error
106	0.64	2.89	YES	YES	YES	NO	NO	YES	YES	YES	
208	0.00	0.00	NO	NO	NO	NO	NO	NO	NO	NO	
215	-0.30	0.00	NO	NO	NO	NO	NO	NO	NO	NO	
101	-0.40	0.00	NO	NO	NO	NO	NO	NO	NO	NO	
214	-1.47	1.92	NO	NO	NO	NO	NO	NO	NO	NO	
116	-2.21	0.00	NO	NO	NO	NO	NO	NO	NO	NO	
207	-3.51	6.14	YES	YES	NO	YES	YES	NO	YES	YES	Type I Error

## 5.6 Design Optimization of a Horizontal Well using a Proxy Model

Frequently, reservoir simulations are performed to optimize the design of a horizontal well. The main goals are to maximize oil recovery and to accelerate oil production. Since each reservoir simulation can provide only one set of desired responses, several simulations must therefore be done until a set of maximum or minimum responses is obtained within limited budget and time. In the previous section, the design-combined proxy model is developed to relate input factors of a reservoir simulation to output response or URF due to production of one horizontal well. Therefore, it can be used as a substitute to the process system or reservoir simulator in this research to approximate output response as illustrated in Figure 5.59. Since the proxy model is modeled as a continuous function, maximum or minimum response within the design hyperspace of the proxy model can be easily searched using available mathematical optimization techniques.

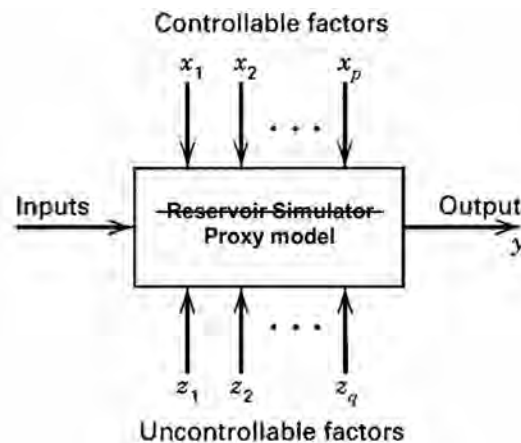


Figure 5.59: Application of a proxy model as a substitute to reservoir simulator

(Adapted from Montgomery [54])

The design-combined proxy model presented in Equation 5.5 is a function of five significant factors and one extra insignificant factor as described earlier. From the equation, WSTANDOFF, LHRATIO, and LRAT are controllable factors which can be optimized during the design. The remaining factors, i.e. PORO, HO#, and OWC,

are uncontrollable factors which are usually in a form of probabilistic distribution due to geological and measurement uncertainties. Conventionally, to optimize a horizontal well design, one must perform Monte Carlo simulation runs on the proxy model by varying the three controllable factors in each run until the optimum P50 value of URF and an acceptable range between P10 and P90 are obtained. The knowledge of main and interaction effects discussed in Section 5.3 could be used to guide the searching of optimum setting. It is essential to note that limitations of the proxy model described in Section 5.4 must not be violated. In addition, more practical limitations specific to a particular reservoir should be taken into account. For example, if a reservoir is very thin, the maximum possible WSTANDOFF that could be designed would be 0.65 in order to maintain drilling tolerance.

Alternatively, JMP Profiler platform can be used for the design optimization. As shown in Figure 5.56, the platform provides an approach to visualize the response surface in hyperspace by seeing what would happen if one or two factor levels are changed at a time. Basically, the platform plots interactive cross-sectional views of the response surface across each design factor. Design optimization can be easily done by adjusting settings of controllable factors, the URF corresponding to the controllable factors and P50 value of uncontrollable factors are calculated and shown in red on the left of the cross-sectional plots. Then, Monte Carlo simulation can be run to evaluate probabilistic distribution of the URF.

## **5.7 Recommendations on Data Surveillance and Acquisition**

Data acquisition and surveillance program is usually put in place to collect necessary information for characterizing geological conditions, assessing reservoir and fluid properties, forecasting production performance, and etc. Unfortunately, there are usually tens of factors involved in a problem. In many circumstances, oil and gas companies need to compromise between limited budget and the cost of surveillance and acquisition to obtain the most beneficial outcome. Thus, it would be wise to spend the budget and effort on acquiring the information which has higher influence on the desired outcome.

In Section 5.2.3.1, it is confirmed that there are five factors having significant influence on ultimate recovery efficiency of a horizontal well. The ranking list of significant factors ordered in descending significance is as follows:

- 1) *PORO* - porosity and its correlated factors such as permeability and thickness of oil-water transition zone
- 2) *WSTANDOFF* - ratio of well standoff to oil-water contact to initial oil column thickness
- 3) *HO* or *HO#* - initial oil column thickness
- 4) *LRAT* - liquid production rate control
- 5) *LHRATIO* - ratio of horizontal well length to reservoir length

Thus, for a horizontal well development program, more budget should be allocated to collect the high-quality information of significant uncontrollable factors which are rock porosity, permeability, initial water saturation, capillary action in fluid transition zone, initial oil column thickness, oil-water contact elevation, relative permeability, and end point saturations. In addition, more effort should be spent on drilling control to get well standoff to oil-water contact and horizontal well length as per designed values.

Since experimental design methodology adopts statistical techniques for making objective conclusions. The accuracy of the conclusions is therefore heavily relied on the quality of the historical data used. This fact points out that proper database management and maintenance is as important as the quality of data collection. As there is more information in the database or new best practices, the designed experiments may be revisited to update and improve the proxy models.



## CHAPTER VI

### CONCLUSIONS AND RECOMMENDATIONS

This chapter concludes important findings from this research. Recommendations for future work are also provided at the end of the chapter.

#### 6.1 Conclusions

In this research, experimental design methodology is applied and proposed as an optimization method for designing a horizontal well in a thin-oil-column reservoir in the Gulf of Thailand. Ultimate recovery efficiency of the horizontal well under primary depletion is selected as the response factor to be optimized. First of all, the research begins with defining a large list of factors which could influence the ultimate recovery factor by brainstorming. The listed factors are then screened out by subject matter experts working in the oil fields in the Gulf of Thailand. To further reduce the number of factors, factors having known mutual correlation are grouped together. Only one factor is selected as a representative of each group. By product, it can also be ensured that factor settings of all subsequent computer experiments are realistic. Consequently, thirteen potential significant factors can be screened out. Petrophysical and engineering data related to the screened factors are then collated from database of the oil fields. As a result, probability and cumulative density functions of these factors can be plotted.

The screened factors are then statistically screened again using a screening experimental design. The objective is to obtain a small group of statistically significant factors which could be used to construct an approximate proxy model for prediction and optimization. In this research,  $2^{13-8}$  fractional factorial design is employed to conduct screening designed experiment. To conduct the experiment, a series of reservoir simulation runs are carried out by varying levels of the thirteen design factors according to the experimental design. As a result, five statistically significant factors can be screened out for subsequent response surface designs. The five factors ordered in descending significance are porosity, well standoff to oil-water

contact, thickness of oil column, liquid production rate control, and a ratio of horizontal well length to reservoir length. Since the screening experiments are conducted at only 2 levels of factors, the analysis of screening might miss some significant factors out if the actual response surface is highly non-linear, the sixth factor, i.e. oil-water contact elevation, is added into the list of significant factors to perform response surface experiments.

The widely used face-centered central composite design is firstly performed to create a quadratic proxy model. It is shown that the obtained quadratic proxy cannot adequately fit and predict response or ultimate recovery factor of the simulated production system. Therefore, another series of reservoir simulation runs are performed according to a maximum entropy design. Maximum entropy designs are a variant of space-filling designs which are suitable for computer experiments and fitting a Gaussian process response surface. Unfortunately, it is found that the obtained Gaussian process proxy can adequately predict the ultimate recovery factor only within the region from where designed experimental points are sampled. Near boundary of the design hyperspace, model prediction is found to be poor because only few experiments are conducted.

Comparison between the two experimental designs reveals that most of central composite design points are at the boundary of the design hyperspace whereas those of the other design are mainly distributed inside the boundary. Due to this fact, the design points and responses of both experimental designs are combined and fitted using a Gaussian process model. The resulting design-combined proxy is thus built on more number of design points which are more spread over the design hyperspace. Cross-validation of the proxy model shows that the model can adequately predict the ultimate recovery factor with improved prediction accuracy.

In summary, the following conclusions can be made;

- 1) Experimental design methodology can be used to optimize horizontal well design in the Gulf of Thailand using the proxy models.
- 2) Five significant factors influencing URF can be screened out from tens of factors. The ranking list of significant factors ordered in descending significance is as follows:

- 2.1) *PORO* - porosity and its correlated factors such as permeability and thickness of oil-water transition zone
- 2.2) *WSTANDOFF* - ratio of well standoff to oil-water contact to initial oil column thickness
- 2.3) *HO* or *HO#* - initial oil column thickness
- 2.4) *LRAT* - liquid production rate control
- 2.5) *LHRATIO* - ratio of horizontal well length to reservoir length

3) To ensure that no significant factors are missed out, the sixth most influence factor on the URF according to the analysis of screening designed experiments, i.e. oil-water contact elevation, is experimented in response surface experiments. Analysis report of the obtained proxy model confirms that oil-water contact elevation is insignificant. Thus, no significant factors are missed out during factor screening.

4) To obtain high accuracy of well performance prediction, acquisition and surveillance of the five significant factors and their correlated factors such as permeability, initial water saturation, capillary pressure, oil-water contact elevation, relative permeability and end point saturation should be performed and maintained with high quality.

5) At a given ratio of well-standoff-to-oil-water-contact to oil-column-thickness, a reservoir having thicker oil column thickness tends to have higher ultimate oil recovery. This is because well standoff to oil-water contact also increases. Therefore, the well is less prone to be within oil-water transition zone and far away from bottom water. As a result, the well can produce oil at higher production rate with less initial water cut and later water breakthrough. Gas cresting is not found to cause negative effect to the production. Instead, its gas lifting effect helps accelerate oil production. This could be because of the limited and small amount of the gas cap.

6) As horizontal well length increases, pressure drawdown required to produce oil at a certain rate is reduced. Moreover, more reservoir fluid volume is susceptible to the pressure drawdown. Thus, water and gas cresting is less problematic. As a result, the longer horizontal well can recover more oil within less period of time.

7) As a ratio of well-standoff-to-oil-water-contact to oil-column-thickness decreases, the influence of oil-water transition zone and oil-water contact dominates performance of a horizontal well. High initial water cut can be observed due to higher initial water saturation near the wellbore. Moreover, the higher initial relative permeability to water and shorter distance between the well to oil-water contact cause water breakthrough to occur much faster. As a result, relatively low amount of oil can be recovered. On the other hand, as the ratio is approaching unity, gas cap has more influence on the well performance. Higher initial oil flow rate and earlier gas breakthrough can be observed as water breakthrough delays. Fluctuation in oil and gas production rates occurs after tubing head pressure reaches its minimum value. This could be attributed to high gas influx along horizontal length which could cause high turbulence flow in the well. Due to the delay in water breakthrough and lifting effect of breakthrough gas, the ultimate recovery factor significantly increases.

8) Porosity and its correlated factors are found to have most influence on the ultimate recovery factor. As porosity increases, oil-water transition zone in the reservoir decreases resulting in smaller initial water cut and delay in water breakthrough. In the meantime, the corresponding increase in reservoir permeability results in greater liquid production rate with smaller pressure drawdown required. Thus, there is also less concern on oil and gas cresting problem. Ultimately, more oil can be recovered from the reservoir

9) It is found that liquid rate production control has an inverse effect on the ultimate recovery factor. As the liquid rate is increased, pressure drawdown in the reservoir is also greater. Consequently, the resultant increase in gas and water cresting tendency causes the horizontal well to shut-in earlier due to high water cut. Thus, less oil can be recovered. However, beyond a certain control rate, no difference in well performance can be observed due to limited deliverability of the well.

10) Interaction effects among porosity, well standoff to oil-water contact, and oil column thickness are found significant. It is found that an increase in one of these factors can amplify the main effect of the other two factors.

11) The developed proxy models can be effectively and quickly used to screen out reservoirs which have high potential for horizontal well development. As a result, workload on reservoir modeling and simulation could be reduced.

## 6.2 Recommendations

1) Some factors such as tubing size, diameter of wellbore, completion type, etc., are kept constant in this research to align with the current working practice. Some are assumed based on the best guess of the subject matter experts due to unavailability of lab or field data, for example, skin factor, wellbore roughness, etc. These factors may be studied to optimize the current practice.

2) It is assumed that the lateral section of the wells in this study is perfectly horizontal. In practice, many horizontal wells have snaking trajectory due to lack of good geosteering. Some lateral sections are straight but slanting. Besides, geometry of the well, multiphase flow along the lateral section and slippage between different fluids could influence the well performance. It is thus interesting to investigate the influence of these factors in the future.

3) Only primary depletion with an artificial lift by a booster compressor is considered in this study. In practice, secondary recovery methods such as waterflood and gas lift are applied to increase more oil recovery and accelerate more oil production. Therefore, additional factor effects related to other artificial lift and EOR methods can be systematically studied further using experimental designs.

4) The information from the horizontal well database used in this research is updated until June 2010 only. As there is more information from ongoing drilling projects, the proxy models constructed in this research should be regularly revisited for update. This is because experimental design methodology is based on statistical method and historical data.

## REFERENCES

- [1] Eric, R.U. et al. Rapid Planning and Execution of the First Multilateral Well in the Gulf of Thailand: Results and Lessons Learned. Paper IADC/SPE 103941, SPE Drilling & Completion (2008): 100-111.
- [2] Maroongroge, V., Sandarusi, K.A., Schmalz, A., Schut, G., and Nucharoen, P. Improved Oil Recovery Through the Use of Horizontal Well in Thin Oil Column: A Case Study from Platong Field, Gulf of Thailand. Paper SPE 80475 presented at the SPE Asia Pacific Oil and Gas Conference and Exhibition, Jakarta, Indonesia (April 2003).
- [3] Upchurch, E.R. et al. Rapid Planning and Execution of the First Multilateral Well in the Gulf of Thailand: Results and Lessons Learned. Paper IADC/SPE 103941 presented at the IADC/SPE Asia Pacific Drilling Technology Conference and Exhibition, Bangkok, Thailand (November 2006).
- [4] Chewaroungroj, J., Varela, O.J., and Lake, L.W. An Evaluation of Procedures to Estimate Uncertainty in Hydrocarbon Recovery. Paper SPE 59449 presented at the 2000 SPE Asia Pacific Con Integrated Modelling for Asset Management, Yokohama, Japan (April 2000): 1-11.
- [5] Cheong, Y.P. et al. Experimental Design Methodology for Quantifying UR Distribution curve – Lessons learnt and still to be learnt. Paper SPE 88585 presented at the 2004 SPE Asia Pacific Oil and Gas Conference and Exhibition, Perth, Australia (October 2004): 18-20.
- [6] United States Department of Energy, Office of Oil and Gas, Energy Information Administration. Drilling Sideways—A Review of Horizontal Well Technology and Its Domestic Application [Online]. 1993. Available from: [http://www.eia.doe.gov/pub/oil\\_gas/natural\\_gas/analysis\\_publications/drilling\\_sideways\\_well\\_technology/pdf/tr0565.pdf](http://www.eia.doe.gov/pub/oil_gas/natural_gas/analysis_publications/drilling_sideways_well_technology/pdf/tr0565.pdf) [2010, Mar 01]
- [7] Joshi, S.D. Horizontal Well Technology. Tulsa, Oklahoma : PennWell Publishing Company, 1991.
- [8] Kuchuck, F.J., Lenn C., Hook, P., and Fjerstad, P. Performance Evaluation of Horizontal Wells. Paper SPE 49539 presented at the 8<sup>th</sup> Abu Dhabi International Petroleum Exhibition and Conference, Abu Dhabi, U.A.E. (October 1998): 733-744.

- [9] Borisov, Ju.P. Oil Production Using Horizontal and Multiple Deviation Wells, Nedra, Moscow (1964). by Stauss, J., Joshi, S.D. Bartlesville, Oklahoma : Phillips Petroleum Co., the R&D Library Translation, 1984.
- [10] Giger, F.M., Reiss, L.H., and Jourdan, A.P. The Reservoir Engineering Aspect of Horizontal Drilling. Paper SPE 13024 presented at the SPE 59<sup>th</sup> Annual Technical Conference and Exhibition, Houston, Texas (September 1984): 16-19.
- [11] Joshi, S.D. Augmentation of Well Productivity Using Slant and Horizontal Wells. Journal of Petroleum Technology (June 1988): 729-739.
- [12] Joshi, S.D. A Review of Horizontal Well and Drainhole Technology. Paper SPE 16868 presented at the Annual Technical Conference, Dallas, Texas (1987).
- [13] Renard, G.I., and Dupuy, J.M. Influence of Formation Damage on the Flow Efficiency of Horizontal Wells. Paper SPE 19414 presented at the Formation Damage Control Symposium, Lafayette, Louisiana (February 1990): 22-23.
- [14] Reiss, L.H. Horizontal Wells' Production After Five Years. Journal of Petroleum Technology (November 1987): 1411-1416.
- [15] Murphy, P.J. Performance of Horizontal Wells in the Helder Field. Journal of Petroleum Technology (June 1990): 792-800.
- [16] Broman, W.H., Stagg, T.O., and Rosenzweig, J.J. Horizontal Well Performance Evaluation at Prudhoe Bay. Paper CIM/SPE 90-124 presented at CIM/SPE International Technical Meeting, Calgary, Canada (June 1990).
- [17] Sherrard, D.W., Brice, B.W., and MacDonald, D.G. Application of Horizontal Wells at Prudhoe Bay. Journal of Petroleum Technology (November 1987): 1417-1425.
- [18] Chaperon, I. Theoretical Study of Coning Toward Horizontal and Vertical Wells in Anisotropic Formations: Subcritical and Critical rates. Paper SPE 15377 presented at the SPE Annual Technical Conference and Exhibition, New Orleans, Louisiana (October 1986).
- [19] Giger, F.M. Analytic 2-D Models of Water Cresting Before Breakthrough for Horizontal Wells. Paper SPE 15378 presented at the SPE 61<sup>st</sup> Annual Fall Meeting, New Orleans, Louisiana. (October 1986).

- [20] Karcher, B.J., Giger, F.M., and Combe, J., “Some Practical Formulas to Predict Horizontal Well Behavior. Paper SPE 15430 presented at the SPE 61<sup>st</sup> Annual Fall Meeting, New Orleans, Louisiana. (October 1986).
- [21] Efros, D.A. Study of Multiplephase Flows in Porous Media (in Russian), Gastoptexizdat, Leningrad (1963). Cited in Karcher, B.J., Giger, F.M., and Combe, J., “Some Practical Formulas to Predict Horizontal Well Behavior. Paper SPE 15430 presented at the SPE 61<sup>st</sup> Annual Fall Meeting, New Orleans, Louisiana. (October 1986).
- [22] Ozkan, E. and Raghavan, R. Performance of Horizontal Wells Subject to Bottom Water Drive. Paper SPE 18545 presented at the SPE Eastern Regional Meeting, Charleston, West Virginia (November 1988).
- [23] Papatzacos, P., Herring, T.U., Martinsen, R., and Skjaeveland, S.M. Cone Breakthrough Time for Horizontal Wells. Paper SPE 19822 presented at the 64<sup>th</sup> SPE Annual Technical Conference and Exhibition, San Antonio, Texas (October 1989).
- [24] Mutalik, P.N., Godbole, S.P., and Joshi, S.D. Effect of Drainage Area Shapes on Horizontal Well Productivity. Paper SPE 18301 presented in the SPE 63<sup>rd</sup> Annual Technical Conference, Houston, Texas (October 1988).
- [25] Vo, D.T., Waryan, S., Dharmawan, A., Susilo, R., and Wicaksana, R. Lookback on Performance of 50 Horizontal Wells Targeting Thin Oil Columns, Mahakam Delta, East Kalimantan. Paper SPE 64385 presented at the SPE Asia Pacific Oil and Gas Conference and Exhibition, Brisbane, Australia (October 2005).
- [26] Penmatcha, V.R., Arbabi, S., and Aziz, K. Effects of Pressure Drop in Horizontal Wells and Optimum Well Length. Paper SPE 37494 presented at the 1997 SPE Production Operations Symposium, Oklahoma City, Oklahoma (March 1997): 801-813.
- [27] Fisher, R.A. Statistical Methods for Research Workers. London: Oliver and Boyd, 1925.
- [28] Box, G.E.P., Hunter, W.G., Hunter, J.S. Statistics for Experimenters. New York City: John Wiley & Sons, 1978.



- [29] Ross, P.J., Taguchi Techniques for Quality Engineering – Loss Function, Orthogonal Experiments, Parameter and Tolerance Design, New York City: McGraw-Hill Book Co. Inc., 1988.
- [30] Vogel, L.C. A Method for Analyzing Multiple Factor Experiments – Its Application to a Study of Gun Perforating Methods. Paper SPE 727-G presented at the 31<sup>st</sup> Annual Fall Meeting of the Petroleum Branch of the American Institute of Mining, Metallurgical, and Petroleum Engineers, Los Angeles (October 1956).
- [31] Sawyer, D.N., Cobb, W.M., Stalkup, F.I., and Braun, P.H. Factorial Design Analysis of Wet-Combustion Drive. Paper SPE 4140 presented at SPE-AIME 47<sup>th</sup> Annual Fall Meeting , San Antonio (October 1974).
- [32] Chu, C. Prediction of Steamflood Performance in Heady Oil Reservoirs Using Correlations Developed by Factorial Design Method. Paper SPE 20020 presented at the 60<sup>th</sup> California Regional Meeting, Ventura (April 1990).
- [33] Damsleth, E., Hage, A., and Volden, R. Maximum Information at Minimum Cost: A North Sea Field Development Study With an Experimental Design. Paper SPE 23139, JPT (December 1992): 1350-1356.
- [34] Aanaonsen, S.I., Eide, A.L., Holden, L., and Aasen, J.O. Optimizing Reservoir Performance Under Uncertainty with Application to Well Location. Paper SPE 30710 presented at the 1995 SPE Annual Technical Conference and Exhibition, Dallas (October 1995).
- [35] Morelon, I., Haas, A., and Massonat, G. Modelling of Geostatistical Parameters Uncertainty in Reservoir Description. Paper presented at the Conference of the Institute of Mathematics and Its Application, Scarborough (March 1995).
- [36] Vincent, G., Corre, B., and Thore, P. Managing Structural Uncertainty in a Mature Field for Optimal Well Placement. Paper SPE 48953 presented at the 1998 SPE Annual Technical Conference and Exhibition, New Orleans (September 1998).
- [37] White, C.D. and Royer, S.A. Experimental Design as a Framework for Reservoir Studies. Paper SPE 79676 presented at the SPE Reservoir Simulation Symposium, Houston (February 2003).

- [38] Peng, C.Y. and Gupta, R. Experimental Design and Analysis Methods in Multiple Deterministic Modelling for Quantifying Hydrocarbon In-Place Probability Distribution Curve. Paper SPE 87002 presented at the SPE Asia Pacific Conference on Integrated Modelling for Asset Management, Kuala Lumpur (March 2004).
- [39] Yeten, B., Castellini, A., Guyaguler, B., and Chen, W.H. A Comparison Study on Experimental Design and Response Surface Methodology. Paper SPE 93347 presented at the SPE Reservoir Simulation Symposium, Houston (January – February 2005).
- [40] Zubarev, D.I. Pros and Cons of Applying Proxy-Models as a Substitute for Full Reservoir Simulations. Paper SPE 124815 presented at the 2009 SPE Annual Technical Conference and Exhibition, New Orleans, Louisiana (October 2009).
- [41] Dejean, J.-P. and Blanc, G. Managing Uncertainties on Production Predictions Using Integrated Statistical Methods. Paper SPE 56696 presented at the 1999 SPE Annual Technical Conference and Exhibition, Houston, Texas (October 1999).
- [42] Venkataraman, R. Application of the Method of Experimental Design to Quantify Uncertainty in Production Profiles. Paper SPE 59422 presented at the 2000 SPE Asia Pacific Conference on Integrated Modelling for Asset Management, Yokohama, Japan (April 2000).
- [43] van Elk, J.F., Guerrero, L., Vijayan, K., and Gupta, R. Improved Uncertainty Management in Field Development Studies through the Application of the Experimental Design Method to the Multiple Realizations Approach. Paper SPE 64462 presented at the 2000 SPE Annual Technical Conference and Exhibition, Dallas, Texas (October 2000).
- [44] Cullick, A.S., Johnson, D., and Shi, G. Improved and More-Rapid History Matching with a Nonlinear Proxy and Global Optimization. Paper SPE 101993 presented at the SPE Annual Technical Conference and an Exhibition, San Antonio, Texas (September 2006).
- [45] Osterloh, W.T. Use of Multiple-Response Optimization to Assist Reservoir Simulation Probabilistic Forecasting and History Matching. Paper SPE

- 116196 presented at the SPE Annual Technical Conference and Exhibition, Denver, Colorado (September 2008).
- [46] Jones, D., Schonlau, M., and Welch, W. Efficient Global Optimization of Expensive Black-Box Functions. Journal of Global Optimization 13 (1998): 455-492.
- [47] Queipo, N.V., Pintos, S., Rincon, N., Contreras, N., and Colmenares, J. Surrogate Modeling-Based Optimization for the Integration of Static and Dynamic Data Into a Reservoir Description. Paper SPE 63065 presented at the Annual Technical Conference and an Exhibition, Dallas, Texas (October 2000).
- [48] Wang, G.G. Adaptive Response Surface Method Using Inherited Latin Hypercube Design Points. Journal of Mechanical Design 125 (2003): 210-220.
- [49] Li, B. and Friedmann, F. Novel Multiple Resolution Design of Experiment/Response Surface Methodology for Uncertainty Analysis of Reservoir Simulation Forecasts. Paper SPE 92853 presented at the SPE Reservoir Simulation Symposium, Houston, Texas (January-February 2005).
- [50] Pan, Y. and Horne, R.N. Improved Methods for Multivariate Optimization of Field Development Scheduling and Well Placement Design. Paper SPE 49055 presented at the SPE Annual Technical Conference and Exhibition, New Orleans, Louisiana (September 1998).
- [51] Guyaguler, B., Horne, R.N. Rogers, L., and Rosenzweig, J.J. Optimization of Well Placement in a Gulf of Mexico Waterflooding Project. Paper SPE 63221 presented at the SPE Annual Technical Conference and Exhibition, Dallas, Texas (October 2000).
- [52] Badru, O. and Kabir, S. Well Placement Optimization in Field Development. Paper SPE 84191 presented at the SPE Annual Technical Conference and Exhibition, Denver, Colorado (October 2003).
- [53] Ozdogan, U., Sahni, A., Yeten, B., Guyaguler, B., and Chen, W.H. Efficient Assessment and Optimization of a Deepwater Asset Development Using Fixed Pattern Approach. Paper SPE 95792 presented at the SPE Annual Technical Conference and Exhibition, Dallas, Texas (October 2005).
- [54] Montgomery, D.C. Design and Analysis of Experiments. 7<sup>th</sup> Edition. International student version. Asia: John Wiley & Sons, Inc., 2009.

- [55] Minitab, Inc. Minitab Statistical Software, Release 16 for Windows. State College, Pennsylvania. Minitab, Inc.: 2009.
- [56] Plackett, R.L. and Burman, J.P. The Design of Optimum Multifactorial Experiments. Biometrika 33 (1946): 305-325.
- [57] Box, G.E.P. and Hunter, J.S. The  $2^{k-p}$  fractional factorial designs, Part I. Technometrics 3 (1961): 311-351.
- [58] Box, G.E.P. and Hunter, J.S. The  $2^{k-p}$  fractional factorial designs, Part II. Technometrics 3 (1961): 449-458.
- [59] Box, G.E.P. and Wilson, K.B. On the Experimental Attainment of Optimum Conditions. Journal of the Royal Statistical Society 13 (1951): 1-45.
- [60] United States Department of Commerce, NIST/SEMATECH. NIST/SEMATECH e-Handbook of Statistical Methods [Online]. 2003. Available from: <http://www.itl.nist.gov/div898/handbook/> [2006, May 01]
- [61] Box, G.E.P. and Behnken, D.W. Some New Three-Level Designs for the Study of Quantitative Variables. Technometrics 30 (1960): 1-40.
- [62] Shewry, M.C. and Wynn, H.P. Maximum Entropy Sampling. Journal of Applied Statistics 14 (1987): 165-170.
- [63] Daniel, C. Use of Half-Normal Plot in Interpreting Factorial Two Level Experiments. Technometrics 1 (1959): 311-342.
- [64] SAS Institute Inc. JMP® 8 Statistics and Graphics Guide. Second Edition. Cary, NC: SAS Institute Inc., 2009.
- [65] Lenth, R.V. Quick and Easy Analysis of Unreplicated Fractional Factorials. Technometrics 31 (1989): 469-473.
- [66] [www.wikipedia.org. Gaussian process](http://en.wikipedia.org/wiki/Gaussian_process) [Online]. 2008. Available from: [http://en.wikipedia.org/wiki/Gaussian\\_process](http://en.wikipedia.org/wiki/Gaussian_process) [2010, February 02]
- [67] Hall, H.R., and Yarborough, L. A new equation of state for Z-factor calculations. Oil and Gas Journal (June 1973).
- [68] Piper, L.D., McCain, W.D., Jr., and Corredor, J.H. Compressibility Factors for Naturally Occurring Petroleum Gases. Paper SPE 26668 presented at the 1993 SPE ATCE SPE Reprint Series No. 52 (1999).
- [69] Lee, Gonzalez, and Eakin. The Viscosity of Natural Gases. JPT (August 1966).

- [70] Valkó, P.P, and McCain, W.D. Jr. Reservoir oil bubble point pressures revisited; solution gas-oil ratios and surface gas specific gravities. J. Pet. Sci. Eng. (2003): 153-169.
- [71] Standing, M.B. A Pressure-Volume-Temperature Correlation for Mixtures of California Oils and Gases. Drill. Prod. Prac. API (1947): 275-287.
- [72] Petrosky, J. and Farshad, F. Pressure Volume Temperature Correlation for the Gulf of Mexico. Paper SPE 26644 presented at the 68th Soc. Pet. Eng. Anna. Tech. Con., Houston, TX (Oct 1993).
- [73] McCain, W. D., Jr. The Properties of Petroleum Fluids. 2nd Ed. Tulsa: PennWell Books (1990).
- [74] Beggs, H.D. and Robinson, J.R. Estimating the Viscosity of Crude Oil Systems. JPT (September 1975): 1140-41.
- [75] Vazquez, M. and Beggs, H.D. Correlations for Fluid Physical Property Prediction. JPT (June 1980): 968-970.
- [76] Osif, T.L. The Effects of Salt, Gas, Temperature, and Pressure on the Compressibility of Water. Paper SPE 13174, SPE Reservoir Engineering, Volume 3, Number 1 (February 1988): 175-181.
- [77] Spivey, J.P., Valkó, P.P., and McCain, W.D., Jr. Coefficients of Isothermal Compressibility of Oilfield Fluid Systems. Unpublished (2003). Cited in Schlumberger. PETREL [Program]. 2009. Schlumberger.
- [78] Meehan, D.N. Estimating Water Viscosity at Reservoir Conditions. Pet. Eng. Int. (July 1980): 117-118.
- [79] [www.process-facility.com](http://www.process-facility.com). Piping – Moody Friction Factor [Online]. 2010. Available from: <http://www.process-facility.com/piping-moody-friction-factor.html> [2010, September 10]

## **APPENDICES**

## **APPENDIX A**

List of Potential Significant Factors Influencing Ultimate Recovery  
Factor of a Horizontal Well

Table A1: Potential significant factors influencing ultimate recovery factor of a horizontal well

No.	Potential Significant Factor	Average Significance Score Subjectively Ranked by Subject Matter Experts <sup>Note 1</sup>	Controllable or Uncontrollable?	Dependent or Independent Factor? (D or I)	Label (C or X) <sup>Note 2</sup>	Remark/Comment
<b><u>Structural &amp; Stratigraphic Properties</u></b>						
1	Reservoir thickness (HRES), ft	9	Uncontrollable	I	X	To collate probability distribution from the existing database.
2	Cross-sectional area of reservoir	0.5	Uncontrollable	D	C	This factor can be calculated from GOC, OWC, fault dip angle, distance between horizontal well to fault, and reservoir thickness.  In practice, deviated wells are drilled parallel to and away from the updip fault at a certain distance of the reservoir candidate for horizontal well drilling to collect petrophysical data. In many cases, the actual hydrocarbon acreage is unknown. Therefore, reservoir boundary effect on fluid flow is studied by defining and using horizontal length-to-reservoir length ratio, LHRATIO.
3	Reservoir acreage, ft <sup>2</sup>	9	Uncontrollable	I	X	
4	Average reservoir dip angle ( $\theta$ ), degree	4	Uncontrollable	I	X	To collate probability distribution from the existing database.
5	Fault transmissibility ( $T_{rf}$ )	0.5	Uncontrollable	I	C	No information in the existing database. Assume that the fault is perfectly impermeable for this study.
6	Fault dip angle, degree	4	Controllable	I	C	According to an earth scientist, fault dip angle general varies from 50 to 60 degree. Using a mid value of 55 degree of the dip angle is advised.
<b><u>Reservoir Rock Properties</u></b>						
7	Porosity ( $\phi$ ), fraction	4	Uncontrollable	I	X	To collate probability distribution from the existing database.
8	Horizontal permeability ( $k_h$ ), md	4	Uncontrollable	I	C	To use an existing k- $\phi$ correlation equation.
9	Anisotropy ( $k_v/k_h$ ), fraction	4	Uncontrollable	I	X	Only one report of vertical permeability tests of core plugs is found. According to an reservoir engineer, the low-, mid-, and high-level anisotropies of 0.1, 0.21, and 1.0 are advised.



Table A1: Potential significant factors influencing ultimate recovery factor of a horizontal well (Continued)

No.	Potential Significant Factor	Average Significance Score Subjectively Ranked by Subject Matter Experts <sup>Note 1</sup>	Controllable or Uncontrollable?	Dependent or Independent Factor? (D or I)	Label (C or X) <sup>Note 2</sup>	Remark/Comment
10	$k_{rhw}$ , $k_{r0w}$ , $k_{rg}$ , md	4	Uncontrollable	I	C	To use generic oil-water and gas-oil relative permeability curves.
11	Residual oil saturation ( $S_{orw}$ ), %	1	Uncontrollable	I	C	A handful of core plug testing data shows that $S_{orw}$ mostly varies from 0.18 - 0.39. No strong correlation with another factor could be obtained with high confidence due to small size of the data. Use an average value of 0.30 for all models.
12	Initial water saturation ( $S_{wi}$ ), %	1	Uncontrollable	I	C	To use a generic Leverette J-function to generate $S_{wi}$ VS depth.
13	Critical gas saturation ( $S_{gc}$ ), %	1	Uncontrollable	I	C	To use the value from the gas-oil relative permeability curve.
14	Heterogeneity (Dykstra-Parson or Geostatistical correlation distance?), dimensionless or ft	4	Uncontrollable	I	C	No information in the existing database. Assume that the simple models in this study are homogeneous.
15	Formation compressibility ( $C_f$ ), $psi^{-1}$	0.5	Uncontrollable	I	C	The sand formations are generally consolidated. Use a constant compressibility value of $8 \times 10^{-6} \text{ psi}^{-1}$ .
<b>Reservoir Fluid Properties</b>						
16	Mobility ratio (M), dimensionless	4	Uncontrollable	D	C	This factor can be calculated from relative permeability and viscosity of oil and gas.
17	Oil gravity (API), ° API	4	Uncontrollable	I	X	To collate probability distribution from existing database.
18	Oil viscosity ( $\mu_o$ ), cp	4	Uncontrollable	I	C	To calculate from a correlation equation.
19	Initial solution gas-oil ratio ( $R_{si}$ ), SCF/STB	4	Uncontrollable	I	C	This factor can be calculated from $P_{bi}$ using a correlation equation.
20	Gravity of gas in gas cap ( $\gamma_g$ ), dimensionless	1	Uncontrollable	I	C	No information in the existing database. Use a generic value of 0.77.
21	Gas viscosity ( $\mu_g$ ), cp	1	Uncontrollable	I	C	No data. To calculate from a correlation equation.
22	Oil compressibility ( $c_o$ ), $psi^{-1}$	0.5	Uncontrollable	I	C	No data. To calculate from a correlation equation.
23	water compressibility ( $c_w$ ), $psi^{-1}$	1	Uncontrollable	I	C	No data. To calculate from a correlation equation.

Table A1: Potential significant factors influencing ultimate recovery factor of a horizontal well (Continued)

No.	Potential Significant Factor	Average Significance Score Subjectively Ranked by Subject Matter Experts <sup>Note 1</sup>	Controllable or Uncontrollable?	Dependent or Independent Factor? (D or I)	Label (C or X) <sup>Note 2</sup>	Remark/Comment
<b><u>Reservoir Fluid Properties (Continued)</u></b>						
24	gas compressibility ( $c_g$ ), $\text{psi}^{-1}$	1	Uncontrollable	I	C	No data. To calculate from a correlation equation.
25	Initial bubble point pressure ( $P_{\text{bp}}$ ), psia	4	Uncontrollable	D	C	This factor can be calculated from initial reservoir pressure, oil gravity and GOC elevation.
26	Initial oil formation volume factor ( $B_{\text{oi}}$ ), psia	1	Uncontrollable	I	C	No data. To calculate from a correlation equation.
27	Capillary pressure ( $P_c$ ), psi	9	Uncontrollable	I	C	$P_c$ - $S_{\text{wir}}$ curves for each porosity value are available in the existing database for building a generic Leverette J-function.
<b><u>Initial Reservoir Condition</u></b>						
28	Initial reservoir pressure ( $P_i$ ), psia	9	Uncontrollable	I	C	To use a $P_i$ - TVDSS correlation equation.
29	Reservoir temperature ( $T_{\text{res}}$ ), °F	0.5	Uncontrollable	I	C	To use a Temperature - TVDSS correlation equation.
30	Initial oil saturation in oil column ( $S_{\text{oi}}$ ), %	1	Uncontrollable	D	C	This factor can be calculated from $S_{\text{wi}}$ .
31	Initial gas saturation in gas cap ( $S_{\text{g}}$ ), %	2	Uncontrollable	D	C	This factor can be calculated from $S_{\text{wi}}$ .
32	Initial gas-oil contact depth (GOC), ft TVDSS	9	Uncontrollable	I	C	This factor can be calculated from OWC and HO
33	Initial oil column thickness (HO), ft TVD	9	Uncontrollable	I	X	To collate the information from the existing database.
34	Initial oil-water contact depth (OWC), ft TVDSS	9	Uncontrollable	I	X	To collate the information from the existing database.

Table A1: Potential significant factors influencing ultimate recovery factor of a horizontal well (Continued)

No.	Potential Significant Factor	Average Significance Score Subjectively Ranked by Subject Matter Experts <sup>Note 1</sup>	Controllable or Uncontrollable?	Dependent or Independent Factor? (D or I)	Label (C or X) <sup>Note 2</sup>	Remark/Comment
<b><u>Driving Mechanism</u></b>						
35	Gas cap size represented as oil PV (MRATIO)	9	Uncontrollable	I	X	To collate the information from the existing database.
36	Aquifer size (AQFRATIO), multiplier of oil PV	9	Uncontrollable	I	X	To collate the information from the existing database.
<b><u>Horizontal Well Placement</u></b>						
37	Horizontal well length (LH), ft	9	Controllable	I	X	To collate the information from the existing database.
38	Well standoff to OWC, ft TVD	9	Controllable	I	X	To collate the information from the existing database.
39	Well standoff to GOC, ft TVD	9	Controllable	D	C	This factor can be calculated from well stand off to OWC and HO.
40	Distance from horizontal well to the updip fault, ft	1	Controllable	D	C	This factor is automatically varied as well standoff to OWC is varied.
41	Orientation direction of horizontal well relative to fault's strike, degree	1	Controllable	I	C	Generally, a horizontal well is preferred to drill in parallel to an updip fault, if possible. Therefore, the well is assumed to be parallel to the fault for all experiments.
<b><u>Drilling and Completion</u></b>						
42	Tubing size ( $d_{t,b}$ ), in	0.5	Controllable	I	C	To use a 2-7/8" tubing size for all models because this size is widely used and can also accommodate high flow rates in the fields.
43	Completion type of horizontal wells	0.5	Controllable	I	C	All horizontal wells have open-hole completion.

Table A1: Potential significant factors influencing ultimate recovery factor of a horizontal well (Continued)

No.	Potential Significant Factor	Average Significance Score Subjectively Ranked by Subject Matter Experts <sup>Note 1</sup>	Controllable or Uncontrollable?	Dependent or Independent Factor? (D or I)	Label (C or X) <sup>Note 2</sup>	Remark/Comment
<b><u>Drilling and Completion</u></b>						
44	Mechanical skin factor ( $S_m$ ), dimensionless	2	Controllable	I	C	This information is not available in the database. It is relatively difficult to control this factor because it depends on many factors, especially experience and workmanship. To assume that there is no skin factor for the objectives of screening and well design.
45	Horizontal well profile (The snaking well profile could affect well performance and be accounted for as an effective length factor?)	0.5	Controllable	I	C	For screening and design purposes, assume that the well is perfectly horizontal.
46	Wellbore diameter ( $d_w$ ), in	2	Controllable	I	C	Only 6-1/8" bit size is used for drilling horizontal section. Thus, wellbore diameter is fixed at 6-1/8".
<b><u>Operational Constraint</u></b>						
47	Liquid production rate (LRAT), STB/day	9	Controllable	I	X	1) Min. liquid flow rate is calculated from min. required oil flow rate and maximum allowable water cut 2) Max. liquid flow rate is the maximum liquid flow rate of 2-7/8" tubing recorded in the field.
48	Well abandonment pressure ( $P_a$ ), psia	2	Controllable	I	C	Its significance depends on the driving mechanism and flowing condition. This factor is indirectly represented by min. tubing head pressure.

**Table A1: Potential significant factors influencing ultimate recovery factor of a horizontal well (Continued)**

Note: 1) Based on your experience, please score the effect of the variables on horizontal well EUR based on the following criteria;

Score	Criteria
0	No effect.
1	The variable effect only SLIGHTLY affects horizontal well URF
4	The variable effect only MODERATELY affects horizontal well URF
9	The variable effect has a DIRECT AND STRONG effect on horizontal well URF

2) Label legend:

Label	Description
C	1) Factor that is held constant because of SME's recommendation or best practice in the fields, 2) Factor that can be correlated from other factors. 3) Factor effect is beyond the objectives of this research.
X	Factor considered to be potential significant factor and need to be experimented to determine what influence it has on the output response and what their optimum setting should be to achieve customer-desired performance.

3) Limiting operation conditions are as follows

3.1) Max. allowable water cut	90%
3.2) Min. required oil flow rate	50 STB/day
3.3) Max. allowable GOR	5 MCF/STB
3.4) Min. allowable tubing head pressure	min. inlet pressure of a booster compressor 100 psig

## **APPENDIX B**

### Probability Distribution and Associated Statistical Analysis of Design Factors

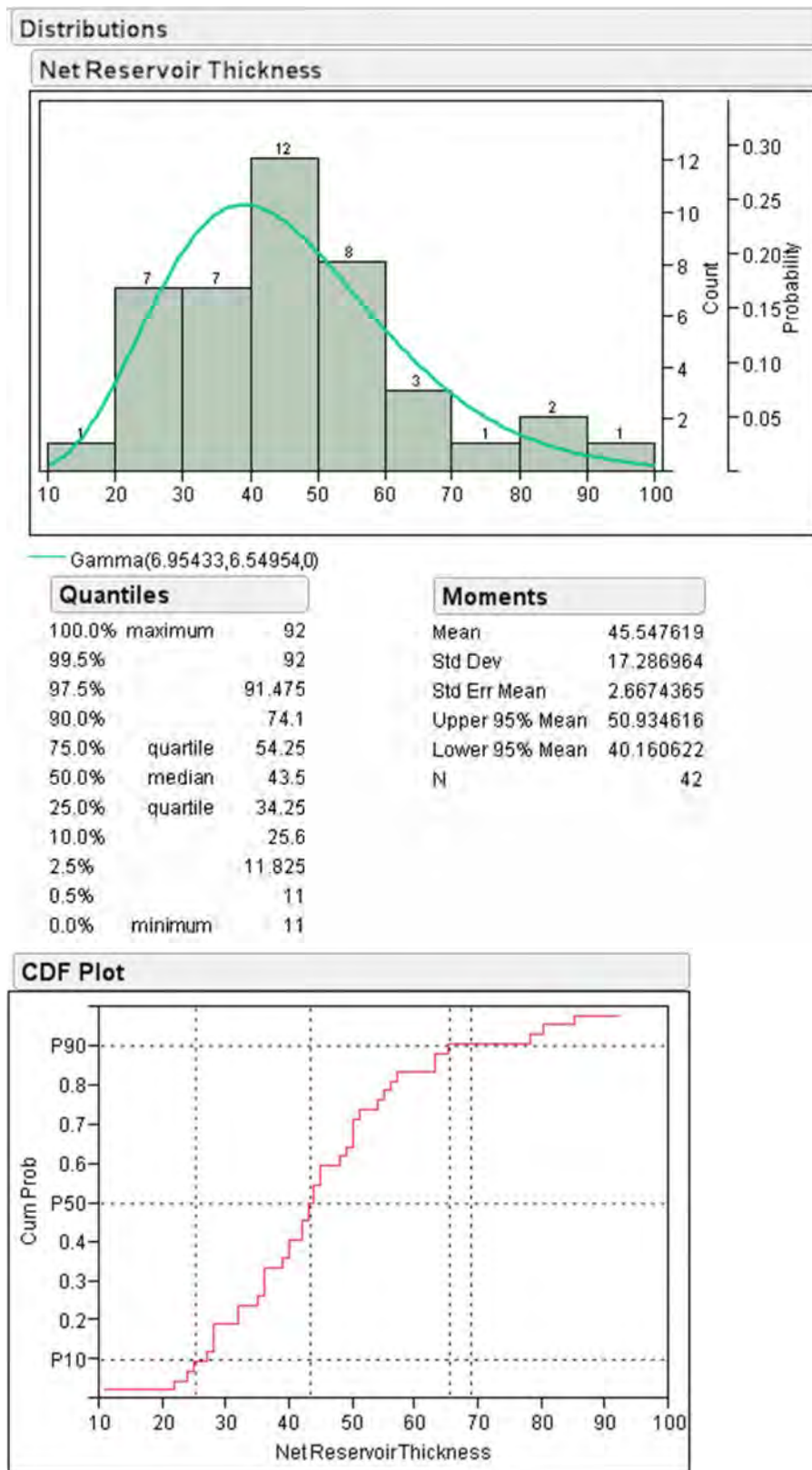


Figure B1: Probability distribution and statistics of reservoir thicknesses

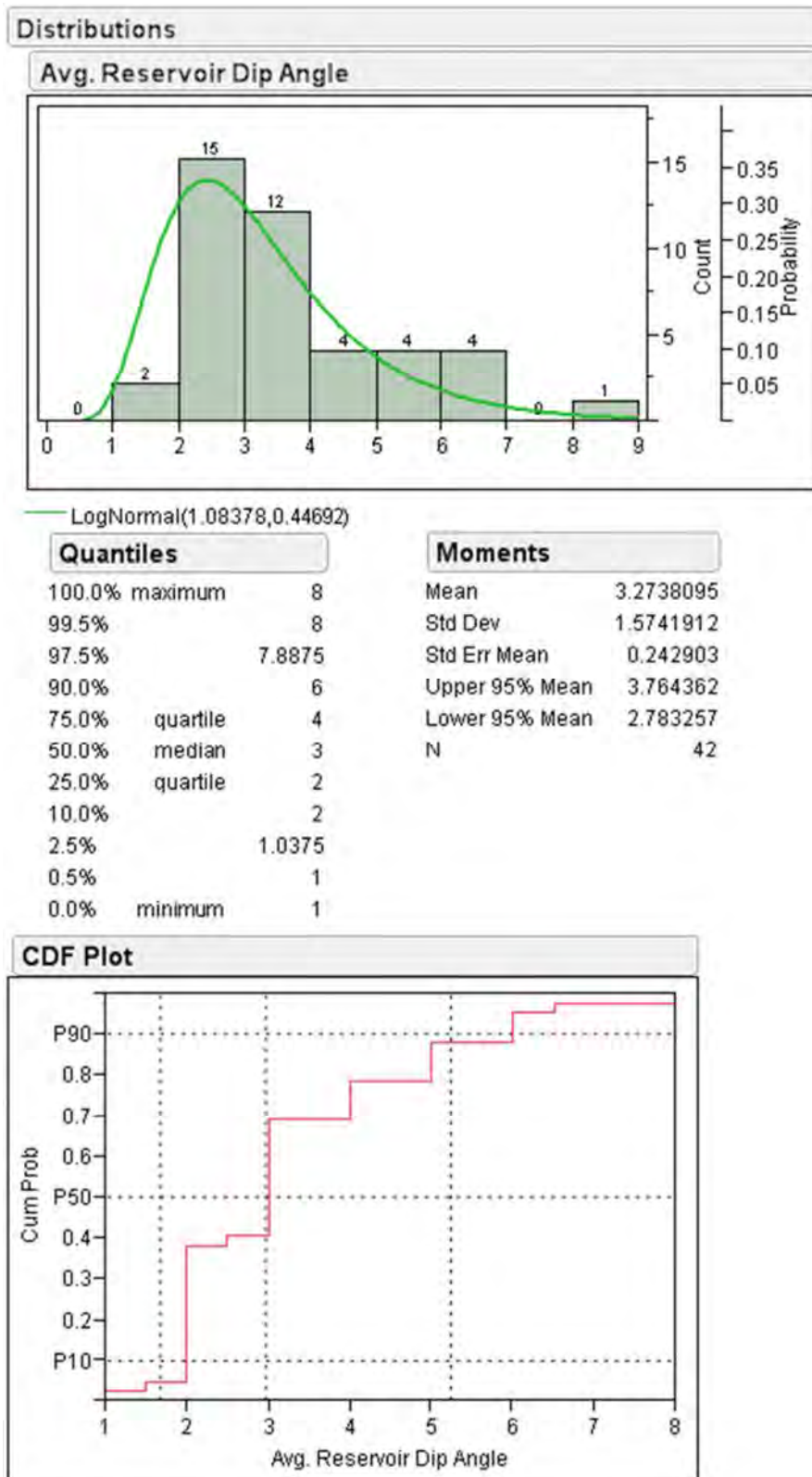


Figure B2: Probability distribution and statistics of reservoir dip angles



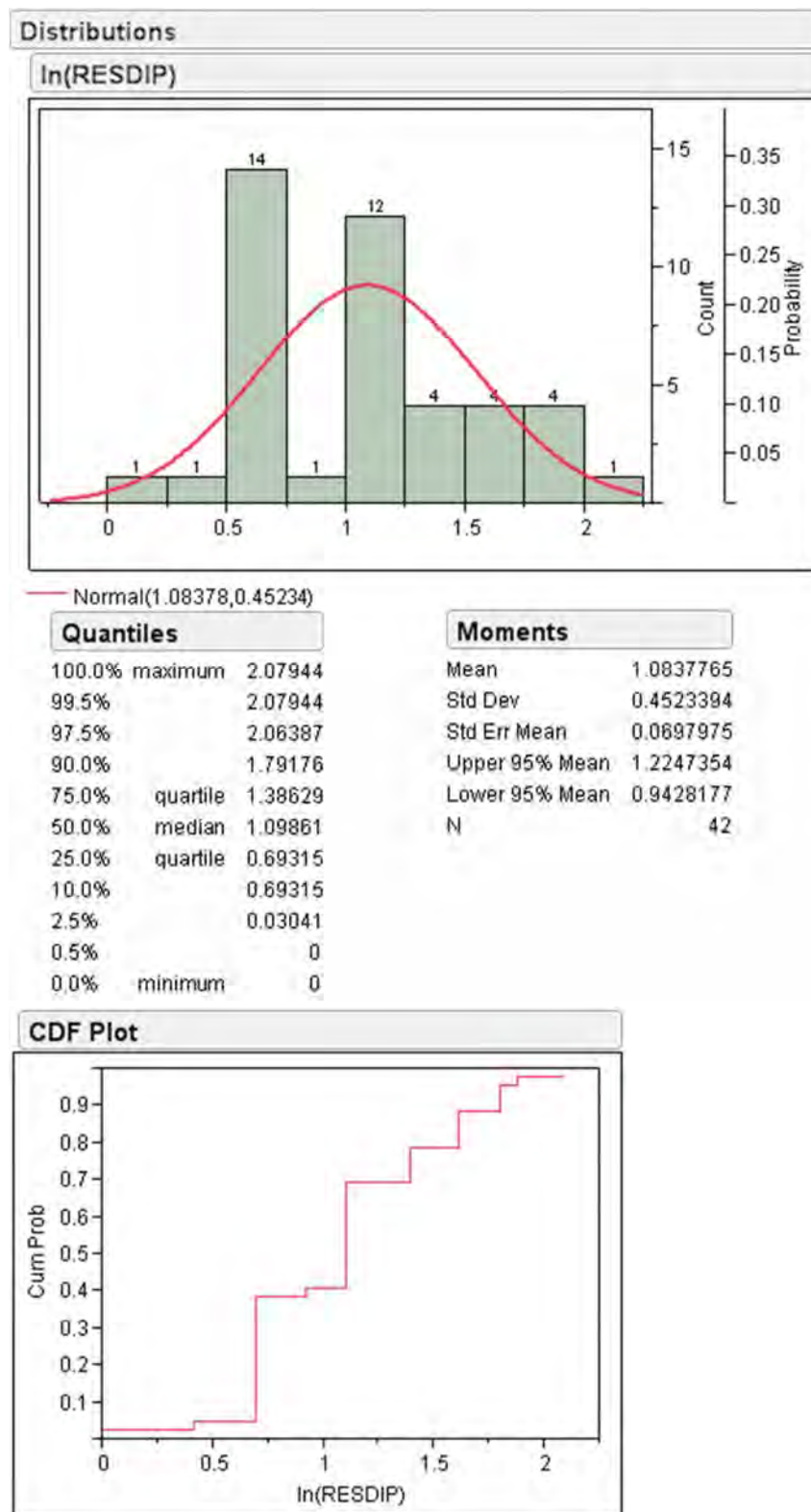


Figure B3: Probability distribution and statistics of transformed reservoir dip angles

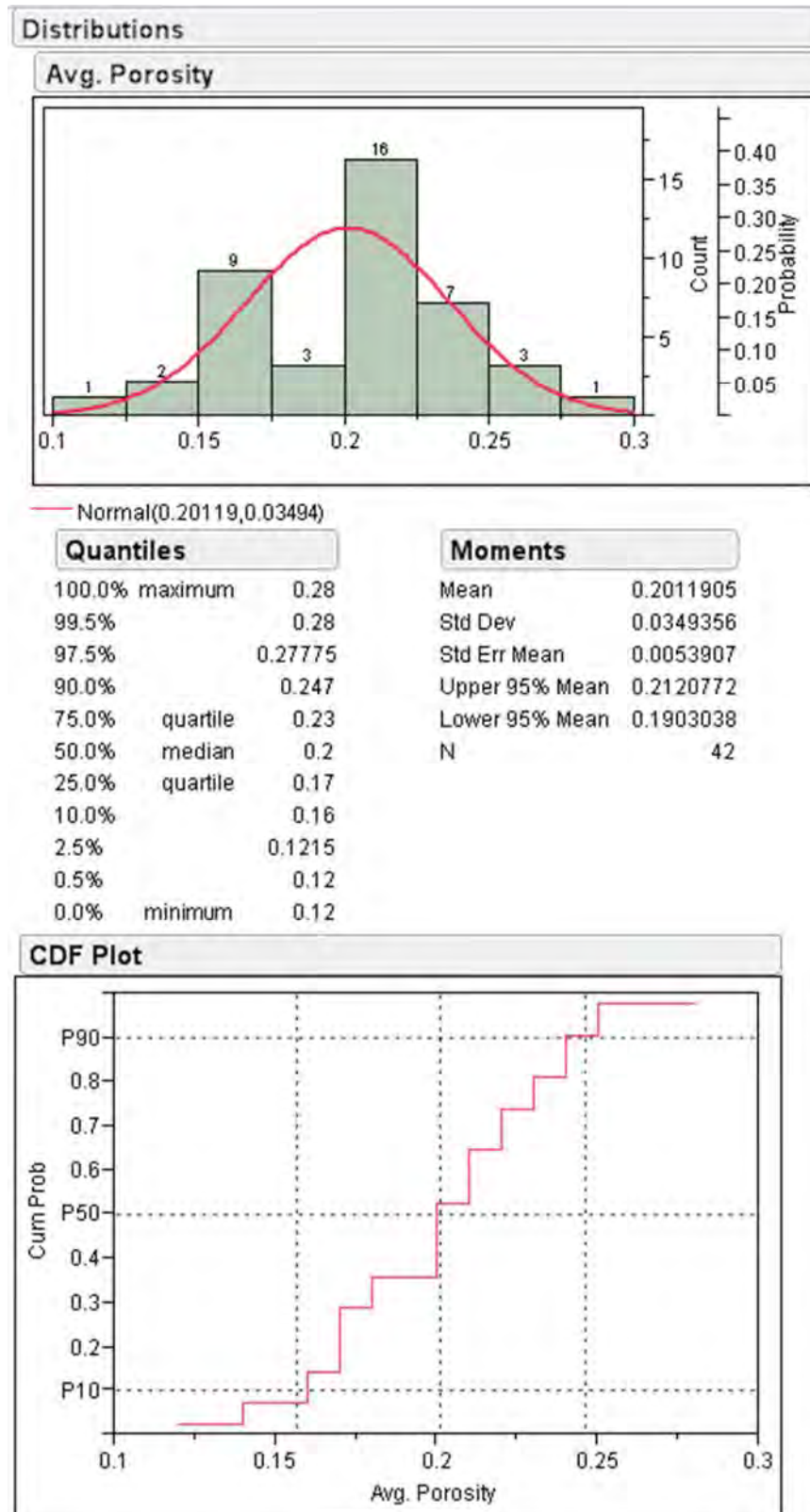


Figure B4: Probability distribution and statistics of porosities

Level	ANISO	$\ln(\text{ANISO}-0.0822)$	Cum. Prob.
Low	0.1	-4.0286	0
Mid	0.21	-2.0573	0.5
High	1	-0.0858	1

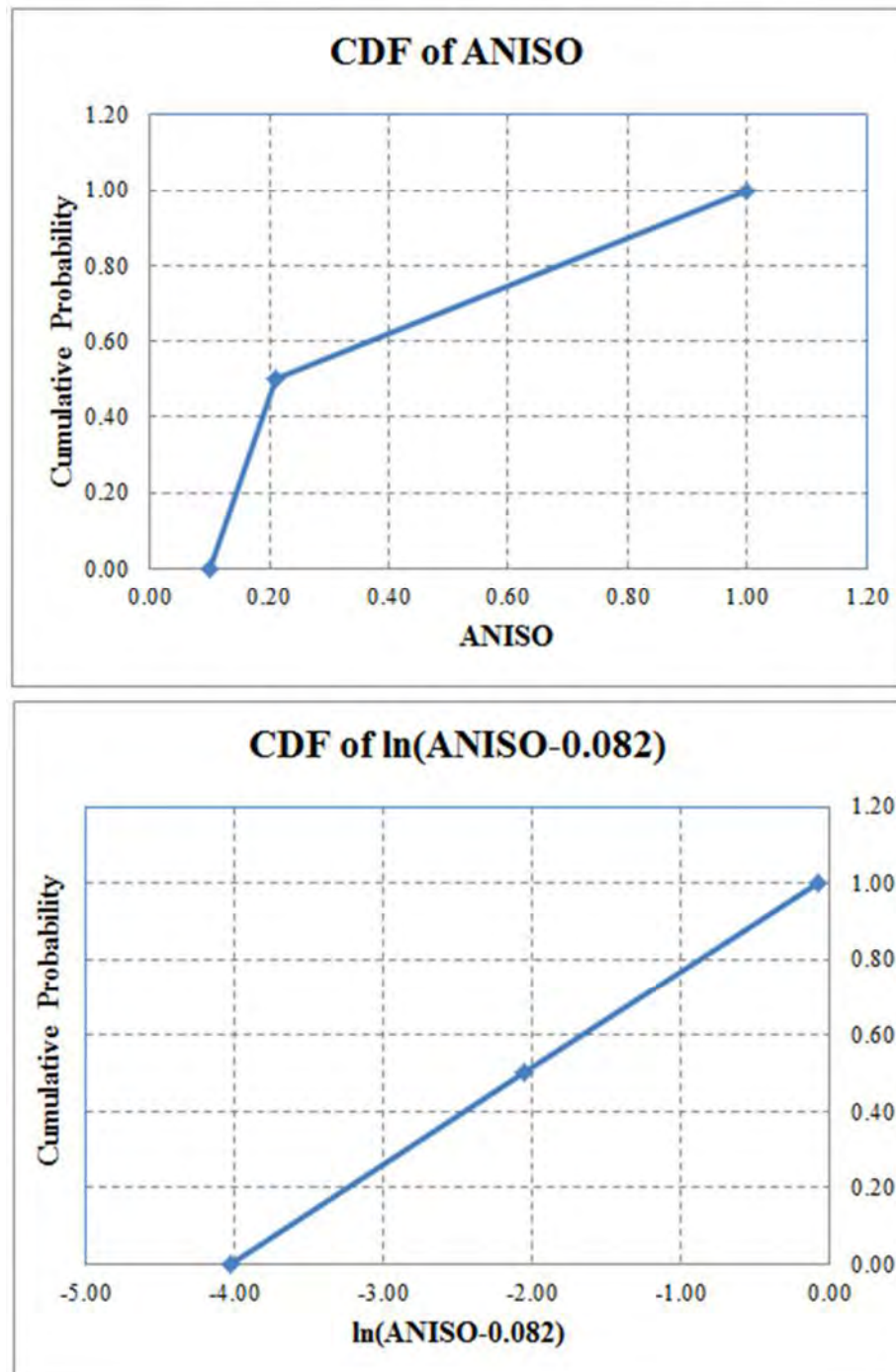


Figure B5: Probability distribution of anisotropies and transformed anisotropies

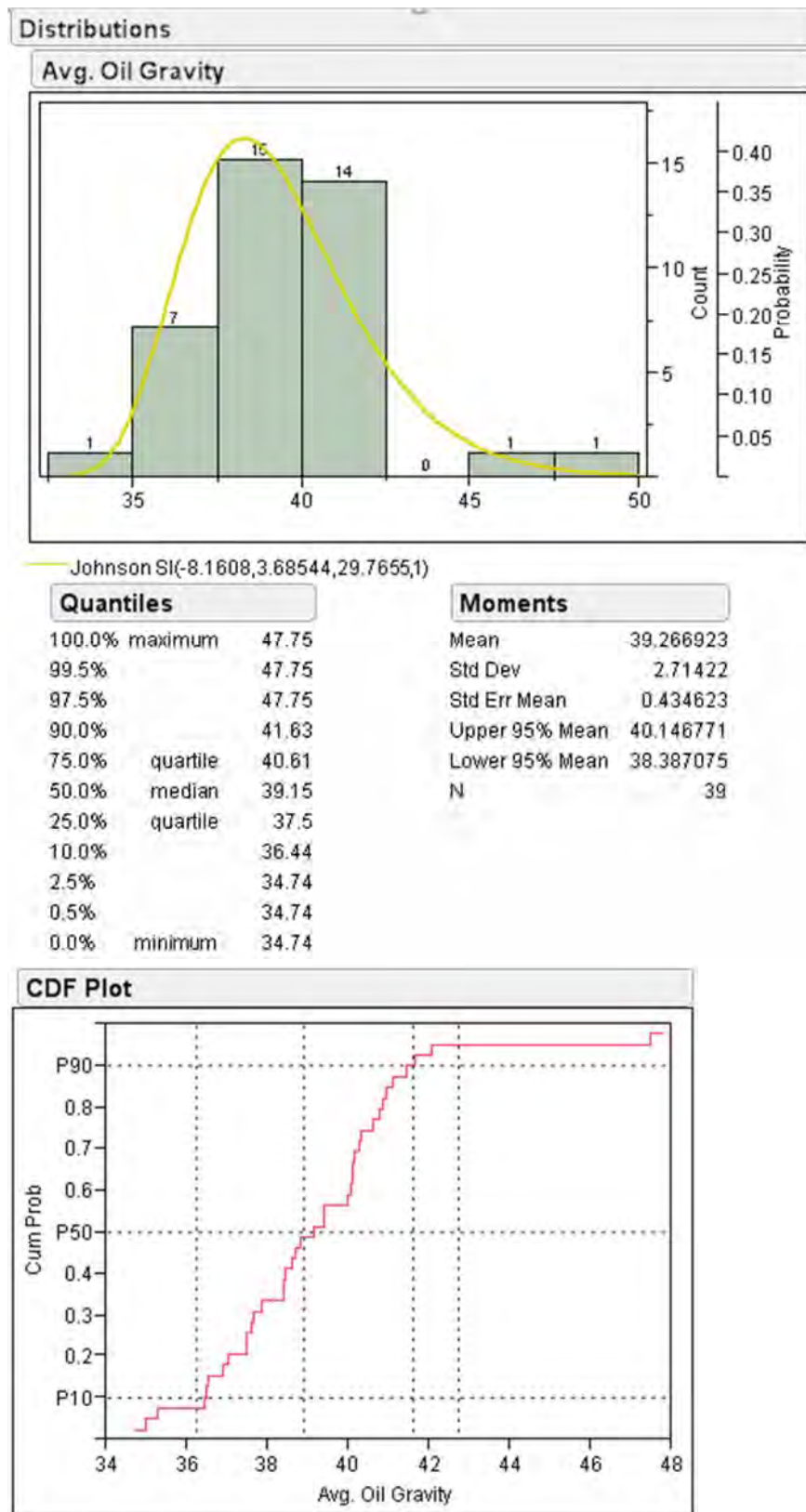


Figure B6: Probability distribution and statistics of oil gravities

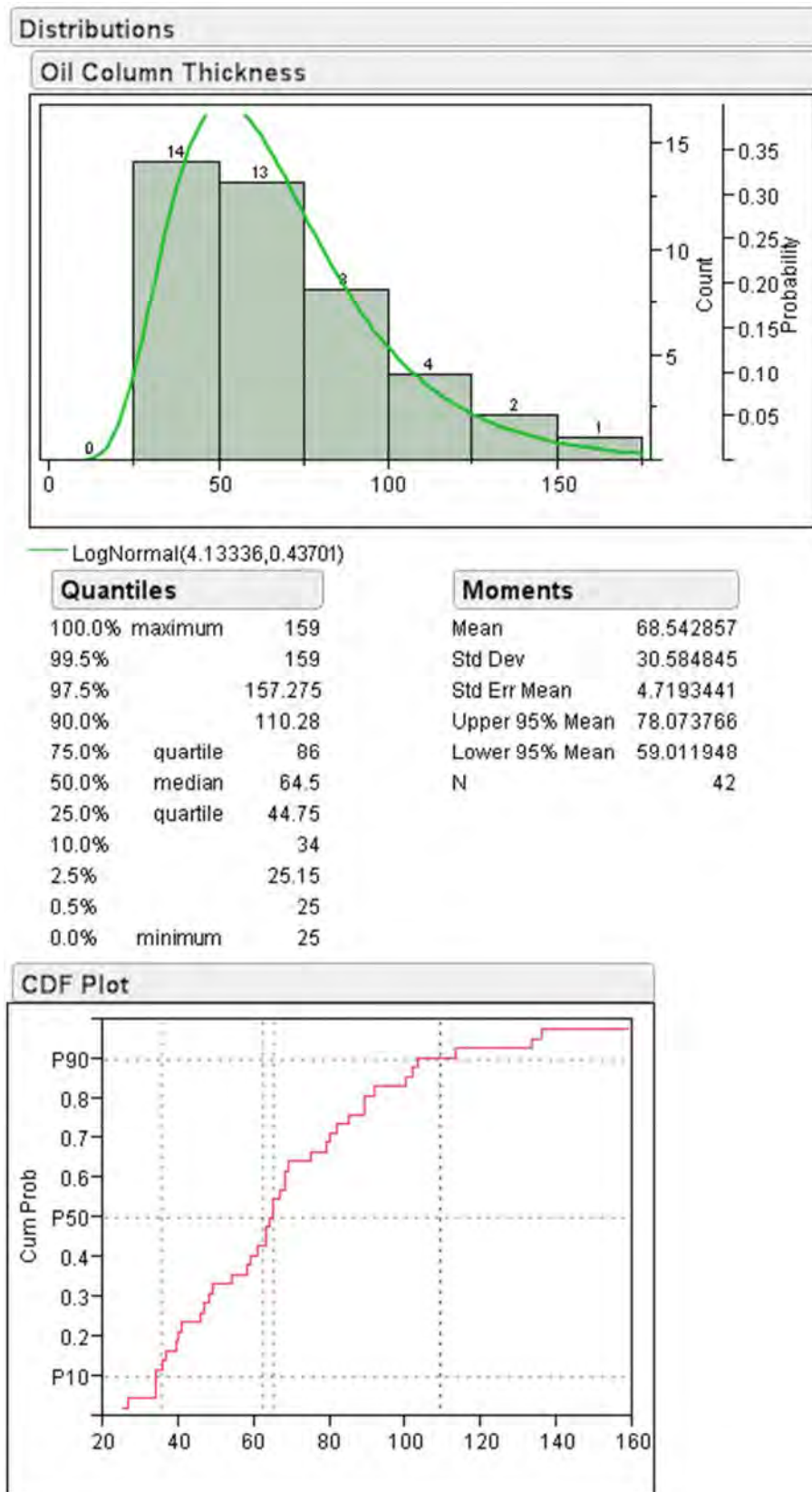


Figure B7: Probability distribution and statistics of initial oil column thicknesses

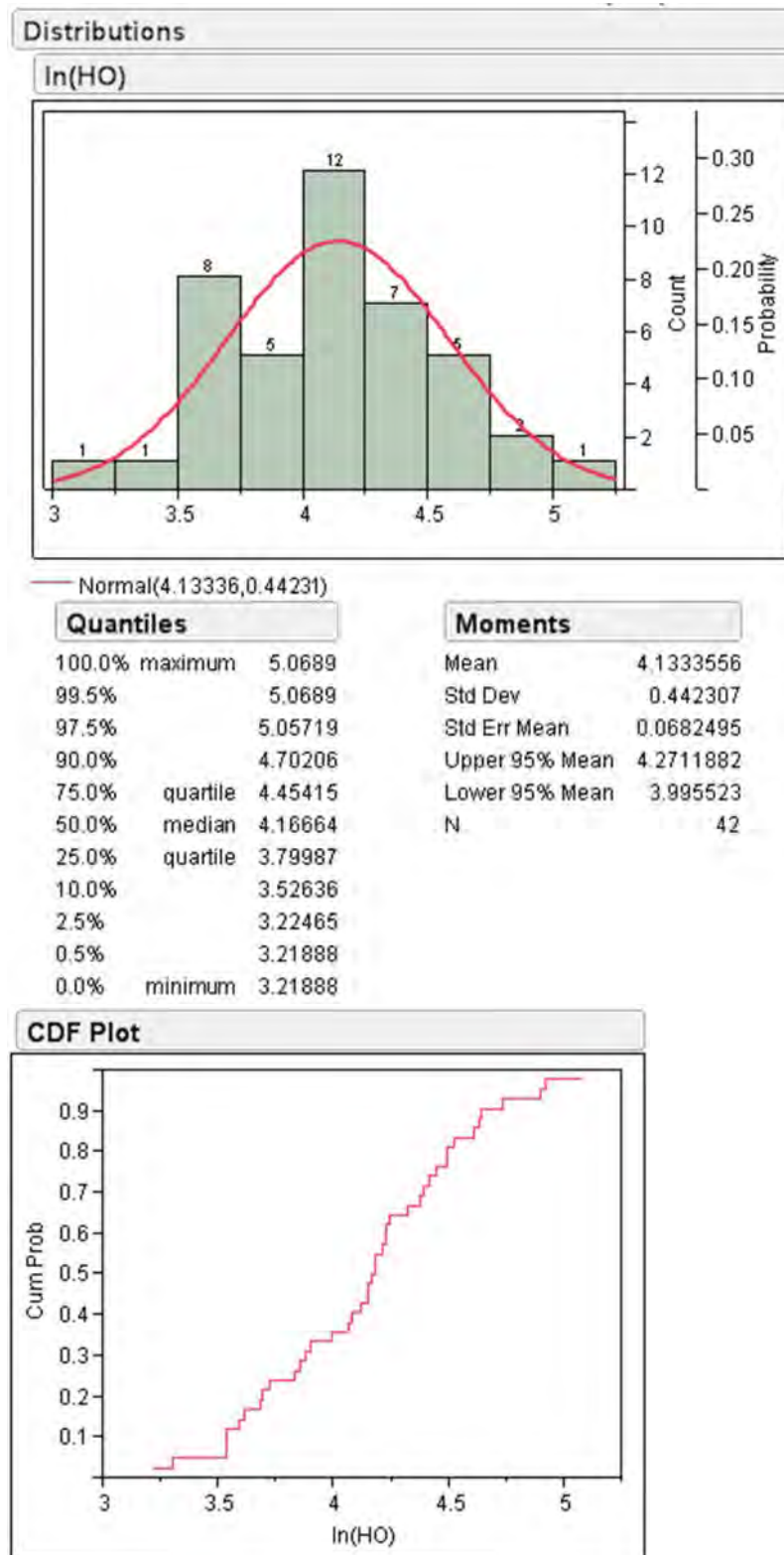


Figure B8: Probability distribution and statistics of transformed initial oil column thicknesses

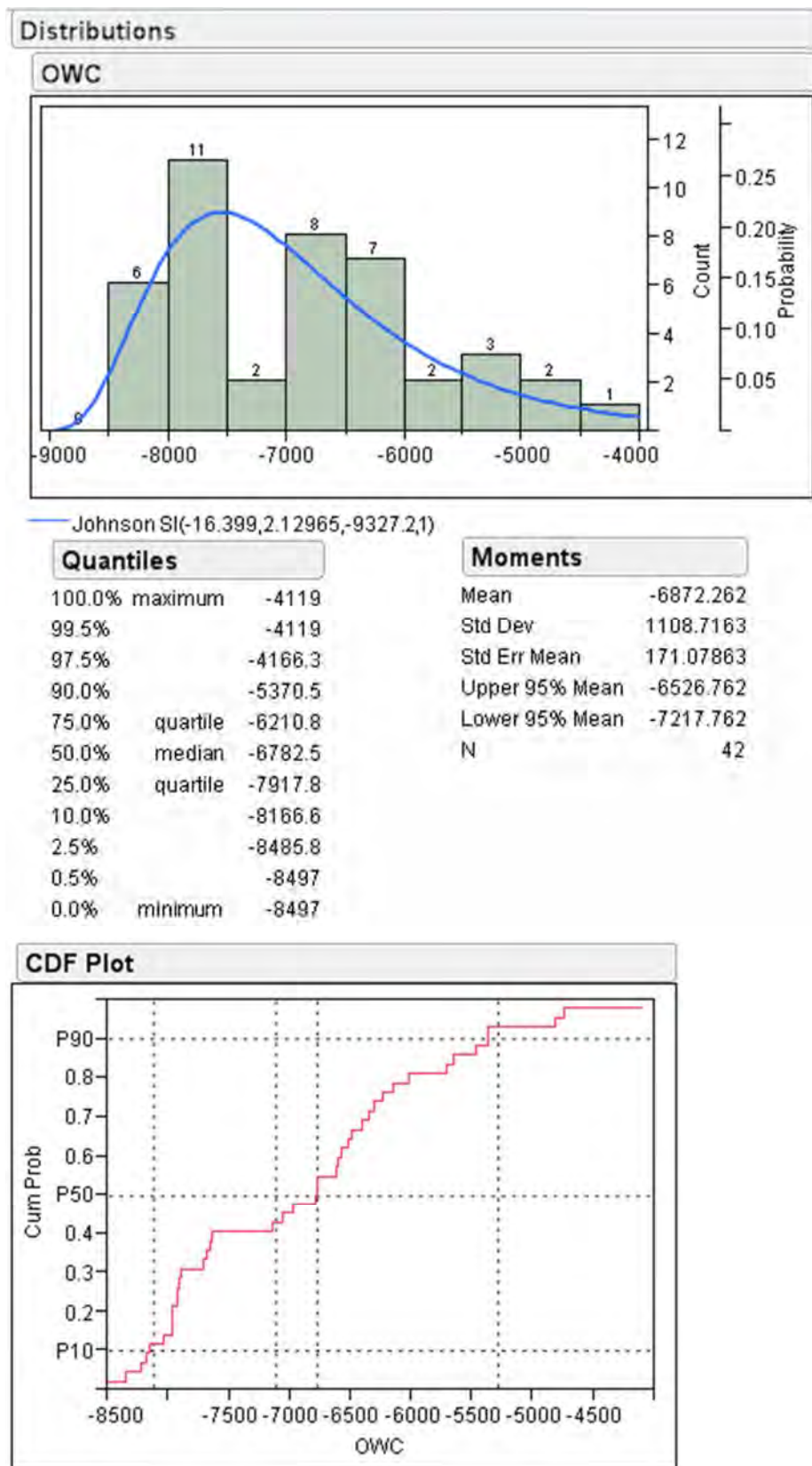


Figure B9: Probability distribution and statistics of oil-water contact elevations

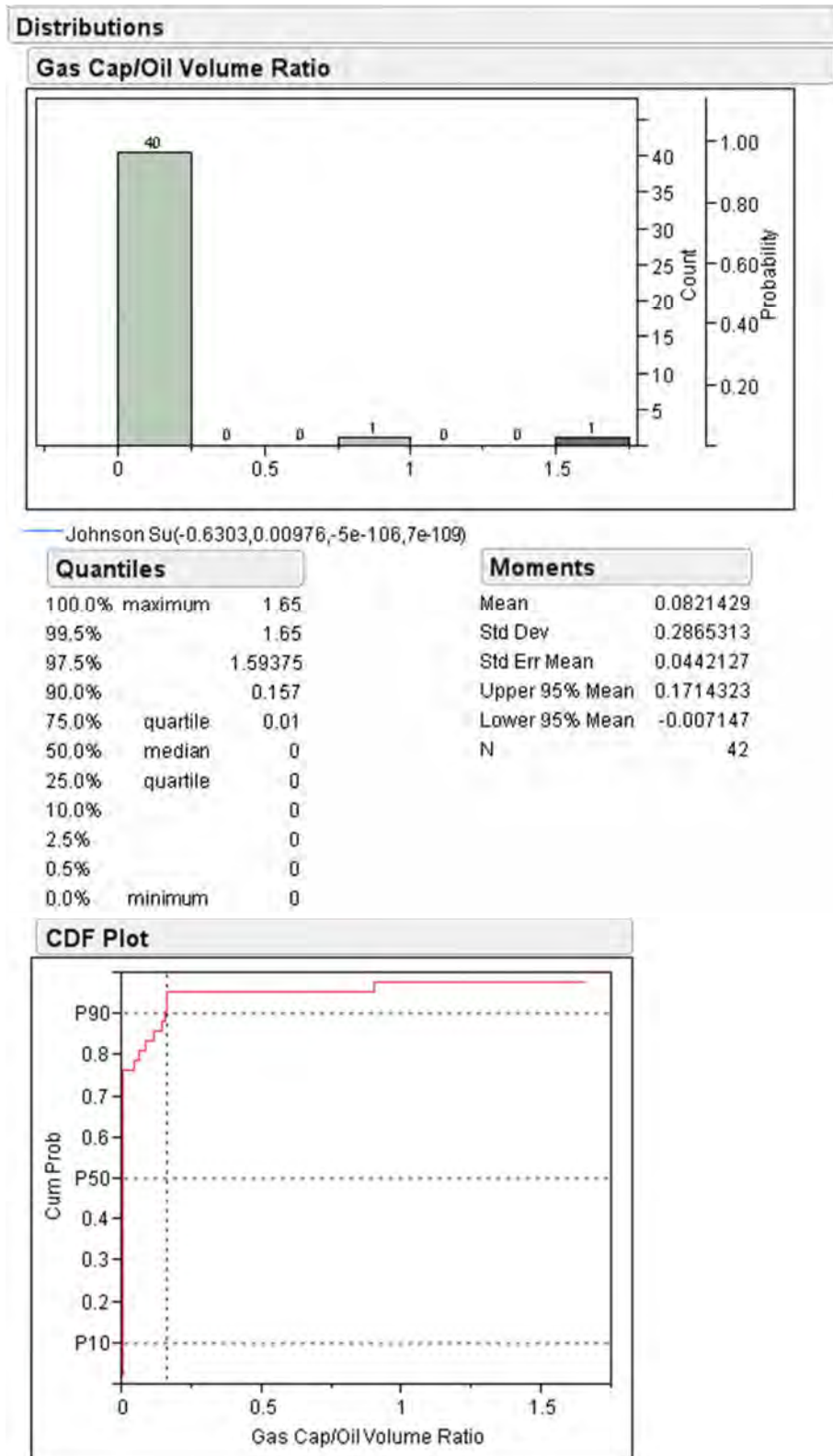


Figure B10: Probability distribution and statistics of gas-cap-volume-to-oil-volume ratios



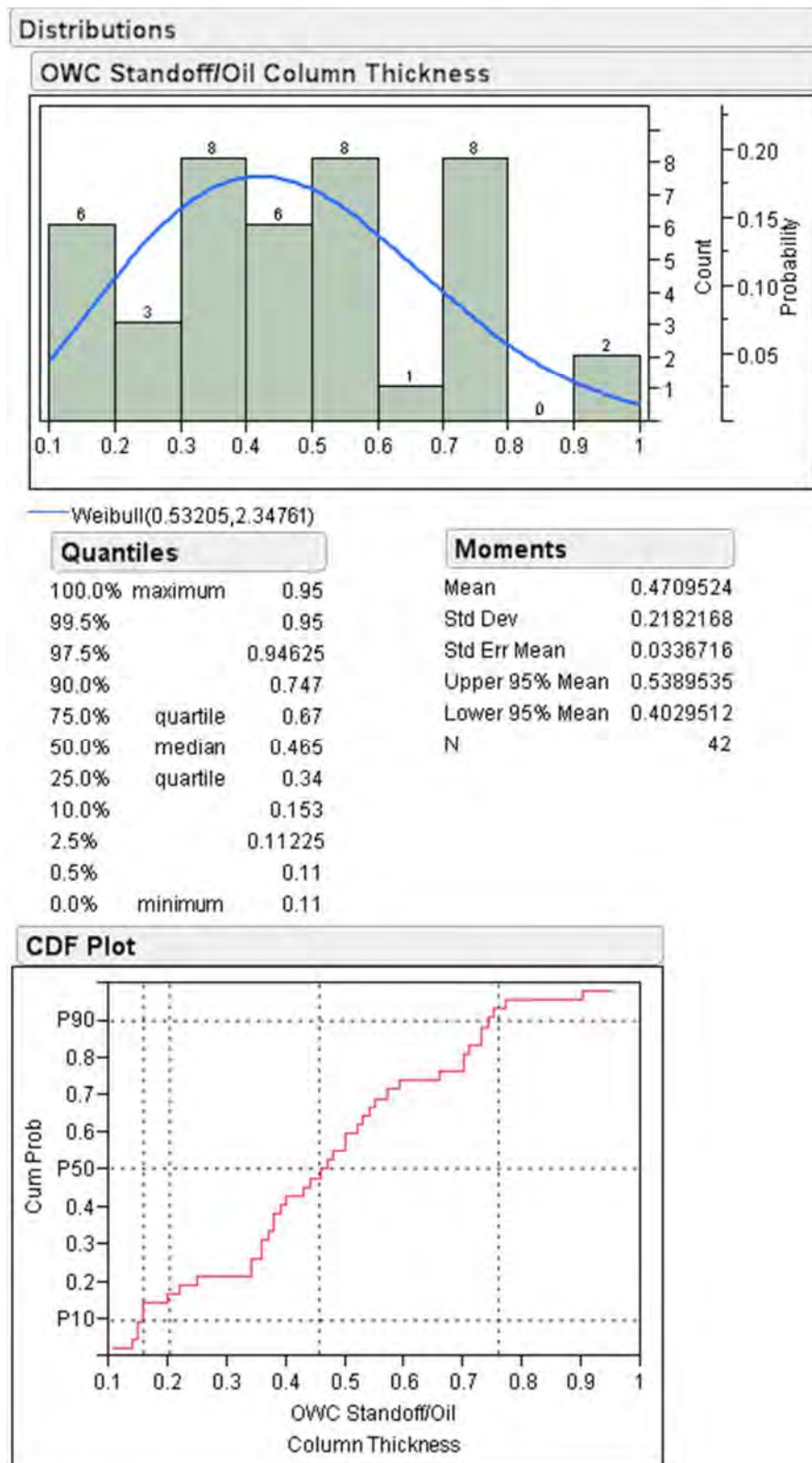


Figure B11: Probability distribution and statistics of well-standoff-to-OWC-to-oil-column-thickness ratios

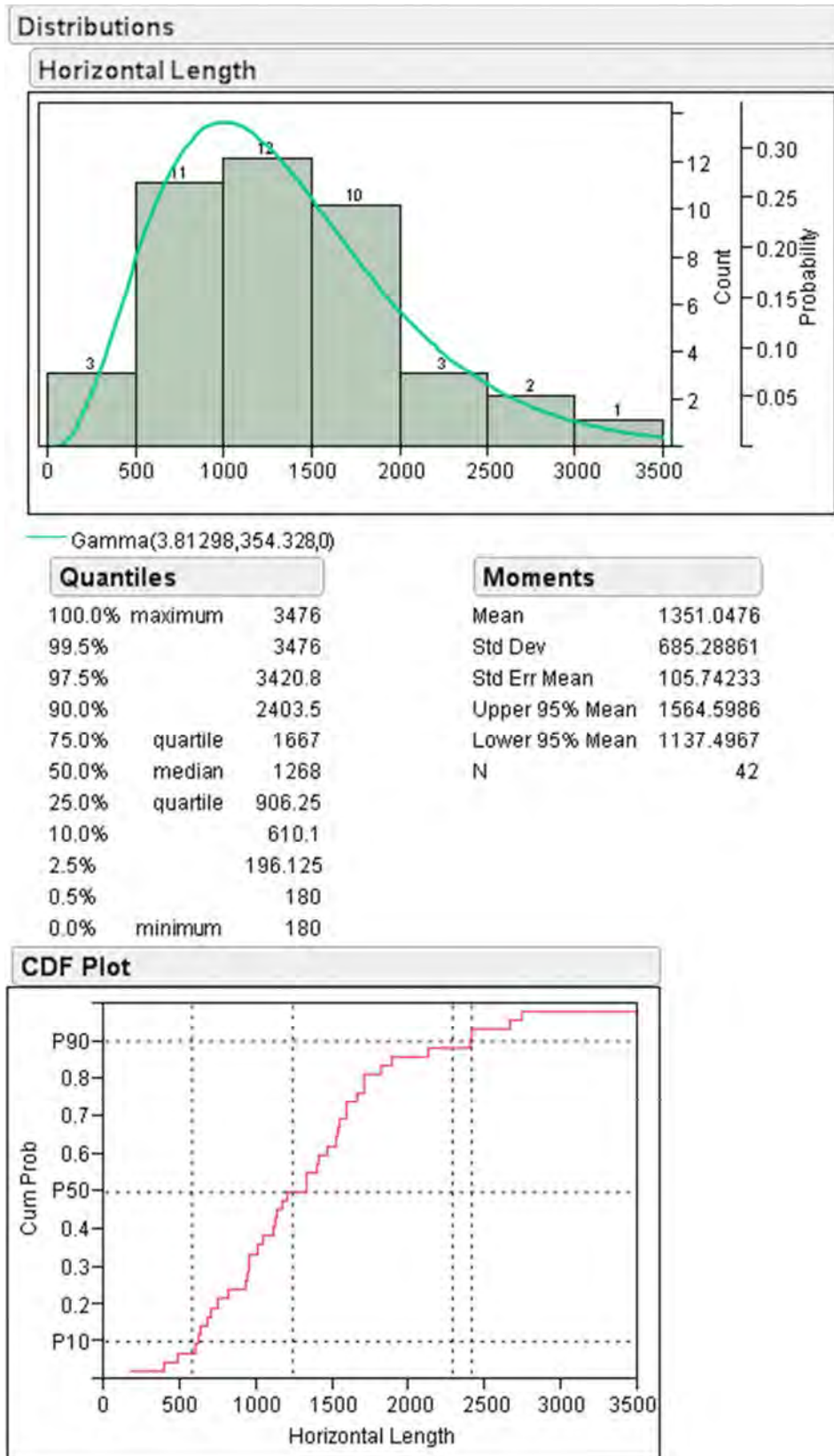


Figure B12: Probability distribution and statistics of horizontal well lengths

## **APPENDIX C**

Design Patterns of Experimental Designs Performed in This Research

Table C1: Design patterns of Resolution IV  $2^{13-8}$  fractional factorial design

Run ID.	Design Pattern	Run ID.	Design Pattern	Run ID.	Design Pattern
1	-----	12	-+++++--	23	+-----+
2	-----+	13	-+----++	24	+-----+
3	---+++++	14	-+++++--	25	++-----+
4	---+-----	15	-+++++--	26	++-----+
5	--+++++	16	-+++++--	27	+++++---
6	--+-----	17	+-----+	28	+++++---
7	---+++++	18	+-----+	29	+++++---
8	---+-----	19	+-----+	30	+++++---
9	-+-----+	20	+-----+	31	+++++---
10	-+-----+	21	+-----+	32	+++++---
11	-+-----+	22	+-----+		

- Note:** 1) "+" = high-level value and "-" = low-level value  
2) The order of design pattern is as follows: OWC, HRES, HO#, LH, LHRATIO, RESDIP#, MRATIO, AQFRATIO, WSTANDOFF, PORO, API, ANISO#, AND LRAT

Table C2: Design patterns of 6-factor faced-center central composite design

Run ID.	Design Pattern	Run ID.	Design Pattern	Run ID.	Design Pattern
1	-----+	16	-++++-	31	+---++-
2	-----+-	17	-+++++	32	+---++-
3	----+---	18	0a0000	33	++++--
4	---++++	19	00a000	34	++++--
5	--+-----	20	000a00	35	+--++--
6	--++---	21	0000a0	36	+--++++
7	--++-+-	22	00000a	37	A00000
8	--++++-	23	000000	38	++----+
9	a00000	24	00000A	39	++--+-
10	-+-----	25	0000A0	40	++-+-
11	-+---++	26	000A00	41	++-+++
12	-+--++	27	00A000	42	+++---
13	-+--+-	28	0A0000	43	+++--+
14	-++---+	29	+-----	44	++++-+
15	-++-+-	30	+---++	45	+++++-

- Note:
- 1) "+", "0", and "-" = high-, mid-, and low-level values, respectively.
  - 2) "A" and "a" = high- and low-level face-centered point.
  - 3) The order of design pattern is as follows: OWC, HO#, LHRATIO, WSTANDOFF, PORO, and LRAT.

Table C3: Design patterns of 6-factor, 45-run maximum entropy design

<b>Run ID.</b>	<b>OWC</b>	<b>HO#</b>	<b>LHRATIO</b>	<b>WSTANDOFF</b>	<b>PORO</b>	<b>LRAT</b>
301	7301.41	3.567	0.380	0.240	0.240	2697.2
302	6360.58	4.171	0.180	0.360	0.160	2565.1
303	7175.97	3.692	0.820	0.400	0.174	2697.2
304	5294.30	3.818	0.940	0.307	0.236	5735.8
305	5796.08	4.473	0.980	0.320	0.224	4414.7
306	7426.86	4.322	0.940	0.427	0.246	715.6
307	5294.30	3.995	0.640	0.387	0.160	55.0
308	6276.04	3.793	0.687	0.360	0.190	55.0
309	7991.36	4.675	0.280	0.440	0.220	4578.4
310	5482.47	4.599	0.600	0.213	0.164	3225.7
311	7928.63	4.222	0.540	0.587	0.234	4150.4
312	5482.47	4.448	0.120	0.320	0.206	2036.7
313	6297.86	4.247	0.620	0.413	0.206	1993.6
314	5796.08	4.297	0.420	0.160	0.212	3754.1
315	7489.58	4.020	0.320	0.421	0.194	847.7
316	5984.24	4.574	0.420	0.400	0.160	847.7
317	5607.91	3.617	0.760	0.160	0.200	2036.7
318	7928.63	4.322	0.440	0.293	0.162	2433.0
319	7050.52	4.222	0.360	0.760	0.188	55.0
320	5294.30	4.133	0.160	0.613	0.204	3357.8
321	7238.69	3.894	0.740	0.173	0.164	4943.1
322	5921.52	4.675	0.100	0.520	0.188	3357.8
323	7113.24	4.010	0.220	0.693	0.160	4546.8
324	7748.65	4.549	0.300	0.160	0.198	55.0
325	7050.52	3.567	0.780	0.533	0.214	2168.8
326	7050.52	3.642	0.260	0.627	0.186	2697.2
327	6736.91	4.196	0.880	0.173	0.224	2961.4
328	6548.74	3.567	0.380	0.627	0.250	5867.9
329	7426.86	3.692	0.260	0.467	0.234	319.2
330	5294.30	3.692	0.520	0.320	0.228	4414.7
331	6705.55	4.257	0.433	0.160	0.178	55.0
332	5733.36	3.970	0.660	0.680	0.246	5339.4
333	6486.02	4.448	0.560	0.547	0.164	4150.4
334	7135.06	4.574	0.280	0.317	0.208	2565.1
335	7994.08	4.020	0.100	0.267	0.210	3225.7

Table C3: Design patterns of 6-factor, 45-run maximum entropy design (Continued)

<b>Run ID.</b>	<b>OWC</b>	<b>HO#</b>	<b>LHRATIO</b>	<b>WSTANDOFF</b>	<b>PORO</b>	<b>LRAT</b>
336	6172.41	4.096	0.120	0.440	0.232	5867.9
337	7113.24	4.096	0.300	0.307	0.210	5471.6
338	7740.47	4.599	0.880	0.707	0.186	5735.8
339	6674.19	4.524	0.980	0.707	0.160	715.6
340	7865.91	4.574	0.960	0.653	0.214	583.4
341	6674.19	3.768	0.760	0.360	0.236	4018.3
342	5482.47	3.869	0.100	0.520	0.224	1244.0
343	5357.02	3.642	0.840	0.653	0.212	3489.9
344	6109.69	3.739	0.180	0.160	0.236	2300.9
345	5733.36	3.617	0.800	0.640	0.174	1508.2

Table C4: Design patterns of the first 18-run maximum entropy design for proxy cross-validation

<b>Run ID.</b>	<b>OWC</b>	<b>HO#</b>	<b>LHRATIO</b>	<b>WSTANDOFF</b>	<b>PORO</b>	<b>LRAT</b>
101	7959.99	3.755	0.950	0.293	0.165	55.0
102	7332.77	4.259	0.100	0.160	0.185	5339.4
103	7803.19	4.322	0.800	0.493	0.180	5009.2
104	6548.74	4.700	0.450	0.160	0.210	4348.6
105	6705.55	3.692	0.650	0.660	0.230	1376.1
106	6548.74	4.133	0.200	0.627	0.180	3027.5
107	6548.74	4.259	0.900	0.160	0.225	2036.7
108	6391.94	3.567	0.350	0.393	0.235	4678.9
109	5451.11	3.944	0.100	0.360	0.200	2697.2
110	5294.30	4.385	0.150	0.493	0.170	5669.7
111	5764.72	4.196	0.450	0.327	0.245	2036.7
112	6078.33	3.755	0.900	0.727	0.160	3688.1
113	8116.80	4.574	0.250	0.293	0.230	3027.5
114	5294.30	4.511	0.850	0.527	0.235	2697.2
115	6862.36	4.385	0.400	0.693	0.220	1045.8
116	5294.30	3.692	0.650	0.260	0.185	385.3
117	6705.55	3.818	0.700	0.327	0.165	2366.9
118	6862.36	4.385	0.800	0.560	0.160	715.6

Table C5: Design patterns of the second 18-run maximum entropy design for proxy cross-validation

<b>Run ID.</b>	<b>OWC</b>	<b>HO#</b>	<b>LHRATIO</b>	<b>WSTANDOFF</b>	<b>PORO</b>	<b>LRAT</b>
201	5607.91	3.818	0.150	0.427	0.205	2366.9
202	5294.30	3.755	0.650	0.627	0.220	5009.2
203	5921.52	3.567	0.250	0.727	0.190	4018.3
204	7175.97	3.818	0.250	0.493	0.160	5339.4
205	5294.30	4.637	0.150	0.593	0.195	1706.4
206	5294.30	4.700	0.900	0.460	0.180	2036.7
207	7803.19	4.511	0.400	0.727	0.205	3688.1
208	7959.99	4.133	0.800	0.327	0.160	4348.6
209	6862.36	4.574	0.600	0.527	0.170	4018.3
210	5607.91	4.259	0.100	0.327	0.185	5339.4
211	6391.94	3.692	0.950	0.427	0.225	385.3
212	6078.33	4.070	0.500	0.160	0.225	3688.1
213	6862.36	3.567	0.850	0.493	0.180	2697.2
214	7646.38	4.322	0.350	0.327	0.165	715.6
215	7175.97	3.567	1.000	0.227	0.180	55.0
216	5764.72	4.448	0.550	0.627	0.225	5669.7
217	5294.30	4.259	0.800	0.160	0.175	2366.9
218	5921.52	4.511	0.400	0.260	0.205	385.3



## **APPENDIX D**

Generic Correlation Equations of Petrophysical Properties of Thin-Oil-Column Reservoirs in the Gulf of Thailand

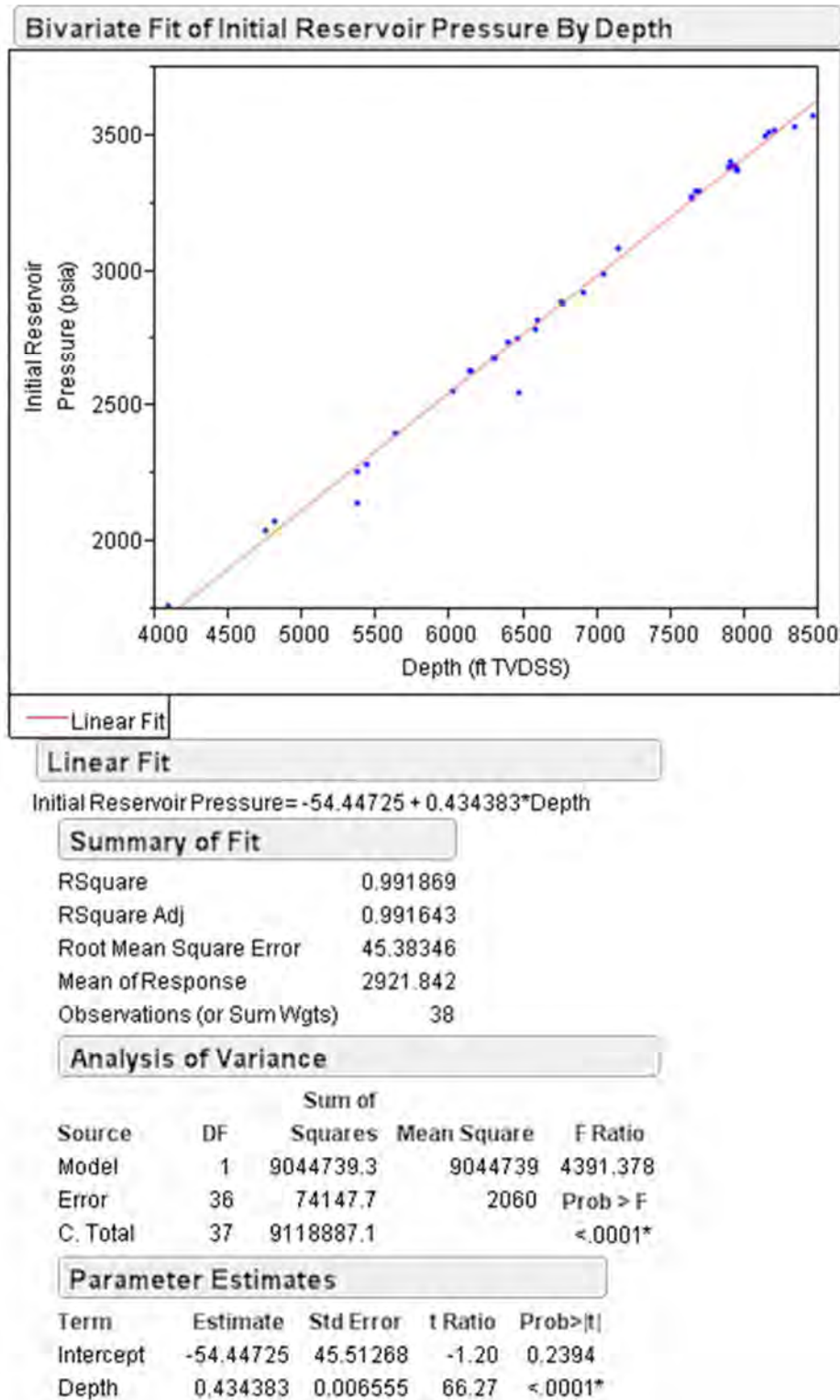


Figure D1: Correlation between initial reservoir pressure and horizontal well depth

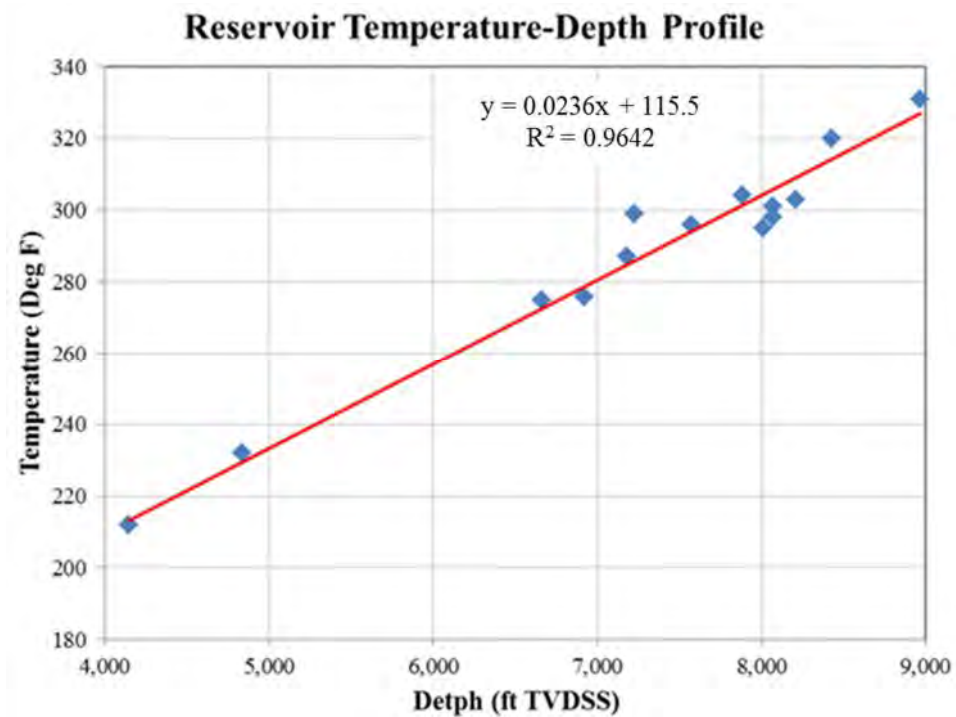


Figure D2: Correlation between initial reservoir temperature and depth

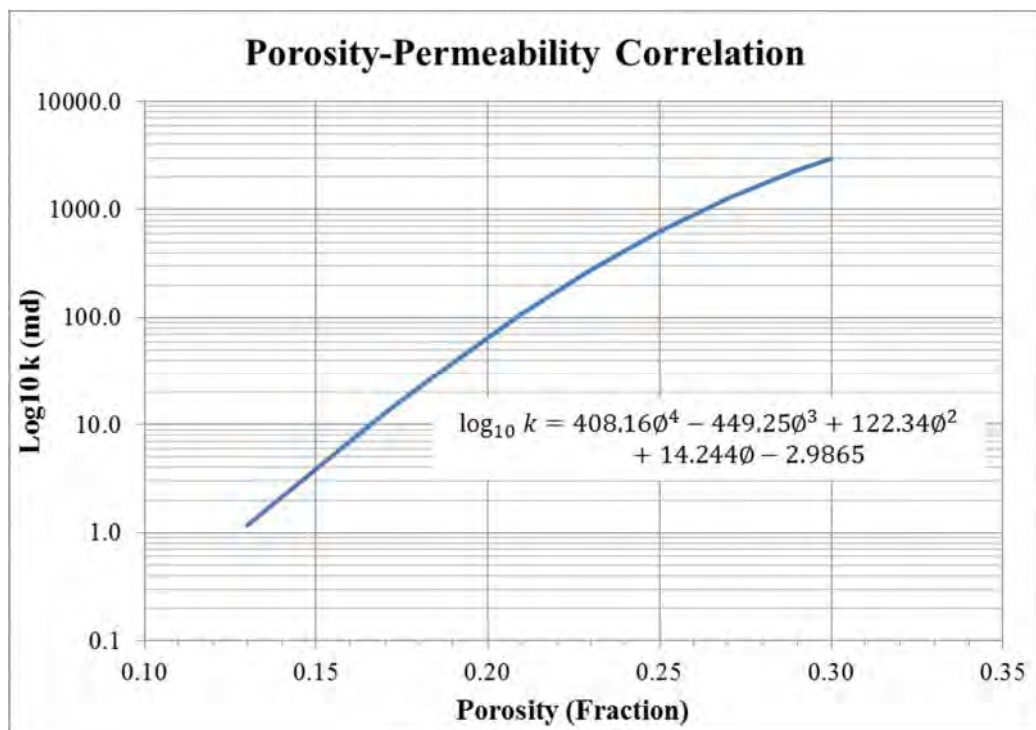


Figure D3: Correlation between porosity and horizontal permeability

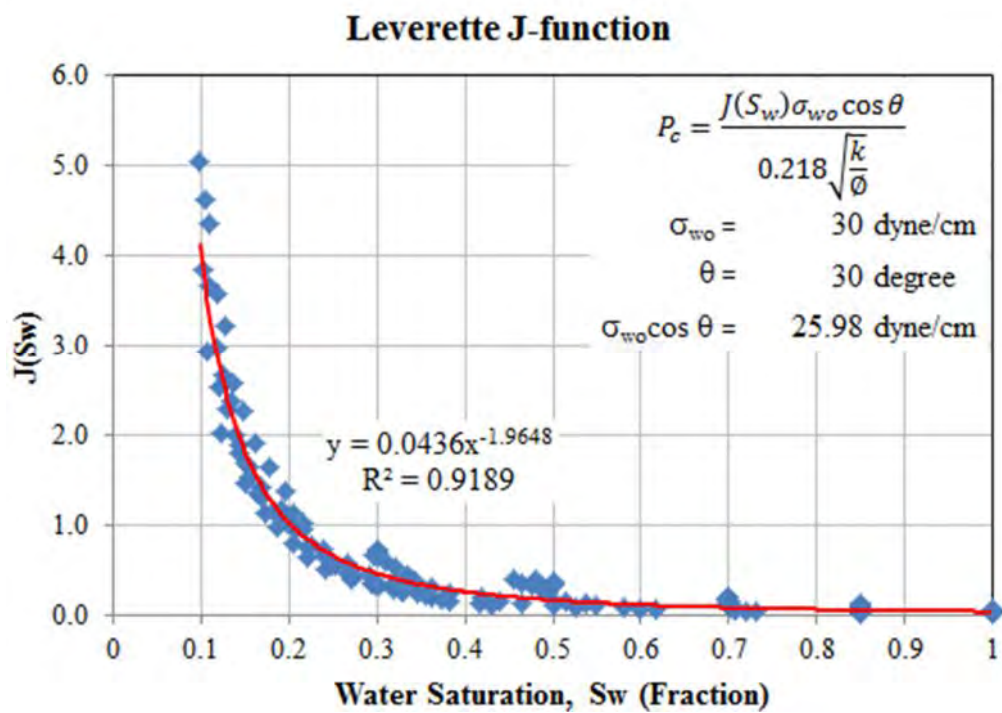
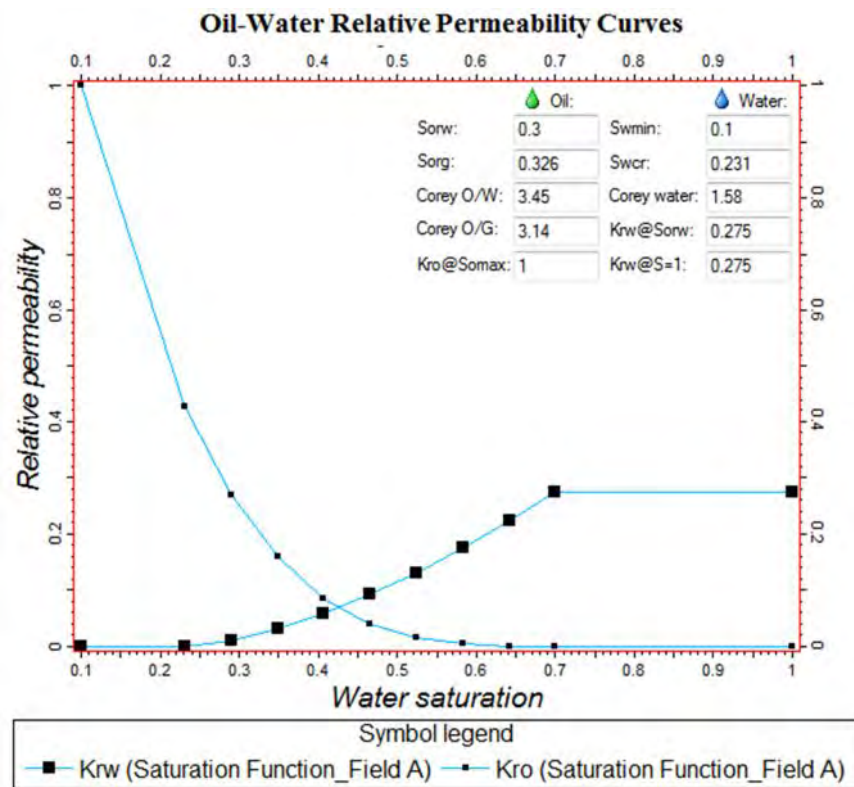
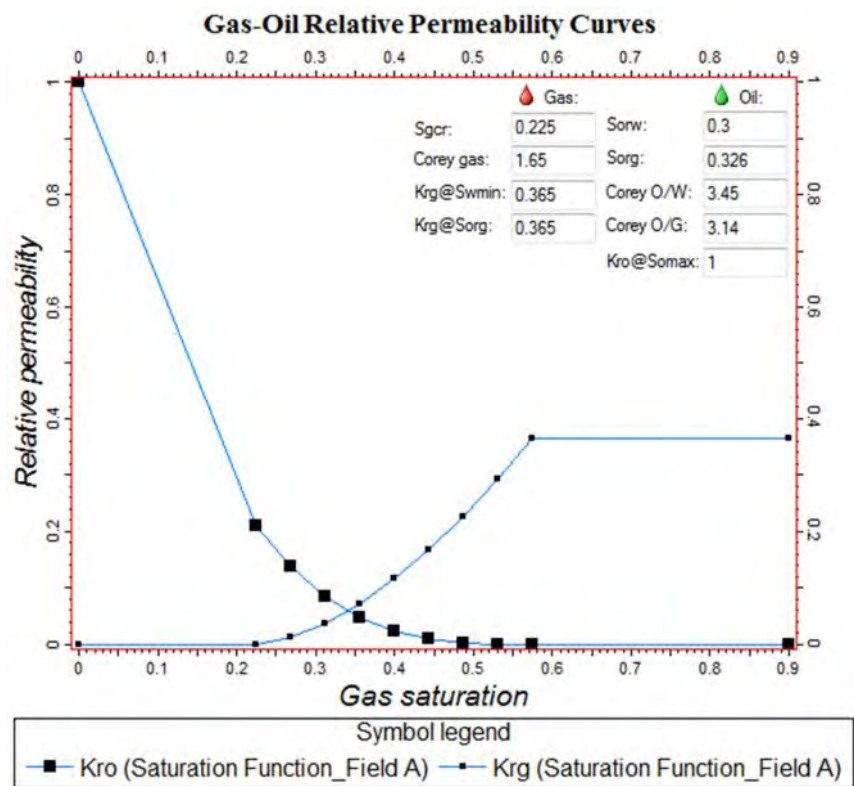


Figure D4: Correlation between Leverette J-function and  $S_w$



(a) Generic oil-water relative permeability curves



(a) Generic gas-oil relative permeability curves

Figure D5: Generic relative permeability curves

## **APPENDIX E**

Experimental Analyses and Results for Building a Gaussian Process  
Proxy used to Predict URF due to Two Vertical Wells

Table E1: Experimental results of the central composite design for vertical well production

Run ID.	Design Pattern	URF (%)	Run ID.	Design Pattern	URF (%)
1V	-----+	0.000	24V	00000A	9.318
2V	-----+-	0.038	25V	0000A0	31.176
3V	----+---	0.000	26V	000A00	16.577
4V	---++++	4.359	27V	00A000	8.757
5V	---+---	0.000	28V	0A0000	16.350
6V	---+-++	8.859	29V	+-----	0.000
7V	---++-+	0.000	30V	+----++	6.369
8V	---++++-	1.312	31V	+---+-+	0.000
9V	a00000	6.667	32V	+---++-	2.106
10V	-+-----	0.000	33V	+---+++	0.000
11V	-+---++	3.787	34V	+---+-+	0.114
12V	-+---+-	0.119	35V	+---+--	0.000
13V	-+---+-	33.809	36V	+---++++	20.153
14V	-+---+-	0.000	37V	A00000	10.459
15V	-+---+-	0.993	38V	+---+++	0.000
16V	-+---+-	0.071	39V	+---+-+	1.373
17V	-+---++	33.760	40V	+---+--	0.377
18V	0a0000	2.682	41V	+---++++	31.952
19V	00a000	3.589	42V	+++---	0.000
20V	000a00	0.310	43V	+++--++	14.695
21V	0000a0	0.000	44V	++++-+	0.316
22V	00000a	0.588	45V	+++++-	44.228
23V	000000	9.318			

Note: 1) "+", "0", and "-" = high-, mid-, and low-level values, respectively.  
 2) "A" and "a" = high- and low-level of face-centered point.  
 3) The order of design pattern is as follows: OWC, HO#, LHRATIO, WSTANDOFF, PORO, and LRAT.

Table E2: Experimental results of the maximum entropy design for vertical well production

Run ID.	OWC	HO#	LHRATIO	WSTANDOFF	PORO	LRAT	URF (%)
301V	7301.41	3.567	0.380	0.240	0.240	2697.2	11.975
302V	6360.58	4.171	0.180	0.360	0.160	2565.1	0.000
303V	7175.97	3.692	0.820	0.400	0.174	2697.2	0.000
304V	5294.30	3.818	0.940	0.307	0.236	5735.8	5.610
305V	5796.08	4.473	0.980	0.320	0.224	4414.7	11.364
306V	7426.86	4.322	0.940	0.427	0.246	715.6	32.324
307V	5294.30	3.995	0.640	0.387	0.160	55.0	0.000
308V	6276.04	3.793	0.687	0.360	0.190	55.0	0.005
309V	7991.36	4.675	0.280	0.440	0.220	4578.4	19.632
310V	5482.47	4.599	0.600	0.213	0.164	3225.7	0.000
311V	7928.63	4.222	0.540	0.587	0.234	4150.4	26.392
312V	5482.47	4.448	0.120	0.320	0.206	2036.7	2.580
313V	6297.86	4.247	0.620	0.413	0.206	1993.6	9.370
314V	5796.08	4.297	0.420	0.160	0.212	3754.1	0.595
315V	7489.58	4.020	0.320	0.421	0.194	847.7	2.173
316V	5984.24	4.574	0.420	0.400	0.160	847.7	0.000
317V	5607.91	3.617	0.760	0.160	0.200	2036.7	0.004
318V	7928.63	4.322	0.440	0.293	0.162	2433.0	0.000
319V	7050.52	4.222	0.360	0.760	0.188	55.0	6.961
320V	5294.30	4.133	0.160	0.613	0.204	3357.8	5.751
321V	7238.69	3.894	0.740	0.173	0.164	4943.1	0.000
322V	5921.52	4.675	0.100	0.520	0.188	3357.8	4.769
323V	7113.24	4.010	0.220	0.693	0.160	4546.8	0.000
324V	7748.65	4.549	0.300	0.160	0.198	55.0	0.001
325V	7050.52	3.567	0.780	0.533	0.214	2168.8	4.154
326V	7050.52	3.642	0.260	0.627	0.186	2697.2	0.042
327V	6736.91	4.196	0.880	0.173	0.224	2961.4	3.945
328V	6548.74	3.567	0.380	0.627	0.250	5867.9	16.950
329V	7426.86	3.692	0.260	0.467	0.234	319.2	12.312
330V	5294.30	3.692	0.520	0.320	0.228	4414.7	4.282
331V	6705.55	4.257	0.433	0.160	0.178	55.0	0.000
332V	5733.36	3.970	0.660	0.680	0.246	5339.4	20.977
333V	6486.02	4.448	0.560	0.547	0.164	4150.4	0.064
334V	7135.06	4.574	0.280	0.317	0.208	2565.1	7.776
335V	7994.08	4.020	0.100	0.267	0.210	3225.7	1.536
336V	6172.41	4.096	0.120	0.440	0.232	5867.9	10.185
337V	7113.24	4.096	0.300	0.307	0.210	5471.6	4.252
338V	7740.47	4.599	0.880	0.707	0.186	5735.8	17.154
339V	6674.19	4.524	0.980	0.707	0.160	715.6	0.100
340V	7865.91	4.574	0.960	0.653	0.214	583.4	22.998



Table E2: Experimental Results of the maximum entropy design for vertical well production (Continued)

Run ID.	OWC	HO#	LHRATIO	WSTANDOFF	PORO	LRAT	URF (%)
341V	6674.19	3.768	0.760	0.360	0.236	4018.3	16.050
342V	5482.47	3.869	0.100	0.520	0.224	1244.0	3.651
343V	5357.02	3.642	0.840	0.653	0.212	3489.9	3.304
344V	6109.69	3.739	0.180	0.160	0.236	2300.9	1.653
345V	5733.36	3.617	0.800	0.640	0.174	1508.2	0.000

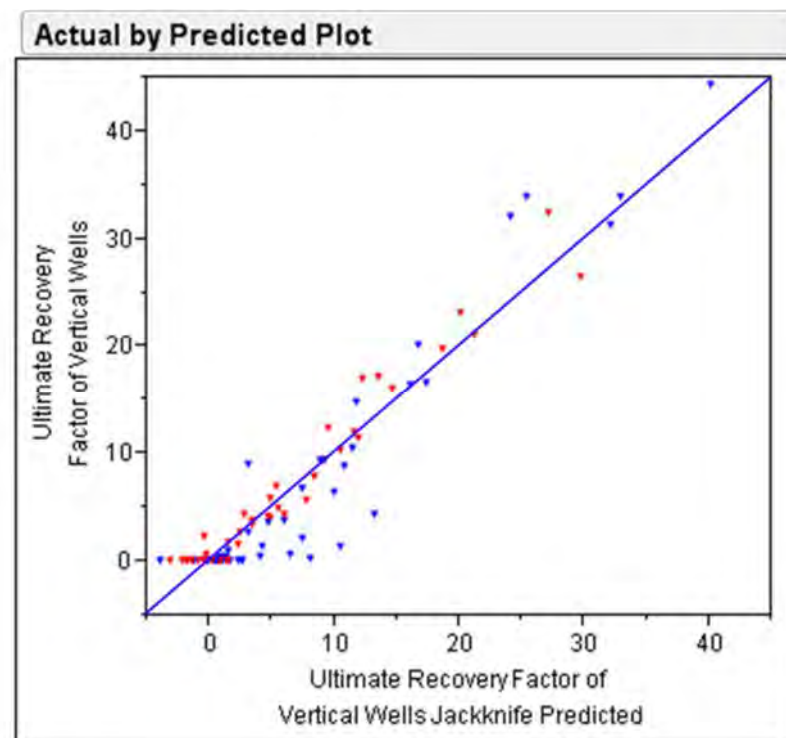


Figure E1: Actual by jackknife predicted plot of the Gaussian process proxy model for vertical well production

Table E3: JMP model report of the Gaussian process proxy model for vertical well production

<b>Model Report</b>		<b>Total</b>		<b>OWC</b>		<b>HO#</b>		<b>LHRATIO</b>		<b>WSTANDOFF</b>		<b>PORO</b>		<b>LRAT</b>	
<b>Column</b>	<b>Theta</b>	<b>Sensitivity</b>	<b>Main Effect</b>	<b>Interaction</b>	<b>Interaction</b>	<b>Interaction</b>	<b>Interaction</b>	<b>Interaction</b>	<b>Interaction</b>	<b>Interaction</b>	<b>Interaction</b>	<b>Interaction</b>	<b>Interaction</b>	<b>Interaction</b>	<b>Interaction</b>
OWC	8.3055e-9	0.0155094	0.0095779	.	.	5.5434e-6	0.0000569	0.0000569	0.0006307	0.0048504	0.0003879	0.0003879	0.0003879	0.0003879	0.0003879
HO#	0.1879122	0.1876818	0.1126879	5.5434e-6	5.5434e-6	.	0.0008684	0.0008684	0.045291	0.027582	0.001247	0.001247	0.001247	0.001247	0.001247
LHRATIO	0.2333011	0.029336	0.0195132	0.0000569	0.0000569	0.0008684	.	.	0.0014342	0.0066087	0.0008547	0.0008547	0.0008547	0.0008547	0.0008547
WSTANDOFF	6.5841148	0.233923	0.1225339	0.0006307	0.0006307	0.045291	0.0014342	0.0014342	.	0.0491401	0.0148931	0.0148931	0.0148931	0.0148931	0.0148931
PORO	169.405	0.637138	0.5433085	0.0048504	0.0048504	0.027582	0.0066087	0.0066087	0.0491401	.	.	.	.	.	.
LRAT	2.9447e-8	0.0349855	0.0119543	0.0003879	0.0003879	0.001247	0.0008547	0.0008547	0.0148931	0.0056483	0.0056483	0.0056483	0.0056483	0.0056483	0.0056483
$\mu$	-0.63118	230.90387	2.309e-10												
$\sigma^2$															
<b>Nugget</b>															
<b>-2*LogLikelihood</b>															

Fit using the Gaussian correlation function.

Nugget parameter set to avoid singular variance matrix.

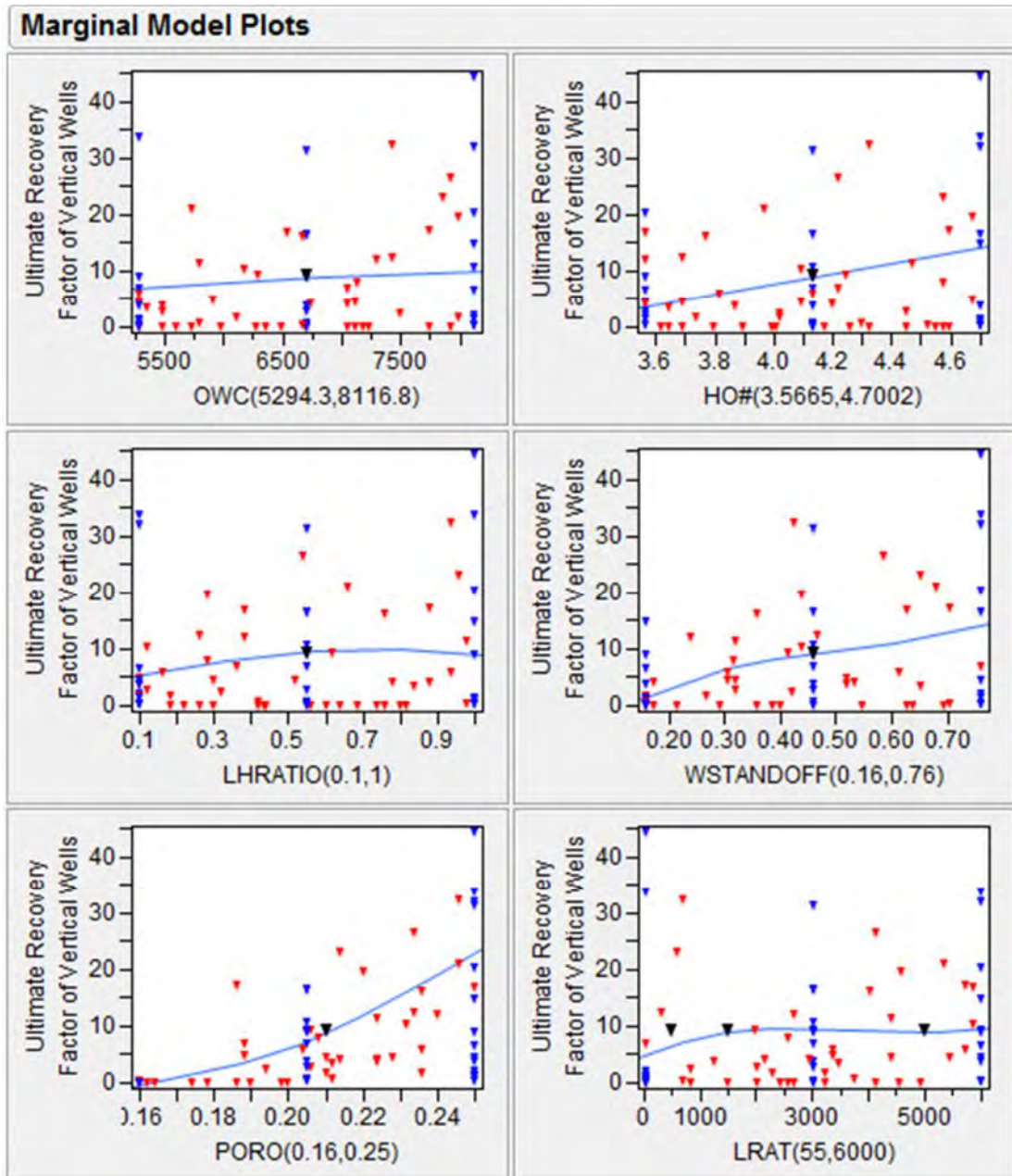


Figure E2: JMP marginal model plots of the Gaussian process proxy model for vertical well production

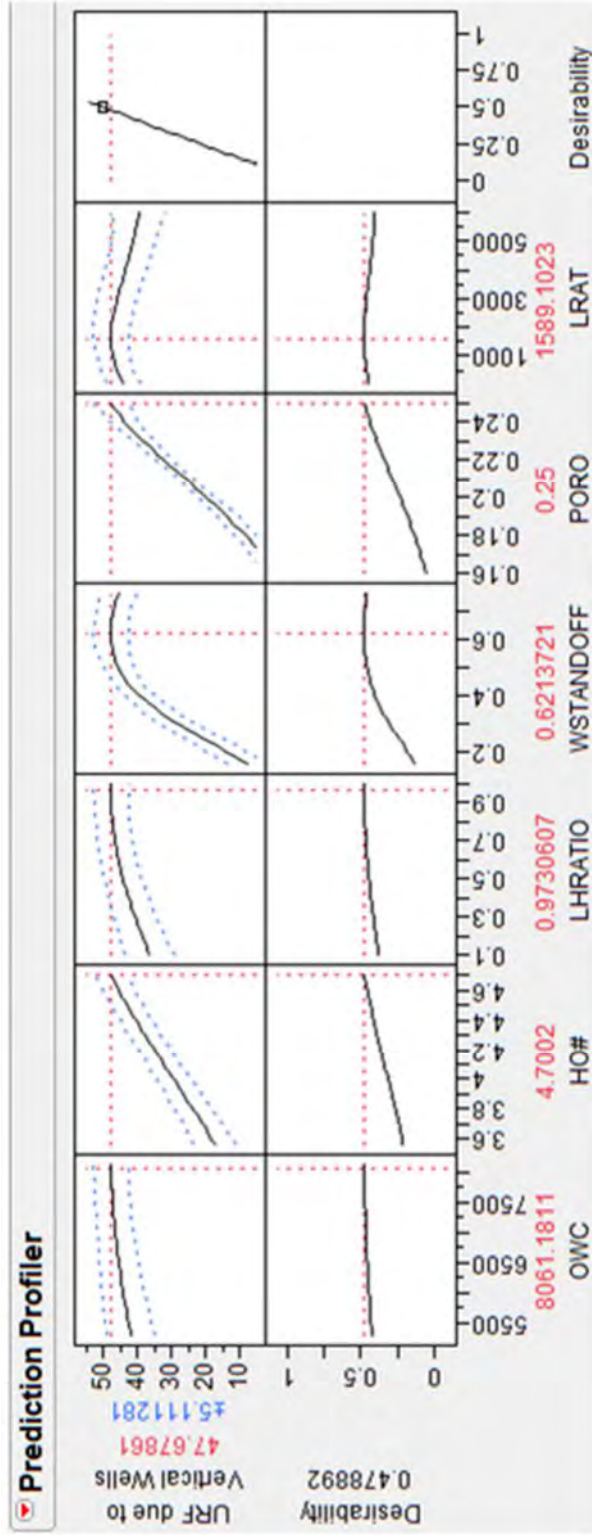


Figure E3: JMP prediction profiler showing optimum factor setting of the Gaussian process proxy model for vertical well production

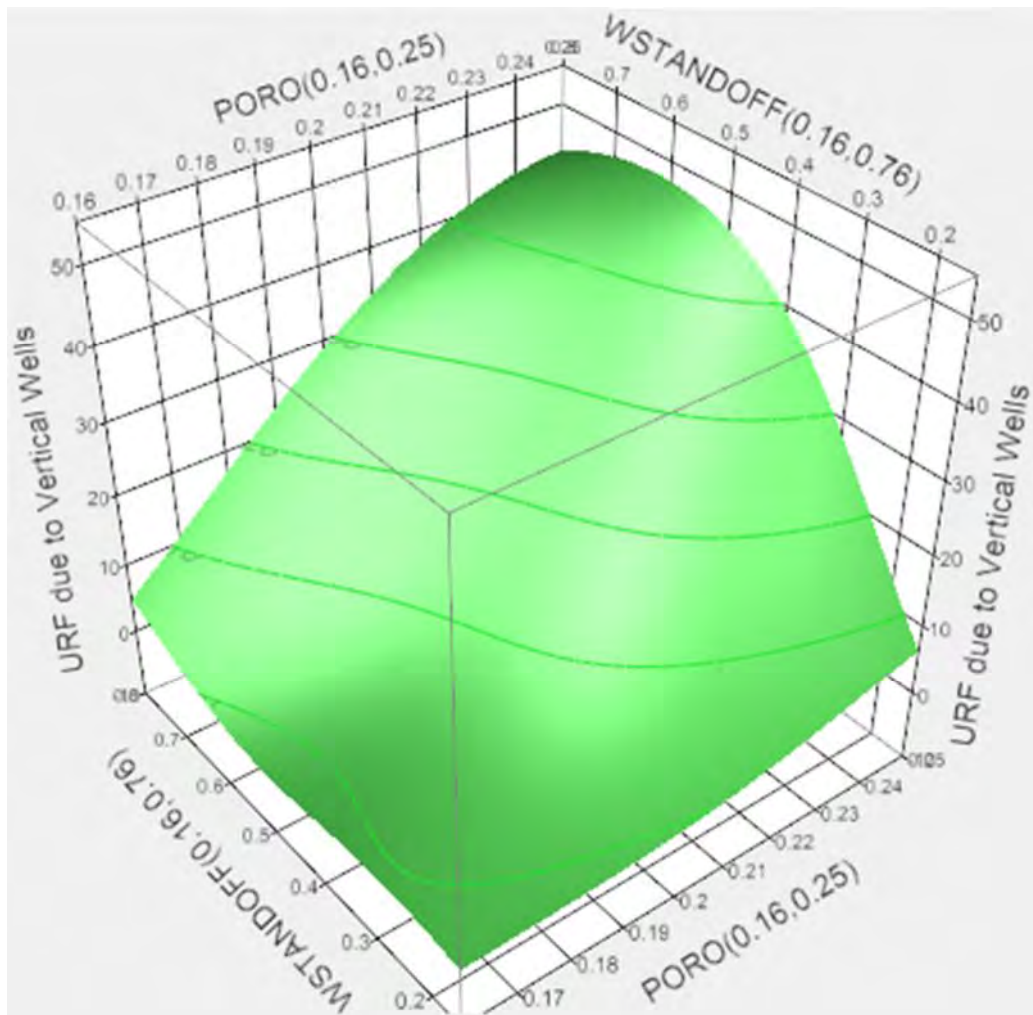


Figure E4: 3D surface plot at the optimum factor setting of the Gaussian process proxy model for vertical well production



Figure E5: JMP interaction profiles at the optimum factor setting of the Gaussian process proxy model for vertical well production

Table E4: Experimental results of the first 18-run maximum entropy design for validating the proxy model for vertical well production

<b>Run ID.</b>	<b>OWC</b>	<b>HO#</b>	<b>LHRATIO</b>	<b>WSTANDOFF</b>	<b>PORO</b>	<b>LRAT</b>	<b>URF (%)</b>
101V	7959.99	3.755	0.950	0.293	0.165	55.0	0.000
102V	7332.77	4.259	0.100	0.160	0.185	5339.4	0.000
103V	7803.19	4.322	0.800	0.493	0.180	5009.2	2.863
104V	6548.74	4.700	0.450	0.160	0.210	4348.6	2.410
105V	6705.55	3.692	0.650	0.660	0.230	1376.1	13.252
106V	6548.74	4.133	0.200	0.627	0.180	3027.5	1.874
107V	6548.74	4.259	0.900	0.160	0.225	2036.7	3.113
108V	6391.94	3.567	0.350	0.393	0.235	4678.9	8.364
109V	5451.11	3.944	0.100	0.360	0.200	2697.2	0.206
110V	5294.30	4.385	0.150	0.493	0.170	5669.7	0.002
111V	5764.72	4.196	0.450	0.327	0.245	2036.7	12.982
112V	6078.33	3.755	0.900	0.727	0.160	3688.1	0.000
113V	8116.80	4.574	0.250	0.293	0.230	3027.5	14.816
114V	5294.30	4.511	0.850	0.527	0.235	2697.2	21.158
115V	6862.36	4.385	0.400	0.693	0.220	1045.8	22.799
116V	5294.30	3.692	0.650	0.260	0.185	385.3	0.000
117V	6705.55	3.818	0.700	0.327	0.165	2366.9	0.000
118V	6862.36	4.385	0.800	0.560	0.160	715.6	0.003

Table E5: Experimental results of the second 18-run maximum entropy design for validating the proxy model for vertical well production

<b>Run ID.</b>	<b>OWC</b>	<b>HO#</b>	<b>LHRATIO</b>	<b>WSTANDOFF</b>	<b>PORO</b>	<b>LRAT</b>	<b>URF (%)</b>
201V	5607.91	3.818	0.150	0.427	0.205	2366.9	0.488
202V	5294.30	3.755	0.650	0.627	0.220	5009.2	8.130
203V	5921.52	3.567	0.250	0.727	0.190	4018.3	0.033
204V	7175.97	3.818	0.250	0.493	0.160	5339.4	0.000
205V	5294.30	4.637	0.150	0.593	0.195	1706.4	9.710
206V	5294.30	4.700	0.900	0.460	0.180	2036.7	0.569
207V	7803.19	4.511	0.400	0.727	0.205	3688.1	21.740
208V	7959.99	4.133	0.800	0.327	0.160	4348.6	0.000
209V	6862.36	4.574	0.600	0.527	0.170	4018.3	0.445
210V	5607.91	4.259	0.100	0.327	0.185	5339.4	0.001
211V	6391.94	3.692	0.950	0.427	0.225	385.3	8.707
212V	6078.33	4.070	0.500	0.160	0.225	3688.1	1.532
213V	6862.36	3.567	0.850	0.493	0.180	2697.2	0.001
214V	7646.38	4.322	0.350	0.327	0.165	715.6	0.000
215V	7175.97	3.567	1.000	0.227	0.180	55.0	0.000
216V	5764.72	4.448	0.550	0.627	0.225	5669.7	23.770
217V	5294.30	4.259	0.800	0.160	0.175	2366.9	0.000
218V	5921.52	4.511	0.400	0.260	0.205	385.3	3.345



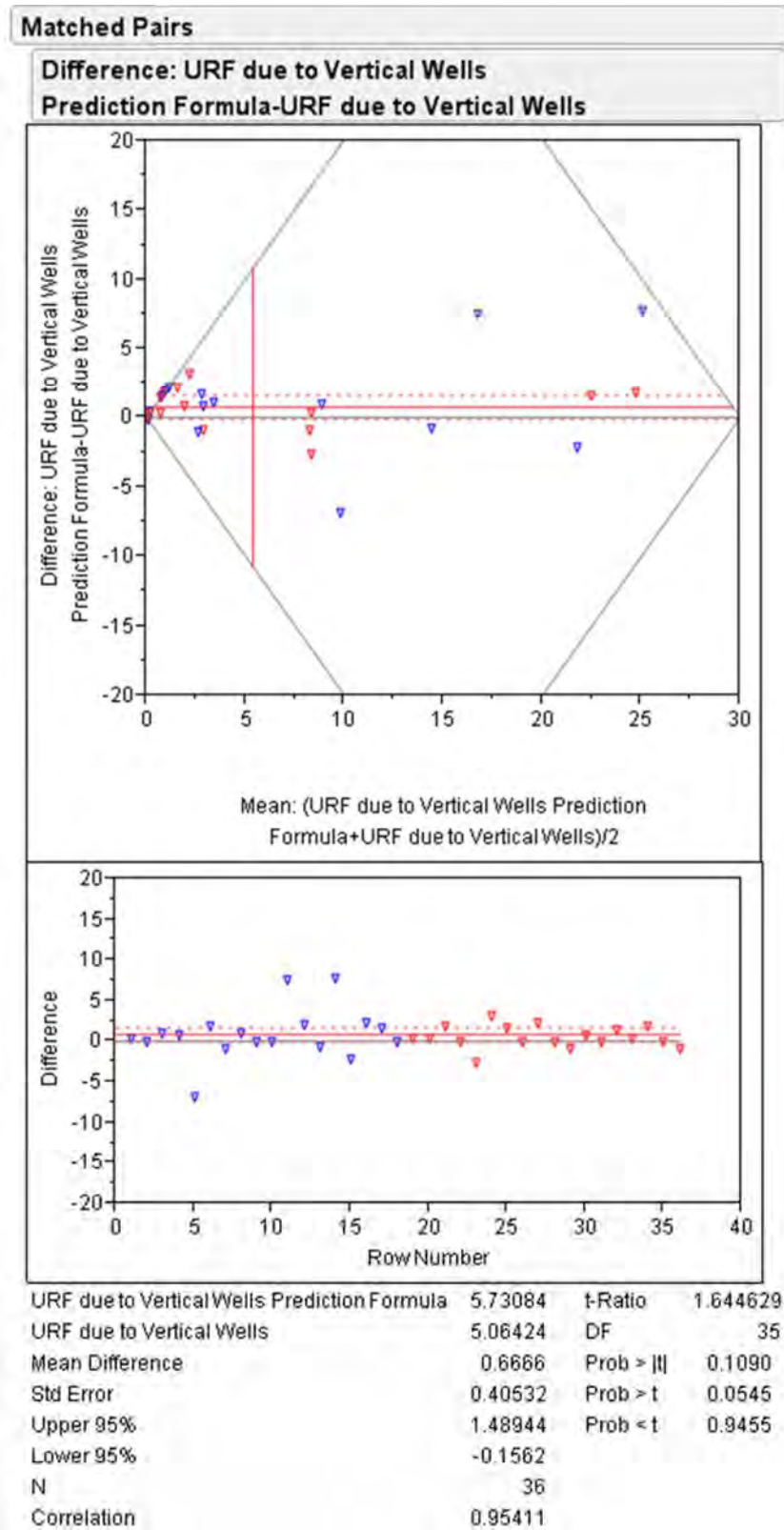


Figure E6: Matched pairs t-test for validating the Gaussian process proxy model for vertical well production

## **APPENDIX F**

Estimation of Oil Production Volume at Break-Even Point of a  
Horizontal Well

### Estimation of Oil Production Volume at Break-Even Point

1) Drilling and completion cost	=	2.700 \$MM/well (Conventional completion = \$250/ft or \$2.7MM/well)
2) Surface facility cost	=	0.300 \$MM/well (High case)
3) Operating cost	=	0.052 \$MM/well/year
4) Maintenance cost	=	0.020 \$MM/well/year
5) Escalation rate	=	3% per year
6) Discount rate	=	10% per year

Year	Description	Escalating factor	Escalated Cost (\$MM)	Discounting factor	Present Value (\$MM)
0	Items 1- 2	1.00	3.000	1.00	3.000
1	Items 3-4	1.03	0.074	0.91	0.069
2	Items 3-4	1.06	0.076	0.83	0.067
3	Items 3-4	1.09	0.079	0.75	0.064
4	Items 3-4	1.13	0.081	0.68	0.062
5	Items 3-4	1.16	0.083	0.62	0.060
6	Items 3-4	1.19	0.086	0.56	0.058
7	Items 3-4	1.23	0.088	0.51	0.056
8	Items 3-4	1.27	0.091	0.47	0.054
9	Items 3-4	1.30	0.094	0.42	0.052
10	Items 3-4	1.34	0.097	0.39	0.050
				<b>Total =</b>	<b><u>3.592</u></b>

If oil price = 70 \$/bbl, equivalent barrels of oil to break-even point = 51,313 bbl

In practice, only a reservoir having OOIP > 1 MMSTB is considered for horizontal well execution.

If average URF = 10%, the minimum recovered oil is 100,000 STB.

#### Conclusion

Economics should be compared at the time that 100,000 STB of oil is produced.

## VITAE

Jirasak Arunmongkol was born on September 08, 1978 in Bangkok, Thailand. In 1999, he obtained his Bachelor of Engineering in Civil Engineering with 2<sup>nd</sup> class honors from Faculty of Engineering, Chulalongkorn University. In 2000, he pursued his Master of Engineering in Civil Engineering in National University of Singapore under NUS research scholarship. After his graduation, he worked as a geotechnical engineer for one and a half year before returning to Thailand in 2004. Subsequently, he starts his career in oil and gas industry by working as an offshore structural engineer. Since 2007, he has expanded his knowledge in upstream sector of the industry by pursuing Master of Engineering in Petroleum Engineering in Chulalongkorn University.

### Conference Paper [Unpublished]:

Arunmongkol, J. and Chewaroungroaj, J. An Application of Experimental Design for Hydrocarbon Recovery from a Horizontal Well in a Thin-Oil-Column Reservoir in the Gulf of Thailand. Unpublished paper presented at the 9<sup>th</sup> Mining, Metallurgical, and Petroleum Engineering Conference, Bangkok, Thailand (2011, January 13-14).